

Ontwikkeling van een connectortechnologie
voor compacte parallelle verbindingen
op basis van plastic optische vezels

Development of a Connector Technology
for High-Density Parallel Interconnects
Based on Plastic Optical Fibres

Thierry Coosemans

Promotor: prof. dr. ir. R. Baets
Proefschrift ingediend tot het behalen van de graad van
Doctor in de Ingenieurswetenschappen

Vakgroep Informatietechnologie
Voorzitter: prof. dr. ir. P. Lagasse
Faculteit Ingenieurswetenschappen
Academiejaar 2006 - 2007



ISBN 90-8578-108-6
NUR 959
Wettelijk depot: D/2006/10.500/66

Promotor:

Prof. dr. ir. Roel Baets

Universiteit Gent, INTEC

Overige leden van de examencommissie:

Prof. dr. ir. Daniël De Zutter, voorzitter	Universiteit Gent, INTEC
Prof. dr. ir. Dries Van Thourhout, secretaris	Universiteit Gent, INTEC
Prof. dr. ir. Jan Van Campenhout	Universiteit Gent, ELIS
Prof. dr. ir. Peter Van Daele	Universiteit Gent, INTEC
Prof. dr. ir. Hugo Thienpont	Vrije Universiteit Brussel, TONA
Ir. Jan Van Koetsem	FCI
Dr. ir Ronny Bockstaele	Phocon

Universiteit Gent
Faculteit Ingenieurswetenschappen

Vakgroep Informatietechnologie (INTEC)
Sint-Pietersnieuwstraat 41
B-9000 Gent
België

Tel: +32 9 264 33 16
Fax: +32 9 264 35 93
<http://www.intec.ugent.be>
<http://www.photonics.intec.ugent.be>

Dankwoord

Zoals U, beste lezer, tijdens de lectuur van dit verslag zult opmerken, is het beschreven onderzoekswerk te situeren in een zeer multidisciplinair vakgebied. Bijgevolg heb ik tijdens mijn verblijf op INTEC de mogelijkheid gehad om met tal van mensen met verschillende achtergrond te kunnen samenwerken, mensen van zowel binnen als van buiten de universiteit. Het lijstje “te bedanken personen” is dan ook vrij lang en ik hoop uit de grond van mijn hart dat ik in dit dankwoord niemand in de kou heb laten staan.

In eerste instantie wens ik professor Lagasse te bedanken voor de mogelijkheid die ik gekregen heb om dit doctoraatswerk uit te voeren, alsook voor het ter beschikking stellen van de INTEC-infrastructuur. Ook wens ik het IWT en de Europese Commissie te bedanken voor hun projectgebonden financiële ondersteuning. Dan is er natuurlijk Prof. Roel Baets, die het aangedurfd heeft mijn promotor te zijn. Tijdens de vele vergaderingen die we samen hebben gehad, heb ik Roel leren kennen als iemand die steeds de nagel op de kop sloeg en altijd nuttige suggesties voor het verdere verloop van het onderzoek naar voren bracht. Bovendien staat hij steeds achter zijn doctoraatsstudenten en heeft hij zich, althans wat mij betreft, een (zeer) geduldig man getoond. Dank je wel Roel.

Binnen de INTEC vakgroep hebben tal van mensen me meer dan een handje toegestoken. An Van Hove stond steeds klaar met haar hot knife en hot plate om POFjes te termineren, Ronny was mijn onuitputbare leverancier van RCLED's en optica-mopjes, en Kris ableerde en simuleerde er lustig op los zodat ik mijn connectortjes kon assembleren. Bovendien zorgde Steven Verstuyft ervoor dat ik mijn gang kon gaan in de clean-room, en ik kreeg steeds de nodige ondersteuning van Hendrik voor wat betreft de meetapparatuur. Ook heb ik het genoeg gehad om in het raamwerk van een aantal projecten met Prof. Peter Van Daele te mogen samenwerken, zodat niet alleen mijn kennis voor wat betreft MOCVD is toegenomen, maar ook mijn culinaire cultuur naar een hoger niveau is getilt. Verder wil ik Luc Haentjes en Marc Declercq mijn dankbaarheid betuigen voor het produceren van de talrijke mechanische stukjes, artistieke foto's en fijne soldeerwerkjes. Ook al de dames van het secretariaat verdienen een pluim voor hun niet aflatende ondersteuning bij het verwerken der administratieve rompslomp.

Zoals gezegd heb ik de mogelijkheid gehad om met tal van mensen van andere vakgroepen, van andere universiteiten of uit de industrie samen te werken. Hierbij denk ik aan Prof. Jan Van Campenhout dankzij wie ik een beter inzicht in het nut van 3D-interconnecties heb vergaard, aan Prof. Hugo Thienpont die me wegwijs heeft gemaakt in de wereld van de micro-optica en aan Valerie en Heidi die me hebben bijgestaan met simulatie resultaten en Wyko metingen. Dankzij de samenwerking met Jan Van Koetssem heb ik voor het eerst ingezien hoe groot het verschil tussen industrie en universiteit wel is. Wim Van Paeppegem en Wim De Waele hebben de lastige mechanische proeven en simulaties voor hun rekening genomen. Tenslotte wil ik Ilse en Camelia bedanken voor het uitvlooiën van mijn schrijfwerk op de “enkele” typo's.

Werken op INTEC is niet alleen een leerrijke ervaring, maar is doodgewoon ook leuk. De rits sympathieke mensen die er komen studeren/werken zorgen voor een

dynamische, aangename sfeer. Gezien het tijds kader van mijn doctoraatswerk heb ik het genoeg gehad om meerdere “generaties” te zien passeren op het labo. Zowel bij de “oudere” garde (Bart, An, Boris, Swa, Tim...) als bij het “jongere” geweld dat koffiekamer van de 39 onveilig maakte (Ronny, George, Smolli, Flick, Bert, Boeggi-boy, Peter-op-de-witte-stoel....), heb ik me als een vis in het water gevoeld. Bedankt jongens, het was tof.

Tenslotte wil ik mijn twee lieve kinderen bedanken om zo lang te wachten tot papa’s boekje eindelijk af is, evenals mijn vrienden en familieleden die nooit zijn beginnen lachen als ik zei dat ik “binnenkort” zou indienen. Eind goed, al goed.

Gent, 2 November 2006

Thierry Coosemans

Nederlandstalige samenvatting

Door de razendsnelle ontwikkeling van de halfgeleidertechnologie in de tweede helft van de 20ste eeuw is de mensheid in staat om steeds groter wordende computers en gegevensverwerkende apparaten te bouwen. De microchip, die de basis vormt van zulke systemen, heeft een rekenvermogen en complexiteit die aan een hoog tempo toenemen. Omdat het verwerkingsvermogen van de chips op zulk een snelle manier toeneemt, neemt ook de uitwisseling van informatie tussen de chips in hoge mate toe. Deze communicatie werd tot nu toe altijd gedaan over koperen transmissielijnen. Echter, door de groeiende data overdracht is een steeds dichter netwerk nodig met steeds smallere koperbaantjes. Dit beperkt de bandbreedte van de transmissielijnen aanzienlijk. Niettegenstaande dat er allerlei technieken ontwikkeld worden om de bandbreedte te vergroten, voorziet men toch dat op een bepaald ogenblik in het volgende decennium, de lijnen in grote dataverwerkende systemen de informatiestromen niet meer zullen kunnen ondersteunen. Multimode optische vezels kunnen hiervoor een oplossing bieden. Voor typische afstanden in grote computers leveren ze een hoge bandbreedte, en kunnen ze dus hoge datasnelheden aan. Bovendien kunnen ze door hun kleine diameter (typisch $125\ \mu\text{m}$) op kleine afstanden van elkaar in parallelle bundels geplaatst worden zodat men een nog grotere samengestelde datasnelheid per chip kan bekomen. Plastic optische vezels met een kleine diameter hebben nog een aantal extra voordelen: ze zijn zeer buigbaar en kunnen gemakkelijk met een hoge numerieke apertuur gemaakt worden. Dit wil zeggen dat met deze vezels scherpe bochten gemaakt kunnen worden zonder dat er veel transmissieverliezen optreden, een aanzienlijk voordeel in computersystemen, waarin de ruimte meestal zeer beperkt is. Bovendien kunnen ze d.m.v. eenvoudige en goedkope technieken, zoals het doorsnijden met een verwarmd mes, getermineerd worden. Het grote nadeel van plastic vezel met kleine diameter is dat er heden ten dage geen connectoren bestaan die parallelle bundels kunnen koppelen, naar andere bundels of naar opto-elektronische componenten. Deze doctoraatsthesis geeft een oplossing voor dit probleem en stelt een technologie voor om zulke connectoren te maken.

Tijdens het onderzoekswerk werden twee types plastic optische vezel bekeken. Beide hadden een buitendiameter van $125\ \mu\text{m}$ en hadden een trapvormig index profiel. De ene was echter gemaakt door Asahi Chemical en had een kerndiameter van $61\ \mu\text{m}$; de andere was gemaakt door Toray en had een kerndiameter van $116\ \mu\text{m}$. In eerste instantie werd er aan gedacht om een connector te ontwerpen die gebaseerd was op het principe dat commerciële MT-connectorenTM voor parallelle glasvezels gebruiken. Hierbij worden de vezels via conische buisjes in gaatjes geleid die de vezels op exact de juiste positie houden. Echter, plastic vezels zijn zo buigzaam dat het inbrengen in de conische buisjes zeer moeilijk verloopt en dus zeer arbeidsintensief is. Daarom werd een nieuwe techniek ontwikkeld bestaande uit drie stappen. In een eerste stap werden één-dimensionale bundels ($1 \times N$) gemaakt, die dan in een tweede stap gestapeld werden op een precieze afstand van elkaar. Op die manier maakte men een twee-dimensionale bundel ($M \times N$). In een laatste stap werd deze bundel in een structuur geplaatst die bij koppeling de ene bundel t.o.v. de andere bundel uitlijnt, of die de bundel t.o.v. opto-elektronische componenten uitlijnt.

Voor het vervaardigen van de één-dimensionale bundel werden twee methodes be-

schouwd. De eerste techniek bestond uit het vervaardigen van dunne polymethyl metacrylaat (PMMA) plaatjes met parallelle groefjes erin door middel van laser ablatie met een ArF-gaslaser. Vervolgens werden de vezels in de groefjes gelegd en met UV-lijm vastgezet. Deze methode bleek adequaat zolang de buitendiameter van de vezel goed gecontroleerd was, zoals in het geval van de Toray vezel. Voor de Asahi vezel was dit echter niet zo en een andere methode drong zich op. Hierbij werden twee silicium plaatjes gebruikt waarin v-vormige groefjes geëtst waren. De vezels werden in deze groeven gelegd en tussen de twee plaatjes opgespannen. In het gebied tussen de plaatjes waren de vezels vrij en werden ze overgoten met UV-lijm. Na uitharding van de lijm werd het geheel van lijm en vezels met een verwarmd mes doorgesneden en bekwam men een één-dimensionale bundel. De positie van de vezels in de bundel was tot op $8\ \mu\text{m}$ nauwkeurig.

Voor het stapelen van de bundels werd een methode ontwikkeld die we "virtuele uitlijning" genoemd hebben. Dit is een optische uitlijntechniek waarbij twee bewegende camera's als het ware een virtueel masker creëren waarmee twee verschillende objecten t.o.v. mekaar gepositioneerd kunnen worden. De reden voor de ontwikkeling van deze techniek lag in het feit dat in het algemeen de afstanden tussen de te stapelen vezels te groot zijn om het geheel met voldoende vergroting te kunnen bekijken met één microscoopobjectief enerzijds, en dat de afstanden te klein waren om met twee parallelle objectieven te kunnen werken anderzijds. Een systeem uitwerken waarbij twee camera's een onafhankelijk en bewegend gezichtsveld hebben, bood een oplossing. Het stapelen gebeurt dan in twee stappen: eerst worden de één-dimensionale bundels op de correcte afstand van elkaar gezet door middel van virtuele uitlijning, en vervolgens wordt de UV-lijm, die op voorhand is aangebracht, uitgehard. Virtuele uitlijning blijkt objecten te kunnen positioneren tot op 2% van de gevraagde afstand nauwkeurig. De uiteindelijke positie van de vezel in de twee-dimensionale bundel was tot op $15\ \mu\text{m}$ na bepaald. Voor parallelle optische verbindingen die gebruik maken van Vertical Cavity Surface Emitting Lasers (VCSELS) was deze afwijking aanvaardbaar.

Tenslotte werd virtuele uitlijning ook gebruikt om de twee-dimensionale bundel in de structuur te plaatsen die de bundels uitlijnt bij het koppelen, alsook voor het plaatsen van een aligneerstructuur bij de opto-elektronische componenten. Dit experiment gaf niet het verhoopte resultaat, niet te wijten aan een tekortkoming van de uitlijntechniek, maar eerder aan een verlijmingsprobleem. Dit probleem was echter niet fundamenteel, en op het einde van de doctoraatsthesis worden dan ook suggesties gegeven om dit op te lossen.

Het onderzoekswerk voor deze doctoraatsthesis is uitgevoerd in het raamwerk van twee projecten. In eerste instantie was er het IWT-project: "Studie van connectoren voor parallelle optische interconnecties binnen en tussen elektronische systemen.", ten tweede was er het door de Europese Commissie ondersteunde project: "Optically Interconnected Integrated Circuits".

English Summary

Thanks to the extremely fast evolution of semiconductor technology during the second half of last century, mankind is capable to build large data processing systems that get more complex day by day. The elementary building block of those systems is the microchip, a device with a dramatically increasing processing capability. Together with the growing chip functionality the data exchange between those chips is dramatically increasing as well. Until now the chip-to-chip transmission lines consisted of copper wiring. The increasing functionality of the chip and as a result the growing electrical pin-out, requires a denser wiring network and consequently narrower copper lines. This requirement severely limits the bandwidth of these lines and in spite of a continuous development of bandwidth-enhancing techniques, it is foreseen that in the next decade copper will not be able anymore to accommodate the necessary data traffic within large data processing systems. In other words an interconnect “bottleneck” will occur in large data processing systems. Multimode optical fibres offer a good solution for this problem. For typical interconnect lengths within a large computer rack, they offer a high bandwidth and can cope with high data rates. Moreover, thanks to their small diameter (typically $125\ \mu\text{m}$) they can be placed in dense parallel arrays, resulting in even higher aggregate data-rates per chip. Small diameter Plastic Optical Fibre (“POF”) has some extra advantages: they are very flexible and can easily be made with a high numerical aperture, what reduces transmission losses while bending the fibres with short bending radius. This allows making compact optical links, an important asset for computer systems in which space between printed circuit boards is limited. In addition POFs are cheap and they can be terminated with a fast technique, like for instance hot knife cutting. Drawback is the lack of an adequate connector that couples two-dimensional arrays of small diameters POFs to optoelectronic components or to other POF arrays. This PhD thesis tries to give a solution for that problem and proposes a technology that allows making such connectors. For this study two kinds of small diameter POFs were used, both with a step index profile and an outer diameter of $125\ \mu\text{m}$. One type was made by Asahi Chemical and had a core diameter of $61\ \mu\text{m}$; the other was made by Toray with a core diameter of $116\ \mu\text{m}$. Our first idea was to develop a connector technology that was similar to the existing MT^{TM} connector system. In this system each fiber is introduced in a conical duct that guides the fiber into precise holes that keep the fibers at the exact position. However, the small diameter plastic fibres are so flexible that introducing them in the ducts is extremely difficult and hence labour intensive. Therefore an alternative solution, based on three consecutive steps has been proposed. In a first step, POFs were accurately placed in a $1 \times N$ one-dimensional array. Then, these one-dimensional arrays were stacked at a precise pitch to obtain a two-dimensional $M \times N$ array, called the ferrule. Finally, this ferrule was placed in a structure that assures its alignment with respect to another coupled ferrule, or with respect to an array of optoelectronic dies. For the realization of the one-dimensional arrays, two technologies were developed and evaluated. The first method consisted of ablating u-shaped grooves in thin PolyMethyl MetAcrylate (PMMA) plates by means of a ArF gas laser, consecutively inserting the POFs in these grooves, and finally fixing them with UV-curable glue. This method proved to be satisfactory as long as the outer diameter of the

POF is well controlled. However, this was not the case for the Asahi-made fibre, and another method had to be developed. It consisted of aligning POFs by means of two silicon plates with parallel v-shaped grooves. Those plates were placed at a certain distance from each other and the part of the POFs that was stretched between the plates was immersed in UV-curable glue. After the UV-curing, the glue and POFs were cut with a heated knife and a one-dimensional array was obtained. An accuracy of $8\ \mu\text{m}$ on the positioning of the fibres in the array was achieved.

For the stacking of the one-dimensional arrays to form a ferrule, a method we called “virtual alignment” was developed. This technology was an optical alignment method whereby two independently moving cameras created a virtual mask that allowed aligning two objects with a high precision. The incentive for the creation of this technology was given by the fact that the distances between the fiber arrays were too large for the field of view of one objective, and too small to use two parallel objectives. Implementing two cameras, each with an independent and movable field of view, solved the problem. The stacking of the one-dimensional arrays is carried out in two steps, first the arrays are aligned with respect to each other, than they are fixed by UV-curing the glue that was applied on the arrays prior to the alignment. The “virtual alignment” method alignment proved to be able to position objects within 2 % of the targeted distance. For the accuracy on the positioning of the POFs in the ferrule we achieved $15\ \mu\text{m}$ for the Toray POFs and $20\ \mu\text{m}$ for the Asahi POFs. These figures were acceptable for VCSEL-based interconnect links. Finally we used the virtual alignment method to place the ferrule in a structure for aligning coupled ferrules, and we used it to place a coupling alignment feature near the optoelectronic dies. This experiment did not yield the expected results, mainly due to a glue dispensing problem. However, this problem is not fundamental and solutions are suggested at the end of this PhD thesis.

The research for this PhD was carried out in the framework of two projects: the Flemish government funded project: “Study of Connectors for Parallel Optical Interconnections in and Between Electronic Systems” on the one hand, and the European Commission funded MELARI project: “Optically Interconnected Integrated Circuits” (OIIC) on the other hand.

Contents

1	Introduction	5
1.1	Context	6
1.2	Goal of the PhD Study	9
1.3	Time frame of the research work	10
1.4	Thesis Overview	10
1.5	Publications	11
	Bibliography	13
2	Parallel Optical Transmission Media	15
2.1	Properties of an Adequate Transmission Medium for a Short Distance Optical Parallel Data Link.	16
2.2	Optical Transmission Media	17
2.2.1	Free Space	17
2.2.2	Optical Waveguides	18
2.2.2.1	”Large” planar waveguides	18
2.2.2.2	Glass Fibre	18
2.2.2.3	Other Silica Based Waveguides	20
2.2.2.4	Polymer Waveguides Boards	23
2.2.2.5	Plastic Optical Fibre	26
2.3	Conclusion: What Medium to use for a 1 Meter Parallel Optical Interconnect Link?	28
	Bibliography	30
3	Plastic Optical Fibre	35
3.1	Introduction	36
3.2	POF: State-of-the-Art	37
3.3	Production processes of POF	39
3.4	Small-diameter POF	40
3.4.1	Specifications	40
3.4.2	Mechanical Properties	41
3.4.2.1	Geometrical properties	41
3.4.2.2	Tensile strength and bending	46
3.4.3	Optical properties	48
3.4.3.1	Bandwidth issues	48
3.4.3.2	Light propagation in POF	50
3.4.3.3	Transmission losses	57

3.4.3.4	Influence of bends	64
3.4.3.5	Influence of temperature	67
3.5	Conclusions	67
	Bibliography	69
4	A connector for two-dimensional POF arrays: essential issues and design	71
4.1	Requirements for an adequate connector design	72
4.2	Some important choices to make	73
4.3	Connecting fibre arrays: what happens in the world?	76
4.3.1	One-dimensional fibre array connectors	76
4.3.2	Two-dimensional fibre array connectors	79
4.3.2.1	MT TM -like solutions	79
4.3.2.2	Other possibilities	79
4.3.3	POF/optoelectronics interfaces	80
4.4	Design of a connector system	84
4.4.1	The “stacked array” approach	84
4.4.2	Basic structure of the connector	85
4.4.2.1	POF/POF interfaces	86
4.4.2.2	POF/emitter-detector interfaces	87
4.4.2.3	The alignment spacer at the optoelectronic devices	88
4.4.2.4	Are there alternative solutions for a bent fibre array?	89
4.5	Some brief calculations on the behaviour of bent POF arrays	90
4.6	Connector technologies in the OIIC project	91
4.7	Conclusions	93
	Bibliography	94
5	Optical fibre coupling: efficiencies and tolerances	97
5.1	Interfaces in optical links	98
5.2	Experimental setup	98
5.2.1	Principle	98
5.2.2	The alignment system	100
5.3	End facet termination	103
5.3.1	Comparative study	107
5.3.2	Subsequent coupling and end facets	108
5.3.3	Coupling efficiency and coupling force	108
5.4	Fibre alignment tolerance: theory and experiment	108
5.4.1	Emitter-to-POF coupling	109
5.4.1.1	RCLED/POF interface	109
5.4.1.2	VCSEL/POF interface	123
5.4.2	POF/POF coupling	128
5.4.2.1	Intrinsic losses	128
5.4.3	POF-to-detector coupling	134
5.5	Optical cross-talk	138
5.6	Power budget: calculations on examples	139
5.7	Conclusions	149

Bibliography	151
6 Fabrication of one-dimensional POF arrays	153
6.1 Introduction	154
6.2 The “fibre in groove” method	154
6.2.1 Laser ablation	154
6.2.2 Fixing the POF in the grooves	158
6.3 The “embedded fibres” method	161
6.3.1 Principle and set-up	162
6.3.2 Experimental results	165
6.4 Conclusions	166
Bibliography	169
7 Fabrication of two-dimensional POF arrays	171
7.1 Introduction	172
7.2 “Virtual alignment”	172
7.2.1 Principle and set up	172
7.2.2 Evaluation of the set-up	177
7.3 Stacking POF arrays: assembly of the ferrule	179
7.4 Assembly of the complete connector	184
7.5 Assembly of a RCLED module	186
7.6 Conclusions	190
Bibliography	191
8 Conclusions and perspectives	193
8.1 Highlights and conclusions	194
8.2 POF and interconnect: what is next?	195
Bibliography	197

1

Introduction

IN this introductory chapter we will discuss the technological context and the goals of the research work carried out during this PhD. In addition, a chapter overview will be given as well as a list of national and international publications reporting on the research results obtained during the PhD study.

1.1 Context

About 5000 years ago Babylonian merchants were using counting boards to make their calculations. These boards were made by drawing grids in the sand and pebbles were used to mark the tens, hundreds and thousands. In fact, that ancient civilization used the first primitive computer. Things have changed since then. Electricity was mastered and electronics invented. In 1971 Intel presented the first microprocessor: the Intel 4004 chip. For the first time all the components of a computer (central processing unit, input and output controls) were located on one minuscule chip. It contained 2250 transistors, worked at 800 Khz clock frequency and could cope with 60.000 instructions/sec. Since then, the features on micro-electronic chips have been scaled down dramatically, allowing very high transistor densities. Nowadays processors contain millions of transistors on a square inch which makes them extremely fast and functional. For instance Intel's Pentium 4 processor presented in 2000 operates at 1.5 GHz clock frequency and 1500 million instructions per second, has 478 in/out pins and contains 42 million transistors. Nowadays, the Pentium 4 processors operate at 3.8 Ghz [1]. This rapid increase of chip functionality was already foreseen in 1965 by Gordon Moore who predicted that the number of transistors per integrated circuit would double every 18 months [2]. Linked with the increase of processing capability, the interconnections between the microchips become more complex. This phenomenon is described by Rent's rule: the minimal number of pins G needed by a module is a function of the number of basic functional blocks B in the module [3] :

$$G = t \cdot B^r \quad (1.1)$$

The Rent coefficient t is the average number of connections on a basic functional block. The Rent exponent r has values between zero and one and depends on the complexity of the modules. For complicated circuits $r = 0.6$. And here problems start. On a chip with only perimetric pins, the available space for I/O pads is proportional to \sqrt{B} . However, the number of perimetric metallic pins is limited by mechanical constraints. So in cases where $r > 0.6$ the demand for I/O pads is higher than the perimetric supply. As reported in several cases, turning to area pin-out resolves this pin supply problem [4-6]. However, it does not resolve the data transfer problem in the underlying interconnect substrate. Due to the increasing pin-out the required density of the galvanic interconnect wires in the interconnect substrate can only be obtained by scaling down the cross section of the wires. Yet the amount of data transmitted through a galvanic channel is limited [7]. This is due to the fact that the rise time of data signals is limited by the losses in the transmission line. In a data processing system we can essentially distinguish two kinds of lines: either the loss in the line is dominated by the skin effect ("LC"-lines) or it is dominated by the bulk resistance ("RC"-lines). For an "RC"-line the limiting mechanism is easy to understand intuitively. The 0 %- 90 % rise time at the end of the (unterminated) line happens to be numerically equal to the total RC-time constant of the line:

$$\tau_{rise} \cong RC = R_l C_l l^2, \quad (1.2)$$

with R the d.c. resistance of the line, C the total capacity of the line, R_l and C_l are the resistance and capacity per unit length. R_l is inversely proportional to the cross sectional area of the line, C_l does not depend on the length of the line, only on its geometry. Hence scaling the line with a factor a will not change the rise time, since R_l will be divided by a^2 and l will be multiplied with a factor a . As a result the rise time depends only on the geometry of the line. Since $R \propto l/A$, with A the cross sectional area, and $C \propto l$ for a fixed geometry, we can state that $\tau_{rise} \propto l^2/A$. The maximal bit rate B of the channel is inversely proportional to the rise time τ_{rise} and hence [7]:

$$B = B_0 \frac{A}{l^2}, \quad (1.3)$$

with B_0 a constant, equaling typically 10^{16} for “RC”-lines. Hence the maximal bit rate of the transmission line depends directly on the aspect ratio \sqrt{a}/l . Although the physics of “LC” and “RC”-lines is substantially different, the aspect ratio limit on bit rate capacity shows the same scaling in both cases, and also in the case of so called equalized “LC”-lines [8]. For “LC”-lines B_0 typically equals 10^{15} and for equalized lines B_0 equals 10^{17} . It is hence obvious that the data transfer, through narrow and relatively long (in this context we speak about millimeters or a few centimeter) metallic paths between chips is limited. This limited bandwidth will cause an interconnect “bottleneck” in the near future. However, the forecasted moment on which this “bottleneck” will occur has been postponed continuously during the last years. For instance, following the ITRS ¹ roadmap of 2000 this bottleneck will occur in data processing systems in 2007. The roadmap of 2005 mentions the year 2015. Whatever the correct timing is or will be, it is clear that in case of a two-dimensional interconnect substrate the perimetric pin-out problem remains, but now on substrate level. One solution to this problem consists of stacking electronic chips in a three-dimensional structure [9], but to our opinion the use of optical interconnection links is a more valuable option. Several elements plead in favor of optical interconnects:

- 1: For the covered distances at interconnect level, the bandwidth is independent of the channel length.
- 2: Very high signal (channel) density can be achieved.
- 3: Power consumption is nearly independent of the transmission length. Hence optical interconnects offer the possibility to reduce power consumption for interconnect distances greater than a critical length.
- 4: Thanks to the development of large two-dimensional arrays of detectors and emitters, optics allows area I/O interconnects and hence creates a three-dimensional

¹The International Technology Roadmap for Semiconductors tries to assess the future challenges for the semiconductor industry. It is the result of an interaction between all the main players on the semiconductor market (industry, government, research centers)

interconnect structure.

There are still problems to be resolved though. Highly parallel optical link technology is still in an early stage of development and hence it is costly. The interfacing between the optoelectronic elements and the optical channels needs improvement and the production processes of the electronic board and the optical part should be made more compatible. Eventually a monolithic board with integrated optical and electronic features will be the ideal solution. At this moment we are still far from that point and intermediate, cheap solutions have to be looked for. Besides the time frame, also the level at which the first interconnect “bottleneck” will appear within data processing systems is a point of discussion. Consider therefore a typical rack-based data processing system. As can be seen in figure 1.1, interconnect links can be classified following the packaging level at which they are used. Intercabinet (frame-to-frame) links cover distances from a few meters

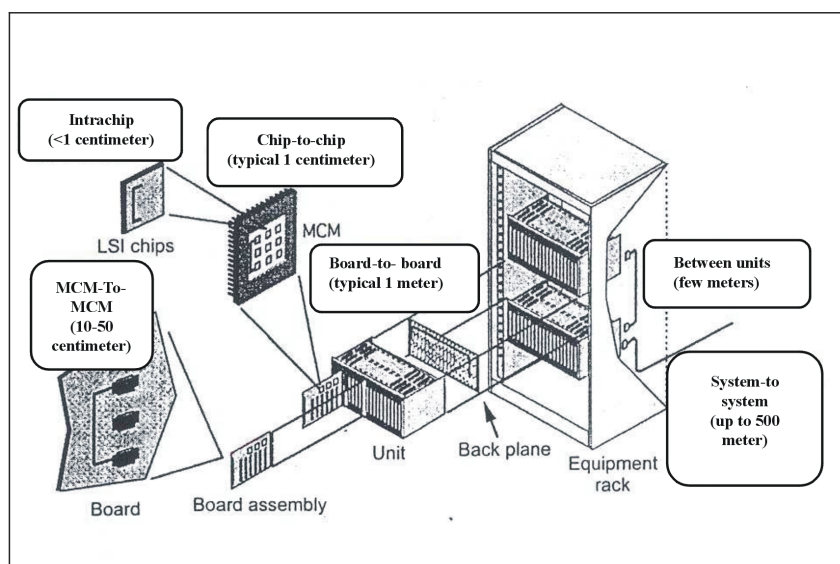


Figure 1.1: Scheme of a rack-based data processing system

up to several hundred meters. For this type of interconnects, parallel optical links are already implemented. At a lower level we distinguish backplane interconnects between units (few meters) and between boards (in the order of 1 meter), as well as multi-chip-module to multi-chip-module (MCM-to-MCM) and chip-to-chip links that vary typically between 10 and 50 cm. Finally we have short chip-to-chip links (few centimeters) and on-chip links (millimeters). The logical next step would be that the following bottleneck would appear on places where the interconnect distances are long and data rates are high, this means on board-to-board level. This reasoning was followed during the late nineties and the beginning of the 21st century, the period in which the research work for this PhD was carried out. This

is easily illustrated by the numerous projects that were dealing with developing optical backplanes and short distance interconnects [10–14]. Several applications like high-bandwidth telecom switch routers, high-end servers and supercomputers were considered as requiring optical parallel optical interconnect links in the near future. However, the burst of the telecom bubble during the first decade of the 21st century tempered severely the demand for higher bandwidth and large data processing systems. Moreover the bandwidth of copper-based links has been severely improved as well, so that all of the intra-cabinet traffic can be accommodated by copper wiring for at least the next 5 years, even for the most demanding applications. As a result the attention of the optical interconnect world has been drawn to a level that did not seem so obvious a few years ago: on-chip optical interconnect. The combination of the fast growing complexity and bitrate with the continuous down-sizing of the features on an electronic chip, makes that the interconnect bottleneck may well appear within the chip. The narrowing of electrical interconnect lines together with a high density of the lines, will give rise to strong capacitive and inductive coupling between these transmission lines resulting in interconnect noise. One can reduce this effect by increasing the wire spacing or by using shielding, both options resulting in a less efficient use of the interconnect resources. This may lead to routing congestion or non-routability. A solution to this problem consists in adding an on-chip optical layer, offering a high-bandwidth interconnect layer that is immune to electromagnetic noise. Nowadays, several labs are doing extensive research on on-chip optical interconnect [15–19].

Despite this evolution of the last years, a revival of the interest in board-to-board optical parallel links can be noticed, but for other applications than originally thought. Certainly high-end servers and computers are still a target but in a more distant future. Applications on the other hand, in which the electrical connector density at the card edges is not sufficient to accommodate the required data traffic may be the first candidates for implementation of these links [20]. Switchcards are a typical example. Applications that run in an EMI-hostile environment, or bandwidth-hungry systems with dense, fast and long off-card interconnects like future game and media platforms, can be other opportunities. Large companies like IBM, Fujitsu, Intel and Agilent perform research on optical backplanes, which proves the serious interest of the industry in this technology [21–24]. Despite this revival, the opinions about the design of the optical link itself are still divided and there is a multitude of technologies and configurations proposed. However, the solution that we will propose in this PhD is based on small diameter Plastic Optical Fibre (“POF”). We will discuss this choice thoroughly in Chapter 2.

1.2 Goal of the PhD Study

The goal of this PhD study is to develop a technology for the fabrication of highly parallel Plastic Optical Fibre-based optical pathways for short distance interconnect links at MCM-to-MCM and board-to-board level (so a typical length of 10 cm to 1 m). More precisely, the research work is focused on the design of a connector structure that aligns a two-dimensional array of small-diameter POF to an array

of emitters and detectors or to another POF array. It is the aim of this work to propose a technology that can, in principle, be automated and that does not make use of expensive materials or very complicated production processes. Since low production costs are a key condition for the future success of optical interconnect, it is of major importance to develop simple and fast production techniques. In this respect we will propose a design that is not necessarily the most “elegant” from a technical point of view, but that offers a simple and feasible solution for the first generation point-to-point short distance interconnect links.

Most of the reported research work has been performed in the framework of two research programs. Firstly there was the Flemish government funded project: “Study of Connectors for Parallel Optical Interconnections in and Between Electronic Systems”. Scope of this project was the development of a backplane-level connector technology for one-dimensional fibre arrays. Secondly there was the European Government funded MELARI project: “Optically Interconnected Integrated Circuits” (OIIC) [25]. The main goal of this project was to establish key technologies and define relevant processing architectures allowing introduction of area (as opposed to edge) optical interconnections for intra- and inter-MCM data exchange. During this project a system demonstrator was built in which three packaged programmable chips were interconnected using parallel small diameter ($125\ \mu\text{m}$) POFs. Each chip is linked to another chip by 128 POFs. An aggregate bit rate (I/O) of more than 10 Gb/s per chip was achieved. This program had its continuation in a second European Government funded project: “Interconnect by Optics” [26].

1.3 Time frame of the research work

All the research work of this PhD work was carried out between 1996 and 2002. As mentioned in the previous paragraphs the forecasts for the introduction of short-distance parallel optical datalinks in large data processing system has been delayed, mainly due to the burst of the telecom bubble. This delay had a double result: in the first place it raised questions about the when and how of the introduction of parallel optics in data processing cabinets, but secondly it also slowed down the development of adequate technologies for the implementation of these parallel optics. In this perspective, the research carried out during this PhD is still relevant. In any case, all the discussions within this thesis concerning the state-of-the-art of parallel optical datalinks, have been updated to the year 2006. In addition, the achieved results of the research work are being discussed within the context of the situation anno 2006 as well.

1.4 Thesis Overview

This thesis is built up in the following way: in Chapter 2 a comparison is made between the possible optical transmission media for short distance interconnect. In the third chapter the used plastic optical fibre for the optical link is discussed. Measurements on its optical and mechanical behaviour are reported. Chapter

4 deals with the design of the optical interconnect link, a layout for the optical interface is proposed. In Chapter 5 we investigate what accuracy on the fabrication of this optical interface needs to be achieved. In Chapter 6 we propose and discuss a fabrication method for one dimensional arrays of plastic optical fibres. Analogously to Chapter 6, Chapter 7 gives a proposal for, and a discussion of, a manufacturing method for two-dimensional POF arrays and very simple connectors. Finally this manuscript ends with Chapter 8: conclusions and perspectives.

1.5 Publications

The work performed during this PhD study gave rise to the following publications in national and international conference proceedings and journals (in chronological order):

1. A. Van Hove, R. Bockstaele, T. Coosemans, B. Dhoedt, R. Baets and P. Van Daele: "Termination and Coupling Experiments for a 1x12 Small Diameter (125 μm) Plastic Optical Fibre Array and POF Coupling to Microcavity LEDs", LEOS Benelux Symposium, Eindhoven, The Netherlands, 26 November 1997, pp. 113-116
2. A. Van Hove, R. Bockstaele, T. Coosemans, B. Dhoedt, R. Baets and P. Van Daele: "Termination and Coupling experiments for a 1x12 Small Diameter (125 μm) Plastic Optical Fibre Array and POF Coupling to Microcavity LEDs", URSI Forum 97, Gent, Belgium, Dec 1997
3. A. Van Hove, T. Coosemans, B. Dhoedt, P. Van Daele, R. Baets, J. Van Koetsem, L. Van den Torren : "Termination of Small Diameter (125 μm) Plastic Optical Fibre for 1x12 Datacommunication", 48th Electronic Components and Technology Conference, Seattle, Washington, 25-28 May 1998, pp.783-789.
4. T. Coosemans, A. Van Hove, R. Baets, P. Van Daele, B. Dhoedt : "Parallel Optical Data Communication Using 125 μm Plastic Optical Fibres: End Facet Termination and Coupling Alignment Using MT Ferrules", 7th International Optical Fibres Conference '98 (POF'98), ISBN 3-905084-55-4, Berlin, 5-8 October 1998, pp. 143-146.
5. A. Van Hove, K. Vandeputte, L. Vanwassenhove, T. Coosemans, S. Verstuyft, R. Baets, P. Van Daele, J. Van Koetsem, L. Van den Torren : "MT-compatible module for coupling LED- to POF-arrays", Third Annual Symposium of the IEEE/LEOS Benelux Chapter, Gent, Belgium, 26 November 1998, pp. 241-244.
6. B. Dhoedt, R. Baets, I. Moerman, P. Van Daele, P. Demeester, T. Coosemans, A. Van Hove, R. Bockstaele, C. Sys, L. Vanwassenhove, : "Microcavity LEDs coupled to POF arrays for parallel optical interconnects", (invited paper), LEOS '98, The 11th Annual Meeting, ISSN 1092-8081, Vol. 2, Orlando, Florida, 1-4 December 1998, pp. 331 - 332.

7. A. Van Hove, K. Vandeputte, L. Vanwassenhove, T. Coosemans, S. Verstuyft, R. Baets, P. Van Daele, J. Van Koetsem, L. Van den Torren : "MT-compatible module for coupling LED- to POF-arrays", URSI Forum '98, Brussels, Belgium, 10 December 1998, pp. 13-16.
8. R. Bockstaele, A. Van Hove, T. Coosemans, C. Sys, I. Moerman, B. Dhoedt, R. Baets, P. Van Daele: "Microcavity LED-Based Parallel Data Link Using Small Diameter (125 μm) Plastic Optical Fibres", Optics in Computing 98, Brugge, Belgium, Proc. SPIE Vol. 3490, 17-20 June 1998, pp. 293-296
9. B. Dhoedt, R. Baets, I. Moerman, P. Van Daele, P. Demeester, T. Coosemans, A. Van Hove, R. Bockstaele, C. Sys and L. Vanwassenove: "Microcavity LEDs Coupled to POF Arrays for Parallel Optical Interconnects", LEOS Annual Meeting, Orlando, USA, 1-4 December 1998, pp. 331-332
10. R. Bockstaele, A. Van Hove, T. Coosemans, C. Sys, I. Moerman, B. Dhoedt, R. Baets, P. Van Daele: "Microcavity LED-Based Parallel Data Link Using Small Diameter (125 μm) Plastic Optical Fibres", Journal of Optics A : Pure and Applied Optics, Vol 1, no 2 (Febr 1999), pp. 233-236
11. R. Bockstaele, T. Coosemans, C. Sys, L. Vanwassenhove, A. Van Hove, B. Dhoedt, I. Moerman, P. Van Daele, R. Baets, R. Annen, H. Melchior, J. Hall, P. Heremans, M. Brunfaut and J. Van Campenhout: 'Realisation and Characterisation of 8×8 Resonant Cavity LED Arrays Mounted onto CMOS Drivers for POF-Based Interchip Interconnections", IEEE Journ. Sel. Topics Quant. Electr, Vol 5, no 2 (March 1999), pp. 224-235
12. K. Naessens, S. Boons, A. Van Hove, T. Coosemans, S. Verstuyft, H. Ottevaere, L. Vanwassenhove, P. Van Daele, R. Baets: "Excimer laser ablated U-groove alignment structure for optical fibre arrays", Fourth Annual Symposium of the IEEE/LEOS Benelux Chapter, Mons, Belgium, 15 November 1999, pp. 187-190.
13. T. Coosemans, A. Van Hove, R. Bockstaele, K. Vandeputte, L. Vanwassenhove, B. Dhoedt, R. Baets, P. Van Daele, J. Van Koetsem and L. Van den Torren: "MT- Compatible Connectorisation of VCSEL and RCLED Arrays to Plastic Optical Fibre Ribbon for Low Cost Parallel Datalinks", EMRS Conference, Strasbourg, France, 1-4 June 1999.
14. A. Van Hove, T. Coosemans, R. Bockstaele, K. Vandeputte, L. Vanwassenhove, B. Dhoedt, R. Baets and P. Van Daele, J. Van Koetsem, L. Van den Torren: "Direct MT-compatible Connectorisation of LED Arrays to Plastic Optical Fibre Ribbon for Low Cost Parallel Datalinks", ECTC 99, San Diego, California 1-4 June 1999, pp. 1096-1102
15. T. Coosemans, A. Van Hove, R. Bockstaele, J. Derluyn, I. Moerman, R. Baets and P. V. Daele: "Optical Data Communication Using Substrate-removed 850 nm RCLEDs and Small Core Fibres", 8th International POF Conference, Chiba, Japan, 14-16 July 1999, pp. 246-249

16. T. Coosemans, A. Van Hove, R. Bockstaele, K. Vandeputte, L. Vanwassenhove, B. Dhoedt, R. Baets, P. Van Daele, J. Van Koetsem and L. Van den Torren: "MT-Compatible Connectorisation of VCSEL and RCLED Arrays to Plastic Optical Fibre Ribbon for Low Cost Parallel Datalinks", *Mat. Science in Semicond. Proc.*, Vol 3 (2000), pp. 475-480
17. K. Naessens, A. Van Hove, T. Coosemans, S. Verstuyft, H. Ottevaere, L. Vanwassenhove, P. Van Daele, R. Baets : "Fabrication of Microgrooves with Excimer Laser Ablation Techniques for Plastic Optical Fibre Array Alignment Purposes", SPIE, Photonics West, Vol. 3933, San Jose, California, 22-28 January 2000, pp. 309-315.
18. T. Coosemans, A. Van Hove, R. Bockstaele et al: "Substrate Removed 850 nm RCLEDs and Small Core (63/125 μm) Plastic Optical Fibers for Optical Data Communication" (Invited Paper) SPIE, Photonics West, San Jose, California, 22-28 January, proc. SPIE Vol 3938 (2000), pp. 160-168
19. T. Coosemans, A. Van Hove, K. Naessens, L. Vanwassenhove, P. Van Daele, R. Baets: "Fabrication of a 2D Connector for Coupling a 4×8 Array of Small Diameter Plastic Optical Fibre (117/125 μm) to MCLED or VCSEL", 50th Electronic Components and Technology Conference, Las Vegas, Nevada, USA, May 2005, pp.1236-1241
20. T. Coosemans, K. Naessens and R. Baets: "Connectors for Parallel Optical Datalinks using 2×8 Arrays of Embedded Small Diameter (125 μm) Plastic Optical Fibres ", 10th International POF Conference, Amsterdam, the Netherlands, 27-30 September, 2001, pp. 147-152

Bibliography

- [1] www.intel.com.
- [2] G. E. Moore, "Cramming more components onto CMOS integrated circuits," *Electronics*, vol. 38, no. 8, 1965.
- [3] J. Van Campenhout, "Optics and the CMOS interconnection problem: A systems and circuits perspective," *Intern. Journ. Optoelectronics*, vol. 12, no. 4, pp. 145-154, 1998.
- [4] J. Depreitere, H. Neefs, H. Van Marck, and J. Van Campenhout, "A quantitative analysis of the benefits of the use of area-I/O pads FPGA's," *Microprocessors and Microsystems*, vol. 22, no. 2, pp. 145-154, 1997.
- [5] V. Maheshwari, J. Darnauer, J. Ramirez, and W. M.-M. Dai, "Design of fpga's with area i/o for field programmable gate arrays," in *Proceedings FPGA 95/SIGDA International Symposium on Field-Programmable Gate Arrays* (A. Press, ed.), (Monterey), pp. 17-23, 1995.
- [6] W. Meleis, M. Leeser, P. Zavracky, and V. M., "Architectural design of a three-dimensional fpga," in *Proceedings of the 17th Conference on Advanced Research in VLSI*, pp. 256-268, September 1997.
- [7] D. Miller and H. Ozaktas, "Limit to the bitrate capacity of electrical interconnects," *Journal of Parallel and Distributed Computing , Special Issue on Parallel Computing with Optical Interconnects.*, vol. 41, pp. 42-52, 1997.
- [8] C. Foster and H. Van Duesen, "Extending the range of copper for fiber channel interconnects," *Electronic Packaging and Production*, pp. 59-64, April 1996.

- [9] M. B. Kleiner, S. A. Kuhn, P. Ramm, and W. Weber, "Performance improvement of the memory hierarchy of risc-systems by applications of 3-d technology," *IEEE Transactions on Component, Packaging and Manufacturing Technology*, vol. 19, pp. 709–718, November 1996.
- [10] L. Galarneu and K. Johnson, "Cheetah project: Cost effective embedding of high performance interconnects." Website: www.htc.honeywell.com.
- [11] R. A. Selfridge, "Incorporation of MT-ferrule and ribbon technology into optical backplane systems," in *Proceedings of the SPIE Photonics West Conference 2000* (SPIE, ed.), vol. 3592, pp. 50–58, January 2000.
- [12] O. Krumpholz, R. R. J. Guttmann, P. Huber, J. Moisel, and M. Rode, "Optical backplane in planar technology," in *Proceedings of the SPIE Photonics West Conference 2000* (SPIE, ed.), vol. 3592, pp. 59–65, January 2000.
- [13] R. A. Nordin, "Advanced optical interconnection technology in switching equipment," *IEEE J. Lightwave Techn.*, vol. 13, pp. 987–994, June 1999.
- [14] K. Vandeputte et al, "Low cost multi-fiber add/drop multiplexer demonstration system," in *Proceedings of the 25th European Conference on Optical Communications (ECOC)*, vol. 1, (Nice, France), pp. 112–113, September 1999.
- [15] <http://picmos.intec.ugent.be>.
- [16] M. Haney, M. Iqbal, M. McFadden, T. Dillon, and D. Prather, "Progress towards optical interconnects for intrachip loba communication," *Proceedings of SPIE, Photonics Packaging and Integration VIII*, vol. 6126, January 2006.
- [17] V. Baukens, *Scalable Micro-Optical Modules for Short Distance Photonic-VLSI Interconnections*. PhD thesis, Vrije Universiteit Brussel, 2001.
- [18] M. Haurylau et al, "On-chip optical interconnect roadmap: challenges and critical directions," in *Proceedings 2nd International Group IV Photonics Conference*, (Antwerpen, Belgium), pp. 17–19, 21-23 September 2005.
- [19] I. O'Connor, "Optical solutions for system-level interconnect," in *Proceedings of the 2004 international workshop on System level interconnect prediction*, (Paris, France), pp. 79 – 88, 14-15 February 2004.
- [20] C. Berger, B. J. Offrein, and M. Schwarz, "Challenges for the introduction of board-level optical interconnect technology into product development roadmaps," *Proceedings of SPIE, Optoelectronic Integrated Circuits VIII*, vol. 6124, January 2006.
- [21] H. Shashikant, S. Lei, D. Kuchta, Y. Kwark, C. Baks, F. Doany, J. Kash, and J. Trehwella, "Thermal-mechanical analysis of terabus high-speed optoelectronic package," in *Proceedings of the Electronic Components and Technology Conference, vol 2*, (Lake Buena Vista, Florida, USA), pp. 1854 – 1858, 31 May - 3 June 2005.
- [22] by A. F. Benner, M. Ignatowski, J. Kash, D. Kuchta, and M. Ritter, "Exploitation of optical interconnects in future server architectures," *IBM Journal of Research and Development*, vol. 755-775, pp. 11–12, July / September 2005.
- [23] A. L. Glebov et al, "Integrated waveguide micro-optic elements for 3D routing in board-level optical interconnects," *Proceedings of SPIE, Photonics Packaging and Integration VIII*, vol. 6126, January 2006.
- [24] E. Mohammed et al, "Optical interconnect system integration for ultra-short-reach applications," *Intel Technology Journal*, vol. 8, pp. 115–128, May 2004.
- [25] M. Brunfaut, W. Meeus, J. Van Campenhout, R. Annen, P. Zenklusen, H. Melchior, R. Bockstaele, L. Vanwassenhove, J. Hall, B. Wittman, A. Neyer, P. Heremans, J. Van Koetssem, R. King, H. Thienpont, and R. Baets, "Demonstrating optoelectronic interconnect in a FPGA-based prototype system using flip-chip mounted 2d-arrays of optical components and 2d POF ribbon arrays as optical pathways," in *Proceedings of the SPIE' 46th annual meeting*, (San Diego, California), July 2001.
- [26] <http://io.intec.ugent.be>.

2

Parallel Optical Transmission Media

IN the first chapter, small core POF was brought up as a possible transmission medium for short distance parallel optical data links. In this chapter we will explain why we consider POF more suitable than other solutions. For that purpose the requirements for an adequate transmission medium are discussed. Then we consider and compare different available media and discuss the advantages and drawbacks of each of them. Finally we conclude this chapter by selecting the most adequate transmission media for the first generation short distance parallel optical datalink.

2.1 Properties of an Adequate Transmission Medium for a Short Distance Optical Parallel Data Link.

The relevant properties that determine the suitability of a medium can be grouped into the following categories: mechanical properties of the medium, optical properties of the medium, susceptibility to the environment and production and mounting costs.

Mechanical Properties Space in data processing systems is very limited. Typical distances between different boards in a rack are in the order of a few centimeters (DIN 41 494). Therefore the path of the optical link often makes a sharp 90° bend. This can be done by e.g. micro mirrors in certain cases, but it can also be achieved by bending a solid waveguide like e.g. a POF. These bends necessarily have a small radius (a few millimeter), hence it is imperative that these waveguides are not plastically deformed by this bending. The effect of the bending has to be considered on the short as well as on the long term. Other features as resistance to torsion and shock are of importance for the automotive and avionics industry, but most of the large data processing systems are standing in a more computer friendly environment and hence these issues are less relevant. Hence they will not be discussed in this dissertation.

Optical Properties The main issues to be considered here are transmission losses and numerical aperture of the medium. Since we consider (short) data links varying in length from a few centimeter up to a meter, a few dB/meter transmission losses can be accepted. This is quite high in comparison with long distance telecommunication systems where 0.25 dB/km absorption loss is standard. The numerical aperture of an optical system defines the maximal angle of light acceptance and/or emission. In order to have a maximal power coupling from the emitter to the transmission medium the NA should be (ideally) at least as large as the NA of the light source, at least if one wants to avoid or minimize the use of micro-optics. If the light source is a laser, this is generally not an issue, since lasers have a very low beam divergence. If, on the contrary, one uses Light Emitting Diodes or Resonant Cavity LEDs the efficiency of the LED-medium coupling heavily depends on the NA since (RC)LEDs have a broad emission pattern. At the end of the optical pathway on the other hand, one prefers a small NA, otherwise part of the emitted light may not hit the detector and the optical power is partially lost. This effect can be decreased by increasing the detector diameter but this slows down the detector⁷. In many cases, a trade-off between both parameters has to be found. Yet, there is one more argument in favour of a higher NA: if the transmission medium needs to be bent, its transmission losses will be lower for a high NA. We will discuss this phenomenon in more detail in the next chapter. Finally, as we will see in Chapter 3, an increased NA causes a decreased bandwidth-length product. However, for distances up to a meter the bandwidth-length product is not a limiting factor and is definitely not an essential issue.

Susceptibility to the Environment In electronic data processing systems, temperatures can rise up to 80° C. A high sensitivity to increased temperatures can result in physical damage as well as in optical losses, and this particularly in combination with moisture. Therefore it is very important that the medium is resistant to such temperatures. Sensitivity to other factors like corrosive gases and liquids is of less importance for the systems we consider.

Cost The cost of the medium is defined by two factors: the cost of producing the medium itself and the cost to install it in the system. The mounting can be done in various ways depending on the transmission medium. Often one needs to prepare the end facets of the medium, to connectorise it and to align it to a transceiver or another transmission medium. How difficult, and hence how expensive these procedures are, depends heavily on the chosen medium. Since the scope of the development of parallel data links is to obtain a cheap and easily producible product, cost is one of the main factors (if not the most important) to take into account.

2.2 Optical Transmission Media

Light can be transmitted from a light source to a detector in two ways: either it propagates through free space and passes through, or is reflected by, optical elements such as (micro)lenses, (micro)mirrors, prisms, Diffractive Optical Elements (DOEs) and Holographic Optical Elements (HOEs), or it is confined within a light guiding structure: a waveguide. It is of course possible to combine different kinds of waveguides or even to combine waveguide- and free space propagation. We will now study these different ways of light transmission in more detail.

2.2.1 Free Space

Free space propagation for optical data links has been proposed and demonstrated in some cases. [1–8]. These links have the advantage that they are capable to interconnect very large arrays of transceivers (for instance 1000×1000 channels) at a very small pitch. By using micro-optics, very compact systems can be realized. Moreover, since the transmission media are in general air and small bits of plastic and glass, a large range of wavelengths can be used without absorption losses. However, free space links have an important drawback: These systems make use of distinct optoelectronic elements (emitters and receivers) and possibly diffractive and refractive optical elements along the optical pathway. All those elements have to be aligned very well with respect to each other, which makes the system very sensitive to e.g. thermal expansion. Moreover, the divergence of the emitted light beams often limits the transmission distance: diverging beams can cause crosstalk and decrease the incident light power on the receiver. Hence free space optical links are well suited for short interconnect distances (a few millimeter to a centimeter) like e.g. intra-chip connections, as has been shown at the Free University of Brussels in the framework of the ESPRIT-OIIC project [1](fig

2.1), but longer links up to 1 meter are difficult to realize. Possible solutions for

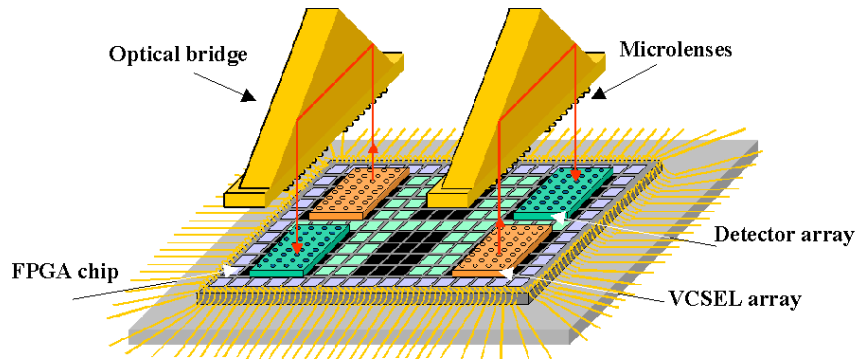


Figure 2.1: Principle of a free space optical interconnect link realized in the OIIC project [1].

somewhat longer links (tens of centimeters) have been suggested: e.g. one can use grin lenses [9], intermediate relay lenses [10–13] or even an auto-active alignment system [14]. However these systems are rather complicated to realize and hence relatively expensive.

2.2.2 Optical Waveguides

2.2.2.1 "Large" planar waveguides

In order to tackle the problem of the alignment of optical elements along the pathway one can use a transparent substrate (e.g. glass) on which optical elements are defined [15–19]. All the optical channels are passing through the same substrate, i.e. there is one common waveguide (fig 2.2). Since all the optical elements are defined on one rigid structure, their mutual alignment is precise and less dependent on environmental circumstances. Large arrays of transceivers with small pitch can be interconnected. However, here again the divergence of the emitted beams is a limiting factor for the transmission distance, so that intermediate relay lenses have to be added. Besides, the tolerances on the parallelism of the sides of the substrate are rather strict. Hence covering a distance of e.g. one meter with such precise substrates is definitely a difficult task.

2.2.2.2 Glass Fibre

Single-mode glass fibre is the standard waveguide in long haul communication such as telecommunication and wide area networks and is widely available. For a communication distance in the range of tens to hundreds of meters (local area networks, interconnects between high speed servers, workstations clusters or supercomputers) multimode glass fibre has been proposed and used for the optical pathway in

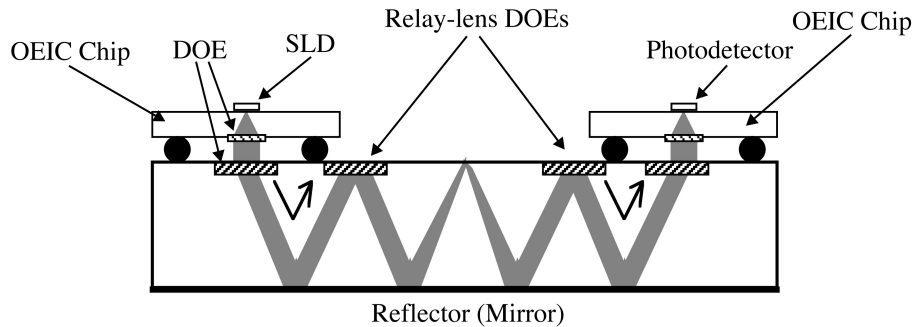


Figure 2.2: Principle of a large planar waveguide link [18]

several parallel interconnect systems. Transmitter and receiver modules for such systems are commercially available, as well as one-dimensional ribbons (1 by 4 to 12 fibres) at a pitch of $250\ \mu\text{m}$. [20–25]. Moreover the connector technology for these ribbons is very mature. Currently larger two-dimensional array connectors have been developed and are commercially available [26–28]. Clearly the knowledge of, and the experience with, glass fibre based interconnect links is vast.

Glass fibre has several advantages: it is not expensive (40 Euro/km) and is very easy to obtain. It has very low absorption losses over a wide wavelength range (0.2 dB/km at 1550 nm and 5-12 dB/km at 850 nm). It is resistant to high temperatures: the melting temperature of glass is 1900°C and glass fibre cables are specified up to 250°C . The geometrical properties are very well controlled: the diameter of the fibre and core cladding concentricity have micrometer accuracy. This is an important issue for coupling losses for two reasons: firstly, while performing fibre to fibre coupling, the transmission losses due to mismatch of fibre diameter or cladding-core non-concentricity are limited. Secondly, the precise control of the outer diameter of the fibre makes it more easy to align the fibre to another fibre or to a transceiver. With glass fibres complicated routing schemes can be fabricated by e.g. embedding them in a flexible foil following a routing pattern as can be seen in figure 2.3 [29, 30]. They can also be embedded inside the printed circuit boards on which the optical components are mounted: the so-called “fibre in board” technology [31, 32], as has been demonstrated in the Brite-Euram Plato project. There are some drawbacks though in the use of glass fibre. The preparation of the end facet of the fibres is time-consuming and delicate: the fibres need to be polished with consecutive different grain sizes which results in an average production time of half an hour for one connector facet. This increases the mounting costs considerably. In addition, the minimal bending radius is relatively large: 1 cm for (standard) glass fibres with $125\ \mu\text{m}$ diameter. This is quite large if an optical pathway (including bends) is situated between adjacent boards with a typical spacing of a few centimeter, and it is definitely a compromising factor for the use of glass fibre for short distance interconnect links. The numerical aperture of commercial fibre is around 0.2 for bandwidth reasons but it is technically possible to produce step index glass fibres with high numerical aperture. As has

been mentioned several multimode glass fibre based parallel interconnect systems are being developed or are already commercially available. They typically cover distances of a few meters up to hundreds of meters. They generally consist of two separate sealed transceiver modules that are interconnected with detachable glass fibre ribbons. In figure 2.4, a transmitter-receiver pair for a 12-parallel multimode glass fibre link is shown.



Figure 2.3: A flexible foil with optical fibres [29, 30]

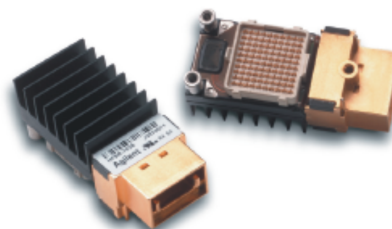


Figure 2.4: The Avago 12-channel optical transmitter and receiver modules

Inside the modules the used transmission medium does not need to be glass fibre. Actually, only part of these interconnect systems that exist, or existed, use glass fibre inside the modules: for instance the OETC [33], the LitebusTM [34], the VixelinkTM [35], the Cheetah [36] and the PAROLITM [37] interconnect links do this. Other systems like the POLO [38], the Optobus [39], the STAR [40] and the ParaBITTM [41] links use polymer waveguides inside the modules. The PONI-1 link [42] modules contain fibre face plates and the Jitney link [43, 44] module uses micro-optics, as well as the POSH modules [45]. A more detailed discussion of the optical interfaces inside these modules will be given in Chapter 4.

2.2.2.3 Other Silica Based Waveguides

Some other glass waveguides can possibly offer a solution for short distance interconnect links. In the first place there are the so called "fibre image guides" (FIGs). These are flexible bundles of small diameter (typical 3-20 μm diameter) glass fibre. There are different ways to make these bundles. One of them is the so called "leached fibre" approach, as used by e.g. Schott Glass: a glass rod with the correct refractive index profile is drawn down to a single fibre, similarly as for the production of standard glass fibre. Here however, the rod has an extra outer layer of acid-soluble glass. Then the fibres are stacked into a hexagonal array, called a multiassembly. This multiassembly is further drawn down to a multirod. A second stacking and drawing follows and a multi-multi-rod is created. Core densities of 2000-15.000 cores/ mm^2 are reached. The obtained rods are cut and polished. Finally the acid-soluble glass layer is removed with an acid bath in order

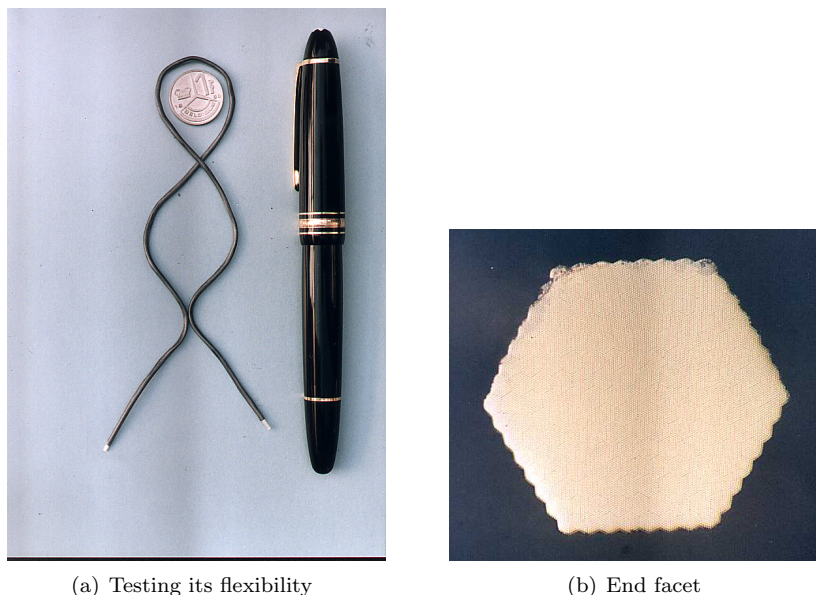


Figure 2.5: A flexible fibre image guide developed in the OIIC project [46]

to detach the individual fibres and obtain a flexible bundle. The ends of the rod have been encased in wax prior to the bath, so at the ends of the bundle the fibres remains together. Parallel links based on fibre guides have been demonstrated at NEC [47, 48], University of Pittsburgh [49], and at IMEC/VUB in the framework of the OIIC project [46] (fig 2.5). Due to its high core densities, dense arrays of datachannels can be transmitted. A parallel link with a pitch of $62.5\mu\text{m}$ was demonstrated [49]. The NA of image fibre can vary between 0.1 and 1.25 and is hence fully adaptable to the requirements of the link. Link lengths of one meter can be easily covered and transmission losses are negligible (10 dB/km). More important for the link loss is the filling factor:

$$\alpha = \frac{S_1}{S_1 + S_2}, \quad (2.1)$$

with S_1 = total fibre-core area and S_2 total cladding and other area. The efficiency of the FIG-FIG and emitter-FIG coupling depends heavily on α . Typical reported values of α vary between 0.5 and 0.6. The minimal bending radius is of the same order as for single glass fibre (1cm for a bundle of 0.5mm diameter), which is relatively large. Further on, no precise connector technology is available for FIGs and the use of FIGs is restricted to point-to-point interconnection links. It is possible to introduce e.g. splitters and combiners but these elements are bulky and complicate the optical link considerably. Finally, until today the production of such a waveguide remains a relatively complex, and hence expensive, process.

Glass Sheets Another promising and certainly elegant solution for the parallel transmission link problem is the use of glass sheets, as e.g. the Optoboard proposed by PPC [50]. The idea is to define waveguides in thin glass sheets and then incorporate these sheets in PCBs (fig 2.6). This technology was included in the “Interconnect by Optics” project [51].

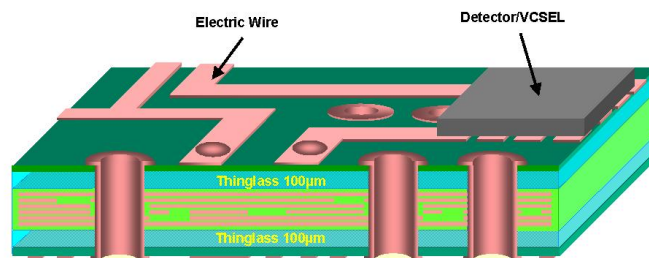


Figure 2.6: An optoelectronic PCB

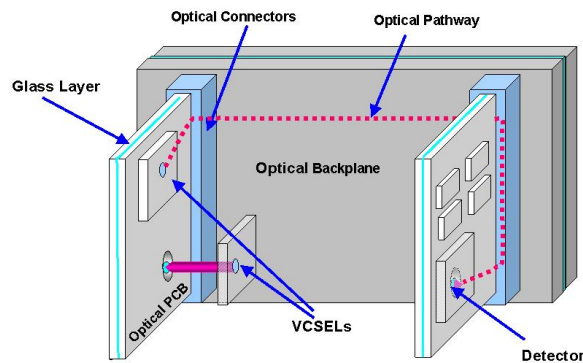


Figure 2.7: The OptoboardTM interconnection scheme

The waveguides can be made by different processes such as etching or embossing. Since glass can resist high temperatures it is certainly compatible with the fabrication process of PCBs and moreover it is a cheap material. Losses of the waveguides are in the order of 10 dB/m at 850 nm. This method would offer a very compact interconnect link (fig 2.7). However the production of multilayer structures, necessary to interconnect two-dimensional arrays of detectors and emitters, remains difficult. Especially the in-and-out coupling of the parallel light beams is complex, and is not fully solved. Hence further development needs to be done in order to obtain a usable and commercial product.

2.2.2.4 Polymer Waveguides Boards

As we mentioned before, polymer waveguides are often used as a part of the optical pathway. One of the first large-scale programs for the development of complete polymer optical pathways is e.g. the POINT project [52]. Here the complete optical pathway would consist of optical waveguide boards: polymer slabs in which multimode waveguides are defined. However, after the collapse of the telecom-bubble the interest in polymer interconnect decreased significantly. Yet, during the last years a renewed interest in polymer waveguides and polymer backplanes can be noticed. Several companies like Fujitsu, IBM, Siemens, Samsung and NTT are working on waveguide-based optical backplanes [53–57]. The definition of the waveguides can be done using a wide range of processes including lithography, wet and dry etching, laser writing, laser etching, embossing and moulding. Polymer waveguides are being developed in several research centers and hence there is a large variety of used materials and production processes. Therefore it is difficult to give a complete overview of all developed waveguides. However we will try to give some examples of the most successful and/or promising products and techniques, used to develop multimode waveguide boards for short distance optical interconnects.

PolyguideTM by DuPont Dupont is one of the pioneers in the field of polymer waveguides and has developed acrylate-based single and multimode waveguides [58]. They have been successfully used in the POINT and POLO project. The waveguides are formed by a photolithographic process followed by a photopolymerisation step (photolocking). Then the waveguide board is given its final thickness by laminating additional layers of polymer. PolyguideTM has a transmission loss of 8 dB/meter at 800 nm. It can resist a temperature of 85° C during 6 weeks and 125° C during 2 weeks. The temperature resistance can be increased up to 150° C by encapsulating the waveguide with polycarbonate. The core thickness of the guides varies between 4 and 200 μm . Geometric features in the waveguiding plane, like the pitch and the width of the waveguides, have an accuracy at sub-micron level. The accuracy on the thickness of the layers is a few micrometer. The numerical aperture can be varied with an accuracy of 0.0055 and numerical apertures between 0.1 and 0.4 have been reported. Higher functionalities like splitters and combiners can be included in the boards. The use of micro-machining techniques such as laser ablation or microtome cutting allows adding alignment features, like e.g. holes for alignment pins, on the polymer board. Polyguide can be used as an independent flexible waveguide board or can be mounted on the electric circuit boards. Currently PolyguideTM is commercialized by Optical CrossLinks under the name GuidelinkTM [59].

AlliedSignal [60, 61] AlliedSignal has developed halogenated acrylate-based polymer waveguides [60]. Unlike Dupont, AlliedSignal uses laser direct patterning for the definition of the waveguide. This allows to deposit the polymer layers on top of the emitter/detector and then write the waveguide as a function of the exact position of the emitter/detector, what results in a highly efficient coupling.

The transmission losses in this polymer are very low: 1 dB/m at 840 nm. The refractive index can be tailored between 1.3 and 1.6 with an accuracy of 0.0001. In this way a large range of numerical apertures can be covered, varying from 0.1 to 0.9. These waveguide are functional up to a temperature of 125° C. They were used in the POINT project. Now AlliedSignal has merged with Honeywell.

NTT NTT developed low loss waveguide-based on deuterated poly-methylmetacrylate (d-PMMA) [62]. The fabrication of the waveguides involves spin-coating, photolithography, and O₂-reactive ion etching. d-PMMA is used for the core and UV curable epoxy is used for the cladding material. Transmission loss is 1.8 dB/meter at 830 nm. The refractive index was controlled in the 1.36-1.49 range with an accuracy of 0.001 and this for 42 μm by 42 μm core-size multimode waveguides.

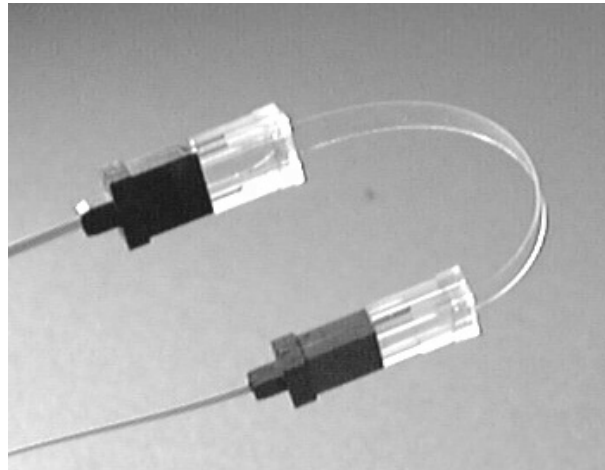


Figure 2.8: A NTT flexible optical waveguide board [63]

These waveguides are being used in the ParaBit [41] module. This technique has been extended to make multilayer waveguides [63]. Finally 12-inch long flexible waveguides have been produced using direct photo patterning in UV-curable epoxy resins (fig 2.8) [63].

Other Research Centers and Fabrication Techniques Siemens and the Fraunhofer Institute for Reliability and Micro-integration fabricate waveguides by hot embossing [64, 65]. The boards are inserted as an optical layer in the (electrical) Printed Circuit Board. In order to resist the high temperatures involved with the fabrication of FR4 (170° C) and with even higher temperature peaks during the soldering (230° C), polycarbonate Cyclo-olefine-copolymers are used [66]. Similar methods have been used at the University of Dortmund [67] to produce 123 μm by 130 μm core waveguides with losses of 17 dB/meter at 855 nm. Finally, embossing is used in several Korean labs and at Epigem [56, 68, 69]. Rubber molds are being used at the Korea advanced Institute of Science and Technology, to cre-

ate perfluorocyclobutane waveguides [70, 71]. The waveguide cores are formed by a rubber mold and then heat cured. Waveguides with a core size of $47\ \mu\text{m}$ by $41\ \mu\text{m}$ and with 40 dB/meter transmission losses at 1300 nm have been realized. A similar technology is used at the University of Texas. Waveguides with a core dimension of 50 by $50\ \mu\text{m}$ and a loss of 0.6 dB/cm at 850 nm were realized [72]. Laser writing seems to be a promising technique for the creation of waveguides. It does not require a photolithography step and can hence be adapted very easily, since no mask is needed. Daimler-Chrysler uses this technique to produce 55 cm long multimode waveguides with a propagation loss of 3 dB/meter at 850 nm [73]. Laser writing has been used to fabricate the waveguides for the STAR project at the Heriot-Watt University [40]. Also IBM used direct laser writing for defining their 50 by $50\ \mu\text{m}$ waveguides with a loss 0.6 dB/cm at 850 nm. Instead of using laser light for direct waveguide patterning one can apply laser ablation to form the waveguides. In this case the non-wanted part of the polymer is ablated away. Multimode waveguides with a loss of 0.13 dB/cm are fabricated at Ghent University [74]. Honeywell and GE developed flexible waveguide boards based on UltemTM (Polyetherimide) as core material [61]. This is combined with benzocyclobutene (BCB) as cladding material. The waveguides are produced by a lithography and a reactive ion etching process. Transmission losses are higher than in the acrylate-based waveguides (30 dB/meter at 830 nm) but the heat resistance is better (180°C). These waveguides were used in the POINT project. Lithographic techniques are quite common as proven by several labs and companies that are using this technology [53, 55, 75–77]. Finally, there is a very original way of fabrication of waveguides used in the SOLNET optical link [78–80] project. In this project multilayer optoelectronic boards are produced. However the polymer is made of photo-refractive material (Polyguide) index of refraction increases when exposed to light. No waveguides are formed before the completion of the multilayer board. Then light is coupled in and hence only at that moment a waveguide is created. This has the advantage that the formed waveguide is well aligned with the optoelectronic elements.

Features of Polymer Waveguide Boards There are two approaches to integrate polymer waveguides in a data system: either the polymer board is part of, or is merged with, the electric board carrying the electric wiring and (opto)electronic components, or the polymer boards are flexible separate units that have to be attached to the electric board with optical connectors. The former case is similar to the glass sheet approach described above and is certainly the most elegant and compact. However it is technically more difficult, yielding reliability issues. In the first place the production of the waveguide layer and the electric layer (including soldering processes) have to be compatible with each other. Recently a lot of research work has focussed on this issue [54–56, 68, 75, 76]. Secondly the light emitter- and detector arrays need to be coupled to the optical layer. For one-dimensional arrays, several solutions have been proposed. Mostly 90° deflection micromirrors are used. These mirrors can be fabricated by means of laser ablation [74], etching [68, 76], machining [41, 53, 68] and tilted exposure [80]. However for two-dimensional waveguide arrays, a three dimensional coupling- and routing

scheme is required and this is very complex to realize. An example of a such a routing scheme is given in [53], where printed circuit boards with two optical layers are used. One way to avoid these routing problems is to implement the 90° deflection not in the optical pathway but in the electronics [54]. By mounting the emitters/detectors on a flexible printed circuit board one can realize a 90° bend, a principle used commonly in commercial parallel fiber-optic transceiver modules. However, for a reliable implementation of this technology in optical backplanes, the packaging of the optoelectronic interface becomes sophisticated and renders this technology complex as well [54]. On the other hand, having a separate optical waveguide board separated from the electric board, solves most of these problems, and it is certainly easier to guide two-dimensional parallel optical arrays [58, 77]. Of course, this solution is less compact and elegant since there are extra boards in the system.

Polymer boards offer quite some advantages. The size and numerical aperture can be controlled by the producer with high accuracy and over a wide range. Moreover a higher functionality can be included in the waveguide design. Routers, splitters, combiners and pitch adapters can be incorporated. They are flexible (few millimeter bending radius) and can easily resist working temperatures common in datacom systems. The waveguides are positioned at an accurate pitch which simplifies the coupling to other arrays or to an emitter/receiver. The end facet termination can be done with a fast technique like laser- or microtome cutting. There are however some drawbacks. It is hard to obtain somewhat longer waveguides and hence to cover a distance of e.g. one meter. In the first place transmission losses are too high. Only recently polymers with low enough losses are being developed. In the second place, the length of the waveguides is limited by most of the involved fabrication techniques. Moreover, the longer the waveguide the more difficult it is to accurately control the thickness of it. Bad control of the thickness complicates the alignment procedure for waveguide-waveguide and waveguide-transceiver coupling. Besides, there is not an adequate connector technology available to couple two-dimensional arrays of polymer waveguides. Remains that the production of these waveguides is still a complicated process at this moment, which makes them expensive devices.

2.2.2.5 Plastic Optical Fibre

Plastic optical fibre has been developed in the late 1960s by DuPont as a medium for illumination. Now however, it is being implemented in local area networks, home and office networks and automotive networks [81, 82]. Currently POF-based transceiver modules are commercially available [25, 83–85]. Recently, a consortium around POF-technology has announced a 10G transmission over 100 meter of graded index plastic optical fibre [86]. In general, the POFs proposed for these applications have a graded index profile and a relatively large diameter (typically $500\ \mu\text{m}$ and up to 2 mm). The graded index profile increases the bandwidth of the fibre by limiting the modal dispersion. The large diameter on the other hand, makes the coupling and termination of fibres really easy which results in cheap tooling and connectors. Moreover it makes the fibres rather strong which

is a clear advantage in for instance automotive applications. In the last years however, there have been new graded index fibres on the market with smaller core diameter [87]. The smaller core allows to use smaller detectors and hence permits to make faster datalinks. Until now, all those graded index-based links are using a single fibre. For short distance parallel interconnect links on the other hand, small diameter ($125\ \mu\text{m}$) step index POF has been proposed. The small diameter allows compatibility with a pitch of $250\ \mu\text{m}$ commonly used in optoelectronics. A 128 channel POF-based, parallel interconnect link has been demonstrated in the OIIC project [88](fig 2.9). Commercially available Polymethyl Methacrylate-based step index fibre was used (core diameter $117\ \mu\text{m}$ /cladding diameter $125\ \mu\text{m}$). small-diameter POF has several advantages. In the first place POF is very flexible and can be bent to a radius of a few millimeter. Moreover, due to its high numerical aperture (0.5), the optical bending losses are low. Thanks to its very simple extrusion production process it is very cheap (25 Eurocent/km)and it is easy and quick to terminate by hot knife cutting or a very short polishing procedure [89]. However, since the general interest in small-diameter POF has been moderate



Figure 2.9: The OIIC system demonstrator

until now, there are only few producers, and hence it is not easy to acquire. The available small-diameter POFs are all PMMA-based which makes them relatively sensitive to high temperatures. In general their working temperature limit is 85°C which is only just above the usual 80°C specification in data processing systems. The transmission losses are about 2-3 dB/meter at 850 nm for the fibres we used in

this PhD. However great effort is put in the development of low loss POFs based on deuterated or perfluorinated polymers and 0.06 dB/meter at 850 nm has already been achieved in a 50 μm core diameter GRIN POF. [87, 90, 91]. Hence, loss is not a fundamental problem. Finally, until now there is no standard technology available for the production of parallel POF connectors and ribbons. Embedding the fibres in UV-curable glue has been proposed as a solution for the fabrication of 1 by 12 POF ribbons at IMEC [89]. Analogous to glass fibre, research is being performed to create POF image guides. So called multi-core POFs were realized at NEC [92] and Asahi Chemical [93]. More details on the fabrication and properties of POF will be given in Chapter 3 .

2.3 Conclusion: What Medium to use for a 1 Meter Parallel Optical Interconnect Link?

The following possible transmission media for short parallel optical datalinks were discussed: free space, "large" planar waveguides, glass fibre, glass and polymer fibre image guides, glass sheets, polymer waveguides and plastic optical fibre. Which one of them would be the most suitable option for the first generation parallel datalinks ? Since we consider links between 10 centimeter and 1 meter let us focus on the most complicated link to realize: a 1-meter link. It is hard to believe that free space propagation and "large" planar waveguides will be able to cover such a distance in the near future. Also, techniques like glass sheets and (polymer) fibre image guides are in a too early stage of development to be an option for the first generation datalinks. Leaves us with polymer waveguides, glass fibre and POF. Let us compare in table 2.1 their relevant properties

Cost will probably be a major criterion to decide whether a transmission link is suitable for a parallel optical link. Since there are no industrialized procedures for mass fabrication of long enough polymer waveguide boards these are relatively expensive at the moment. small-diameter POF and glass fibre on the other hand are commercially available at low prices. Even for prototyped small diameter step index POF the price is low due to its simple fabrication technique. It is hence probable that one will rely on glass- and/or plastic optical fibre for the first generation optical link. However, once the mass production problem of polymer waveguides will be solved, they will certainly be used due to their compactness, heat resistance and easy termination technique. Nevertheless, it will always be complex to construct a three-dimensional routing structure with slab waveguide, due to their inherent two-dimensional structure. This is not the case for fibres, the fact that each fibre can be routed separately allows to build complex routing structures. Comparing POF to GOF we can notice that POF has a smaller bending radius in combination with a high numerical aperture, which allows more compact links. Moreover POF can be terminated with simple techniques. One notices also that the transmission losses of POF and polymer waveguides are in the same order of magnitude, this means: clearly larger than those of glass. However, for the interconnect range we are considering, these losses are almost negligible. Yet, a clear drawback of POF is the absence of connector technology for parallel small

Table 2.1: Overview of Parallel Waveguides

	POF	GOF	Polymer Waveguides
Bending Radius (mm)	2	10	2
Connectors	not available	available	not available
Fabrication	simple	standard industrial process	complex
Losses at 850nm (dB/meter)	0.06	0.0001	0.05
Termination	simple and fast	time consuming	simple and fast
Max Working Temp (° C)	85	120	120
Numerical Aperture	0.2-0.9	0.2-1	0.1-0.9
3D-structures	Relatively Simple	Relatively Simple	Complex

diameter fibres. This thesis wants to give a solution to that problem: by proposing a new technology for the fabrication of these connectors we want to prove that small-diameter POF is a valuable candidate for short distance optical interconnect links of the first generation.

Bibliography

- [1] H. Thienpont, C. Debaes, V. Baukens, H. Ottevaere, P. Vynck, P. Tuteleers, G. Verschafelt, B. Volckaerts, A. Hermanne, M. Hanney, and I. Veretennicoff, "Plastic micro-optical interconnect modules for parallel free-space inter- and intra-mcm data communication," *Proceedings of the IEEE, Special Issue on 'Short distance Optical Interconnects for Digital Systems*, 2000.
- [2] B. Dhoedt, P. De Dobbelaere, J. Blondelle, P. Van Daele, P. Demeester, and R. Baets, "Monolithic integration of diffractive lenses with LED-arrays for board-to-board free space optical interconnect," *Journal of Lightwave Technology*, vol. 13, pp. 1065–1073, June 1995.
- [3] A. Walker et al., "Optoelectronic systems based on InGaAs complementary-metal-oxide-semiconductor-smart-pixel arrays and free space optical interconnects," *Applied Optics*, vol. 37, pp. 2822–2830, May 1998.
- [4] M. W. Haney, M. P. Christensen, P. Milojkovic, G. J. Fokken, M. Vickberg, B. K. Gilbert, J. Rieve, J. Ekman, P. Chandrami, and F. Kiamilev, "Description and evaluation of the fast-net smart pixel-based optical interconnection prototype," *Proceedings of the IEEE*, vol. 88, pp. 819–827, June 2000.
- [5] E. M. Strzelecka, D. A. Ouderback, B. J. Thibeault, G. B. Thompson, K. Bertillon, and L. A. Coldren, "Parallel free-space optical interconnect based on arrays of vertical-cavity lasers and detectors with monolithic microlenses," *Applied Optics*, vol. 37, pp. 2811–2821, May 1998.
- [6] C. J. Henderson, B. Robertson, D. Gil Leyva, T. D. Wilkinson, D. C. O'Brien, and G. Faulkner, "Control of a free space adaptive optical interconnect using a VCSEL array transmitter and FLC SLM for beam steering," *Proceedings of SPIE, Micro-optics, VCSELS and Photonic Interconnects*, vol. 5453, pp. 270–279, April 2004.
- [7] Y. Tissot, G. Russell, K. Symington, and J. Snowdon, "Optimization of reconfigurable optically interconnected systems for parallel computing," *Journal of Parallel and Distributed Computing*, vol. 66, pp. 238–247, February 2006.
- [8] C. Debaes, M. Vervaeke, B. Volckaerts, J. Van Erps, L. Desmet, H. Ottevaere, P. Vynck, V. Gomez, A. Hermanne, and H. Thienpont, "Low-cost plastic micro-optics for board level optical interconnections," *Proceedings of SPIE, Photonics Packaging and Integration*, vol. 6126, pp. 17–23, January 2006.
- [9] V. Baukens, *Scalable Micro-Optical Modules for Short Distance Photonic-VLSI Interconnections*. PhD thesis, Vrije Universiteit Brussel, 2001.
- [10] R. L. Morisson and B. Buchholz, "Extensible, low-chromatic-sensitivity, all-diffractive-optics relay for interconnecting optoelectronic device arrays," *Applied Optics*, vol. 37, pp. 2925–2934, May 1998.
- [11] Y. Liu, B. Robertson, G. C. Boisset, M. H. Ayliffe, R. Iyer, and D. V. Plant, "Design implementation and characterization of a hybrid optical interconnect for a four-stage free space optical backplane demonstrator," *Applied Optics*, vol. 37, pp. 2895–2914, June 1998.
- [12] B. Robertson, "Design of an optical interconnect for photonic backplane applications," *Applied Optics*, vol. 37, pp. 2975–2983, May 1998.
- [13] D. T. Neilson and E. Schenfeld, "Plastic modules for free space optical interconnects," *Applied Optics*, vol. 37, pp. 2944–2952, May 1998.
- [14] K. Hirabayashi, T. Yamamoto, S. Matsuo, and S. Hino, "Board-to-board free space optical interconnections passing through boards for a bookshelf-assembled terabit-per-second-class ATM switch," *Applied Optics*, vol. 37, pp. 2985–2995, May 1998.
- [15] H. Sasaki, K. Kotani, H. Wada, T. Takamori, and T. Ushikubo, "Scalability analysis of diffractive optical element-based free space photonic circuits for inter-optoelectronic chip interconnections," *Applied Optics*, vol. 40, pp. 1843–1855, April 2001.
- [16] G. Kim and R. T. Chen, "Three-dimensionally interconnected multi busline bidirectional optical backplane," *Optical Engineering*, vol. 38, pp. 1560–1566, September 1999.

- [17] S. Natarajan, C. Zhao, and R. T. Chen, "Bi-directional optical backplane bus for general purpose multi-processor board-to-board optoelectronic interconnects," *IEEE J. Lightwave Techn.*, vol. 13, pp. 1031–1040, June 1995.
- [18] S. Sinzinger and J. Jahns, "Integrated micro-optical imaging system with a high interconnection capacity fabricated in planar optics," *Applied Optics*, vol. 36, pp. 4729–4735, 1997.
- [19] J. Ellis, R. Mays, Jr, D. Griffiths, H. Bi, J. Choi, W. Jiang, and R. T. Chen, "Holographic optical elements for optical backplane bus targeted at high speed data transfer," *Proceedings of SPIE, Photonics Packaging and Integration VIII*, vol. 6126, January 2006.
- [20] <http://www.emcore.com>.
- [21] <http://www.zarlink.com/opticalsolutions>.
- [22] <http://www.picolight.com>.
- [23] <http://www.intel.com>.
- [24] <http://www.lasermate.com>.
- [25] <http://www.avagotech.com>.
- [26] T. Ohta, S. Shida, K. Takizawa, T. Airikawa, and Y. Tamaki, "Two dimensional array optical fiber connector," *Fujikura Technical Review*, pp. 18–22, 2000.
- [27] "Design and performance of very high density multi-fibre connectors employing monolithic 60 fibre ferrules," *IEEE photonics technology letters*, vol. 11, pp. 1446–1448, november 1999.
- [28] <http://www.furukawaamerica.com>.
- [29] R. A. Nordin, "Advanced optical interconnection technology in switching equipment," *IEEE J. Lightwave Techn.*, vol. 13, pp. 987–994, June 1999.
- [30] <http://www.nel-world.com>.
- [31] G. De Pestel, "Parallel optical interconnection for future broad band systems based on fiber-in-board technology," in *Proceedings of the ECTC conference*, pp. 532–534, 1996.
- [32] G. De Pestel, "Multifiber electro-optical modules compatible with the fiber-in-board technology," in *Proceedings of the LEOS Annual Meeting*, no. 5, pp. 224–225, 31 October-4 November 1994.
- [33] Y.-M. Wong et al, "Technology development of a high-density 32-channel 16-Gb/s optical datalink for optical interconnection applications for the optoelectronic technology consortium (oetc)," *Journal of Lightwave Technology*, vol. 13, pp. 995–1013, June 1995.
- [34] B. Chan et al, "Packaging aspects of the litebus parallel optoelectronic module," *Micronews*, vol. 6, Third Quarter 2000.
- [35] S. Swirhun et al, "The p-vivelink multichannel optical interconnect," in *Proceedings of the Electronic Components Conference*, pp. 316–320, 1996.
- [36] L. Galarneu and K. Johnson, "Cheetah project: Cost effective embedding of high performance interconnects." Website: www.htc.honeywell.com.
- [37] D. Kuhl et al, "Paroli- a parallel optical link with 15 Gbit/s throughput in a 12 channel wide interconnection," in *Proceedings of the 6th international Conference on Parallel Interconnects*, (Anchorage), October 1999.
- [38] K. H. Hahn et al, "Gigabyte/s data communications with the polo parallel optical link," in *Proceedings of the Electronic Components and Technology Conference*, (Orlando, Florida), pp. 301–307, May 1996.
- [39] L. J. Norton et al, "Optobus: A parallel interconnect solution," in *Proceedings of the LEOS '97 10th Annual Meeting. Conference*, vol. 2, (San Fransisco), pp. 189–190, November 1997.
- [40] N. Sual, F. Tooley, A. Fritze, J. Gourlay, J. Dines, A. . McCarthy, A. Walker, and F. Bresson, "Multimode planar lightwave circuits using direct write of polymers," in *Proceedings of the Optics in Computing Conference (SPIE, ed.)*, vol. 4089, (Quebec), pp. 54–60, June 2000.

- [41] K. Katsura, M. Usui, N. Sato, A. Ohki, N. Tanaka, N. Matsuura, T. Kagawa, K. Tataeno, M. Hikita, R. Yoshimura, and Y. Ando, "Packaging for a 40-channel parallel optical interconnection module with an over- 25- Gbit/s throughput," *IEEE Transactions on Advanced Packaging*, vol. 22, pp. 551–559, November 1999.
- [42] P. Rozenberg et al, "The poni-1 parallel optical link," in *Proceedings of the Electronic Components and Technology Conference*, (San Diego), pp. 763–769, June 1999.
- [43] M. Cohen, G. Johnson, D. Kuchta, P. Pepeljugoski, J. Trehwella, S. Quimet, and S. Spanoudis, "Packaging aspects of the Jitney parallel optical interconnect," in *Proceedings of the Electronic Components and Technology Conference*, (Seattle), pp. 1206–1215, May 1998.
- [44] G. Johnson et al, "Relaxed tolerance plastic components for use in low cost gigabyte/sec parallel optical data interconnect," in *Proceedings of the POF Conference*, (Paris), pp. 64–67, October 1997.
- [45] L. A. Buckman Windover et al, "Parallel-optical interconnects faster than 100 Gb/s," *Journal of lightwave technology*, vol. 22, pp. 2055–2063, September 2004.
- [46] C. Rooman, M. Kuijk, D. Filkins, B. Dutta, R. Windisch, R. Vounckx, and P. Heremans, "Low-power short-distance optical interconnect using imaging fiber bundles and CMOS detectors," in *Proceedings of the IEEE LEOS Summer Topical Meetings on Electronic-enhanced Optics*, (Adventura, FL.), pp. 49–50, 24-26 July 2000.
- [47] H. Kosaka, M. Kajita, Y. Li, and Y. Sugimoto, "A two-dimensional optical parallel transmission using a vertical cavity surface emitting laser array module and an image fiber," *IEEE Photonics Technology Letters*, vol. 9, pp. 253–255, February 1997.
- [48] Y. Lin, T. Wang, H. Kosaka, S. Kawai, and K. Kasahara, "Fiber image guide based bit-parallel optical interconnects," *Applied Optics*, vol. 35, pp. 6920–6933, December 1996.
- [49] D. M. Chiarulli, S. P. Levitan, P. Derr, R. Hofmann, B. Greiner, and M. Robinson, "Demonstration of a multichannel optical interconnection by use of imaging fiber bundles butt coupled to optoelectronic circuits," *Applied Optics*, vol. 39, pp. 698–703, February 2000.
- [50] "www.ppc-electronic.ch."
- [51] <http://io.intec.ugent.be>.
- [52] Y. Liu, "Polymer optical interconnect technology (point)- optoelectronic packaging and interconnect for board and backplane applications," in *Proceedings Electronic Components and Technology Conference*, (Orlando, Florida), pp. 308–315, May 1996.
- [53] A. L. Glebov et al, "Integrated waveguide micro-optic elements for 3D routing in board-level optical interconnects," *Proceedings of SPIE, Photonics Packaging and Integration VIII*, vol. 6126, January 2006.
- [54] C. Berger, B. J. Offrein, and M. Schwarz, "Challenges for the introduction of board-level optical interconnect technology into product development roadmaps," *Proceedings of SPIE, Optoelectronic Integrated Circuits VIII*, vol. 6124, January 2006.
- [55] H. Schröder et al, "Waveguide and packaging technology for optical backplanes and hybrid electrical-optical circuit boards," *Proceedings of SPIE, Optoelectronic Integrated Circuits VIII*, vol. 6124, January 2006.
- [56] K. B. Yoon et al, "Optical backplane system using waveguide-embedded PCBs and optical slots," *Journal of lightwave technology*, vol. 22, pp. 2119–2127, September 2004.
- [57] <http://www.keytech.ntt-at.co.jp>.
- [58] J. Marchegiano, B. Booth, C. Chang, R. Furmanak, D. Graham, and R. Yohannan, "Polyguide technology for passive optical interconnects," in *Proceedings of the Photonics West-OE-Laser Conference*, vol. 2690, (San Jose/California), pp. 3614–368, February 26 -March 3 1994.
- [59] <http://www.opticalcrosslinks.com>.
- [60] L. Eldada and L. Shaklette, "Advances in polymer integrated optics," *IEEE journal of Selected Topics in Quantum Electronics*, vol. 6, pp. 54–67, January/February 2000.

- [61] Y. Liu, "Polymer waveguide applications in multi-chip modules (mcms) and board level optical interconnects." Technical Report GE Corporate Research and Development, December 1997.
- [62] R. Yoshimura, M. Hikita, S. Tomaru, and S. Imamura, "Low-loss polymeric optical waveguides fabricated with deuterated polyfluoromethacrylate," *Journal of Lightwave Technology*, vol. 16, pp. 1030–1036, June 1998.
- [63] M. Hikita, S. Tomaru, and S. Imamura, "Multi-layer and flexible polymeric optical waveguides," in *Proceedings of the 10th International POF Conference*, (Amsterdam), pp. 133–138, September 2001.
- [64] E. Griese, "Optical interconnections on printed circuit boards," in *Proceedings of the Optics in Computing Conference* (SPIE, ed.), vol. 4089, (Quebec), pp. 60–71, June 2000.
- [65] E. Griese, "A high -performance hybrid electrical-optical interconnection technology for high-speed electronic systems," *IEEE Transactions on Advanced Packaging*, vol. 24, pp. 375–383, August 2001.
- [66] D. Krabe and W. Scheel, "Optical interconnects by hot embossing for module and PCB technology," in *Proceedings of the Electronic Components and Technology Conference*, (San Diego , California), pp. 1164–1176, June 1999.
- [67] F. Mederer, R. Jager, H. Unold, T. Michalzik, K. Ebeling, S. Kehmacher, A. Neyer, and E. Griese, "3-Gb/s Data transmission with GaAs VCSELs over PCB integrated polymer waveguides," *IEEE Photonics Technology Letters*, vol. 13, pp. 1032–1033, September 2001.
- [68] E. hang Lee, S. G. Lee, B. H. O, S. G. Park, and K. H. Kim, "Fabrication of a hybrid electrical-optical printed circuit board(EO-PCB) by lamination of an optical printed circuit board (O-PCB) and an electrical printed circuit board (E-PCB)," *Proceedings of SPIE, Photonics Packaging and Integration VIII*, vol. 6126, January 2006.
- [69] <http://www.epigem.co.uk>.
- [70] B.-T. Lee, M.-S. Kwon, J.-B. Yoon, and S.-Y. Shin, "Fabrication of polymeric large-core waveguides for optical interconnects using a rubber molding process," *IEEE Photonics Letters*, vol. 12, no. 1, pp. 62–64, 2000.
- [71] X. Zhao, S. P. Smith, S. J. Waldman, G. M. Whitesides, and M. Prentiss, "Demonstration of waveguide couplers fabricated using microtransfer molding," *Applied Physics Letters*, vol. 71, no. 8, pp. 1017–1019, 1997.
- [72] C. Choi et al , "Flexible optical waveguide film fabrications and optoelectronic devices integration for fully embedded board-level optical interconnects," *Journal of lightwave technology*, vol. 22, pp. 2168–2175, September 2004.
- [73] J. Moisel, H. H. J. Guttmann, O. Krumpholze, and M. Rode, "Optical backplanes utilizing multimode polymer waveguides," in *Proceedings of the Optics in Computing Conference* (SPIE, ed.), vol. 4089, (Quebec), pp. 72–78, June 2000.
- [74] G. Van Steenberge, N. Hendrickx, P. Geerinck, E. Bosman, S. Van Put, J. Van Erps, H. Thienpont, and P. Van Daele, "Development of a fabrication technology for integrating low cost optical interconnects on a printed circuit board," *Proceedings of SPIE, Photonics Packaging and Integration VIII*, vol. 6126, January 2006.
- [75] B. S. Rho et al , "PCB-compatible optical interconnection using 45 degrees-ended connection rods and via-holed waveguides," *Journal of lightwave technology*, vol. 22, pp. 2128–2134, September 2004.
- [76] <http://electronicmaterials.rohmhaas.com>.
- [77] J. sung Kim and J.-J. Kim, "Stacked polymeric multimode waveguide arrays for two-dimensional optical interconnects," *Journal of lightwave technology*, vol. 22, pp. 840–844, March 2004.
- [78] T. Yoshimura, J. Roman, Y. Takahashi, Wen-Chou, V. Wang, and M. Inao, "Self-organizing lightwave network (SOLNET) in optical interconnections," in *Proceedings of the Optics in Computing Conference* (SPIE, ed.), vol. 4089, (Quebec), pp. 321–332, June 2000.

- [79] T. Yoshimura et al, "Three-dimensional chip-scale optical interconnects and switches with self-organized wiring based on device-embedded waveguide films and molecular nanotechnologies," *Proceedings of SPIE, Photonics Packaging and Integration VIII*, vol. 6126, January 2006.
- [80] T. Yoshimura et al, "Self-organized lightwave network based on waveguide films for three-dimensional optical wiring within boxes," *Journal of Lightwave Technology*, vol. 22, pp. 2091–2099, September 2004.
- [81] W. Baierl, "Evolution of automotive networks," in *Proceedings of the 10th POF Conference*, (Amsterdam), pp. 161–168, September 2001.
- [82] N. Schunk, K. Panzer, E. Baur, W. Kuhlmann, K. Streubel, R. Wirth, and C. Karnutsch, "IEEE 1394b POF transmission system 500mbit/s versus 50m 0.3 NA POF," in *Proceedings of the 10th POF conference*, (Amsterdam), pp. 65–71, September 2001.
- [83] <http://www.firecomms.com>.
- [84] <http://www.infineon.com/pof>.
- [85] <http://www.luceat.it>.
- [86] <http://www.www.pofto.com/downloads/PRPOF.pdf>.
- [87] [HTTP://www.chromisfiber.com](http://www.chromisfiber.com).
- [88] M. Brunfaut, W. Meeus, J. Van Campenhout, R. Annen, P. Zenklusen, H. Melchior, R. Bockstaele, L. Vanwassenhove, J. Hall, B. Wittman, A. Neyer, P. Heremans, J. Van Koetssem, R. King, H. Thienpont, and R. Baets, "Demonstrating optoelectronic interconnect in a FPGA-based prototype system using flip-chip mounted 2d-arrays of optical components and 2d POF ribbon arrays as optical pathways," in *Proceedings of the SPIE' 46th annual meeting*, (San Diego, California), July 2001.
- [89] A. Van Hove, *Termination and Interconnection Technology for Parallel Optoelectronic Systems*. PhD thesis, Ghent University, Faculty Applied Sciences, Dept of Information Technology, Sint Pietersnieuwstraat 41, 9000 Gent , Belgium, 2001.
- [90] Y. Koike, "POF technology for the 21st century," in *Proceedings of the 10th POF Conference*, (Amsterdam), pp. 5–8, September 2001.
- [91] Y. Koike and M. Naritomi, "Graded-refractive-index optical plastic material and method for its production," U.S. Patent 5 783 636, July 1998.
- [92] Y. Li, "Board-level 2-d data-capable optical interconnection circuits using polymer fiber-image guides," *Proceedings of the IEEE*, vol. 88, pp. 794–805, June 2000.
- [93] S. Teshima and H. Munekuni, "Multi-core POF for high-speed data transmission," in *Proceedings of the POF conference*, (Berlin), pp. 135–142, October 1998.

3

Plastic Optical Fibre

AFTER a short overview of the state-of-the-art of plastic optical fibre technology, we will focus on the properties of the small-diameter POFs used for the experimental work carried out during this PhD study. Theoretical and experimental aspects of mechanical as well as optical issues will be discussed.

3.1 Introduction

Before starting a more elaborate discussion on the properties of POF, let us briefly repeat some fundamentals of fibre optics. Since in this PhD work we only make use of fibres with a step index profile, we will limit the discussion to this kind of fibre. Moreover, we will see that POFs are highly multimodal and hence ray theory can be applied [1].

A step index fibre consists of a cylindrical core region with refractive index n_1 and a cladding sheath with refractive index n_2 , whereby $n_1 > n_2$. If a light ray strikes the interface between core and cladding, it is refracted following Snell's law (figure 3.1):

$$n_1 \sin \alpha = n_2 \sin \alpha' \quad (3.1)$$

One can see that when the condition

$$\alpha = \alpha_c = \arcsin\left(\frac{n_2}{n_1}\right) \quad (3.2)$$

is fulfilled, the angle of refraction α'_c becomes 90° . For larger angles ($\alpha_1 > \alpha_c$) the light is reflected completely into the core region. This is called Total Internal Reflection (TIR). In terms of the complementary angle θ the condition for TIR becomes:

$$\theta < \theta_c = \arccos\left(\frac{n_2}{n_1}\right) \quad (3.3)$$

Note that this phenomenon can only occur when $n_1 > n_2$. To the critical angle

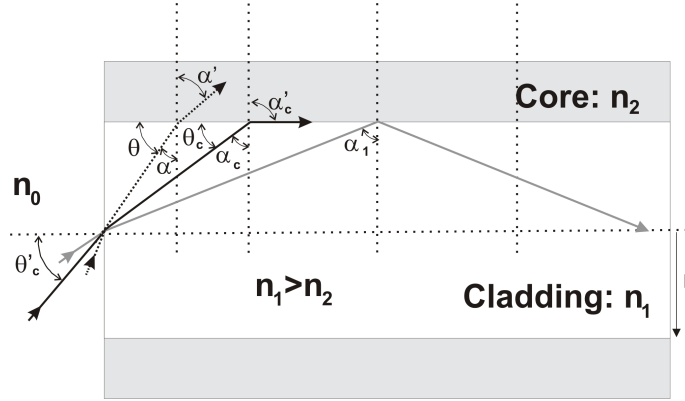


Figure 3.1: Reflected and refracted rays in a step index fibre

θ_c a ray launching angle θ'_c corresponds, following the equation:

$$n_0 \sin \theta'_c = n_1 \sin \theta_c \quad (3.4)$$

Only the light that is emitted from a light source with an angle smaller than θ'_c will be accepted by, and propagate in, the optical fibre. The quantity $n_0 \sin \theta'_c$ is called

the Numerical Aperture of the fibre. In lots of cases the emitter is positioned in air and $n_0=1$ and hence $NA = \sin \theta'_c$. Working out equation 3.4 yields:

$$NA = n_1 \cos(\alpha_c) = n_1 \cos\left(\arcsin \frac{n_2}{n_1}\right) = n_1 \cos\left(\arccos \sqrt{1 - \left(\frac{n_2}{n_1}\right)^2}\right) \quad (3.5)$$

and hence the numerical aperture can be expressed in terms of the refractive indexes of the fibre:

$$NA = \sqrt{n_1^2 - n_2^2} \quad (3.6)$$

For a POF with a typical NA of 0.5 this corresponds to an angle θ'_c of 30° outside the fibre, and to angle θ_c of 20° in the core. However, not every ray that is launched within the numerical aperture propagates through the fibre. Due to conditions of constructive interference at the core-cladding interface only a limited number of ray directions is allowed. Such a ray direction is called a mode and corresponds to a certain angle α of reflection at the core-cladding interface (and hence to a launching angle θ'). The number of modes in a fibre is given by [2]

$$m = \frac{1}{2} \left(\frac{\pi d}{\lambda} NA \right)^2 \quad (3.7)$$

With λ the wavelength of the light and d the diameter of the core. When $m > 1$ the fibre is called a multimode fibre and when $m = 1$ it is called a single mode fibre. Plastic fibres are in general highly multimodal. For instance a POF with a core diameter of $62 \mu\text{m}$ and numerical aperture 0.5 has about 5000 modes at a wavelength of 980 nm.

3.2 POF: State-of-the-Art

As has been mentioned in the previous chapter, POF was first introduced in the late sixties by DuPont as a medium for illumination. Since then, one has realized that POFs could be used as well as a data transmission medium and, especially spurred by Japanese manufacturers and researchers (in particular Prof. Koike of the Keio university [3]), there have been fast developments in POF technology the last years. Whereas glass fibre remains the prime transmission medium for long distance telecommunications there is an opportunity for POF to replace silica fibre on mid-range distances varying from tens of meters to a couple of hundreds of meters. Several applications like Local Area Networks, home- and office networks and automotive networks [4–6] have been suggested. At this moment POF-based optical links are commercially available [7–10]. POF is proposed as a cheap and easy-to-mount alternative for silica glass fibre. Indeed, the possibility to easily fabricate large diameter (up to a few millimeter) POF reduces significantly the installation cost since low tolerance connectors can be used. Moreover the end facet is obtained by a simple hot knife cutting procedure and it is relatively immune to dust. In addition plastic it not as brittle as glass which makes POFs

easier to handle. Hence, a large part of the effort in the quest for better POFs deals with the development of low loss, large diameter, and high bandwidth fibre. However, in order to obtain still higher data rates, small core graded index POF has become available recently. Nexans and Chromis Fiberoptics are two examples of companies that have developed such fibres with core diameters between 50 and 120 μm .

The first generation POFs however, had a step refractive index profile and were polymethyl methacrylate-based (PMMA). An important disadvantage was the high transmission loss at classical telecom wavelengths 1300 and 1550 nm. The main cause of this loss is the absorption of light due to vibrating C-H bonds in the methacrylate molecules (formula PMMA see figure 3.2). By replacing the H atoms by deuterium or by F (fluorination), the resonance peak is shifted towards the deeper infrared region and the absorption is reduced [11] as can be seen in figure 3.3. Even better results, especially at 1300 nm, were obtained with the intro-

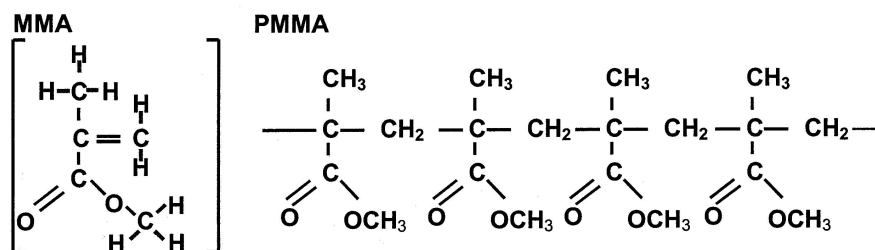


Figure 3.2: Structure of PMMA

duction of the polymer CYTOPTM. The monomer formula can be seen in figure 3.3: it contains no C-H bonds and is cyclic. Theoretically the transmission losses of fluorinated polymers can be as low as that of standard silica fibre [3]. However, intrinsic scattering losses, due to variations of the refractive index, and extrinsic scattering losses, due to e.g. core-clad imperfections and microvoids, still prevent values lower than 15 dB/km at 1300 nm [12, 13].

Bandwidth is another important issue for the implementation of POF in local area networks. There are two ways to increase bandwidth: decrease the numerical aperture of a step index fibre or create a fibre with a parabolic index profile (graded index fibre). The first solution is the most simple since the creation of a step index profile is less complex than that of a graded index profile (see paragraph 3.3). Transmission lines at 500 Mbit/s over 50 meter using a 0.3 numerical aperture were reported [14]. However the fibre bandwidth can be increased significantly more by creating a graded index POF [15]. Recently a 10 Gbps link with 100 meter POF was realized [16]. The first commercially available graded index fibre was produced by Asahi Glass, was called "Lucina" and was made of CYTOPTM. A bandwidth-length product of 300 Mhz.km at 850 nm and 1300 nm has been measured as well as a transmission loss of 40 dB/km at the same wavelengths. Nexans used Cytop as well for its POF, achieving a loss of 20 dB/km at 850 nm. During the research work of this thesis, the industry hardly put any effort in the

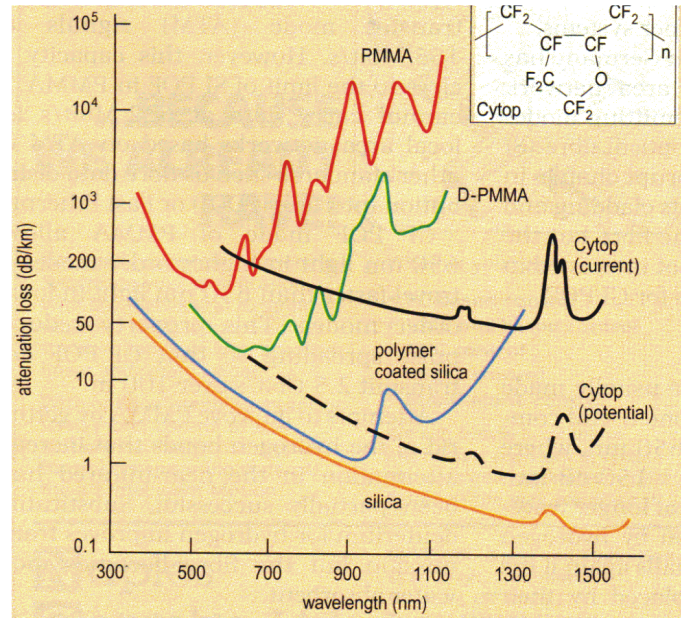


Figure 3.3: Evolution of the transmission losses in POF

development of small diameter fibres. Since at that moment there was no immediate commercial interest in this POF, only few manufacturers produced them. The fibres we obtained were made of PMMA, had a step index profile and had a large NA (0.5). However, we will show that these properties do not form an obstacle for their use in short distance interconnections.

3.3 Production processes of POF

Plastic optical fibre can be made in two ways. Either it is fabricated by a direct process or it is drawn from a preform with a given index profile, similar to the production process of glass fibre. In the case of direct fabrication different variations are possible [17–19]. A standard method is co-extrusion (figure 3.5): Polymerized core and cladding materials in the form of granules are melted and hot drawn by passage through a co-extrusion head containing two coaxial dies. The first one defines the diameter of the core. At its exit, the molten plastic surrounds the core and the whole passes through the second die that defines the external diameter. When the fibre has cooled sufficiently it is drawn by a capstan and rolled onto a drum for storage. This technology is straightforward for step index fibre. However, for graded index-like profiles, the co-extrusion process has to be expanded to several layers. Yet, this creates a refractive index profile that is evolving stepwise (Multi-Step-Index), generally resulting in a worse dispersion behavior than in case of a real continuous index profile, although it has been shown that by increasing the number of layers, a quite satisfactory result can be obtained [20]. Other direct

fabrication technologies are batch extrusion, melt spinning and direct UV-cross linking [19].

Co-extrusion can be used as well to make a preform. In case of a step index fibre the preform consists of a polymer core cylinder with a high refractive index that is concentrically sheathed in a cladding tube with a lower index. It is then heated (190 to 230° C) and drawn, through a diameter gauge (figure 3.4).

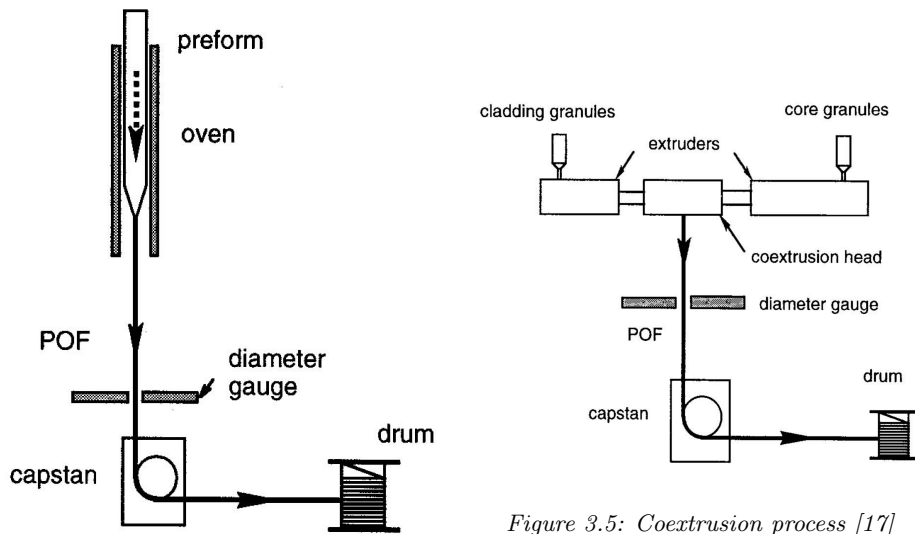


Figure 3.5: Coextrusion process [17]

Figure 3.4: POF drawing from a preform [17]

Preforms with a real graded index profile can be obtained by chemical vapour deposition (CVD), outside vapour deposition (OVD), vapour phase axial deposition (VAD), photo-copolymerization methods and interfacial-gel polymerization techniques [20–24].

3.4 Small-diameter POF

Two kinds of small diameter step index POF were purchased and were object of study. The Toray PGR-125 POF is a commercially available product and was in fact developed more as a light guide or for sensing purposes more than for data transmission. The Asahi Chemical Luminous TB/125 on the contrary, was a prototype POF without specific applications.

3.4.1 Specifications

Toray PGR-125 POF As mentioned this Toray POF is a commercially available product and is hence well specified. It has a step index profile created by a polymethyl methacrylate (PMMA) core and a fluorinated cladding layer. The

numerical aperture is 0.5. The core diameter is 116 μm and the overall diameter is 125 μm . Transmission losses are specified at 0.3 dB/m at 650 nm and around 2 dB/meter at 800 nm wavelength. Temperature range for permanent use: $-40/+70^\circ\text{C}$.

Asahi Chemical Luminous TB 62/125 POF Since this fibre was developed as a prototype it is less specified. Similar to the Toray POF the core is made of PMMA and the cladding of fluorinated PMMA. Diameter of the core is 62.5 μm and the overall diameter is specified at 25 μm . The refractive index of the core is 1.492 and that of the cladding is 1.41 resulting in an NA of 0.49. The attenuation was not specified.

These properties were studied experimentally and a discussion will follow in the next paragraphs.

3.4.2 Mechanical Properties

3.4.2.1 Geometrical properties

Compared to glass fibre the geometry of POFs is less tightly controlled. Nevertheless, a good control of the geometry is an important issue for efficient POF coupling (POF to emitter/detector or POF to POF). The following factors have to be taken into account:

Diameter of the core Since almost all the light is transported in the core of the fibre, it is clear that if one couples a fibre to another fibre there will be loss of light when a POF with a large core diameter is coupled to a POF with a smaller core diameter (figure 3.6). In this case, the power loss at a POF/POF interface is

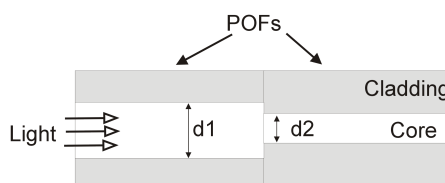


Figure 3.6: Coupled POFs with different core radii

described by the following equation (in dB) [25]:

$$\text{loss}[\text{dB}] = -10 \log \left(\frac{d_2}{d_1} \right)^2 \quad \text{if } d_1 > d_2 \quad (3.8)$$

, with d_1 and d_2 the respective core diameters. The core diameter has been measured extensively for the two considered POFs. Therefore POFs were inserted in a MT^{TM} -ferrule for parallel glass fibres (1×12), and were then cut with a hot knife along the end facet of the ferrule. The end facet, now containing the cross-sections of the fibres, was then looked at with a microscope and the core and outer diameter were measured. The accuracy of this measurement was 1 μm . This generated

the following results:

Toray PGR 125:

In order to estimate the diameter several 0.5 meter long pieces were cut every 1 cm and the core and outer diameter were measured with a microscope. In addition a longer piece of 2.5 meter was cut every 5 cm. Both experiments generated similar results in terms of average, standard deviation, minimum and maximum values. As can be seen in figure 3.7 the core diameter varies around an average value of

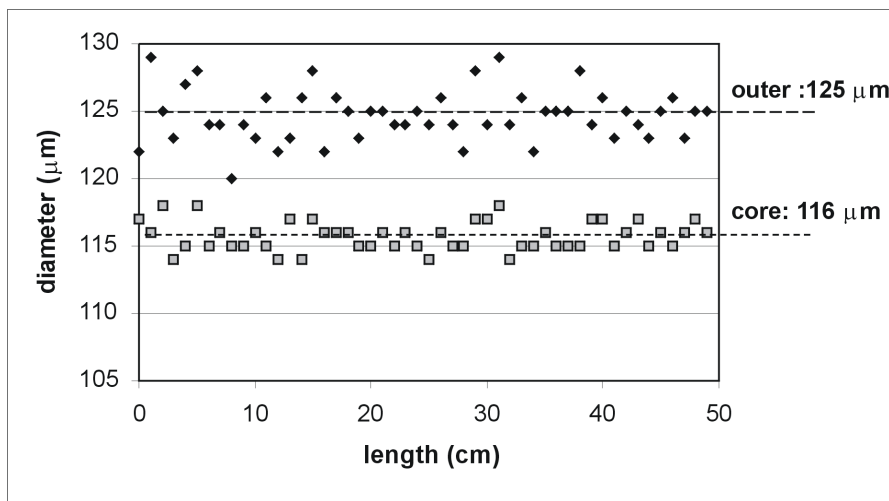


Figure 3.7: Core and outer diameter of the Toray PGR 125 POF as a function of the fibre length

$115.8 \approx 116 \mu\text{m}$. The standard deviation is $1 \mu\text{m}$ and the maximum and minimum values are $118 \mu\text{m}$ and $114 \mu\text{m}$, respectively.

In order to get an idea of the effect of the varying core diameter on coupling losses one can calculate the average power loss due to core diameter mismatch while coupling two POFs, and this following equation 3.8 and the diameter distribution shown in figure 3.8. 64 % of the POF/POF couplings have no losses (light goes from small diameter to larger diameter) while 36 % show losses with an average of 0.1 dB. The total average coupling loss is 0.04 dB per coupling. The worst case is generated by a 118 to 114 μm diameter coupling: 0.3 dB.

It is clear that the variation of the core diameter will affect the efficiency of the emitter/POF coupling as well as the POF/detector coupling. However the effect will heavily depend on the chosen parameters for the emitter and detector. For instance if we choose a laser as a light source, the effect will be much smaller than in case of a Light Emitting Diode. Also the diameter of the emitter/detector is of importance. In chapter 5 emitter-detector/POF couplings will be studied and an example will be given.

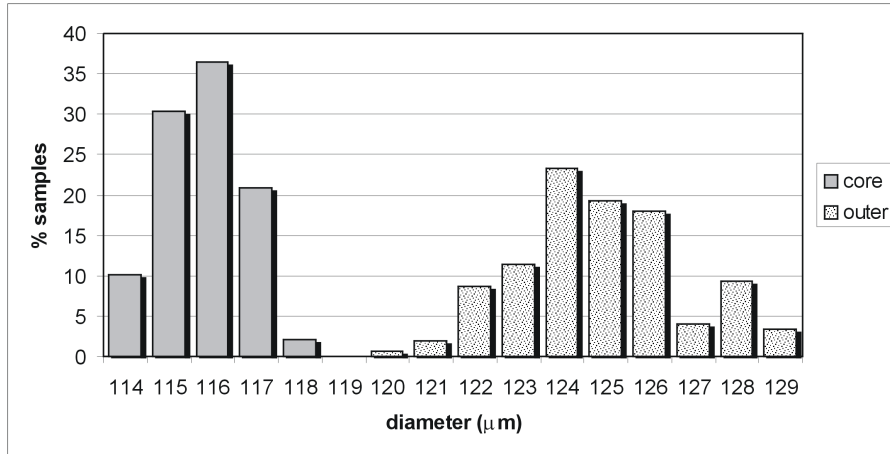


Figure 3.8: Distribution of the measured diameters (Toray POF)

Asahi Luminous TB 62/125 The diameter of the POF varies over the length of the fibre in a different way than in the case of the Toray POF (figure 3.9). Besides

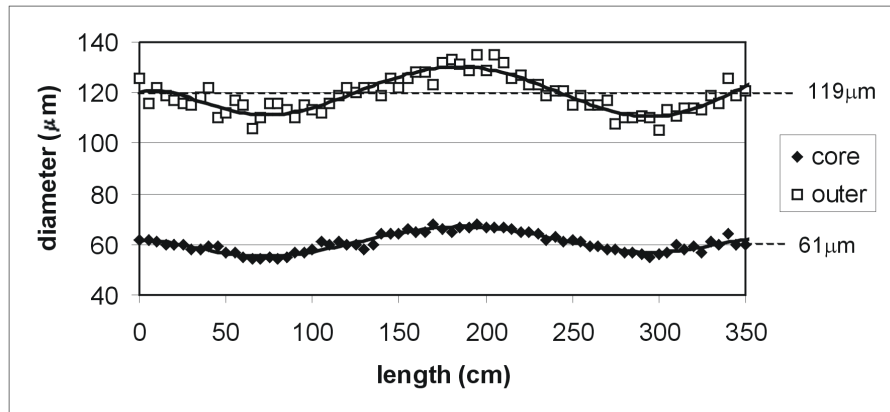


Figure 3.9: Evolution of the diameter as a function of the length for the Asahi POF

the "rapid" fluctuations of a few μm similar to the case of the Toray POF, there is a "slower" and larger fluctuation with a period of around 2 meter. This results in a lower accuracy on the diameter. Following values were measured: average: $60.74 \mu\text{m} \approx 61 \mu\text{m}$, standard deviation: $3.8 \mu\text{m}$, minimum value $54 \mu\text{m}$, maximum value $68 \mu\text{m}$. We can see from figure 3.10 that the measured values are more spread than in case of the Toray POF. The influence of the core diameter on the efficiency of a POF/POF coupling can be calculated in the same way as mentioned above: 53.5 % of the couplings are lossless and 46.5 % show losses. (average 0.68 dB). The total average loss per POF-POF coupling = 0.32 dB. The worst case is generated

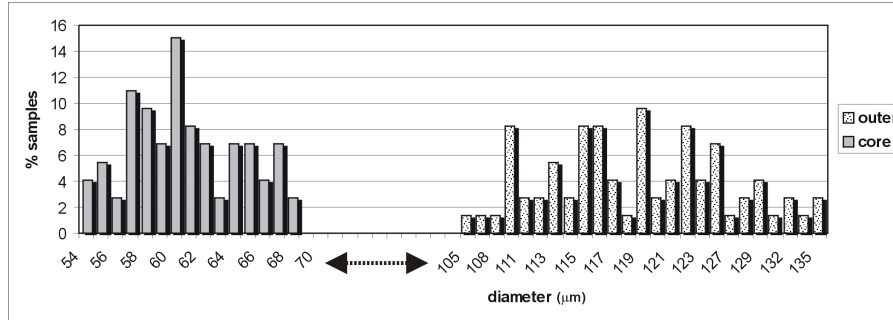


Figure 3.10: Distribution of the measured core and outer diameters (Asahi POF)

by a 68 to 54 μm fibre coupling: 2 dB!

The core diameter of a standard multimode glass fibre has a maximum deviation of 3 μm . Note that the values measured for the Toray POF are comparable. For the Asahi POF on the other hand, the specifications are definitely worse.

Outer diameter Fibres are aligned in connectors generally by inserting them in precise V-grooves or holes. This alignment relies on the accuracy of the outer diameter of the POF. It is easy to see that when the diameter of the fibre is smaller than that of the hole, the accuracy on the position of the fibre decreases (see figure 3.11) This results in a radial offset of the coupled fibers. Following [25]

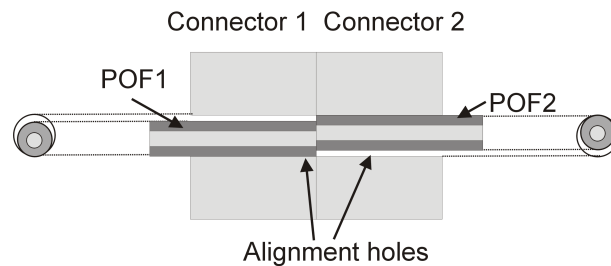


Figure 3.11: Radial misalignment while coupling to POFs, caused by the varying outer diameter of the fibre.

the transmission loss as a function of the radial offset x is given by:

$$\text{loss}[\text{dB}] = -10 \log \left(\frac{2}{\pi} \left(\arccos\left(\frac{x}{d}\right) - \frac{x}{d} \sqrt{1 - \left(\frac{x}{d}\right)^2} \right) \right) \quad (3.9)$$

The outer diameter of both types of fibre was measured in the same way as the core diameter.

Toray PGR 125:

As can be seen from figure 3.7 the cladding varies more than the core. Following

values were measured: average: $124.8 \mu\text{m} \approx 125 \mu\text{m}$, standard deviation $2.0 \mu\text{m}$, minimum value: $120 \mu\text{m}$, maximum value $129 \mu\text{m}$. Figure 3.8 shows the distribution of the measured diameters.

Asahi TB 62/125

Similarly as for the core there is a "fast" variation superposed on a slowly varying one. This results in the following specifications: average: $119.1 \mu\text{m} \approx 119 \mu\text{m}$, standard deviation $7.1 \mu\text{m}$, minimum value $105 \mu\text{m}$, maximum value $135 \mu\text{m}$. From figure 3.10 one can see that here again, the measured values are widely spread. Hence the Asahi POF geometry is clearly less controlled than the Toray one.

Core-cladding concentricity Similar to a varying outer diameter, core-cladding non-concentricity generates a radial offset of the cores. However, it is more complicated to measure the non-concentricity than the diameter. Yet, since core-cladding non concentricity and varying outer diameter yield the same offset while coupling fibres, it is relevant to measure their combined effect on the coupling efficiency of POFs. An estimation method has been worked out. POFs were kept in a commercially available MT^{TM} ferrules. These are ferrules used in connectors for 1×8 to 1×12 glass fibres. The alignment of the ($125 \mu\text{m}$ diameter at $250 \mu\text{m}$ pitch) fibres relies on an array of very precise holes ($\pm 0.5 \mu\text{m}$, [26]) in which the fibres are inserted (figure 3.12). When two MT ferrules are coupled, this set of holes is aligned to the similar set in the mating ferrule by means of two ($700 \mu\text{m}$ diameter) guiding pins. Toray POFs were inserted in these ferrules and by scanning the

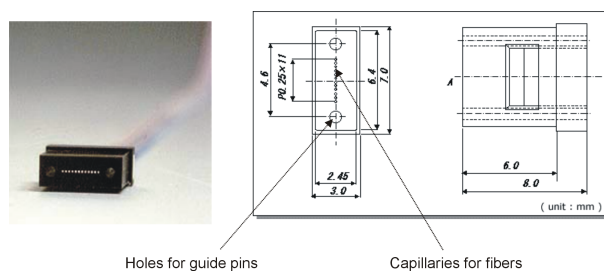


Figure 3.12: MT^{TM} ferrule

fibres with a light source the position of the fibres was measured. By a simulation of ferrule-coupling one can estimate the effect of the non-concentricity of core and hole. This simulation was done in the following way: after the coordinates of the POF cores in a ferrule were experimentally determined, the best fit between the measured values and an ideal (1×12) array was calculated. This was done for different ferrules. Then the mating between different pairs of ferrules was simulated with the boundary condition that the ideal arrays were overlapping perfectly. In this way, one assumes that the guiding pin system aligns perfectly. Hence, the radial offset is caused by the combined effect of the offset of the holes, the varying outer diameter of the fibres, and the core-cladding non-concentricity (hereby neglecting the variation of the hole diameter). Following [26], the average radial

offset between two mated holes is $1.28 \mu\text{m}$ which corresponds to an average loss of 0.06 dB. The calculated average radial offset between POF cores was $4.8 \mu\text{m}$ corresponding to 0.23 dB average loss. A typical simulation of two coupled 1×12 POF arrays can be seen in figure 3.13. Roughly speaking, the joined effect of

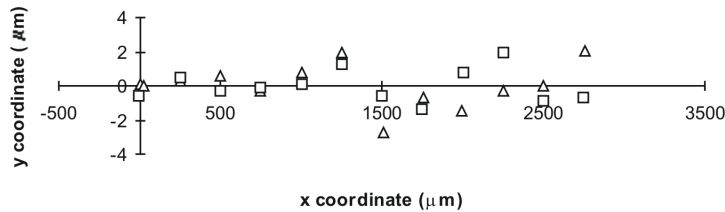


Figure 3.13: A simulated mating of two 1×8 arrays. The triangles give the positions of the POF cores in the first ferrule, the squares in the second ferrule.

core-cladding non-concentricity and varying outer diameter causes an average loss of $0.23 - 0.006 \text{ dB} = 0.17 \text{ dB}$ per POF/POF coupling.

For the Asahi POF such experiments have not been carried out but it is easy to understand that since the geometry of the fibre is far less controlled, these effects on the coupling efficiency will be considerably larger than in the case of the Toray POF.

3.4.2.2 Tensile strength and bending

The susceptibility of POF to external forces is a complex matter. The effects of external forces have to be studied on the long term as well as on the short term, and for single as well as for repeated incidents. An extended discussion of the necessary tests and characterizations to get a complete picture of the mechanical strength of a POF, can be found in [17, 18, 27]. Issues like bending, tensile strength, torsion resistance, impact resistance and transverse compressive strength are treated. It is not in the scope of this PhD work to investigate these parameters thoroughly. However, in view of the realization of compact links, the bending of fibres, and hence the closely related tensile strength, is particularly important to us. It is possible to calculate the minimal bending radius of a fibre starting from its tensile strength. Therefore extensive strain-tension tests were carried out on the considered POFs¹. A universal material testing machine type INSTRON 4505, was used [28].

Toray PGR 125:

The experimental results of several strain tension-tests can be seen in figure 3.14. The fibres deform elastically until about 3% strain. The tension σ_{max} in the fibre at this point is hence $F_{max}/\text{cross section fibre} = 0.86 \text{ N}/0.012\text{mm}^2 \approx 70 \text{ N/mm}^2$.

¹Carried out by Wim De Waele, Dept Mechanical Construction & Production, Ghent University

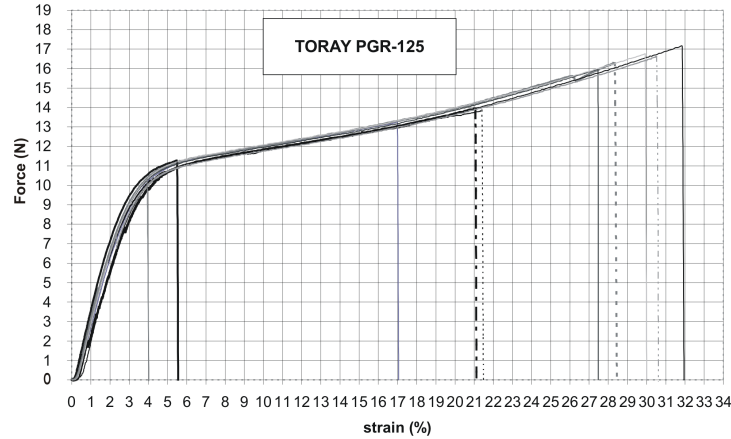


Figure 3.14: Strain-force diagram for Toray POF at room temperature

For higher strains the POF enters the domain of plastic deformation and eventually breaks. The breaking point varies from fibre to fibre, probably due to the fact that the measurement setup was not really adapted to perform tests on POF. More precisely, the clamping system regularly caused some damage on the fibre surface. However, in the elastic region the measurements were very reproducible. The E-modulus of the fibre can be calculated as follows:

$$E = \frac{\sigma}{\varepsilon}, \quad (3.10)$$

with ε the strain. For this type of POF the average $E = 2333 \text{ N/mm}^2$. When bending the fibre the highest tension will occur at the outer surface of the fibre and is given by :

$$\sigma = \frac{E \cdot r}{R}, \quad (3.11)$$

with r the radius of the fibre and R the bending radius. Hence the minimal bending radius $R_{min} = (E \cdot r) / \sigma_{max} = 1.7 \text{ mm}$. It is customary for manufacturers to take a 50 % margin and in that case the minimal bending radius would be 3.4 mm. However, POFs have been bent down to a radius of 2 mm without any damage.

Ahasi Luminous TB 62/125

The behavior of the Asahi POF is quite different, as can be seen in figure 3.15. It appears that this POF is more brittle and extremely sensitive to initial damaging by the clamping system. Therefore the different samples break at completely different strain points. It is also possible that the varying geometry of the cross section plays a role in the different plastic behavior of the samples. In the elastic region however the different samples show a more uniform behavior. The fibres deform elastically until 2.5 % strain. The average force needed for this strain is 0.56

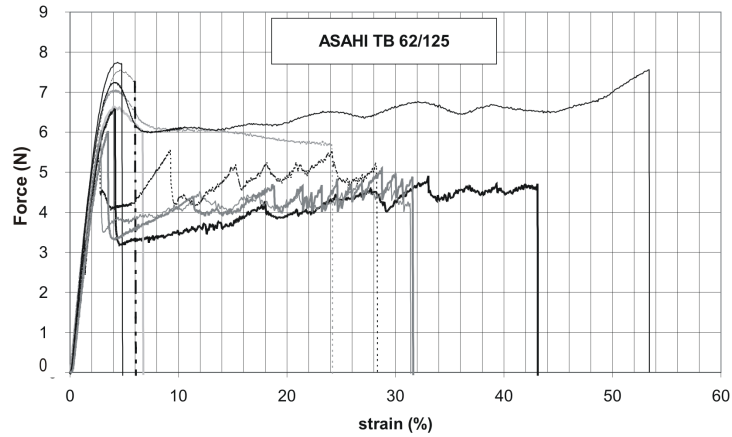


Figure 3.15: Strain-force diagram for Asahi POF at room temperature

N and hence $\sigma_{max} = 46 \text{ N/mm}^2$. The E-modulus is consequently 1825 N/mm^2 , definitely lower than the Toray modulus. The minimal bending radius becomes 2.5 mm, or with a 50 % margin 5 mm. We have bent POFs down to 2 mm radius without plastic deformation, but this had to be done with great care in order to avoid damaging the fibre.

3.4.3 Optical properties

3.4.3.1 Bandwidth issues

Data are transmitted through a fibre as a train of light pulses. Such a light pulse consists of a superposition of rays, each with a different angle of reflection $< \alpha_{lim}$. It can be seen from figure 3.1 that rays with a larger angle α have to travel a longer way to reach the end of the fibre than the rays with a smaller angle. Hence the different ray components of a pulse will arrive at different moments at the output of the fibre. In other words the pulse broadens as it travels along the fibre (figure 3.16). Beyond a certain distance the consecutive pulses will overlap and can not be distinguished from each other, hence the information carried by the signal is lost. It is easy to see that this pulse overlap will occur beyond a shorter fibre length as the data rate increases. In other words: the higher the data rate, the shorter the fibre has to be in order to transfer a correct signal. This relationship can be expressed by the following equation:

$$\text{Bandwidth} - \text{length product} = \text{constant} = B \cdot L, \quad (3.12)$$

with B the bandwidth and L the length of the fibre. The bandwidth of a transmission line is defined as the highest possible frequency of a sinusoidal intensity modulated signal, that will be received at the end of the transmission line with a decrease of modulation depth of less than 3dB. Maximal bandwidth and bit rate

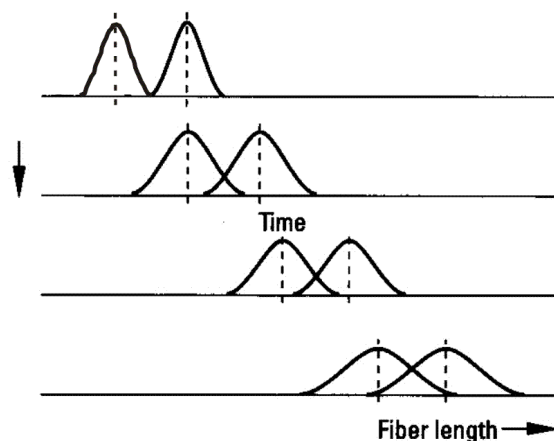


Figure 3.16: Pulses broaden due to dispersion and eventually overlap

are directly related by the following (approximative) rule : [29]:

$$\text{Bitrate} = 2B \quad (3.13)$$

The phenomenon of pulse broadening caused by the different angles of reflection for the different modes is called modal dispersion. It can be described by means of the delay difference $\delta\tau$ that expresses the difference in propagation time for the slowest and the fastest mode.

$$\frac{\Delta\tau}{L} \approx \frac{n_1 - n_2}{c}, \quad (3.14)$$

with c the speed of light in vacuum. For the considered POFs the delay time difference is about 270ns/km. The bandwidth is at least half the bit rate so:

$$B \approx 2\Delta f \approx \frac{1}{\Delta\tau} \quad \text{and hence : } \Delta f \cdot L = \frac{c}{2(n_1 - n_2)} \quad (3.15)$$

For the used POFs this means a bandwidth-length product of about 1.8 MHz·km. Hence the maximal bit rate that can be transmitted through 1 meter of POF is 3.6 GBit/sec, which is clearly sufficient for most optical interconnect applications. Besides modal dispersion, other mechanisms can cause pulse broadening. It was noticed that even for single mode fibres some dispersion effects occurred. This is due to the non-monochromaticity of the used light emitters and hence this phenomenon is called chromatic dispersion. It can be subdivided into two phenomena: material dispersion and waveguide dispersion. Material dispersion is caused by the fact that the refractive index of a material is wavelength dependent. It can be shown that a disturbance of a wave travels with a velocity, called the group velocity, that is different from the phase velocity of the wave. Since the group velocity

is a function of the refractive index of the material the different spectral components of the pulse propagate at different speeds, and eventually arrive at different moments at the end of the fibre. Yet, even if the refractive index would not be dependent on the refractive index the different spectral components would travel at a different group velocity. This phenomenon only occurs in waveguides and is hence called waveguide dispersion. It is caused by the fact that the group velocity is dependant on the wavelength, even with the refractive index constant. The greater the wavelength, the more the light penetrates into the cladding, in which the phase velocity is higher. Hence longer wavelengths will propagate faster, even though by the same mode. However, in highly multimodal fibres like the considered POF, the effect of chromatic dispersion is negligible compared to intermodal dispersion [17].

3.4.3.2 Light propagation in POF

In order to understand the optical properties of a fibre it is relevant to know the propagation properties of light inside the fibre. It is by understanding the behavior of the light in the POF that phenomena like transmission and bending losses can be explained. As explained in section 3.1, the considered POFs are highly multimodal. Whether all the possible modes are excited depends on different factors. In the first place the used light source defines the "initial conditions": if a light source launches light over a broad angular range many modes of the fibre are excited. On the other hand, if light is emitted at a narrow angle only a part of the modes are excited, and it takes a certain propagation distance to "fill up" the other modes. How fast this process occurs depends on how fast light power is converted from one mode to another. This mode coupling is induced by some intrinsic factors of the fibers, like irregularities in the structure of the fibre or at the core-cladding interface, and by external factors like bending or pressure. Eventually the light in the fibre will evolve to an Equilibrium Mode Distribution, independent of the initial launching conditions. In order to investigate this behavior, experiments were carried out making use of two light sources with a different emission pattern: Resonant Cavity Light Emitting Diodes (RCLED) and Vertical Cavity Surface Emitting Lasers (VCSEL).

Resonant Cavity Light Emitting Diodes RCLEDs are "enhanced" light emitting diodes: by placing the (light emitting) active layer between two mirrors the efficiency of the diode increases (figure 3.17). The resonant cavity, formed by these two mirrors, is responsible for an enhancement of the extraction efficiency: a larger part of the photons emitted by the active layer can escape from the diode into the air [30]. Moreover the emitted light beam is narrower than the lambertian emission pattern of a classical LED [31]. A Total quantum efficiency of 22.3 % (emitted photons/total injected electrons) has been achieved for AlGaAs-based RCLEDs with 2 mm diameter [32]. Smaller AlGaAs-based RCLEDs (diameter 70-40 μm), especially designed for maximal power coupling into the numerical aperture of a POF (0.5), have been developed at our department. The overall

quantum efficiency of the RCLEDs was about 10 %. About $\pm 27\%$ of the emitted light is launched into the N.A. of the fibre, resulting in a maximum overall quantum efficiency of 2.7 % into the POF. The overall quantum efficiency into the POF is defined as the number of photons in the POF divided by the number of electrons injected in the RCLED [33]. The wavelength is 980 nm and these devices have been produced in 8×8 arrays. The issue of the RCLED-to-POF coupling will be treated in more detail in Chapter 5.

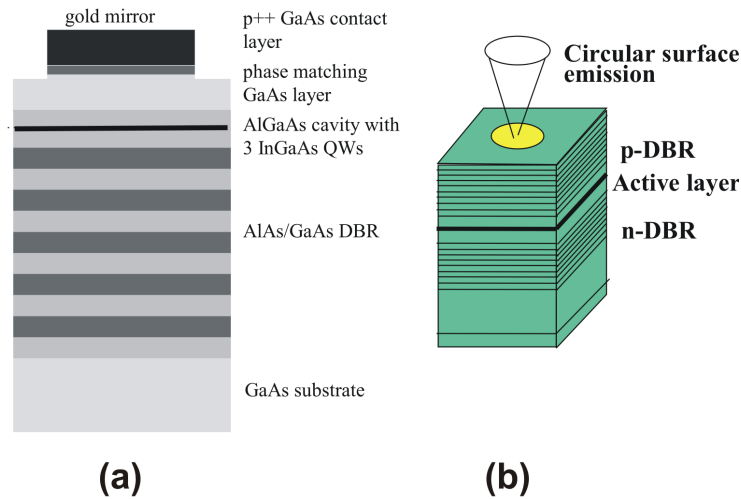


Figure 3.17: (a): layer structure of the used RCLEDs, (b): schematic layer structure of a VCSEL

Vertical Cavity Surface Emitting Lasers Similar to a RCLED a VCSEL consists of an active layer sandwiched between two mirrors. Here however, the active layer and the mirrors (both Distributed Bragg Reflectors, reflection about 99 %, figure 3.17) are designed in such a way that a lasing effect occurs when a current above threshold is injected. As a result a low-divergence light beam is emitted. The AlGaInP-based VCSELs used for the following experiments have been developed in the European Esprit long term BREDELS project [34]. They have a wavelength of 663 nm and are produced in 1×8 arrays. The diameter of the aperture is $15 \mu\text{m}$.

RCLEDs and VCSELs: which emitter to choose for a parallel POF-based optical interconnect link? It is not in the scope of this PhD study to present a thorough discussion about the choice for the best light source for a short distance parallel interconnect link. However, this choice has its consequences for the design of the optical pathway. Hence it is certainly appropriate to summarize and compare some of the properties of VCSELs and RCLEDs. Main issues to be

discussed are efficiency, speed, reliability, manufacturability, uniformity

- **Efficiency:** Compared to the achievable 3.7 % overall quantum efficiency into the numerical aperture of a POF for a RCLED, the VCSELS show a better result, at least if the injected drive current exceeds the threshold current. A VCSEL has a typical total extraction efficiency of about 50 %. In addition the light is emitted in a cone with a typical divergency of $10\text{-}15^\circ$, hence all the light falls into the N.A. of the POF. As a result a total quantum efficiency of 45-50 % into the fibre is a typical value. However, if a VCSEL is driven with a current lower than its threshold current, it is more appropriate to use a RCLED since RCLEDs are more efficient than non-lasing VCSELS. It is clear that for such small drive currents the emitted power is low. Hence a lot will depend on the amount of optical power needed at the detector end of the link. Transmission losses in the waveguide and coupling efficiency play a decisive role in this matter. Hence the specifications of the waveguide, the used wavelength, the detector diameter and accuracy of the different alignments weigh heavily on the selection of an adequate light source ².
- **Speed:** RCLEDs and VCSELS with the same diameter can be modulated at about the same speed [33]. Yet, in practice VCSELS are mostly much smaller than RCLEDs and hence faster. Moreover if a bias drive current is used the VCSEL remains above threshold and the modulation speed increases greatly (up to tens of GHz). However, chip interconnects demand a low power consumption and hence a bias current is to be avoided. The VCSEL manufacturers are tackling this problem with a continuous attempt to reduce the threshold current.
- **Manufacturability:** The structure of a RCLED is in general simpler than that of a VCSEL. A VCSEL has two complicated DBRs while a RCLED has only one more simple DBR. E.g. the DBR of the RCLEDs grown in our lab consists of 5 pairs only, while a typical VCSEL DBR has tens of pairs. The manufacturing complexity for VCSELS makes it more difficult to obtain uniform arrays. In the early days a 10 % non-uniformity was achieved. However, this number is decreasing rapidly and has reached a few percent, comparable to RCLEDs. Yet, due to their relative simple structure RCLEDs are intrinsically cheaper and extremely reliable devices.

Conclusion: Although RCLEDs are outclassed by VCSELS (speed and efficiency) they can offer a cheap and reliable solution for short distance parallel links, especially in configurations where the speed requirements are modest. (e.g. 622 Mbit per second per channel)

²A more precise elaboration on the calculation of the trade-off current can be found in [33]

Far field emission pattern experiments When light is coupled into a POF it undergoes several phenomena. As has been mentioned in paragraph 3.1 and 3.4.3.1 it propagates in distinct modes, each with a different group velocity. The power distribution of these modes is not invariable, but changes as the wave propagates along the fibre. Beyond a certain distance, the so called coupling length L_C , the distribution reaches a "steady state": the Equilibrium Mode Distribution (EMD). Beyond L_C the modes are fully coupled and the power distribution is independent of the launching conditions. The varying power distribution finds its cause in several mechanisms. In the first place higher order modes (larger angle θ) travel over a longer distance to cover a certain fibre length L , than the lower order modes. It is easy to see from figure 3.1 that if a ray parallel to the symmetry axis of the fibre travels over a length L , the ray with angle θ travels over a distance $L/\cos(\theta)$. For a fibre with NA 0.5 this means a 6 % longer way for the highest order mode. As a consequence the higher order modes are absorbed more than the lower order ones. Besides that, the higher the mode, the more it is reflected at the core cladding interface. The number of reflections per unit distance traveled is given by:

$$N = \frac{\tan \theta}{2r} \quad (3.16)$$

This gives for a fibre with NA 0.5 and diameter 100 μm , 3600 reflections per meter. Even within the angle of total internal reflection, reflections are not perfect (10^{-5} to 10^{-4} loss per reflection) and some power is lost. Due to the large number of reflections these losses are higher for higher order modes [35, 36]. Finally one can take the effects of the Goos-Haenchen-Shift into account: rays reflecting at the core-cladding interface penetrate somewhat in the cladding, and the greater the angle of incidence, the deeper the penetration. Since the absorption loss in the cladding is substantially higher than in the core [35], this causes extra losses. Considering the totality of these effects it is clear that higher order modes will be attenuated substantially more than lower order modes and that a large part of the power in the EMD is carried by lower order modes. However, the above described mechanisms are not sufficient to describe the evolution towards EMD. As a result of fibre anomalies such as microbends, cracks, microvoids, diameter variations, roughness of the core-cladding interface and density fluctuations of the polymers, the light is scattered as it propagates along the fibre. In this way power is exchanged from one mode to another. This is called mode coupling. It appears that the core-cladding interface roughness is the main source of light scattering [37]. This phenomenon was described by Gloge in 1972 [38, 39] who used a diffusion model (analogous to a diffusion process known in e.g. thermodynamics) to describe light propagation in fibres. This model includes the angle(mode) dependent attenuation as well as mode mixing processes. Gloge assumed that rays reflected at the core-cladding interface do not follow Snell's law but their angle is changed slightly according to a Gaussian random distribution. This means that power is mainly coupled from one mode to an adjacent mode. This also means that higher order modes have more chances to be scattered into the cladding than lower order modes. Eventually the higher order modes will be attenuated strongly until EMD

is reached. This results in an increased bandwidth. Whereas the bandwidth is inversely proportional to the fibre length in the first part of the POF, beyond the coupling length it becomes inversely proportional to the square root of the fibre length. The distance L_C over which EMD is reached depends on the strength of the coupling: the stronger the scattering (the lower the quality of the fibre) the faster EMD is reached. By launching the light with an emission pattern close to EMD the coupling length can be reduced. Experiments to measure L_C have been carried out [40] and yield values of 15-20 meter for a PMMA step index POF with a NA of 0.5 and a diameter of 1 mm. This is short compared to glass fibre which has a typical L_C of several kilometers.

For POF lengths up to 1 meter EMD will never be reached. Hence the mode distribution depends strongly on the launching conditions. In order to investigate this issue, several experiments were carried out. RCLEDs at 980 nm wavelength and VCSELs at 663 nm were coupled to 1 meter long Toray and Asahi POFs and the far field emission pattern was measured. This is done by rotating a light detector around the end facet of the fibre, with a rotation radius of ± 30 cm. Then, consecutive pieces of 10 cm were cut and the far field pattern was measured. In this way the evolution of the mode distribution during the light propagation through the fibre can be appreciated.

From figure 3.4.3.2 we can see that already after a short piece of POF (10 cm) the power distribution changes dramatically compared to the launching pattern. This can be partially explained by calculating the Fresnel transmission and reflection coefficients for the plastic/air interface [41]. Light with increasing incidence angle

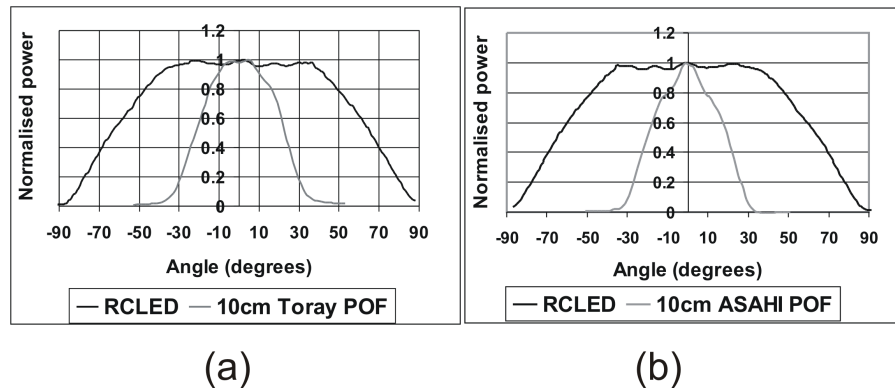


Figure 3.18: Far field emission pattern of 10 cm POF compared to the RCLED pattern.
(a) Toray POF (b) Asahi POF

θ will be reflected more. At angles close to 90° the reflection is total. However, within the aperture of the POF, (-30° to 30°) the reflection coefficient stays low (typical 4 %) and still the mode pattern changes from a quasi Uniform Mode Distribution (all angles within the aperture carry the same power) to a rapidly decaying curve. Obviously the higher order modes are already strongly attenuated in the first 10 cm. Since the distance is too short for considerable absorption losses, the loss is most likely due to scattering and non perfect reflections at the core cladding

interface. We can also note from figure 3.4.3.2 that there is some power carried at angles larger than the numerical aperture. Rays outside the numerical aperture transmit a portion T to the cladding each time they reflect on the core-cladding interface. T is given by [1]:

$$T = \frac{4\sin\theta\sqrt{\sin^2\theta - \sin^2\theta_c}}{(\sin\theta + \sqrt{\sin^2\theta - \sin^2\theta_c})^2} \quad (3.17)$$

A plot of this function for POF with a NA of 0.5 can be seen in figure 3.19. Note that the loss increases rapidly for angles larger than the 20° angle of total internal reflection. For a ray with an angle of 21° e.g. the loss is 70 %. This means that

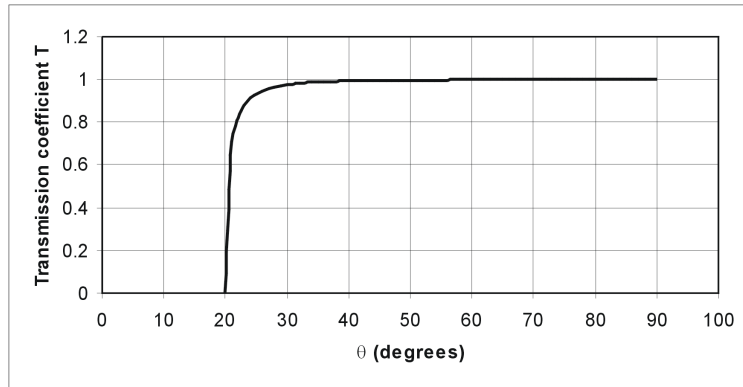


Figure 3.19: Transmission coefficient into the core cladding interface as a function of θ for refracting rays

after 4-5 reflections almost nothing remains of this ray. Following equation 3.16 it bounces about 330 times in a 10 cm piece of $116 \mu\text{m}$ core POF, for a $60 \mu\text{m}$ core POF about the double. Hence there are no refracted rays anymore in the core that could be responsible for the light outside the NA of the fibre. Probably this light is caused by so called cladding modes: rays that are coupled into the cladding and that satisfy total internal reflection conditions at the cladding-air interface ($\sin\alpha \approx 1/1.5 \Rightarrow \alpha_c(\text{plastic} - \text{air}) = 40^\circ$). We can also notice in figure ?? that the contribution of the light outside the NA is lower for the Asahi POF than for the Toray POF. This is in agreement with the cladding modes assumption: the cladding of the Asahi POF is 6 times thicker than that of the Toray POF. Since the attenuation of the light in the cladding is clearly higher than in the core it is logical that cladding modes will attenuate faster in fibres with thicker cladding. It is of course also possible that part of the light measured outside the NA is caused by scattering at the core-cladding interface.

We can see the same effect for longer pieces of POF. After 1 meter of Asahi POF the cladding modes have disappeared completely (figure 3.21) while for the Toray POF there is still power above 30^0 (figure 3.20). These figures also prove the attenuation of higher order modes by showing narrower patterns for larger fibre lengths. This is particularly clear for the Toray POF. It is less clear for the Asahi

case, in particular for 1 meter POF length. Here, the far field power is very low

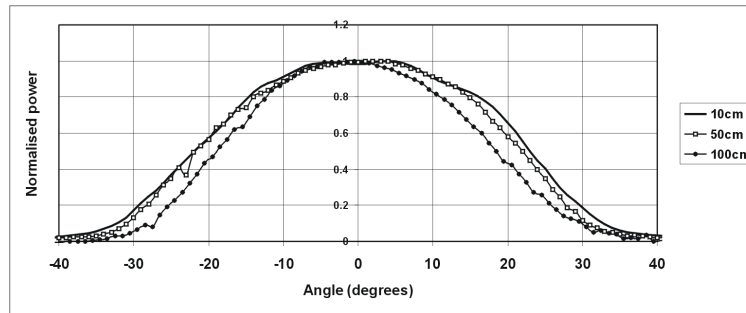


Figure 3.20: Far field of Toray POF for different fibre lengths with RCLED light source

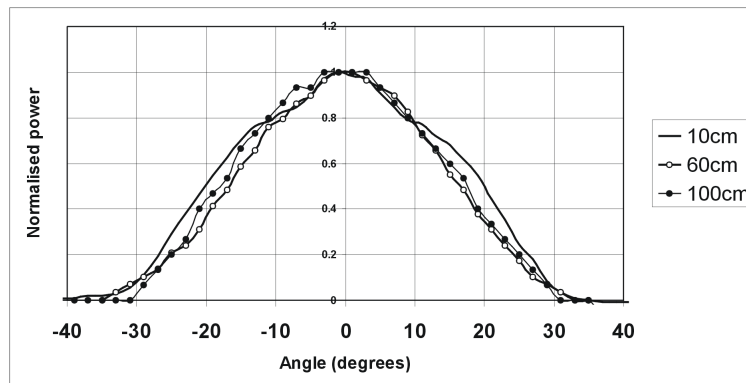


Figure 3.21: Far field of Toray POF for different fibre lengths with RCLED light source

(nanoWatts) and hence the pattern is difficult to measure due to its sensitivity to fluctuations caused by scattering effects and changes in the background light. (In general the fluctuations on the measured patterns can be explained by scattering at the imperfect end facet of the POF)

The effect of mode coupling through scattering can be seen in figures 3.22 and 3.23. Light is coupled in with a narrow VCSEL beam. The power in the side lobes of the laser is probably too low to couple a considerable amount of power into cladding modes, and hence no power is measured in the fibre far field pattern above 30° . What can be noticed though, is the broadening of the pattern as the fibre gets longer. This can only be explained by mode coupling through scattering. It has to be noticed that for the Asahi fibre there is an initial broadening in the first 20 cm, but for longer lengths this broadening is not so obvious. How long it takes to reach EMD can not be derived from these patterns. To that end, experiments with longer POFs are necessary. These experiments have been carried out for the Toray POF in [42] and a coupling length of 7 meter is estimated. A measurement of EMD can be seen in figure 3.24. Notice that the field is limited between -25°

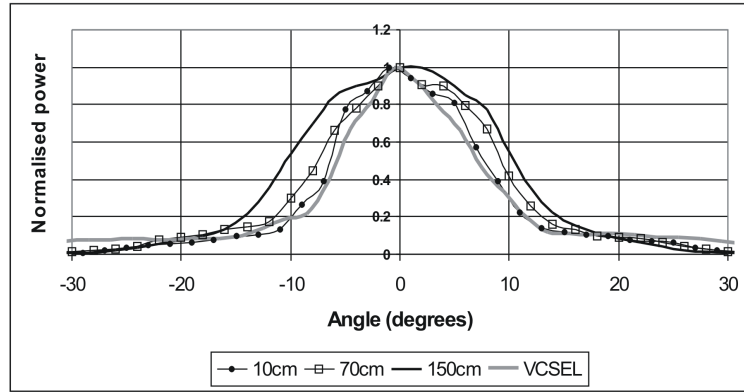


Figure 3.22: Far field Toray POF for different fibre lengths and with VCSEL light source

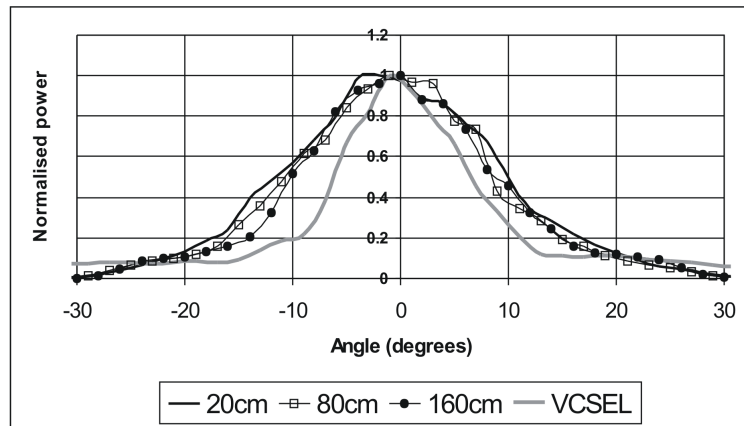


Figure 3.23: Far field Asahi POF for different fibre lengths and with VCSEL light source

and $+25^\circ$, hence higher order modes are completely attenuated.

The main conclusion of this experiment is that for the interconnect distances we consider (10 cm up to 1 meter) the mode distribution, and hence the emission pattern, depend strongly on the launching conditions. This is particularly important for the coupling between fibre and detector since issues like coupling efficiency and crosstalk depend on the fibre emission pattern.

3.4.3.3 Transmission losses

When designing an interconnect link it is of extreme importance to know the power loss when light is propagating in a POF. Therefore we experimentally determine the attenuation coefficient of POF, first by means of a white light source and a spectrum analyzer, secondly by using RCLED and VCSEL light sources.

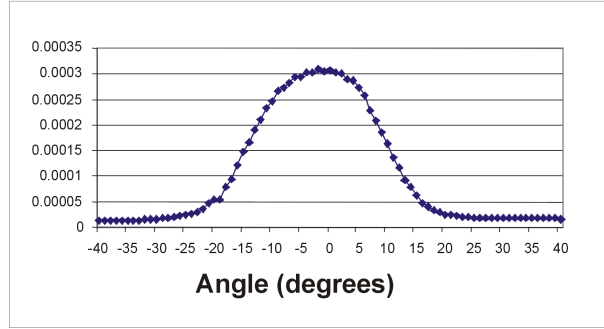


Figure 3.24: EMD far field of Toray POF

As mentioned in paragraph 3.2, transmission losses are caused by two phenomena: scattering and absorption. In the first part of the fibre however, we have to add losses due to so called tunneling rays. Rays propagating in fibres can be split up in two groups: meridional rays that cross the symmetry axis of the fibre (and hence stay in one plane), and skew rays that do not cross the axis but follow an helical path through the fibre. Part of these skew rays fulfill apparently the condition of total internal reflection but still radiate energy to the cladding. This happens when the skewness is too high [1] and the curvature of the core surface induces reflection losses. These rays are called tunneling rays. In ref [1] the part of the fibre where tunneling rays are present is called the zone of spatial transient, beyond that zones the light is propagating in a spatial steady state. An estimation of the spatial transient length L_t with a diffuse light source is given by;

$$L_t = \frac{r}{2\theta_c} e^{V/2}, \quad (3.18)$$

with r the radius of the core, θ_c the critical angle for total internal reflection, and V the V-number of the fibre:

$$V = \frac{2r\pi}{\lambda} \sqrt{n_{co}^2 - n_{cl}^2} = \frac{2r\pi}{\lambda} .NA \quad (3.19)$$

For the Toray POF: $V=185$, $L_t = 1.2 \cdot 10^{33}$ km and for the Asahi POF: $V=92$, $L_t = 4.10^{12}$ km at 980 nm wavelength. These are enormous values compared to e.g. standard multimode glass fibres that have a transient length of 300 meter (with $V = 20$, $r=25 \mu\text{m}$ and $\theta_c = 0.14$) The above mentioned equation starts from the assumption that when illuminating the fibre with a diffuse source, half of the power is carried by skew rays. Hence this large value can be explained by the high number of modes in POF. In practice there are always skew rays present in the POF since all the rays (meridional and skew rays) will be extinguished by scattering and absorption before the transient length is reached.

Experimental results Transmission losses in the first meter POF were measured using the cut back method. A white light source was coupled in a 2 meter

long Toray POF and the outgoing power as a function of the wavelength was measured with a spectrum analyzer. Then a piece of 150 cm was cut and the spectrum was measured again and compared with the first spectrum. In this way the loss per length can be determined for each wavelength. The attenuation spectrum can be seen in figure 3.25: Attenuation at 980 nm was about 11 dB/meter, 1.1 dB/meter

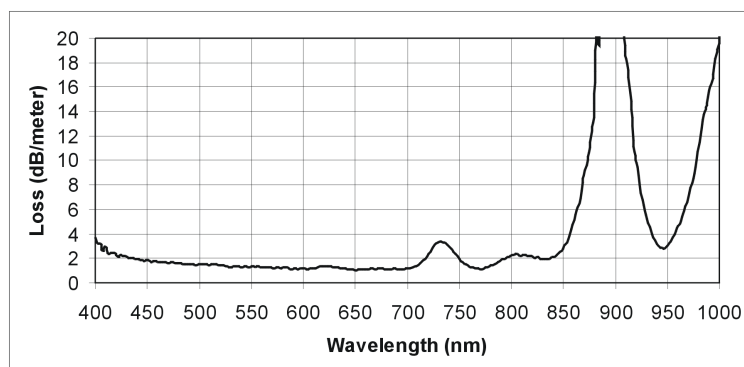


Figure 3.25: Attenuation spectrum Toray POF

at 633 nm and 1.35 dB/meter at 663 nm. In order to test the validity of these measurements another experiment was carried out [42]: the transmission loss at 633 nm was measured with a Helium-Neon laser. The POF was wound several times around a cylinder to introduce mode coupling and fill up the aperture. An average value of 1.1 dB/meter was found, which corresponds with the first experiment.

In order to estimate the transmission losses appearing in short links using VCSELs and RCLEDs similar experiments were carried out. Pieces of 1.5 meter POF were cut down with steps of 10 cm and the outgoing power was measured. A RCLED at 980 nm wavelength and a VCSEL at 663 nm were used. In case of a constant attenuation coefficient over the length of the fibre, the light power evolves following:

$$P(z) = P_0 e^{-\alpha \cdot z} \quad (3.20)$$

With z the length of the fibre, P_0 the initial power and α the (constant) attenuation coefficient. If the power is expressed on a logarithmic scale this relationship becomes linear. Hence, by expressing the light power in $\text{dBm} = 10 \cdot \log(P/1\text{mW})$, one can simply obtain the loss in dB/length by taking the slope of the straight line in the z -Power diagram. The power in function of z for a Toray POF with VCSEL light can be seen in figure 3.26. The power decreases almost linearly and taking the tangent of the straight line yields a value of 1 dB/meter (averaged over different measurements). However, looking in more detail at the curve shows that the curve is slightly bent down and that hence the attenuation coefficient is not completely constant. Taking the derivative $dP(z)/dz$ gives the extinction per unit length at a position z in the fibre. A plot of dP/dz as a function of z is given in

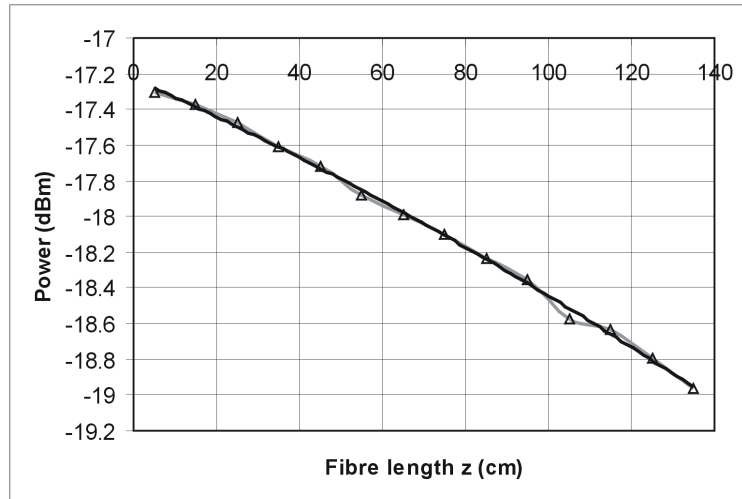


Figure 3.26: Outgoing power of a Toray POF as a function of the length, with a 663 nm VCSEL light source

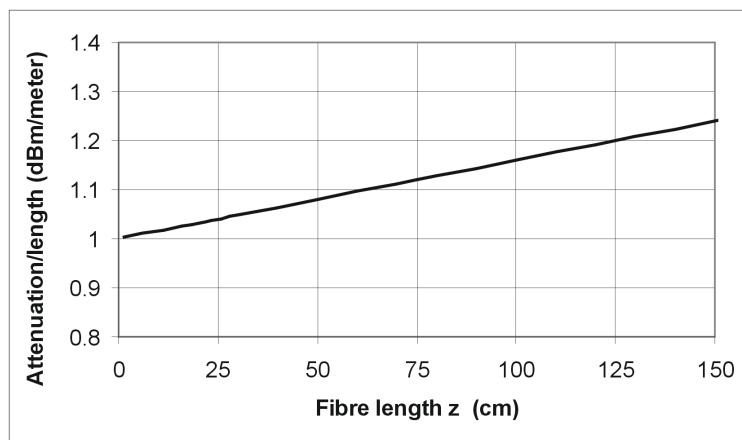


Figure 3.27: Attenuation coefficient as a function of the fibre length for a Toray POF, 663 nm VCSEL light source

figure 3.27. As we can see the attenuation/length increases slowly with increasing z . Probably this is due to power transfer from lower order modes to higher order modes by scattering, as we concluded from the far field experiments. Higher order modes are attenuated more and hence the attenuation coefficient increases slightly when the light propagates in the fibre. The behavior of the attenuation coefficient at 663 nm in the Asahi POF is slightly different. As can be seen in figure 3.28 $P(z)$ decreases linearly. An average attenuation/length of 1.3 dB/meter was found. This is in agreement with the far field measurements we made for this type

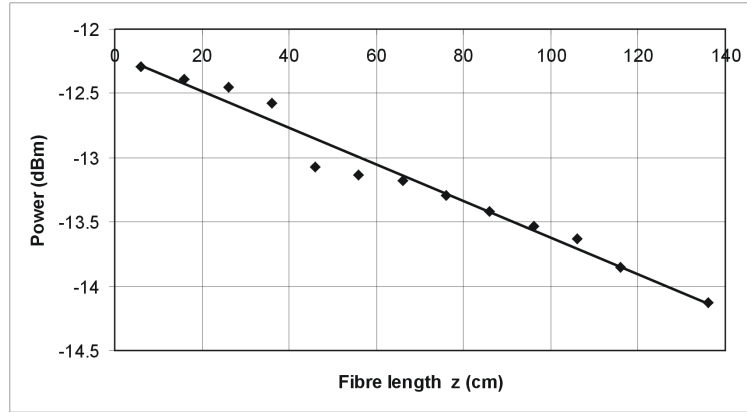


Figure 3.28: Outgoing power of an Asahi POF as a function of the length, with a 663 nm VCSEL light source

of POF: the mode distribution did not seem to change a lot after 20 cm. The power attenuation with RCLED coupling shows a completely different behavior. Looking at the power evolution at 980 nm in the Toray POF one notices that the power-z relationship is not linear but follows an exponential curve (figure 3.29). Calculating the derivative $P(z)/dz$ yields a diagram that can be seen in figure 3.30. dP/dz is a descending straight line and hence the extinction decreases linearly

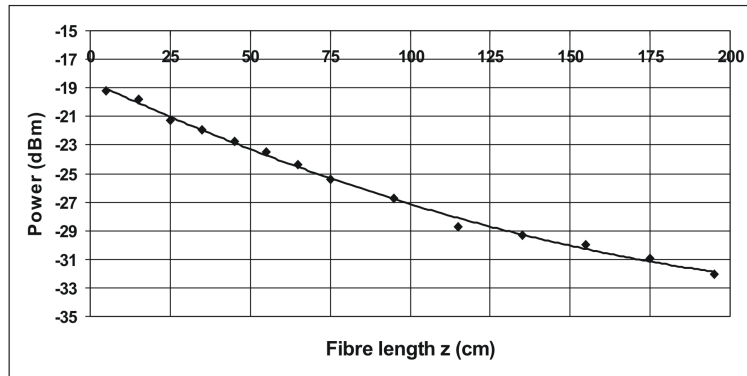


Figure 3.29: Outgoing power of a Toray POF as a function of the length with a 980nm RCLED light source

as the light propagates in the fibre. This can be partially explained by looking at the far field measurement (figure 3.20) with 980 nm RCLED light. The vanishing cladding- and higher order modes cause decrease of the extinction coefficient as a function of z , since they are the most attenuated. However, the disappearance of higher order modes cannot explain the great rate at which the absorption coefficient decays. Whereas the initial value is 11 dB/meter, after 1 meter it becomes

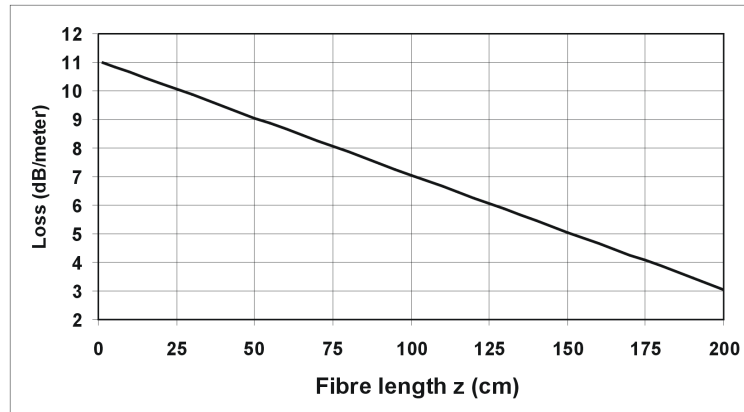


Figure 3.30: Attenuation coefficient as a function of the fibre length for a Toray POF with 980 nm RCLED light source

7 dB/meter. A look at the spectrum of the LED clarifies this phenomenon (3.31). Wavelengths between 940 and 1020 nm are clearly present. Given that the ab-

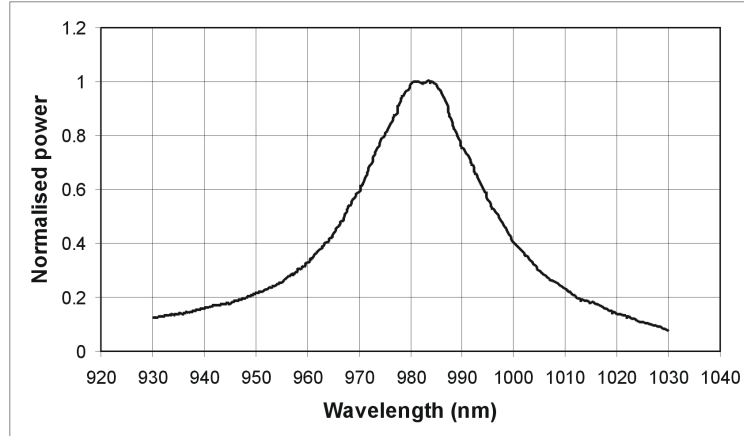


Figure 3.31: Spectrum of the 980 nm RCLED

sorption strongly varies over this range, as can be seen in spectra provided by PMMA POF producers (figure 3.3) and by our own spectral measurement (figure 3.25), the different wavelength components will be attenuated at a clearly different rate. In other words, the spectrum of the RCLED light will be altered over the length of the fibre. Wavelengths with a lower attenuation coefficient will, beyond a certain propagation length, carry most of the power even if their initial power contribution was low. This can be easily understood by means of the following example. Let us say that the RCLED emits 0 dBm power (=1 mW) in a narrow band around 982 nm (centre wavelength of the spectrum), then it will emit e.g.

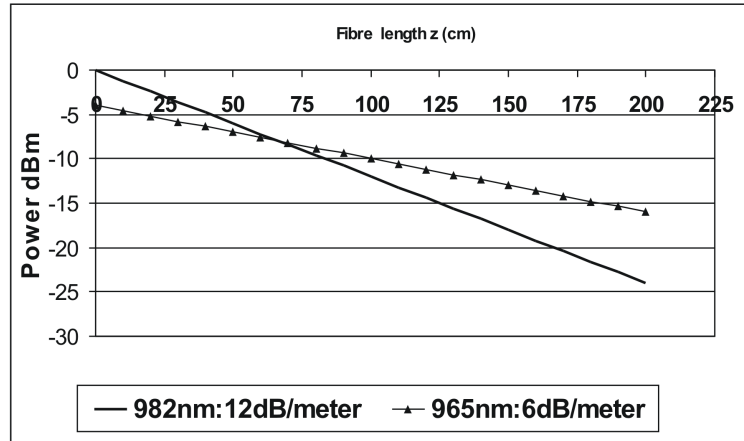


Figure 3.32: Power evolution of two spectral components of the RCLED in function of fibre length

-4 dBm at 965 nm. From figures 3.3 and 3.25 we can estimate that losses will be around 12 dB/meter for 980 nm and around 6 dB/meter for 965 nm. Comparing the power at both wavelengths as a function of the propagation length in the fibre one can see that beyond 75 cm the 965 nm wavelength carries more power than 980 nm. Hence the attenuation coefficient will evolve from a number close to the 980 nm coefficient to a lower value determined by the low loss wavelength components. For the Asahi POF a similar behavior with 980 nm RCLED light can be seen (figure 3.33). Here the attenuation/length varies from an initial 13 dB/meter to 7 dB/meter at $z = 1$ meter. Two main conclusions can be drawn

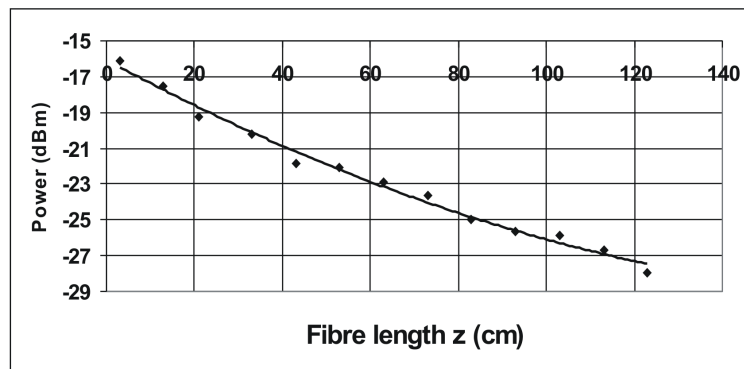


Figure 3.33: Outgoing power of an Asahi POF as a function of the length, with a 980 nm RCLED light source

from these loss measurements. When designing an optical link and calculating the power budget using an attenuation spectrum, one will make a fair estimation loss

of the transmission losses inside a fibre if a VCSEL is used, thanks to the VCSEL narrow spectrum (typical linewidth of 0.5 nm) If a RCLED is chosen as a light source one has to look carefully at its spectrum. For instance, in case of 980 nm RCLEDs, taking the 980 nm attenuation coefficient is a worst case approach, since part of the spectrum will be clearly less attenuated.

3.4.3.4 Influence of bends

Bends are important for two reasons: they can cause optical losses and can cause mode coupling resulting in a change in the mode distribution. Both effects have been studied experimentally.

Bending losses In a bend there are only leaky rays: all the rays independent of their reflection angle loose energy while propagating through the bend. These losses are caused by two phenomena: refraction and tunneling. From figure 3.34 it is easy to see that some rays that are below θ_c in the straight part of the fibre, exceed it in the bend and are hence refracted. They loose their power

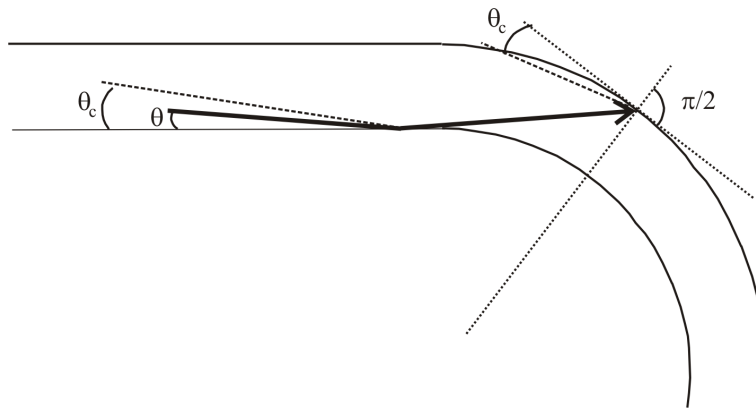


Figure 3.34: Bound rays can be refracted at a bend

following equation 3.18. The other rays, with $\theta < \theta_c$ in the bend, also radiate power due to a tunneling effect caused by the bent surface of the fibre. The effects of these phenomena have been studied experimentally. A Toray POF is wound around a cylinder with radius 5 mm. While the fibre is being wound the outgoing power is measured and hence the power loss in function of the bending distance is monitored. This experiment was repeated for 7.5 and 15 mm radius. The results can be seen in figure 3.35. Consider the case of $R/r = 96$ (equivalent to a bending radius of 5 mm). For a bending distance starting from 150 (corresponding to a bend of 90°) up to 1800 (corresponding to 3 full turns of 360°) the loss increases strongly due to refracted rays. Afterwards the loss evolves to a clearly slower growth solely caused by tunnelling effects. For the larger bending radii the same evolution occurs but the refraction losses are evidently lower since fewer rays will not satisfy the total internal reflection conditions. Notice that for a 90° turn at 5

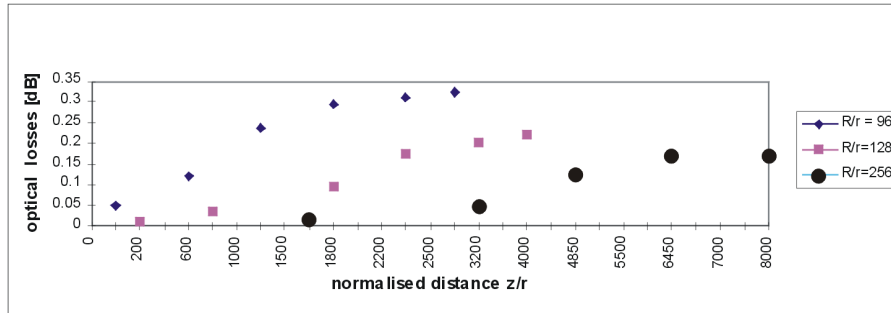


Figure 3.35: Bending losses for a Toray POF as a function of the bend length and for different bending radii

mm radius the loss is only 0.05 dB. In fact, down to a bending radius of 2 mm a loss of 0.1-0.3 dB for a 90° bend was measured. Similar values for the Asahi POF were found. These low values are due to the relatively large numerical aperture of POF. As a matter of fact these losses are negligible in the context of a power budget calculation for an interconnect link and hence small 90° bends are definitely acceptable.

Bends and modes Yet one more aspect of bends has to be looked at. It is known that bends are a source of mode coupling [1] and hence they can influence the mode distribution and as a consequence the far field emission pattern, which in turn influence the POF-detector coupling efficiency or cause optical crosstalk at detector level.

As we will see in the next chapter, typical places to introduce 90° bends in an optical pathway, are just after the light source and just before the detector. Hence experiments were carried out to simulate these situations both with a VCSEL and with a RCLED source. We focused on bends with a 2 mm bending radius since this is about the smallest we can go from a mechanical point of view. In the case

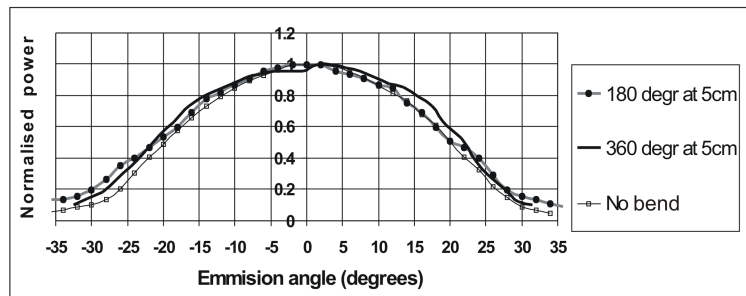


Figure 3.36: Far field pattern of a Toray POF bent at 5 cm from the detector end, for different bend lengths, with 2 mm bending radius and 850 nm RCLED light source

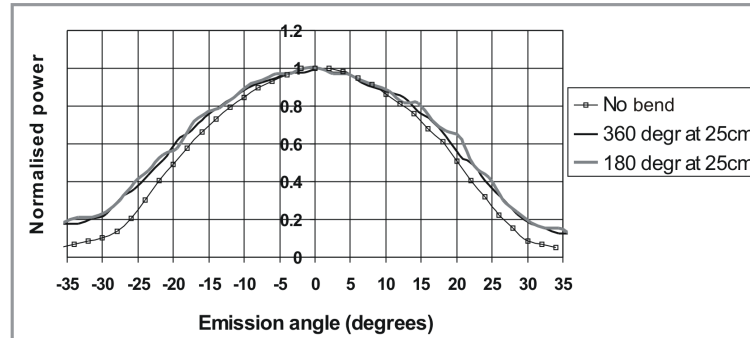


Figure 3.37: Far field pattern of a Toray POF bent at 25 cm from the detector end, for different bend lengths, with 2 mm bending radius and a 850 nm RCLED light source

of a RCLED source the mode distribution is only slightly disturbed by a bend. A 50 cm long Toray POF was bent at 5 cm from its end (detector side) with a 2 mm bending radius. As can be seen from figure 3.36 the far field gets slightly broader at a turn of 180° , and a limited amount of light gets refracted into the cladding. For a 90° turn no difference with the “bendless” situation was measured. A turn of 360° gives no clear difference compared to a 180° turn. The same effects can be seen when the fibre is bent at larger distance from its end facet. The same experiment was done at 25 cm from the end of the POF and similar results were obtained (see fig 3.37). Obviously the mode coupling effects in the straight fibre are not strong enough to annihilate (over 25 cm) the changes that occurred at the bend. Also the excited cladding modes are probably still present at the end of the fibre. More clear effects can be seen when coupling the POF to a VCSEL. A 1 meter long Toray POF was coupled to a 663 nm VCSEL. Figures 3.36 and

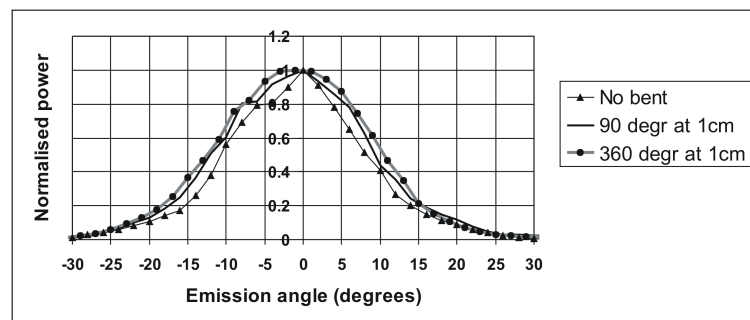


Figure 3.38: Far field pattern of a Toray POF bend at 1 cm from the detector end, for different bend lengths, with 2 mm bending radius and a 663 nm VCSEL light source

3.37 show that the far field broadens somewhat in a bend, but stays within the numerical aperture. Bending the fibre at different distances from the end yields

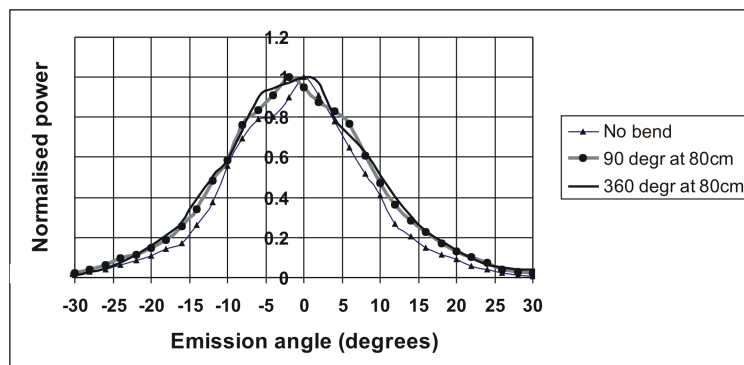


Figure 3.39: Far field pattern of a Toray POF bend at 80 cm from the detector end, for different bend lengths, with 2 mm bending radius and a 660 nm VCSEL light source

similar results. Here again, the disturbance generated in the bend is maintained as the light propagates in the fibre. Note that the first 90° turn seems to be the most important for the mode coupling effects: winding the POF an extra 270° turn does not cause a clear change.

As a conclusion we can state that 2 mm bends do not cause real problems for interconnect using small-diameter POF. Losses are limited and the change of the emission pattern seems only important when the mode distribution consists mostly of lower order modes. The far field emission pattern stays mainly within the numerical aperture and hence unexpected problems with optical crosstalk at the detector side will not occur.

3.4.3.5 Influence of temperature

Due to the polymer structure of POF, it is relatively sensitive to heat. Manufacturers generally specify a maximal working temperature of 70° C for PMMA POF. Heating measurements on the Toray POF have been performed [42]. A 2 meter long POF was heated in a closed box. Up to 75° C no optical degradation was observed. At 85° C optical losses appear and at 90° plastic deformation occurs. The experiments were carried out in a relatively dry environment. However, the combination of moisture and heat decreases in general the maximal working temperature. Heat-moisture test are hence necessary to get a complete picture of the POF's heat resistance.

3.5 Conclusions

In this chapter we have studied in detail some relevant properties of two kinds of small-diameter POF that could be used for the fabrication of parallel short distance interconnect links. Comparing the specifications and the experimental results of these POFs yields the results listed in table 3.1. In general both POFs

Table 3.1: Specifications small-diameter POF

	Toray PGR-125	Asahi Chemical Luminous TB62/125
core material	PMMA	PMMA
Cladding material	Fluorinated PMMA	Fluorinated PMMA
Index Profile	Step index	Step index
Core Diameter (μm)	aver: 116 range: 114-118	aver: 61 range: 54-68
overall diameter (μm)	aver: 125 range: 120-129	aver: 119 range: 105-135
Numerical aperture	0.5	0.5
Attenuation (dB/m @ 663 nm)	1	1.3
Minimal bending radius (mm)	2	2 brittle

show a similar behavior, except for the tolerance on the diameter and the relative brittleness of the Asahi POF. Especially the former might cause a problem for alignment purposes. Not that this is not an intrinsic problem of small core POF (as shown by the Toray POF) but entirely due to the fact that the Asahi POF is a prototype for which the production process is not optimized yet.

Bibliography

- [1] S. Allan W and J. D. Love, *Optical waveguide theory*. 733 Third Avenue, New York 10017: Chapman and Hall, 1983.
- [2] D. Gloge, "Weakly guiding fibres," *Applied optics*, vol. 10, pp. 2252–2258, Octobre 1971.
- [3] Y. Koike, "POF: From past to the future," in *Proceedings of the Seventh International POF Conference*, (Berlin), pp. 1–8, Octobre 1998.
- [4] W. Baierl, "Evolution of automotive networks," in *Proceedings of the 10th POF Conference*, (Amsterdam), pp. 161–168, September 2001.
- [5] N. Schunk, K. Panzer, E. Baur, W. Kuhlmann, K. Streubel, R. Wirth, and C. Karnutsch, "IEEE 1394b POF transmission system 500mbit/s versus 50m 0.3 NA POF," in *Proceedings of the 10th POF conference*, (Amsterdam), pp. 65–71, September 2001.
- [6] Y. Koike, "POF technology for the 21st century," in *Proceedings of the 10th POF Conference*, (Amsterdam), pp. 5–8, September 2001.
- [7] <http://www.firecomms.com>.
- [8] <http://www.infineon.com/pof>.
- [9] <http://www.luceat.it>.
- [10] <http://www.avagotech.com>.
- [11] N. Tanio and Y. Koike, "What is the most transparent polymer?," in *Proceedings 6th international POF conference*, (Paris), pp. 33–34, Octobre 1996.
- [12] Y. Koike and T. Ishigure, "Status and challenges of GI-POF in the data-com area," in *Proceedings of the 27th European Conference on Optical Communication*, vol. 1, (Amsterdam), pp. 72–73, Octobre 2001.
- [13] A. Appajaiah and L. Jankowski, "A review on aging or degradation of POFs: Polymer chemistry and mathematical approach," in *Proceedings of the 10th international POF conference*, (Amsterdam), pp. 317–323, Septembre 2001.
- [14] N. Schunk, K. Panzer, E. Baur, W. Kuhlmann, K. Streubel, R. Wirth, and C. Karnutsch, "IEEE 1394b POF transmission system 500Mbit/s versus 50m 0.3 NA POF," in *Proceedings of the 10th international POF conference*, pp. 65–71, 2001.
- [15] T. Ishigure, Y. koike, and J. W. Fleming, "Optimum index profile of the perfluorinated polymer-based GI polymer optical fibre and its dispersion properties," *Journal of lightwave technology*, vol. 18, pp. 178–184, february 2000.
- [16] <http://www.www.pofto.com/downloads/PRPOF.pdf>.
- [17] A. Weinert, *Plastic Optical Fibres*. Munchen, Germany: Publicis MCD Verlag, 1999.
- [18] J. Marcou, *Plastic Optical Fibres: Practical Applications*. Chisester, UK: John wiley and sons, 1997.
- [19] <http://www.fia-online.co.uk/pdf/Presentation/L4478.pdf>.
- [20] M. Ferenets, H. Myllymaki, K. Grahn, A. Sipila, and A. Harin, "Manufacturing methods for multistep index plastic optical fibre materials," *Autex Research Journal*, vol. 4, pp. 164–174, December 2004.
- [21] Y. Koike, T. Ishigure, and E. Nihei, "High-bandwidth graded-index polymer optical fibre," *Journal of lightwave technology*, vol. 13, pp. 1475–1489, july 1995.
- [22] M. Sato, T. Ishigure, and Y. Koike, "Thermally stable high bandwidth-graded-index polymer optical fibre," *Journal of Lightwave Technology*, vol. 18, pp. 952–958, July 2000.
- [23] O. Park and S. Im, "A new fabrication method of graded index polymer optical fibre preform," in *Proceedings of the 10th international POF conference*, (Amsterdam), pp. 341–347, September 2001.
- [24] F. G. van Duijnhoven and C. W. Bastiaansen, "Monomers and polymers in a centrifugal field: a new method to produce refractive-index gradients in polymers," *applied optics*, vol. 38, pp. 1008–1013, February 1999.

- [25] W. van Etten and J. van der Plaats, *Fundamentals of Optical Fiber Communications*. Hertfordshire, UK: Prentice Hall, 1991.
- [26] T. Statake, T. Arikawa, P. W. Blubaugh, C. Parsons, and T. K. Uchida, "MT multifiber connectors and new applications," in *Proceedings of the 44th Electric Components and Technology Conference*, (Washington D.C.), pp. 994–999, May 1994.
- [27] <http://www.agc.co.jp/lucina/english.Files/english.html>.
- [28] [HTTP://www.instron.us](http://www.instron.us).
- [29] J. Gowar, *Optical Communication systems*. Prentice Halls, 1984.
- [30] R. Bockstaele, T. Coosemans, C. Sys, L. Vanwassenhove, A. Van Hove, B. Dhoedt, I. Moerman, P. Van Daele, R. Baets, R. Annen, H. Melchior, J. Hall, P. Heremans, M. Brunfaut, and J. Van Campenhout, "Realisation and characterisation of 8x8 resonant cavity LED arrays mounted onto CMOS drivers for POF-based interchip interconnections.," *IEEE Journ. Sel. Topics Quant. Electr.*, vol. 5, pp. 224–235, March 1999.
- [31] R. Bockstaele, C. Sys, J. Blondelle, H. De Neve, B. Dhoedt, I. Moerman, P. Van Daele, and R. Baets, "Microcavity leds with an overall efficiency of 4 % into a numerical aperture of 0.5," in *LEOS Summer Topicals* (69-70, ed.), 1997.
- [32] H. De Neve, J. Blondelle, P. Van Daele, P. Demeester, R. Baets, and G. Borghs, "Recycling of guided mode light emission in planar microcavity light emitting diodes," *Appl. Phys. Lett.*, vol. Vol. 70-7, pp. 799–801, 1997.
- [33] R. Bockstaele, *Resonant Cavity Light Emitting Diode Based Parallel Interconnections*. PhD thesis, Ghent University , faculty Applied Sciences, Dept Information Technology, St-Pietersnieuwstraat 41 , 9000 Ghent, Belgium, 2000.
- [34] J. D. Lambkin, T. Calvert, B. Corbet, J. Woodhead, S. Pinches, A. Onischenko, T. Sale, J. Hosea, P. Van Daele, K. Vandeputte, A. Van Hove, A. Valster, and J. Mcinerney, "Development of a red VCSEL-to-plastic fiber module for use in parallel optical data links," vol. 3946, pp. 95–105, Jan. 2000.
- [35] C. A. Bunge, *Polymerfaser Dmpfuns- und Ausbreitungsmodell*. 1999.
- [36] C. Bunge, O. Ziemann, J. Krauser, and K. Petermann, "Effects of light propagation in step index polymer fibres," in *Proceedings of the 8th international POF conference*, (Chiba, Japan), pp. 113–117, July 1999.
- [37] C. Hahn, H. Poisel, and H. Karl, "Modelling and simulating transmission characteristics of polymer optical fibres," in *Proceedings of the 10th International POF Conference*, (Amsterdam), pp. 113–114, September 2001.
- [38] D. Gloge, "Optical power flow in multimode fibres," *The Bell System Technical Journal*, vol. 51, pp. 1767–1781, Octobre 1972.
- [39] D. Gloge, "Impulse response of clad optical multimode fibres," *The Bell System Technical Journal*, vol. 52, pp. 1767–1781, July-August 1973.
- [40] G. Jiang, R. Shi, and A. Garito, "Mode coupling and equilibrium mode distributions conditions in plastic optical fibre," *IEEE phot techn letters.*, vol. 9, pp. 1128–1130, August 1997.
- [41] F. Pedrotti and L. Pedrotti, *Introduction to optics*. 1992.
- [42] A. Van Hove, *Termination and Interconnection Technology for Parallel Optoelectronic Systems*. PhD thesis, Ghent University, Faculty Applied Sciences, Dept of Information Technology, Sint Pietersnieuwstraat 41, 9000 Gent , Belgium, 2001.

4

A connector for two-dimensional POF arrays: essential issues and design

WHEN designing a connector system for parallel POF links there are different possible routes to follow. Therefore we will commence this chapter by determining the requirements for an adequate connector. We will continue with summing up and comparing some essential options and choices that have to be considered when developing the connector design. Then a literature overview of existing connector and interfacing solutions for parallel fiber arrays and modules will be given. Finally a rough design and production scheme for a parallel POF connector system will be presented.

4.1 Requirements for an adequate connector design

The data system environment in which parallel connectors are to be used is characterized by two main constraints: space is limited and the temperature can go up to about 80°C. Controlling the effects of high temperature is principally a matter of choosing the right (combination of) materials and providing an adequate cooling system. It is not in the scope of this thesis to carry out an extensive study of possible connector materials. However, while developing a manufacturing method for connectors we bore in mind that this method should allow to use similar, if not the same, materials for the different components of the connector as well as for the fibers. In this way the thermal deformation of the connector caused by different coefficients of expansion is minimized. Therefore we will propose an all-polymer approach for the design, well knowing that an elaborate search for suitable polymers would be necessary later on.

On the other hand, the possibility to produce a compact connector system was of great concern to us, and hence our attention was mainly focused on this matter during the development of the manufacturing scheme. In addition, we took into account the following aspects of the production process where possible:

- **Manufacturability** Manual work should be omitted as much as possible since it increases the costs of a device considerably. Ideally a product is made in a fully automated way and with a high yield. Hence, when working out a manufacturing scheme, one should keep the idea of automation in the back of one's mind.
- **Simplicity** A connector system should be made in a simple way, minimizing the number of production steps and the number of connector components, again for cost reasons.
- **Reliability** A good device should perform continuously at the same (high) level during a long period and under different circumstances. However, this feature depends largely on the chosen materials and long-term research on the physical and chemical behaviour of these materials is imperative. The necessary time and evaluation techniques were not available during the research for this thesis and hence no thorough discussion about this matter will be given.
- **Scalability** Considering the future large number of (dense) optical channels between electronic chips and MCMs, it is of great importance that the proposed production technology stays applicable independent of the (growing) number of fibres in the arrays.

4.2 Some important choices to make

A multiple fibre connector has two main features: in the first place it aligns its fibres in an array with well-controlled pitch. In general, this alignment is assured in the central part of the connector, called the ferrule. Secondly, it contains a structure that aligns its fibre array to that of the mating connector or to a detector/emitter array. An example can be seen in figure 4.1, where a commercially available 1×8 MTTM ferrule is shown. The fibres are inserted in an accurate array of centrally located capillary holes. In addition, the ferrule contains part of the coupling alignment structure, namely the guide pin holes. Mating ferrules are aligned using steel guide pins that fit tightly in these holes alongside the fibre array (figure 4.2). Apart from the ferrule, a connector contains housing for protection

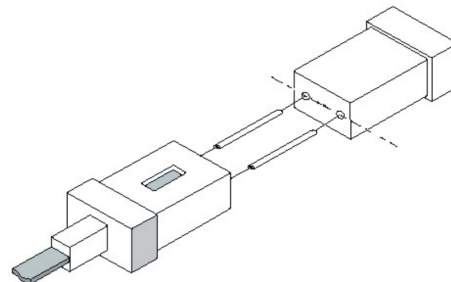
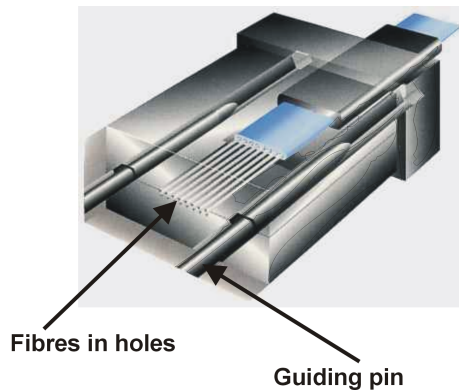


Figure 4.2: Coupled MTTM ferrules

Figure 4.1: Principle of a MTTM ferrule

against mechanical damage and dust¹. Although the design of a compact and reliable housing is of great importance, this is not in the scope of this thesis, and no further attention will be paid to it.

The principle of a central fibre array and peripheral alignment pins can certainly be copied for a parallel POF interconnect link. However, in such a link two kinds of interfaces are possible, as can be seen in figure 4.3: POFs need to be connected to the detector/emitter on the one hand, and they possibly need to be coupled to other POFs on the other hand. For the latter case a simple connector structure can be proposed. Actually, a monolithic ferrule containing the fibre array as well as holes for guide pins would be the ideal solution. If this is technically not feasible, a system consisting of two blocks, i.e. the fibre array and a block for the guide pins, would be a possibility (figure 4.4). Fibre to fibre couplings rely on physical contact and in principle no additional features, like e.g. intermediate waveguides or optics, are necessary. For the POF/emitter-detector interface the situation is more complicated. The lack of space at backplane level implies that possibly the emitted/received light has to make a 90° bend, on a very short distance (figure 4.5). This bend can be implemented in several ways: a first possibility is to incorporate

¹In single fibre connectors the housing is often used to align the ferrules

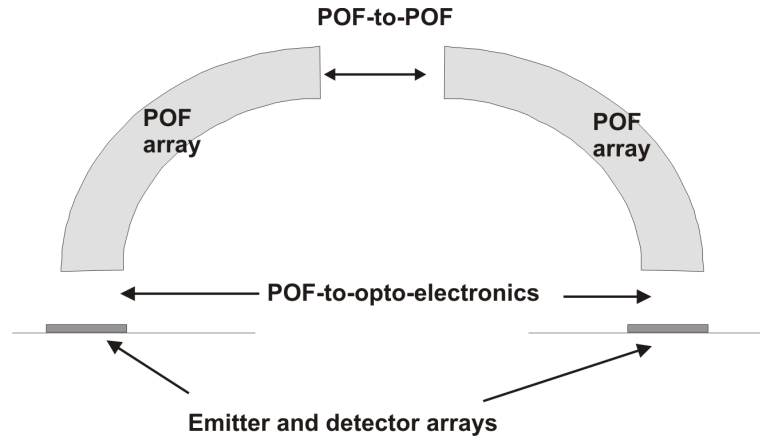


Figure 4.3: The different interfaces in an interconnect link

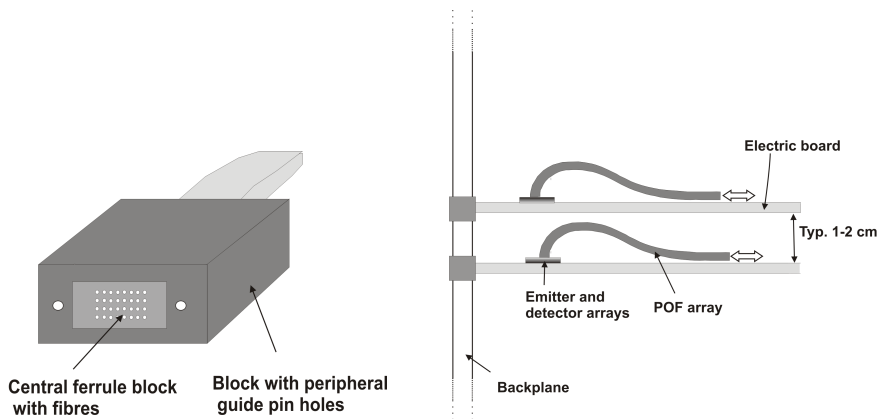


Figure 4.4: Ferrule consisting of two blocks Figure 4.5: A MCM to MCM link has to make a 90° bend, going from the vertically emitting/receiving optoelectronic elements to a horizontal direction parallel to the electronic board.

it into the connector itself and the connector couples directly to the optoelectronic elements (figure 4.6a). This is certainly the simplest solution since it requires only one interface (and hence coupling alignment), namely at POF/emitter-detector level. A disadvantage is the fact that the connector is inserted vertically, which can cause damage to the optoelectronic elements. Hence another protective intermediate layer between the fibres and the detector/emitter is necessary. In addition this layer should assure permanent protection of the optoelectronics against dust, mechanical damage and if possible moisture, even when the fibre connector is not plugged in. In other words it should seal the optoelectronic module more or less

hermetically. Preferably, it should not require any form of alignment. Possible solutions are encapsulating polymers (glob tops) or fused silica plates [1, 2]. It is clear that in the case that the connector would be permanently fixed on the module, it could serve itself as a sealing mechanism. However, fixed optical links show considerable less flexibility than (un)pluggable ones and hence the effort to render optoelectronic modules hermetic is worthwhile. Another way to implement

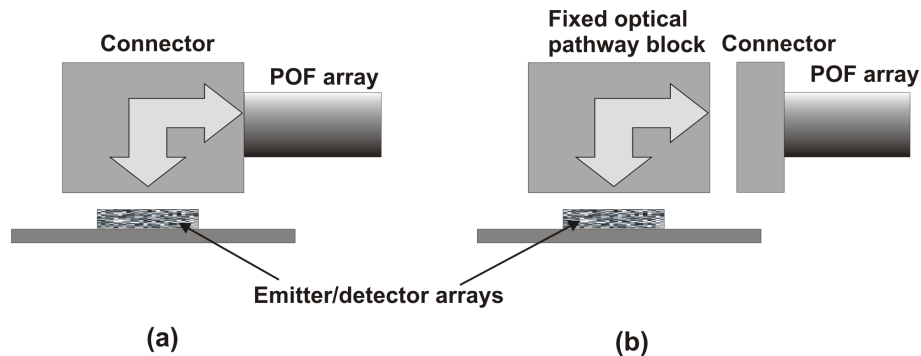


Figure 4.6: (a): the 90° bend is included in the connector (b): the 90° bend is included in a separate fixed optical pathway block to which the actual fibre array connector couples

a 90° bend is to place it in a so called “optical pathway block” (figure 4.6b): an intermediate and fixed optical pathway above the detectors/emitters. This set-up allows to merge two functions: protection and hermetic sealing of the optoelectronic module on the one hand and construction of the 90° bend on the other hand. Moreover, it allows horizontal insertion which limits the risks of damaging the optoelectronic elements. The damage risk can even be reduced more by “pigtailling” the optical pathway block with a waveguide or fibre array so that the coupling to the POF array is moved away from the optoelectronic interface (figure 4.7). However, in the case of a fixed optical pathway block there are two interfaces:

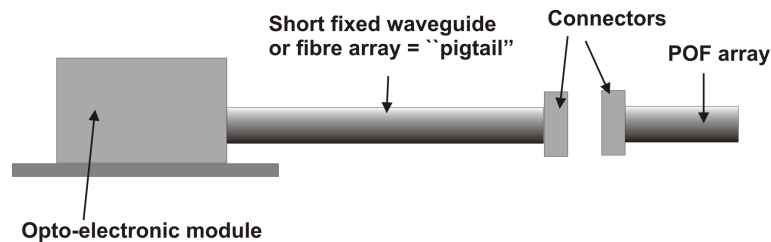


Figure 4.7: Optoelectronic module with “pigtail”

POF/optoelectronics and POF/POF, requiring two coupling alignments. As a result this option will be more complicated, and hence more expensive, than the former one. Moreover it turns out to be relatively “space consuming”. However, we will see in the next paragraph that manufacturers often use a fixed intermedi-

ate optical pathway for their optoelectronic modules, if only for sealing reasons. Moreover a variety of options to realize a 90° deflection is used.

Whether we choose to use an optical pathway block or not, an additional alignment structure that is fixed on the optoelectronic board is necessary. For instance one can use a thin spacer plate that has precise holes in which the guide pins of the connector fit (figure 4.27). This approach has been used in the OIIC-project [3]. Hence a complete connector system consists of the actual connectors containing the fibres, an alignment structure at the optoelectronics level, and possibly an optical pathway block or a sealing mechanism.

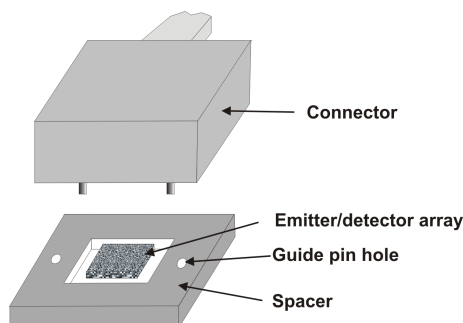


Figure 4.8: POF/optoelectronics interface: the alignment is performed by the spacer plate guide pin holes

Finally one has to consider the use of (micro-)optics. It has been shown that the coupling efficiency at the emitter/POF and the POF/detector interface can increase if micro-optics are used [4], depending on the configuration of POFs and emitters/detectors. However, implementing micro-optics severely complicates the production process. Hence one has to evaluate carefully the trade-off between the cost and the added value of micro-optics.

4.3 Connecting fibre arrays: what happens in the world?

One-dimensional fibre arrays have been used for more than a decade now and hence several reliable connectors for these arrays have been developed and commercialized. In this paragraph we will give a brief overview of the connector types on the market. In addition we look at the state-of-the-art of the two-dimensional fiber connectors and at the different ways the industry considers the fibre/optoelectronics interface.

4.3.1 One-dimensional fibre array connectors

Most of the commercially available connectors for $1 \times N$ fibre arrays are based on MTTM ferrules. This ferrule was designed by NTT and is commonly used for 1×8

to 1×12 parallel optical fibre cables. It is produced under license of NTT by Furukawa and Fujikura and is used to couple glass fibres to other glass fibres or to other optical waveguides like in the case of some optical transceiver modules. It consists of a monolithic block that contains capillaries at $250 \mu\text{m}$ pitch to hold the fibres at the one hand, and holes for the pin guiding system at the other hand. The fibres are inserted in the fibre holes by sliding them from the backside of the ferrules into the capillaries. Then they are fixed with high- T_g , low-shrinkage and hard glue. Finally the ferrule end facet is polished.

Generally, the ferrule is placed in a housing that fits in an intermediate adapter part called the coupler. This part couples the connector to another identical connector or some other configuration of waveguides. The function of this housing system is three-fold: firstly it protects the ferrule from dust and mechanical damage, secondly it contains a spring system that pushes the ferrules against a mating ferrule or another optical interface, thus assuring physical contact between the optical interfaces, and finally it pre-aligns the ferrules in order to facilitate an easy insertion of the alignment pins. Many companies like for instance FCI, US Conec, Molex, Tyco, Amphenol, and Fitel, produce or have produced MTTM-based connectors. A schematic view of such a complete connector system can be seen in figure 4.9. The connectors shown on this figure are called Multi-fiber Push-On

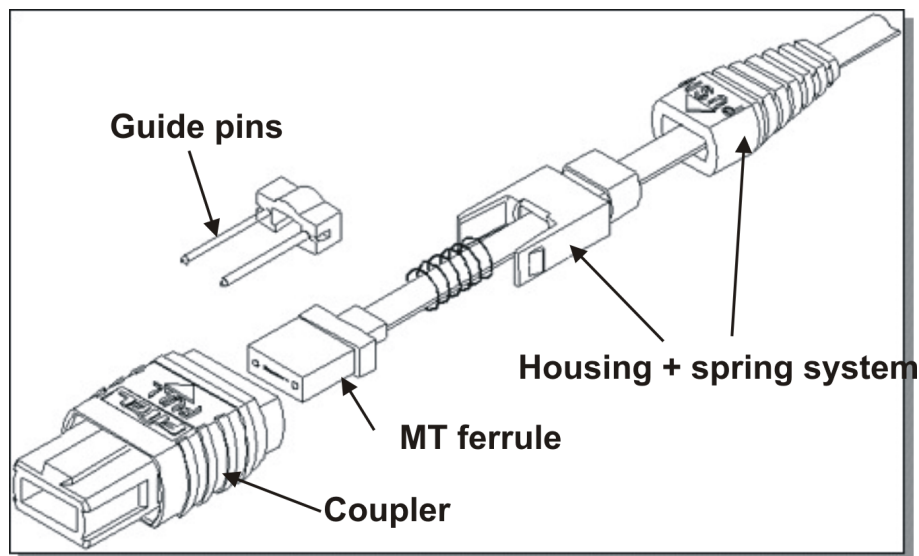


Figure 4.9: A schematic view of an “exploded” 1×12 optical fibre connector (Fitel)

(MPO) connectors, other standards are e.g. MT-RJ, MPX.

The monolithic MTTM ferrules are typically produced by transfer molding of a thermosetting glass-filled epoxy-resin. The resin shows high flow characteristics and low shrinkage. During transfer molding a mold is filled with a mix of resin and hardener at low-pressure, followed by a slow curing process. The capillaries as well as the guide pin holes are formed by pins that are positioned in precise V-grooves

in the mold [5]. The combination of the chosen material with the manufacturing process allows to obtain very precise structures, with accuracies in the order of 1 μm [6].

In order to save production time some manufacturers switched from transfer molding to the faster injection molding. During this process a thermoplastic polymer is injected in a mold at high pressure and afterwards a short curing process is applied. Although injection molding was a less precise technique than transfer molding a while ago, similar results on the accuracy of the ferrule dimensions are achieved nowadays [7].

Some companies have developed an alternative for the monolithic ferrule namely a two-part ferrule. Here, the fibres are sandwiched between two sets of V-grooves as can be seen in figure 4.10. These ferrules offer the advantage that the injection molding procedure is simpler than for the monolithic case. Moreover typical problems with "through hole" insertion like fiber breaking (due to tight tolerances) in the capillaries are omitted. These ferrules can be made with injection and transfer molding in case plastics are used. Some producers, like for instance Rohm and Haas, provide structures in ceramics, silica or silicon [8]. In this case etching techniques or, more common, micro-machining is used to produce the V-grooves. This technique is not as suitable for mass production as molding, but offers the possibility to develop customer-defined designs. However, the big disadvantage of the two-parts ferrule is the fact that this technology is not scalable to two-dimensional fibre arrays. Hence it never became a big success.

As mentioned before, the miniaturization is an important issue and hence the connector manufacturers put great effort in the development of so called "Small Form Factor" connectors. A typical example of such a connector is the MT-RJ connector (figure 4.11).

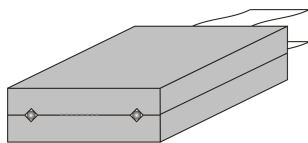


Figure 4.10: Principle of a ferrule consisting of two superposed parts with V-grooves

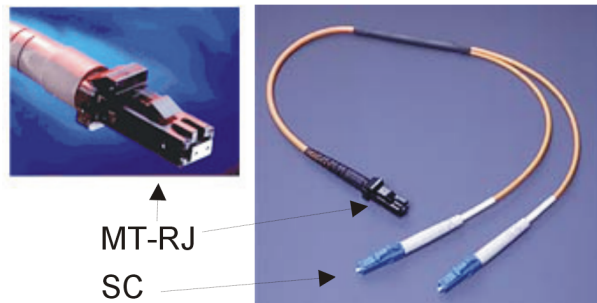


Figure 4.11: MT-RJ connector containing 2 fibres, the size is comparable to that of a standard single fibre SC connector

4.3.2 Two-dimensional fibre array connectors

4.3.2.1 MTTM-like solutions

Commercially available connectors for 2-D arrays are mainly based on the same MTTM ferrules as described above [9–12]. These monolithic ferrules are nowadays commercially available for 2×8 to 6×12 fibres (figure 4.12) and the same production techniques as for the 1-D ferrules are used. However, here multiple rows of core pins are used in the mold to form the rows of fibre capillaries [13, 14].

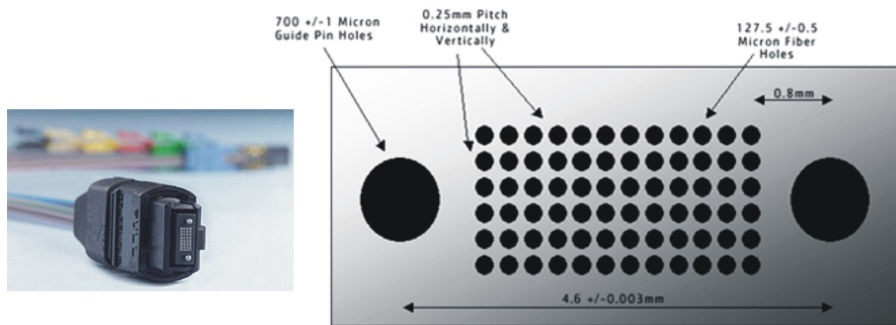


Figure 4.12: Picture and end facet scheme of a 6×12 MT ferrule (molex)

4.3.2.2 Other possibilities

Not many other options than the MTTM-like solutions are commercially available. Ferrules based on V-grooves can be found for $2 \times N$ arrays [15]. It is difficult though to expand the V-groove technology to larger arrays unless one succeeds to stack plates thinner than the fibre pitch (figure 4.13). Since this is typically $250 \mu\text{m}$, it

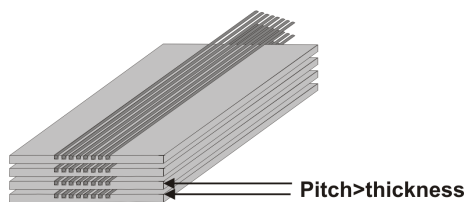


Figure 4.13: Stacked arrays need to be thin

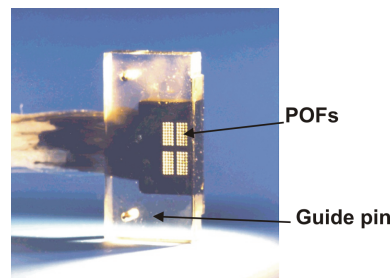


Figure 4.14: The OIIC “drilled hole” connector

is obvious that this is not an easy task. However, exactly this technology has been proposed in the framework of the OIIC project for the second generation connectors [16, 17]. We will discuss this choice elaborately in section 4.4. This technique was also applied by Y. Aoki who stacked silicon plates at a pitch of $500 \mu\text{m}$ [18].

Another existing technique, which was used in the OIIC project for the first generation connectors, is the use of micro-drilled plates: small holes for the fibres as well as for the guide pins are drilled in thin plastic plates as can be seen in figure 4.14 [16]. Micro-drilling is also used for the production of commercially available 2-D ferrules by the company Fiberguide [19]. Alternatively the holes can be made by etching or laser ablation [19, 20].

4.3.3 POF/optoelectronics interfaces

Fibre arrays are rarely coupled straight to emitters/detectors in commercial parallel fibre modules. More precisely, between the connector that the customer plugs into the optoelectronic module, and the actual optoelectronic elements there is an intermediate waveguide, equivalent to what we called the “optical pathway block” in paragraph 4.2. Different reasons are causing this choice of the manufacturers. In the first place, manufacturers prefer to perform the delicate coupling between the intermediate pathway and the emitter/detector themselves in well controlled circumstances, and subsequently make it permanent. In this way a sealed coupling is obtained. The less sensitive pathway/POF coupling can then be done by the customer. Moreover it is (relatively) easy to make it MTTM-compatible. Secondly, the vast majority of the commercially available parallel modules are based on silica fibres. So, if the optical path needs to be deflected by 90° in order to lay the fibres parallel with the underlying printed circuit board one needs to bend the glass fibres themselves. Considering the relatively large minimal bending radius of standard glass fibre (1 cm), this will consume a considerable amount of (precious) space, and moreover the fibres risk to be damaged during their handling. It is hence useful to introduce an intermediate optical or electrical path that can realize this 90° bend in a more compact way. As we will see, this has been implemented in almost as many different ways as there were different parallel optical modules developed during the last decade. Unfortunately, most of these modules did not survive the burst of the telecom bubble few years ago.

Probably the most obvious option to realize the 90° bend is to turn the emitters/detectors themselves. Such a construction was used for example in the PONI

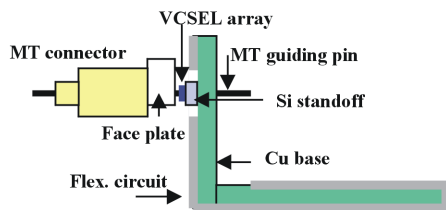


Figure 4.15: Coupling scheme of the PONI module

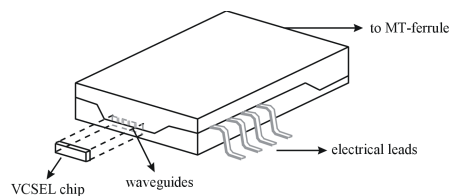


Figure 4.16: The OPTOBUS Guidecast module

link [21]. A schematic view of the coupling mechanism can be seen in figure 4.15. The optoelectronic elements were mounted on a flexible printed circuit board that

was bent over 90° . Direct coupling via a fused silica faceplate was used. The principle of turning the detector/emitter array has been used by Motorola for the development of their OptobusTM link, although here an intermediate waveguide was used. The Tape Automated Bonded lead frame, on which the emitter/detector arrays were attached, was bent. The intermediate waveguide system, called GuidecastTM, was formed by gluing together two molded cladding structures using an optical compound. The emitter/detector arrays were brought in intimate contact with the GuidecastTM. Pin holes in the lead frame and in the GuidecastTM package allowed passive alignment of the optoelectronic arrays to the waveguide. At the external facet the GuidecastTM was MTTM-compatible. A similar technique was used in IBM's LITEBUS, although here the intermediate polymer waveguide was replaced by a silicon structure with precisely etched V-grooves holding glass fibre stubs. Gore's nLighten module contained the same structure as well, but in this device the intermediate glass fibres were held by plastic molded V-grooves [22, 23]. Intermediate glass fibre arrays were also used in the PAROLI module made by Infineon Technologies. Here however, the optoelectronic die arrays were parallel with the electronic board and the light is deflected over 90° by a 45° mirror (figure 4.17). The coupling unit consisting of a plastic molded part containing precise V-grooves holding the intermediate glass fibres, was polished with an angle of 45° [24]. The polished facet was metal coated in order to obtain a reflecting surface. The external side of the coupler was made MTTM compatible. The principle of intermediate glass fibres polished over 45° with a metal coating has been adopted in the OETC project [25]. However, here the fibres were kept in silicon V-grooves. 90° -Deflecting mirrors were also used in some

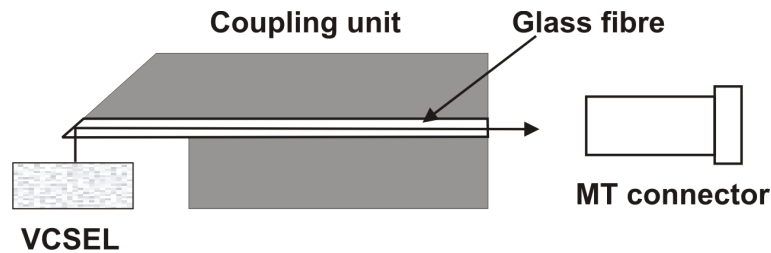
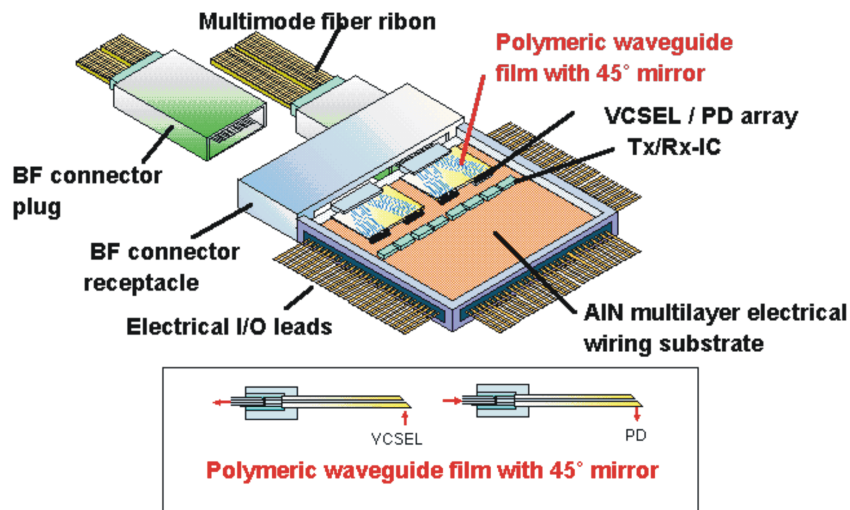


Figure 4.17: Optical coupling principle in the Paroli module

modules containing polymer waveguides like those proposed in the POLO and the POINT program [1, 26]. For example in the POINT project different polymer waveguides (PolyguideTM, Allied Signal acrylic, Ultem) were connected to optoelectronic arrays making use of this mirroring system. An optoelectronic module with a Polyguide waveguide connecting VCSELS with the external interface has been developed. Microtome cutting was used to obtain the 45° facet [27]. At the external interface the waveguide was kept in an MT-like connector. Polyguide (now called GuidelinkTM) is very suitable for micro-machining and hence precise mechanical features, like holes or cut-outs, on the Polyguide waveguide are used for passive alignment towards the optoelectronic dies or the external interface. Rather sophisticated was NTT's Parabit module, in which glass fibre stubs and

Polymeric waveguide film with 45° mirror for ParaBIT
 (Parallel inter-Board optical Interconnection Technology :
 -An over 25 Gbs-throughput 40 ch optical interconnection)



20-ch Polymeric optical waveguide film

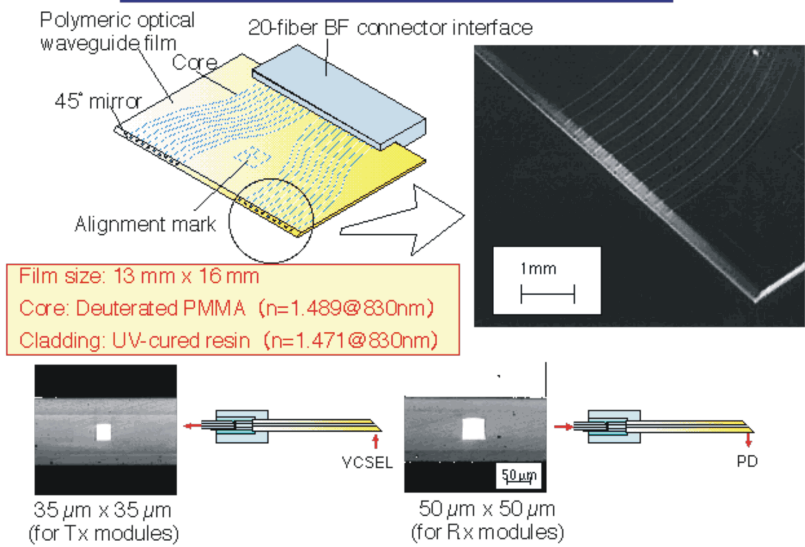


Figure 4.18: Scheme of the Parabit module

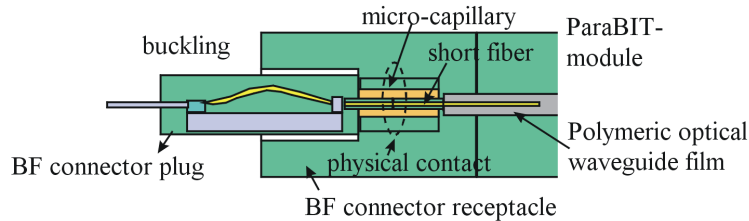


Figure 4.19: Principle of the bare fibre coupling

polymer waveguides were combined. As can be seen in figure 4.18, a polymer waveguide sheet was used to couple the light away from the VCSELS or towards the photodiodes. A diamond sawed 45° end facet was used to deflect the light over 90° . Towards the external interface the waveguide was butt-coupled to fixed short pieces of glass fibres kept in micro glass capillaries. The function of these fibres was to protect the polymer waveguide from damage when the fibre connector is plugged in. The particularity of this module laid in the design of the fibre connector. It did not have a flat polished end facet but contained short pieces of bare fibres at the interface. Those fibres fitted exactly in the capillaries but for easy insertion they had a conical tip (figure 4.19). Physical contact between the fibres was assured by the buckling force of the coupled connector plug. The advantage of this approach was that differences in fibre length did not cause a decreased coupling efficiency since physical contact was obtained for each fibre individually. For classical connectors containing a ferrule and a spring system the uniformity of the fibre length becomes difficult when large connector end facets need to be polished, causing degraded coupling efficiencies. “Bare fibre” connectors with 24 parallel fibres were presented [28]

Finally we have to mention IBM’s Jitney parallel optical module. Here micro-optics was used to deflect the light over 90° . This deflection is done by a coupler mirror consisting of parallel transparent vanes. On the rounded surface a metal coating is laid in order to reflect the light towards the fibres or the detector/emitter array (figure 4.20). The lens as well as its housing were made of molded plastic parts and were designed in such a way that they could be passively aligned to the emitter/detector arrays, making use of alignment pins attached to the optoelectronic package [29]. Yet, the alignment of different optical elements had to be done very accurately and hence IBM decided to omit micro-optics for their commercial LITEBUSTM modules [30]

The modules that we have discussed were all for $1 \times N$ fibre arrays. At a certain moment, companies like Xanoptics or Teraconnect have been presenting $M \times N$ links [31]. However, the exact interfacing scheme has not been revealed clearly yet. And here again, the collapse of the telecom bubble at the beginning of the century prevented those companies from being successful.

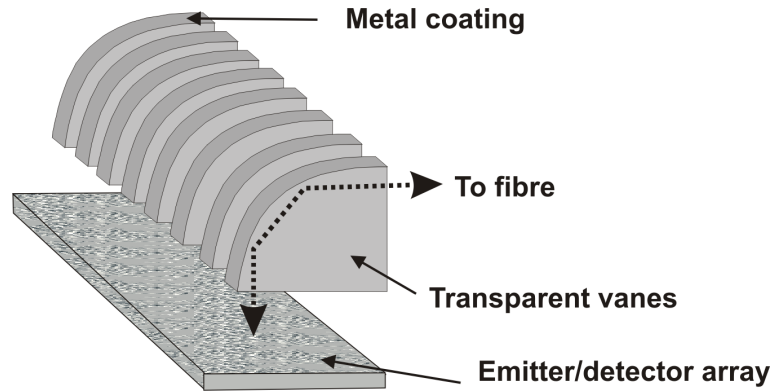


Figure 4.20: The Jitney coupler lens

4.4 Design of a connector system

Simplicity was the main credo when we developed a connector design. Therefore we will present a production scheme that is applicable on the POF/POF as well as on the POF/detector-emitter interface. In addition the use of optics or intermediate waveguides at the POF/emitter-detector interface is omitted. In the next chapter we will motivate this choice. This paragraph first focuses on the design of the actual connector containing the fibres and then discusses the complete connector system, i.e. including the alignment structures fixed at the optoelectronic board.

4.4.1 The “stacked array” approach

Connectors based on a fiber-through-hole principle like the above mentioned MTTM ferrule-based ones are developed for silica fibre, and are not suitable for POFs. Due to the POF's lack of rigidity it is really hard and labour-intensive to introduce an array of fibres into such a ferrule. Moreover the risk of fibre breakage in the capillaries is considerable which decreases the production yield. The argument that POF is a cheap alternative for silica fibre loses its value at that moment. Nevertheless this approach has been tried out in the framework of the OIIC-project and generated good results [16]. 130 μm . Holes for the POFs were drilled in 500 μm thick PMMA plates as well as 700 μm holes for the guide pins. The main advantage of this approach is that all the alignment structures are together in one piece, so only one very precise component needs to be made. However, the difficult task of introducing the fibre in the holes urged us to adopt another technology for the second generation connectors in the OIIC-project. This new technology is based on the stacking of one-dimensional arrays to form a two-dimensional array. Therefore one first needs to realize a one-dimensional array with a thickness smaller than the pitch of the fibres, which was 250 μm in our case. Such an array can be made by e.g. manufacturing thin plates containing U-grooves in which the POFs can be laid and fixed (figure 4.21). In this way the fibre-through-hole method is avoided. In the framework of the OIIC project the use of such U-grooved plates have been

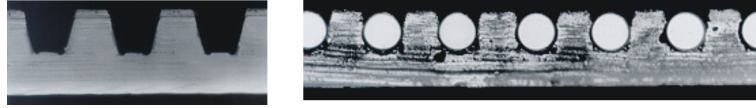


Figure 4.21: Cross section of thin plates with U-grooves made in the framework of the OIIC project. Left: empty U-grooves, right: fibres are introduced in the grooves

proposed as well as another technology for the fabrication of one-dimensional arrays, that we called “embedding fibres” [16, 17]. We will go into more details on these technologies in chapter 6. After the fabrication of these arrays one needs to stack them in order to obtain a two-dimensional array. One could rely on the thickness of the one-dimensional plates to keep the exact fibre pitch while stacking, however this turned out to be technically difficult. No technology seemed to be available to produce one-dimensional arrays with a precise thickness, at least at low cost. E.g it is possible to produce V-grooved plates with a well controlled thickness, but this would require an expensive polishing procedure. Therefore it was necessary to look for a stacking method that can stack the one-dimensional plates at precise pitch independent of the thickness of these arrays. We developed a technique for this purpose that we baptized “Virtual Alignment”. Chapter 7 will deal extensively with this assembling method.

4.4.2 Basic structure of the connector

Once the two-dimensional POF array (i.e. the ferrule) is created, an additional structure to assure alignment during the connector coupling, is necessary. An obvious solution would be to use a “square ring” shaped structure that contains precise holes in which alignment pins fit tightly (figure 4.22). Yet a problem

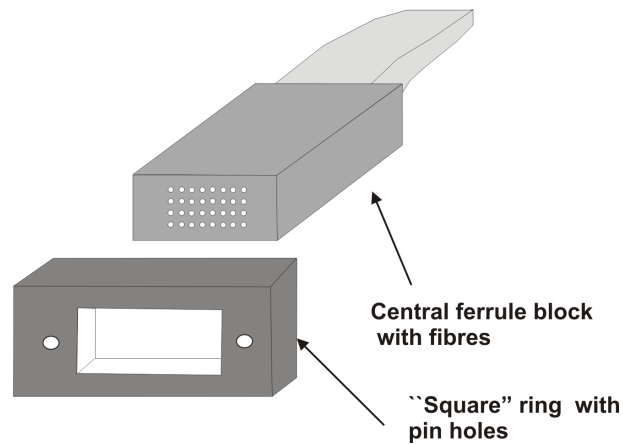


Figure 4.22: ‘Square’ ring fits around the central ferrule containing the fibres

can occur when this option is chosen. Generally, precise holes with small diameter (typically $700\mu\text{m}$) are only obtained in thin plates, due to restrictions of the various production processes to make these holes. It is e.g. easy to understand that a micro-drill with a diameter of $700\mu\text{m}$ has a limited length. Therefore it is doubtful that these thin alignment plates will resist to the friction of pins sliding in and out during consecutive couplings. A solution for this problem would be to reinforce the alignment plate with a more rigid structure, containing less precise sheaths with a larger diameter and fix the guide pins in these sheaths as in figure 4.23. However,

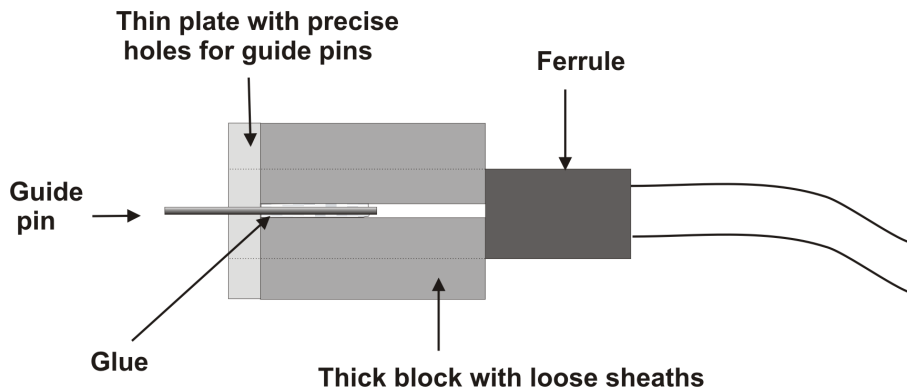


Figure 4.23: The thin plate with precise holes is reinforced with a stronger structure

the fixed guide pins prevent the connector to be coupled to another connector and hence this system would only work in an optical pathway without POF/POF interfaces. This was e.g. the case in the OIIC system demonstrator [17]. However, if one prefers to dispose of a certain degree of freedom when (re)configuring the optical pathway in a data processing system, it is probably useful that POF arrays can be coupled to other POF arrays. Hence a solution similar to the sliding-pin-system of the MTTM-based connectors seems adequate. We propose the following build-up for a connector: instead of using a “square ring” we suggest to use U-shaped blocks each having two U-grooves that can contain half a guiding pin as in figure 4.24. By sandwiching the ferrules between two U-shaped blocks a sheath is created in which the guide pins can slide. The U-grooves have been made at our laboratory with laser ablation, a technique that we will further discuss in chapter 6². The exact positioning of the ferrule with respect to the sheaths can be done with the same “virtual alignment” technology as for the stacking of the plates.

4.4.2.1 POF/POF interfaces

In the case of POF/POF coupling the simple structure described above forms a basic connector system that does not need additional features like e.g. an intermediate adaptor. These connectors can just be coupled by sliding them both over a pair of alignment pins until physical contact is reached. A simple clamping system

²Carried out by Kris Naessens, Faculty Applied Sciences, Dept of Information Technology, Ghent University

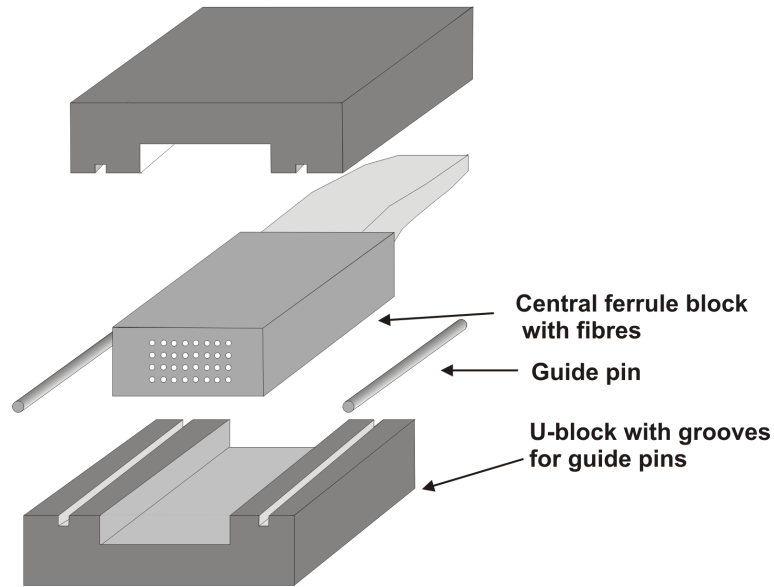


Figure 4.24: Sheaths for the guide pins are formed by superposing two U-grooves

to fasten the contact, like it e.g. for MTTM ferrules (figure 4.25) may be useful though, and should be conceived. Unfortunately we did not succeed to do this within the time frame of this thesis.

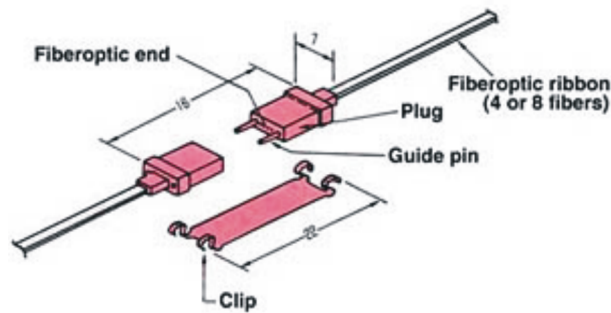


Figure 4.25: MT ferrule with clamping system

4.4.2.2 POF/emitter-detector interfaces

The situation at the POF/emitter/detector interface is more complicated since a 90° turn has to be implemented. We propose the technically most simple solution, i.e. a system with only one optical interface: optical pathway blocks (OPB's) are omitted and the insertion of the connectors is done vertically. We decided on this issue after having studied the different manufacturing possibilities. We

concluded that the advantage of horizontal insertion would not outweigh the extra complications of the production process. So the same basic connector structure as for the POF/POF interface is used. One way to implement a 90° bend in the optical link while keeping this basic connector structure is to pack the bend in the housing system of the connector (figure 4.26). The bent POFs are then loosely and unguided incorporated in the connector head. This technique has not been used during this PhD but has been successfully applied in the framework of the OIIC project [17].

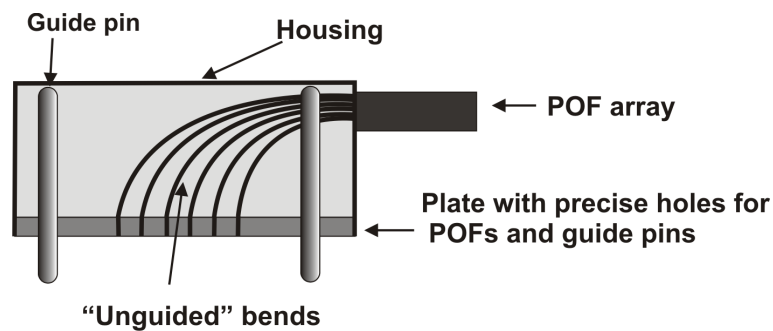


Figure 4.26: Schematic view of the first generation POF connector in the OIIC project

4.4.2.3 The alignment spacer at the optoelectronic devices

Now that we decided on the structure of the fibre connector we need to define a coupling alignment structure that is fixed at the optoelectronics board. The simplest way is to add a spacer plate that is fixed at a precise position around the emitter/detector as in figure 4.27. The spacer plate contains holes in which guide pins fit. It fulfills two functions: it assures the alignment of the fibre connector with respect to the emitter/detector chips and it forms a stop to prevent the end facet of the connector from touching the optoelectronic elements. Yet, for an optimized coupling efficiency the space between the end facet of the connector and the optoelectronic devices should be as small as possible and hence the thickness of the plate must be well adjusted. Also in case an intermediate sealing layer is added, like e.g. a fused fibre plate, the thickness of the spacer should be precise since it would define the distance between the sealing layer and the optoelectronic elements.

The pin holes in the spacer plate can be made e.g. by micro-drilling. However, similar to the situation in paragraph 4.4.2 the spacer plates have to be thin, and hence it is better to fix the alignment pins permanently in the spacer plate. This does not cause coupling problems since the pins can slide freely in and out of the coupled fibre connector. As we will briefly discuss in chapter 7 there are several ways to position this spacer plate with respect to the optoelectronic chips but we propose to use the same “virtual alignment” procedure as for the stacking of the one-dimensional POF arrays. In addition to the spacer plate a sealing mechanism is necessary. We used a fused silica plate with satisfactory results. Certainly glob

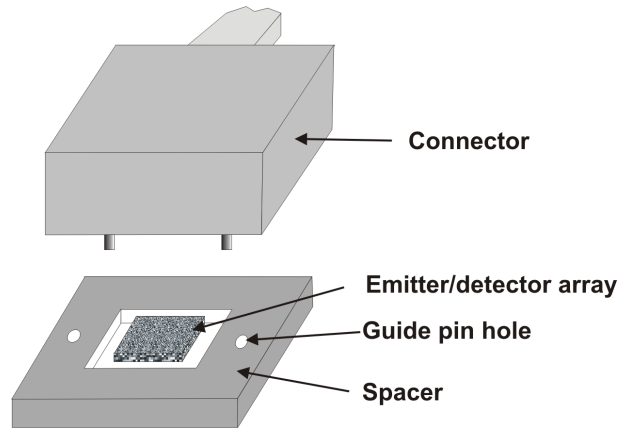


Figure 4.27: Connection scheme with spacer

tops offer cheaper solutions but no sufficient time for studying this possibility was available during this thesis.

4.4.2.4 Are there alternative solutions for a bent fibre array?

As we saw in section 4.3.3, bent 2-D arrays of waveguides or fibres are not being implemented in commercial modules. Instead, a 90° deflection mirror or a flexible printed circuit board is used. The former option is definitely inadequate for 2-D arrays for the simple reason that the emitted light will have diverged considerably when it reaches the fibres, resulting in a high coupling loss and possibly in optical crosstalk. For a VCSEL emitter the loss may be limited due to its low divergence but for a RCLED the setup will surely fail. At the receiver side the same problems will occur due to the relatively large numerical aperture of POF. On the other hand a flexible Printed Circuit Board certainly offers a solution. However it is our feeling that the bent POF array is a simpler option: whether a flexible PCB is used or not a POF connector has to be made. So basically the difference between both solutions is: do we bend a PCB or do we bend a POF array? If we use 'loose' bends as described above no additional complicated technical efforts are needed. The implementation of a bent PCB seems slightly more complex. But what is probably more important, is the fact that the bent PCB option consumes more space since the interfacing, (including alignment features and large detector/emitter areas in case of highly parallel links), happens in a vertical plane, perpendicular to the electric boards. In view of the limited space between electric boards this has to be avoided. In the case of the bent POF arrays though, the (small) bending radius of the POF defines the height of the optical module together with the connector's housing and the spacer plate thickness. For instance the OIIC "drilled hole" connector was only 3.5 mm high [16]. It is clear that this reasoning only holds for "direct coupling" links and not for links containing a separate optical pathway block, since such a block implies a vertical interface plane.

4.5 Some brief calculations on the behaviour of bent POF arrays

In order to estimate the feasibility of the proposed connector design some preliminary calculations were carried out. More precisely the behaviour of a POF array when bent over small radius was investigated. Therefore we carried out the following “gedankenexperiment”: consider a small cube with edges of 1 cm length and consider a 8×8 POF array with pitch $250 \mu\text{m}$ and with fibre diameter $125 \mu\text{m}$.

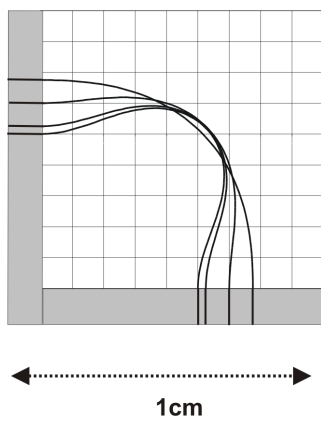


Figure 4.28: POF length 11mm

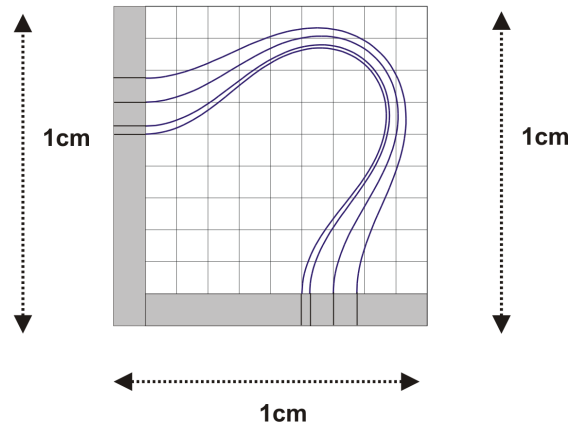


Figure 4.29: POF length 16mm

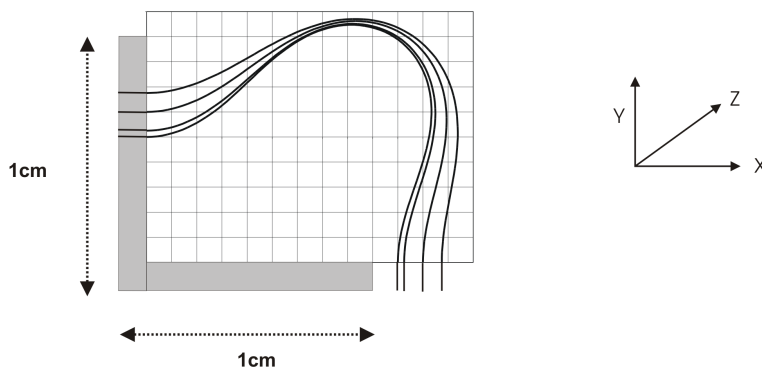


Figure 4.30: POF length 21mm

Is it then possible to insert in the cube this POF array bent over 90° , without damaging the fibres? And if so, what is the ideal length of the fibers, considering that all the fibres have the same length? We put the boundary condition of all the fibres having the same length, since this imitates the real situation the best.

POFs would have all the same length and then be bent together.

The bent array was simulated using a finite element model allowing to calculate the shape a fibre will assume when it is bent³. The result of these calculations can be seen in figures 4.28, 4.29 and 4.30. We assumed that the fibres were held at their ends in two plates of 1mm thick. The calculations have been carried out for one row of fibres lying in the X-Y plane, perpendicular to the “bending axis” (Z-axis). This simplification can be justified by the fact that when all the fibers lying in the considered plane can assume a form so that they do not touch or push against the other fibres in the row, they will actually remain in that plane after the bending. Hence they will not be touching the adjacent rows and as a result the complete array can be bent without problems.

So by varying the length of the fibres we can find out if there is an ideal length for which all the fibres (1) can fit in the $1 \times 1 \times 1$ cm volume and (2) are not stretched or disturbing each other. We can see from figure 4.28 that when the fibres are too short they will interfere with each other and hence problems might occur in the bent array. When the length increases the fibres are lying next to each other without really touching (fig 4.29) and hence it is shown that an 8×8 array can make a 90° turn and be confined in a cube of $1 \times 1 \times 1$ cm. When the length is still increased the bend will no longer fit in the cube and can be damaged if included in the cube. In figure 4.30), the fibres are drawn in their most compact form, without stretching and overlapping each other. As we can see they do no longer fit in the foreseen volume. Clearly, there is an optimal length and in the studied case this is about 16 mm.

4.6 Connector technologies in the OIIC project

The goal of the OIIC project was to propose solutions that could tackle the upcoming bottleneck in large data-processing systems. Therefore this project focussed on establishing key technologies and defining relevant processing architectures that allow introduction of area (as opposed to edge) optical interconnections for intra- and inter-MCM data exchange. In order to show the feasibility of these technologies different demonstrators were built. In the first place there was the system demonstrator [3, 32]: in this setup field programmable gate array (FPGA) chips were optically interconnected (figure 4.31). The main goal of this demonstrator was to show the advantages of massively parallel optical interconnects in electrical systems. The systems consisted of a multi-FPGA system with three optoelectronic FPGAs. Each FPGA was provided with two 8×8 detector arrays, and two 8×8 emitter arrays, which amounts to 256 optical channels per FPGA. The optoelectronic dies were flip-chip mounted on the chips. The central FPGA was connected with its two neighbours by a 10 cm long fixed OPB containing 8×16 Toray POFs. The OPBs are detachable from the FPGA chips to allow easy assembly. The two outer FPGAs can be connected together with two 8×8 POF bundles containing a connector. Two versions were built: one based on RLED arrays, the other based

³Carried out by Wim Van Paepegem, Department of Mechanical Construction and Production, Faculty Applied Sciences, Univ.Ghent

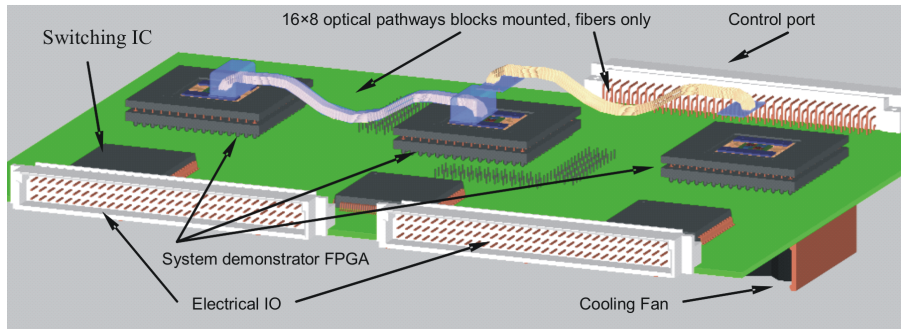


Figure 4.31: CAD rendering of the demonstrator design showing a simplified view of the demonstrator, with the three optoelectronic FPGA chips on sockets. On the left, a mounted and encapsulated optical pathway; and on the right, a partially assembled 8x16 fibre bundle with end “hole”-plate only is shown.

on VCSEL arrays. Both components were developed within the consortium and emitted at 980 nm. A data rate of 90 Mbit/s per optical channel was obtained for both demonstrator types. This resulted in a maximal aggregate data rate of 11.52 Gbit/s for a fully populated FPGA. This rate was essentially limited by the maximum operating clock frequency of the FPGAs. The optical pathway and transmitter/receiver circuit would have allowed more than double this rate.

As we mentioned in paragraph 4.4.2.4, the POF connector was based on a plate with precisely drilled holes, and a vertical insertion scheme was chosen. Each connector was housing 128 fibres, and two connectors could be coupled to one FPGA. The alignment of the connector with respect to the optoelectronic dies was done with alignment pins, fitting in a precision spacer that was placed on the FPGA packaging with a master tool. On top of the OPB a lid, that could be fixed with screws, was placed. This lid pushed the OPB on the spacer, via a spring on top of the OPB. A schematic view and a picture of this configuration can be seen in figure 4.32 In addition to the system demonstrator several technology demonstra-

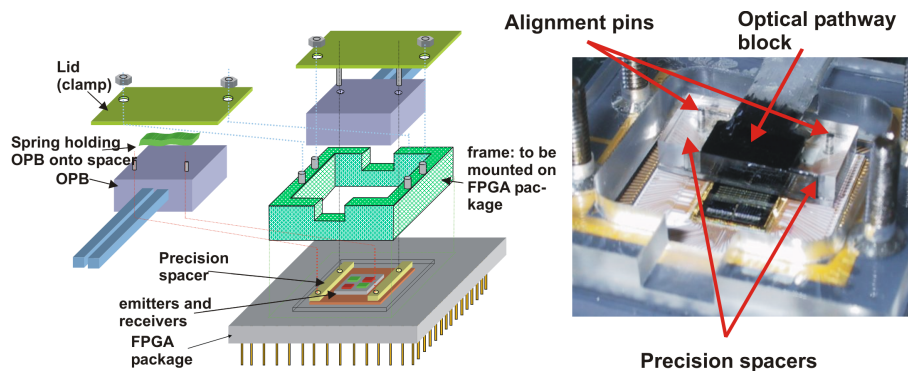


Figure 4.32: Schematic view of “vertical insertion connector” for the optical pathway blocks for the system demonstrator.

tors were built. The aim of these setups was to show the performance of certain newly developed subsystems for optical links. One of the technology demonstrators aimed for an even higher data rate of 1Gbit/channel and was called “Gigalink”. Therefore smaller detectors were necessary, and as a consequence the Asahi POF was to be used, since the “larger” Toray POF would generate too much losses at the fibre/detector interface. Knowing how difficult it was to insert the flexible POFs in narrow holes, the connector solution proposed in this PhD was adopted. Two-dimensional arrays were obtained by stacking one-dimensional arrays, and this stack was sandwiched between two U-shaped blocks with holes or grooves for alignment pins. Patchcords with 4×8 POFs were realized.

In addition demonstrators based on free space interconnects [33] and imaging fiber bundles [34] were realized in the framework of the OIIC project. However, the research work for this PhD was not related to these setups.

4.7 Conclusions

The main goal of this chapter was to come up with an adequate connector design for two-dimensional POF arrays. Therefore we discussed the main assets a connector should have: temperature resistance, compactness and reliability. Moreover the production process should be simple, scalable and allow automation. Then we distinguished different options when developing a design. An important choice in this context is the question whether or not a 90° bend is included at the fibre connector, or in a separate and fixed optical pathway block at the POF/detector/emitter interface. In the next paragraph we described that a large part of the manufacturers of parallel optical modules use an intermediate pathway in which the 90° deflection is realized by a 45° mirror system. We also found out that most of the commercially available fibre connectors are based on fibre-through-hole MTTM ferrules, a technique not suitable for (too flexible) small-diameter POFs. Hence another connector design, based on the stacking of one-dimensional POF arrays, was proposed. By sandwiching the stacked array structure between two U-blocks containing V-grooves for guide pins a basic connector structure was obtained, usable for POF/POF as well as for the POF/emitter-detector interface. We chose to use a configuration without separate optical pathway block and with vertical insertion at the POF/emitter-detector interface. The 90° deflection of the optical path at this interface is achieved by “loosely” bent POFs, included in the connector. This choice was validated by calculations using a finite element model. Finally we focused on the advantages the “stacked array” approach may have in terms of reducing the data channel delay.

Bibliography

- [1] K. H. Hahn et al, "Gigabyte/s data communications with the polo parallel optical link," in *Proceedings of the Electronic Components and Technology Conference*, (Orlando, Florida), pp. 301–307, May 1996.
- [2] R. Bockstaele and P. De Pauw, "Fabrication of a low-cost module for gigabit ethernet transceivers," *Proceedings of SPIE*, vol. 4942, pp. 44–53, April 2003.
- [3] M. Brunfaut, W. Meeus, J. Van Campenhout, R. Annen, P. Zenklusen, H. Melchior, R. Bockstaele, L. Vanwassenhove, J. Hall, B. Wittman, A. Neyer, P. Heremans, J. Van Koetssem, R. King, H. Thienpont, and R. Baets, "Demonstrating optoelectronic interconnect in a FPGA-based prototype system using flip-chip mounted 2d-arrays of optical components and 2d POF ribbon arrays as optical pathways," in *Proceedings of the SPIE' 46th annual meeting*, (San Diego, California), July 2001.
- [4] V. Baukens, *Scalable Micro-Optical Modules for Short Distance Photonic-VLSI Interconnections*. PhD thesis, Vrije Universiteit Brussel, 2001.
- [5] A. Nishimura, T. Ohta, T. Arikawa, and Y. Tamaki, "Low loss MPO connector," *Fujikura Technical Review*, pp. 12–16, 2001.
- [6] T. Statake, T. Arikawa, P. W. Blubaugh, C. Parsons, and T. K. Uchida, "MT multifiber connectors and new applications," in *Proceedings of the 44th Electric Components and Technology Conference*, (Washington D.C.), pp. 994–999, May 1994.
- [7] "Injection molded multi-fibre optical connector using thermoplastic resin," *Fujikura Technical Review*, pp. 17–23, 2001.
- [8] <http://electronicmaterials.rohmhaas.com>.
- [9] www.furukawa.co.jp.
- [10] www.molex.com.
- [11] <http://www.usconec.com>.
- [12] <http://www.amphenol-fiberoptics.com/default.CFM>.
- [13] "Design and performance of very high density multi-fibre connectors employing monolithic 60 fibre ferrules," *IEEE photonics technology letters*, vol. 11, pp. 1446–1448, november 1999.
- [14] T. Ohta, S. Shida, K. Takizawa, T. Airikawa, and Y. Tamaki, "Two dimensional array optical fiber connector," *Fujikura Technical Review*, pp. 18–22, 2000.
- [15] www.haleos.com.
- [16] B. Wittman, M. Jonck, A. Neuer, F. Mederer, R. King, and R. Michalzik, "POF-based interconnects for intra-computer applications," *IEEE Journal of selected topics in Quantum electronics*, vol. 5, pp. 1243–1248, september/october 1999.
- [17] <http://oiic.intec.ugent.be/>.
- [18] Y Aoki et al, "2-dimensional alignment-free optical interconnect using micro-optical bench," *Proceedings of the 7th Micro-optics Conference, Makuhari, Japan*, pp. 294–297, july 1999.
- [19] www.fiberguide.com.
- [20] G. Proudley, "Fabrication of a two-dimensional fibre optic array for an optical crossbar switch," *Optical Engineering*, vol. 33, pp. 627–635, feb 1994.
- [21] P. Rozenberg et al, "The poni-1 parallel optical link," in *Proceedings of the Electronic Components and Technology Conference*, (San Diego), pp. 763–769, June 1999.
- [22] "nlighten parallel fiber optical data link." <http://www.goreelectronics.com>.
- [23] C. Mueller, M. Donhowe, S. Kilcoyne, T. Lowes, R. Martin, and C. Theorin, "nLighten parallel optical modules," *Proceedings*, vol. 20-28, 2000.
- [24] D. Kuhl et al, "Paroli- a parallel optical link with 15 Gbit/s throughput in a 12 channel wide interconnection," in *Proceedings of the 6th international Conference on Parallel Interconnects*, (Anchorage), October 1999.

- [25] Y.-M. Wong et al, "Technology development of a high-density 32-channel 16-Gb/s optical datalink for optical interconnection applications for the optoelectronic technology consortium (oetc)," *Journal of Lightwave Technology*, vol. 13, pp. 995–1013, June 1995.
- [26] Y. Liu, "Polymer optical interconnect technology (point)- optoelectronic packaging and interconnect for board and backplane applications," in *Proceedings Electronic Components and Technology Conference*, (Orlando, Florida), pp. 308–315, May 1996.
- [27] J. Marchegiano, B. Booth, C. Chang, R. Furmanak, D. Graham, and R. Yohannan, "Polyguide technology for passive optical interconnects," in *Proceedings of the Photonics West-OE-Laser Conference*, vol. 2690, (San Jose/California), pp. 3614–368, February 26 -March 3 1994.
- [28] K. Katsura, M. Usui, N. Sato, A. Ohki, N. Tanaka, N. Matsuura, T. Kagawa, K. Tataeno, M. Hikita, R. Yoshimura, and Y. Ando, "Packaging for a 40-channel parallel optical interconnection module with an over- 25- Gbit/s throughput," *IEEE Transactions on Advanced Packaging*, vol. 22, pp. 551–559, November 1999.
- [29] M. Cohen, G. Johnson, D. Kuchta, P. Pepeljugoski, J. Trehwella, S. Quimet, and S. Spanoudis, "Packaging aspects of the Jitney parallel optical interconnect," in *Proceedings of the Electronic Components and Technology Conference*, (Seattle), pp. 1206–1215, May 1998.
- [30] B. Chan et al, "Packaging aspects of the litebus parallel optoelectronic module," *Micronews*, vol. 6, Third Quarter 2000.
- [31] <http://www.compoundsemiconductor.net/articles/magazine/8/3/5/1>.
- [32] L. Vanwassenhove, R. Baets, M. Brunfaut, J. Van Campenhout, J. Hall, K. Ebeling, H. Melchior, A. Neyer, H. Thienpont, R. Vounckx, J. V. Koetsem, P. Heremans, F. Lentens, and D. Litaize, "Two-dimensional optical interconnect between CMOS IC's," in *Proceedings of the Electronic Components Conference*, pp. 231 – 237, 2000.
- [33] H. Thienpont, C. Debaes, V. Baukens, H. Ottevaere, P. Vynck, P. Tuteleers, G. Verschafelt, B. Volckaerts, A. Hermanne, M. Hanney, and I. Veretennicoff, "Plastic micro-optical interconnect modules for parallel free-space inter- and intra-mcm data communication," *Proceedings of the IEEE, Special Issue on 'Short distance Optical Interconnects for Digital Systems*, 2000.
- [34] C. Rooman, M. Kuijk, D. Filkins, B. Dutta, R. Windisch, R. Vounckx, and P. Heremans, "Low-power short-distance optical interconnect using imaging fiber bundles and CMOS detectors," in *Proceedings of the IEEE LEOS Summer Topical Meetings on Electronic-enhanced Optics*, (Adventura, FL.), pp. 49–50, 24-26 July 2000.

5

Optical fibre coupling: efficiencies and tolerances

ASSURING an efficient optical coupling is the main property of a good connector. Since the efficiency of a coupling is a direct function of the precision of the positioning of the optical elements, it is essential to know what tolerances on this positioning are allowable. This is the issue of this chapter: determining the accuracy on the alignment of the optical elements needed for an acceptable coupling. Therefore we will study the effects of misalignments on the optical coupling efficiency. We will do this for three kinds of interfaces, RCLED/fibre, POF/POF and POF/detector. For each of those interfaces a theoretical model is used to estimate the alignment tolerances and, when possible, the model is completed with experimental results. Prior to these results a brief description of the used experimental setup will be given, as well as a short discussion of possible techniques for the end facet preparation of POFs. The chapter will be concluded with power budget calculations for a complete optical link, yielding practical values for the alignment tolerances.

5.1 Interfaces in optical links

As has been mentioned there are three kinds of interfaces in an optical link: emitter/fibre, fibre/fibre and fibre/detector. The optical coupling efficiency at these interfaces is not only function of the accuracy of the alignment structures but also depends on the configuration of the optical link: the geometric and the optical properties of the emitter/detector and those of the POF influence the maximal coupling efficiency thoroughly. The chosen link configuration is the result of a trade-off between different parameters like power consumption, data transmission rate and complexity. This study has been carried out for the OIIC System Demonstrator and the OIIC Gigalink, resulting in four possible link configurations, as well as in a set of parameters used for the link components [1, 2]. It is certainly not in the scope of this chapter to repeat this exercise and therefore we will rather use the proposed OIIC parameters and devices as a starting point for coupling efficiency calculations. In this way we will obtain concrete values for alignment tolerances to be taken into account at the optical interfaces when designing and fabricating the fibre connectors.

Power coupling efficiency can be improved by introducing micro-optics at the interfaces (besides the butt-coupled POF/POF interface). This matter has been discussed elaborately in [2]. However, we mentioned in the previous chapter that the use of micro-optics is omitted in our design and hence we will limit our discussions to cases without optics. Finally, the coupling efficiency equally depends on the roughness of the optical end facet of the optoelectronics and the fibres. For the emitters and detectors the optical end facet is mainly achieved by polishing or cleaving, generating high quality surfaces. For silica fibre polishing is also used yielding excellent results as well. However for POF, different technologies for the end facet preparation are possible.

5.2 Experimental setup

5.2.1 Principle

When useful, and possible, experiments have been carried out in order to verify the theoretical optical coupling models. For instance for RCLED/POF couplings the transmission loss has been estimated using a ray tracing program. For this interface it is certainly useful to carry out experiments to validate this model. On the other hand, for multimode fibre/fibre couplings the transmission efficiency has been described extensively in the literature [3–5]. However, for this case experiments can show the dependence of transmission efficiencies on light launching conditions or on POF bends. In some other cases the necessary devices were not available for experiments (VCSELS and Detectors).

In order to carry out the experiments for measuring alignment tolerances a dedicated setup has been assembled. The principle of this setup can be seen in figure 5.1. The figure shows the setup in case one wants to measure the alignment tolerance on a POF/POF coupling. A light source is coupled to an optical Y-splitter. This device splits an incoming optical channel into two optical channels with a

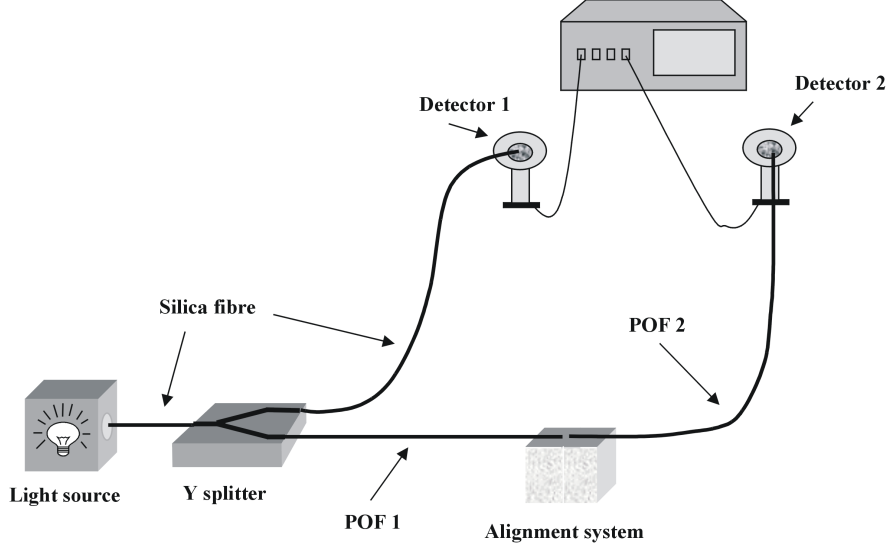


Figure 5.1: Principle of coupling efficiency setup: POF/POF coupling

fixed power dividing ratio. Mostly we used silica-fibre-coupled Helium Neon Laser as light source. One exit of the splitter is coupled to a light detector (detector 1) by means of a glass fibre. The other exit of the splitter is coupled to a plastic fibre (POF 1), which is then coupled to another plastic fibre (POF 2) by means of an alignment system. This system allows to alter the position of the end facets of the coupled POFs with respect to each other. By doing this alteration one can see the influence of the (mis)alignment of the fibres on the power coupling efficiency. Prior to the alignment experiment the ratio:

$$R = \frac{P_{POF1o}}{P_{GOFo}} \text{ or in dB: } R_{[dB]} = 10 \cdot \log \left(\frac{P_{POF1o}}{P_{GOFo}} \right) \quad (5.1)$$

is measured, with P_{GOFo} the power emitted from the glass fibre (detector 1) and P_{POF1o} the power emitted from POF 1 (detector2). Since the power split ratio of the Y-splitter is constant, the emitted power by POF 1 can be derived at all times from the power measured at the glass fibre at detector 1. Then POF 1 is coupled to POF 2 and the POF/POF coupling efficiency in function of the offset is measured. The coupling efficiency is given by the simple equation

$$\eta = \frac{P_{POF1o}}{P_{POF2i}}, \quad (5.2)$$

with P_{POF2i} the power captured by POF 2. The power measured at detector 2 (P_{POF2o}) is the power accepted by POF 2, diminished by the transmission losses LF of the second POF, with

$$LF = \frac{P_{POF2o}}{P_{POF2i}} \text{ or in dB: } LF_{[dB]} = 10 \cdot \log \left(\frac{P_{POF2o}}{P_{POF2i}} \right) \quad (5.3)$$

The transmission loss has been measured following the methods described in Chapter 3. Substituting 5.1 and 5.3 in 5.2, one obtains;

$$\eta = \frac{P_{POF2o}}{P_{GOFo} \cdot LF \cdot R} \quad (5.4)$$

Power can be expressed in dBm units.

$$Power_{(dBm)} = 10 \cdot \log \left(\frac{Power_{(mW)}}{1 \text{ mW}} \right), \quad (5.5)$$

with $Power_{(mW)}$ the power expressed in milliwatts. Expressing equation 5.4 in dB and dBm yields a logarithmic efficiency:

$$\eta_{[dB]} = P_{POF2o(dBm)} - P_{POF2i(dBm)} - R_{[dB]} - LF_{[dB]} \quad (5.6)$$

Since η is smaller than 1, $\eta_{[dB]}$ is negative. The term ‘‘coupling loss’’ (L_c) is often referred to as $\eta_{[dB]}$ multiplied by -1, and hence is a positive number. In the case of a RCLED/fibre coupling experiment the incoming POF is replaced by a light source (fig 5.2). Here a Y-splitter is omitted since the emitter has to be coupled directly to the POF. Hence it is important that the light source has a stable output power. In practice this experiment has only been carried out for a RCLED/POF

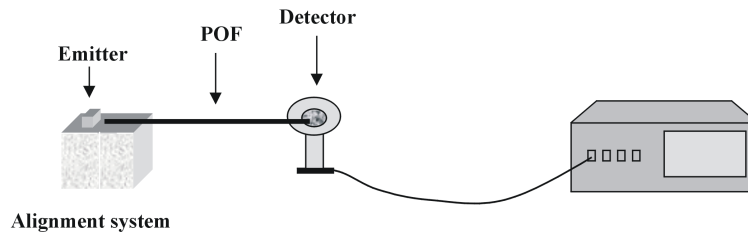


Figure 5.2: Principle of coupling efficiency setup: source-to-POF coupling

interface. The output power of the RCLEDs has been monitored as a function of time and drive current and it appeared that they were more than stable enough to deliver a constant power during a coupling experiment. Here the efficiency becomes:

$$\eta = \frac{P_{POFo}}{P_{Emit} \cdot LF}, \quad (5.7)$$

or in dB:

$$\eta_{[dB]} = P_{POFo(dBm)} - P_{Emit(dBm)} - LF_{[dB]}, \quad (5.8)$$

with P_{POFo} the power measured at the end of the POF and P_{Emit} the power emitted by the emitter (RCLED).

5.2.2 The alignment system

This part of the setup allows to couple two optical devices in a fully automated way. The position of the devices with respect to each other can be altered following six degrees of freedom: three rotations and three translations (figure 5.3). By

changing the position of the devices following one of these directions and simultaneously measuring the transmitted optical power, one can study the influence of misalignment in that particular direction. As can be seen in figure 5.4 and

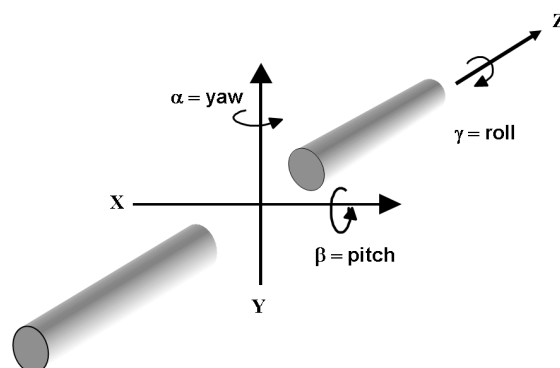


Figure 5.3: Rotations and translations implemented in the coupling setup

figure 5.5, the alignment system consist of two units. The left block contains the translations (X,Y,Z) and the right block contains the rotations α , β , γ (also named yaw, pitch, roll). The axes can be altered automatically and are driven

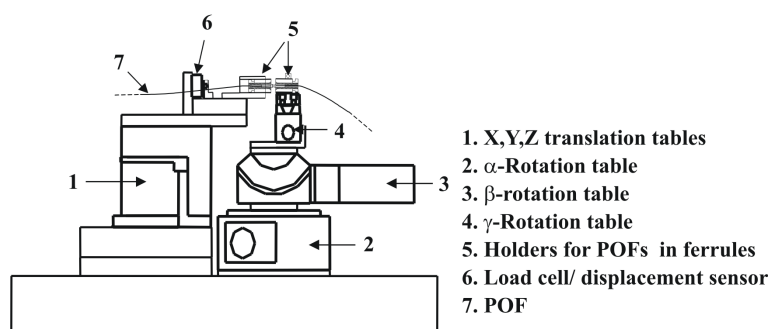


Figure 5.4: Alignment system

by DC motors. The rotations have an accuracy of 0.05° and a repeatability of 0.006° . The translations have a specified accuracy of 0.06 % and a repeatability of $1 \mu\text{m}$. However for the translations a considerable backlash was present (up to $20 \mu\text{m}$). Backlash in a mechanical system is the loss of motion between driving and driven elements due to clearance between parts. This occurs in particular when the movement changes direction: then the aimed position and the real position of the translation table are different. This problem was overcome by moving the translation tables always in the same direction when performing measurements.

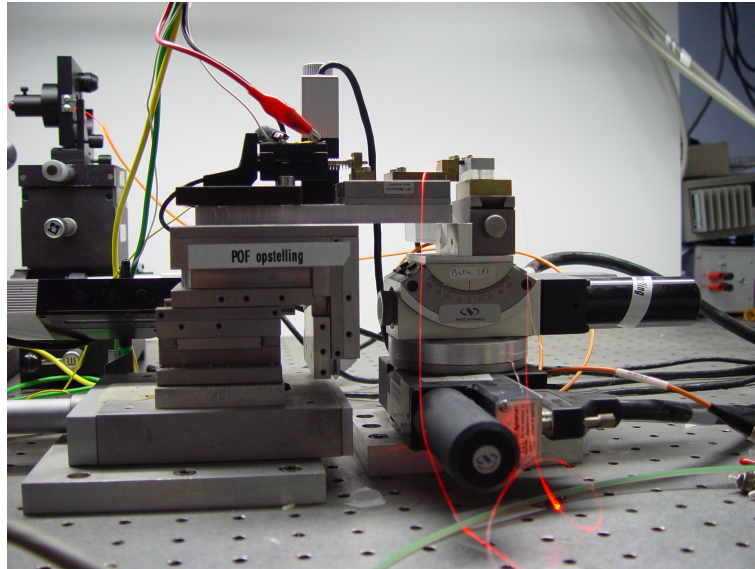


Figure 5.5: Picture of the alignment setup. On top of the blocks there are two holders containing $MT^{\text{T}M}$ ferrules with POFs. For the other interfaces other holders were developed. On the left block the displacement sensor can be seen.

When a backward translation had to be done a larger back-and-forth movement was carried out. Figure 5.6 explains this principle: suppose we make a translation from starting point a to point b . Then the order is given to return to point a . However, due to the backlash L , the real position is now in point c . In order to get back to point a one can add an additional movement towards point d , this time without backlash since backlash occurs when the direction of the movement is changed. In practice the movement is done straight from b to d . Returning now towards point a in the opposite direction annihilates the first backlash and point a is reached.

On top of the translations block a load cell for measuring coupling force is mounted. Since the Z-axis applies the coupling force in case of physical contact between the coupled elements, the cell is mounted parallel with the Z-axis. Alternatively a conductive plastic potentiometer was mounted in the case of delicate interfaces like POF/RCLED couplings. This potentiometer allowed to measure small displacements. It was mounted in such a way that as soon as physical contact between the coupled elements occurred, the potentiometer value is altered. In this way damage was avoided and also the zero point of the Z-axis could be defined. Both load cell and potentiometer were read out digitally. The system was steered by an extensive custom Labview program. It allowed fast optimization of the optical coupling as well as fast scanning following the 6 axes, with or without physical contact of the coupled elements.

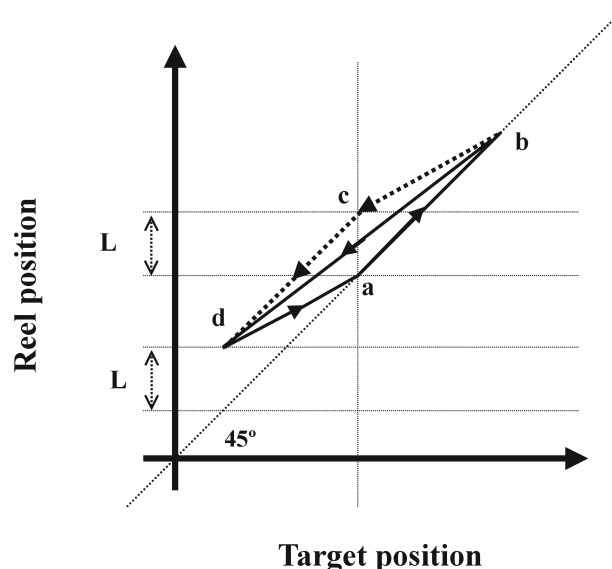


Figure 5.6: Backlash in a mechanical system:

5.3 End facet termination

Theoretical estimations for coupling efficiency are generally assuming that the end facets of the fibres are perfect. However, in reality the end facets have a certain roughness causing coupling losses. Finding a method for adequate POF termination has been a major issue in our laboratory. Extensive results on this matter can be found in [6]. This work describes how four different terminations methods have been investigated. Polishing, hot plate flattening, hot knife cutting and glue termination. For testing these methods, POFs were introduced in standard MT ferrules for $125\ \mu\text{m}$ silica fibre and fixed with UV-curable glue. Then the different termination methods were applied on those ferrules and a comparative study on the end facet quality was carried out. Before discussing these results let's first have a brief look at the investigated termination technologies.

Polishing This method is similar to the classical polishing method used for silica fibre. However for POFs the processing time is in the order of a few minutes, which is a lot shorter than for silica fibre. In our lab three polishing steps were proposed, using AlOx and CeOx polishing grains. The grain size is about $30\ \mu\text{m}$ for the first step, $3\text{-}9\ \mu\text{m}$ for the second step, and as small as $0.3\ \mu\text{m}$ for the final step. A photograph of a polished end facet can be seen in fig 5.7.

Hot plate flattening This technique consists of pushing the ferrule with POFs against a glass plate at $120\ ^\circ\text{C}$ during 0.5 seconds (fig 5.8). The facets of the POFs are melted and rendered flat (figure 5.8). For a good flattening, the fibres need a protrusion of about 0.150 mm with respect to the ferrule facet, prior to the

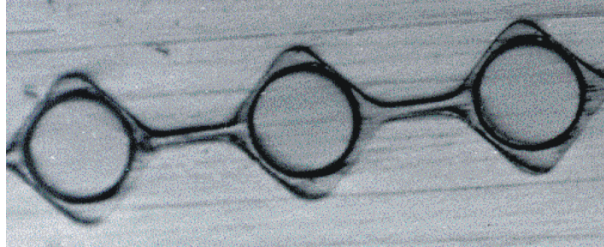


Figure 5.7: Polished end facet of a POF array

flattening process. Also crucial are the contact time and the temperature of the plate.

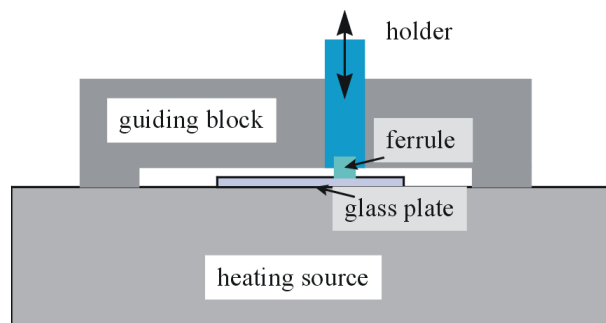


Figure 5.8: Hot plate setup: the ferrule is fixed in a holder that slides in the guiding block. In this way the ferrule facet can be brought parallel to the hot glass plate.

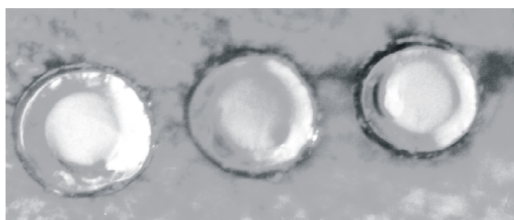


Figure 5.9: : Array of hot plate flattened POF facets

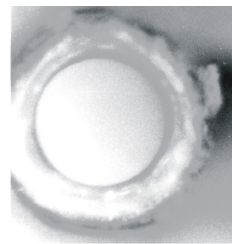


Figure 5.10: Hot plate flattened POF facet

Hot knife cutting The fibres are cut with a razor blade at 110 °C. As can be seen in figures 5.11 and 5.12, a setup allowing a precise positioning of the razor blade with respect to the fibre end facet has been built. It is of great importance that the knife slides smoothly over, and parallel with, the end facet of the ferrule. Other important parameters are the cutting speed and the knife temperature. A photograph of a hot cut fibre and a fibre array can be seen in figures 5.13 and

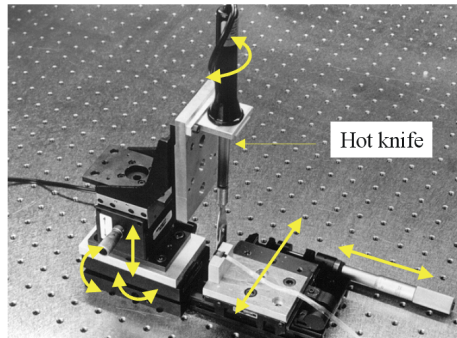


Figure 5.11: Hot knife set-up with three rotation and translation stages.

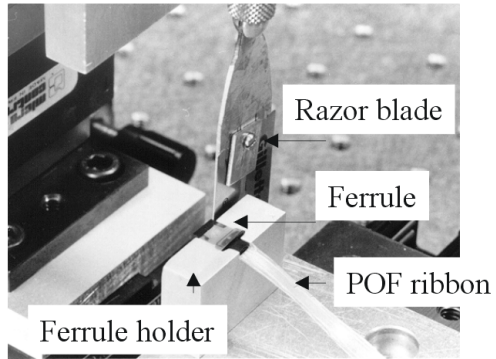


Figure 5.12: Detail of hot knife set-up : the razor blade is slid along the ferrule facet

5.14 respectively. It is possible though, after gaining some experience, to do the cutting by hand. This of course, makes hot knife cutting a fast and user friendly technique. In addition, if a slight roughness remains on the fibre facet after the cutting, it can be removed by a very short polishing procedure as can be seen in figure 5.15 (10-20 s, grain size $0.3 \mu\text{m}$).

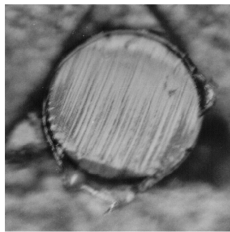


Figure 5.13: Hot knife cut POF array

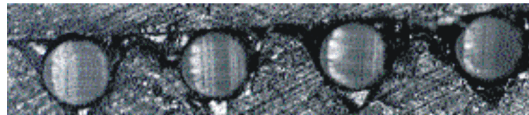


Figure 5.14: End facet of POF cut with hot knife

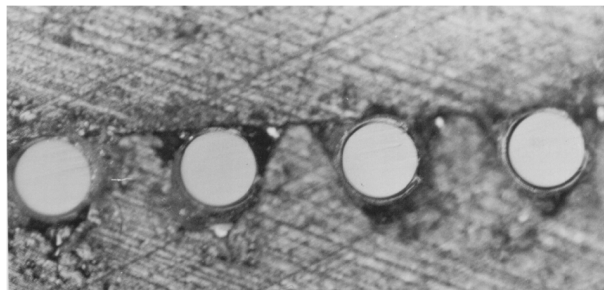


Figure 5.15: Hot cut POF array after short polish procedure

Glue termination Glue termination is not a complete fibre termination technique as such, but it is a process that can be applied after polishing or hot knife cutting. It consists of laying a thin layer ($\pm 15 \mu\text{m}$) of optically flat hard glue on top of the fibre facets. In our lab it has been applied on hot cut fibres. The deposited polymer annihilates the possible remaining roughness on the fibre end facet and a final polishing step after the cutting becomes unnecessary. However, a more important feature is that the end facets are now protected from mechanical damage. The procedure is depicted in figure 5.16. First, an elastomer film with an opti-

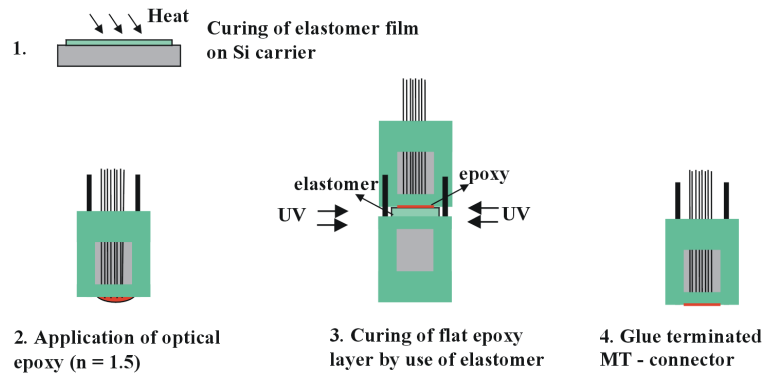


Figure 5.16: The glue termination procedure

cally flat surface is formed by heat curing. To this end, a two-component silicone elastomer (Dow Corning, Sylgard 184) is carefully mixed, avoiding air bubbles, and deposited on an optically flat surface, like a silicon wafer or a glass plate. By further curing in an oven (1 hour @ 90°C), the silicone elastomer is hardened to a flexible rubber-like substance, which can easily be peeled off from the carrier material. As a result we obtain a transparent elastomer film with an optically flat interface. Then a small amount of optically clear, UV-curable, index-matching glue is deposited on the interface of the optical MT connector, containing POFs. The fibres have a slight protrusion of only a few μm . The drop of glue is deposited in the middle of the connector interface and only a small amount of it is used to avoid the glue reaching the guiding pin holes. The connector interface with the uncured glue layer is pressed against the elastomer film. To ensure a correct positioning of the elastomer film without angle inclination, the elastomer film itself is laid on an empty standard MT ferrule, which can be correctly positioned to the filled MT ferrule by the connector guiding pins. The optically flat side of the elastomer film makes contact with the glue drop on the connector. After UV-curing the glue layer, the elastomer film can easily be removed from the connector interface and a hard, thin ($\pm 15 \mu\text{m}$) optically clear glue layer has been formed on the plastic fiber array at the connector interface.

5.3.1 Comparative study

Experiments have been carried out in order to evaluate the different termination methods. Therefore a series of ferrules with Toray POFs was prepared following the different techniques. Each ferrule was then coupled to another ferrule prepared with the same termination technique and the coupling loss per fibre was measured. The experimental setup was similar to the one in figure 5.1, except for the alignment of the POFs: the ferrules are simply mated using alignment pins and light was subsequently launched in all the fibres of the ferrule. The result of these experiments can be seen in table 5.1. As has been explained in Chapter 3

Table 5.1: Experimental evaluation of different POF termination methods

Termination method	Average loss (dB)	Standard deviation (dB)
Polishing	0.40	0.30
Hot plate flattening	0.45	0.30
Hot knife	0.60	0.40
Glue termination	0.55	0.20
Hot knife+ polishing	0.42	0.28

the coupling loss due to the variation of the numerical aperture of the coupled fibres, as well as to geometric imperfections of the POF and the ferrule, is 0.36 dB ($\sigma = 0.14$ dB). By subtracting this number from the total measured loss shown in table 5.1, one obtains the loss due to end facet roughness (under the assumption that full physical contact between mated fibres was achieved). These values are very low and surely comparable to those obtained for the classical polishing method applied for silica fibres. As we can see, polishing and hot plate flattening generate similar losses, and hot knife cutting generates a slightly higher value. However, an additional short polishing step decreases the loss to a similar value. Considering the user friendliness of hot knife cutting, this technology appears to be indicated for small core POF termination. It is possible though, that an additional end facet protection is necessary and than a glue termination layer can be useful. The losses are somewhat higher in that case, probably due to Fresnel

losses and fibre separation. Fresnel losses can occur when the glue facets are not completely parallel and a gap exists between the end facets. Also, by adding an additional polymer layer without a confining core-cladding interface structure, the POF end facets become in fact separated along the Z-axis. As we will see in the following paragraphs this results in coupling losses.

5.3.2 Subsequent coupling and end facets

The question whether a protective end facet layer is necessary was investigated. with the following experiment: two Toray POFs were mated for 500 consecutive times and the transmitted power was monitored. The outcome of the experiment can be seen in figure 5.17. The transmitted power remains roughly the same. Hence damage would rather occur due to the environmental circumstances or careless handling, than due to the actual coupling itself.

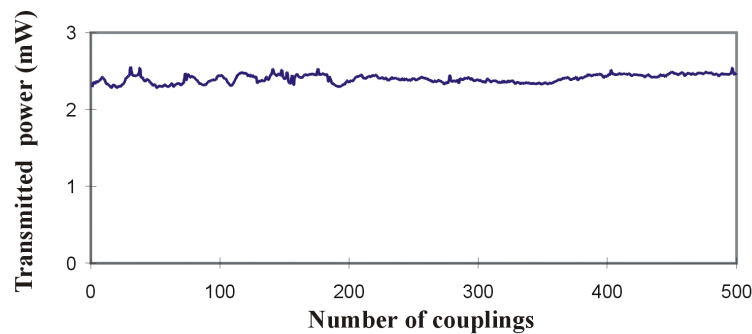


Figure 5.17: Evolution of the transmitted power during 500 subsequent Toray POF couplings

5.3.3 Coupling efficiency and coupling force

Forces up to 20N are used in commercially available parallel glass fibre connectors (Typically 9 N for single fibre connectors). This relatively high force is necessary to assure full physical contact between the fibres. Due to the elasticity of PMMA the applied forces do not need to be so high in the case of small diameter POFs. On the contrary, the force should not be greater than 1 N in the case of coupled Toray POFs, as an experiment shows us in figure 5.18. The coupling efficiency decreases with increasing force, probably due to deformation of the end facet.

5.4 Fibre alignment tolerance: theory and experiment

The next section discusses the effect of misalignments at the optical interfaces in a link on the power coupling efficiency. For each interface we estimated the coupling

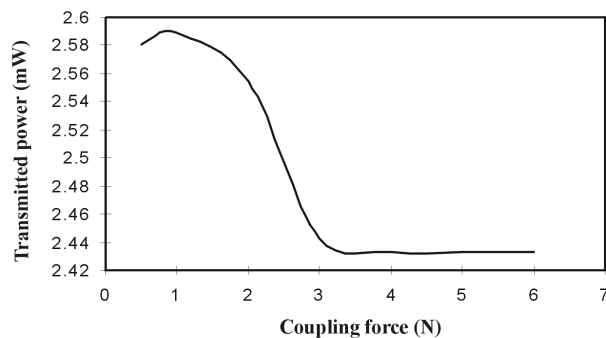


Figure 5.18: Transmitted power as a function of the coupling force, for Toray POF

efficiency as a function of the offset using a theoretical model, and carried out evaluating experiments where possible and/or useful. If intrinsic coupling losses may be present for the devices we are considering, they are of course also studied and estimated. Let us now start our discussion there where the light starts its way through the link: at the emitter/fibre interface.

5.4.1 Emitter-to-POF coupling

Two possible configurations have been studied: RCLED/POF and VCSEL/POF interfaces. The RCLED/POF interface is studied more thoroughly than the latter interface for the following reasons: (1) The coupling of semiconductor laser light into fibres is elaborately described in the literature [3] and is hence thoroughly known. (2) RCLED arrays were fabricated in our laboratory, offering us the possibility for extensive testing. VCSELs on the other hand were hard to obtain during this PhD, at least in a “naked” chip form, suitable for coupling experiments. (3) It will become clear after the following sections that the alignment tolerances at VCSEL/POF level are clearly looser than at the RCLED/POF interface. As a consequence a connector that is suitable for RCLED-based links, will certainly be suitable for VCSEL-based links as well.

5.4.1.1 RCLED/POF interface

The model A theoretical model for the estimation of the coupling losses has been developed. There are no straightforward analytical equations to describe the optical coupling of a RCLED to a POF. Therefore a ray tracing program called ASAP has been used. How a RCLED/POF coupling is modeled can be seen in figure 5.19. A measured far field emission pattern is used to simulate the emission pattern of the RCLED. The POF is modeled by a non-transparent screen containing a hole with the diameter of the POF core on the one hand, and a detector screen at large distance at the other hand. The diameter of the detector is so that only rays up to an incidence angle defined by the numerical aperture of

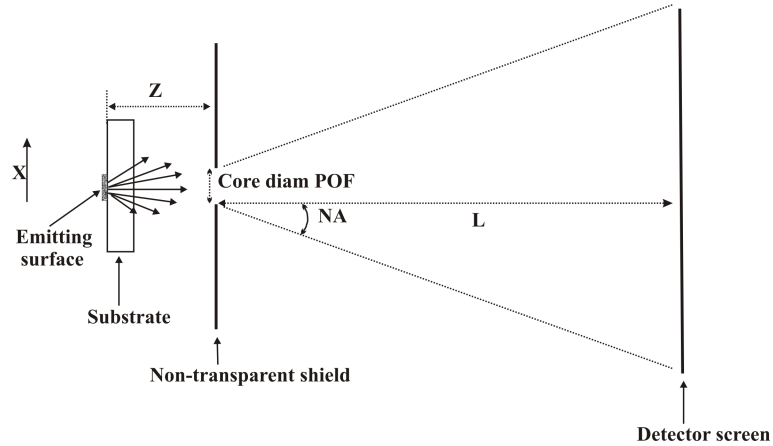


Figure 5.19: Ray tracing model of a RCLED/POF coupling

the fibre reach the detector. So in the case of the POFs, rays with an incidence angle larger than 30° will pass aside the detector. Moreover, a thin layer with the refractive index of the POF core is put on the detector in order to simulate Fresnel losses.

Intrinsic losses due to properties of RCLED and POF Even with perfect alignment of the RCLED and the POF the coupling efficiency may be limited by the properties of the optical elements themselves. Differences in diameter or a mismatch between the emission pattern of the RCLED and the numerical aperture of the POF, can cause coupling losses.

Emission pattern and numerical aperture Although the used POFs have a considerably large numerical aperture, RCLEDs emit light over angles larger than the acceptance angle of a POF. The POFs have an aperture of about 0.5, corresponding to a maximal acceptance angle of 30° in air. Hence all the light emitted by the RCLEDs at an angle higher than 30° will not be propagated through the fibre. The resulting loss can be estimated starting from the far field

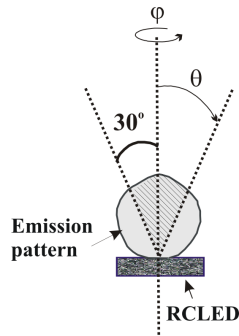


Figure 5.20: RCLED/POF coupling: part of the emitted light does not fall within the numerical aperture of the POF.

emission pattern of the RCLED. This has been visualized in figure 5.20. Under the assumption that every part dS of the active surface of the RCLED emits following the far field pattern, and that the far field pattern is rotationally symmetric, one can calculate the optical coupling efficiency. Since the total power emitted by dS in a solid angle ω is given by

$$P = \int_{\omega} I d\omega \quad (5.9)$$

With I the radiance of the RCLED. Using: $d\omega = \sin(\theta)d\theta d\varphi$, the power emitted by dS in the solid angle defined by a cone with opening angle θ_{max} becomes:

$$p_{\theta} = 2\pi \int_0^{\theta_{max}} I \sin(\theta) d\theta \quad (5.10)$$

Calculating the power for the cone defined by the numerical aperture of the fibre, and dividing this by the total power emitted by dS yields:

$$\eta = \frac{p_{\theta_{max}}}{p_{total}} = \frac{\int_0^{\theta_{max}} I \sin(\theta) d\theta}{\int_0^{\frac{\pi}{2}} I \sin(\theta) d\theta}, \quad (5.11)$$

with θ_{max} equaling 30° for an numerical aperture of 0.5. For the RCLEDs we used during our experiments the optical coupling η was typically between 20 and 30 %. It is possible to design RCLEDs with a higher optical coupling efficiency, in other words with a narrower emission pattern, but then the quantum efficiency of RCLED itself decreases, and more drive current is needed. The RCLEDs were designed to have a maximum for the total extraction efficiency:

$$\eta_{total} = \frac{\text{Number photons in numerical aperture POF}}{\text{Number electrons injected in RCLED}} \quad (5.12)$$

The far field emission pattern of these RCLEDs is close to that of a Lambertian emitter, which have an optical coupling efficiency η of about 25 %. A more ample explanation on this issue can be found in [7].

Although the optical coupling efficiency was estimated from the far field pattern, we carried out experiments to verify this model. The total emitted power of a RCLED was measured by butt-coupling it to a detector. Then, the RCLED was coupled to a short piece of POF and the output power (p_{total}) at the other end of the POF was measured. After taking into account the transmission losses of the POF, the power coupled into the numerical aperture ($p_{\theta_{max}}$) is easily found back and the optical coupling efficiency is simply calculated. The measured values turned out to be 5 to 10 % higher than the predicted ones (up to 40 % coupling efficiency in certain cases). This can be explained by the fact that fibres can propagate cladding modes, as discussed in Chapter 3. Given that usually the length of a POF during an experiment was only about 35 centimeter, cladding modes can certainly be present at the detector side of the POF. In other words the POF has a slightly higher numerical aperture than specified, resulting in a considerable increase of the accepted power. This can be seen in figure 5.21. The maximal coupling efficiency as a function of the numerical aperture of the POF

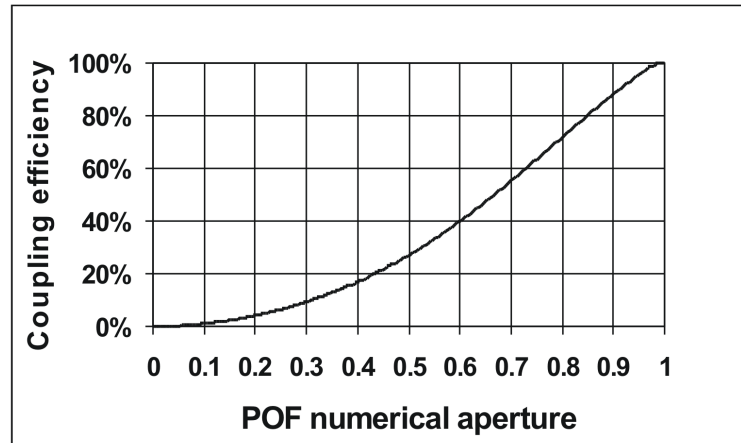


Figure 5.21: Coupling efficiency of RCLED/POF interface as a function of the numerical aperture of the POF

is calculated with equation 5.11, for a typical RCLED emission pattern. One can see that e.g. an increase from 0.5 to 0.6 in numerical aperture (30 to 36°) results in a 13% coupling efficiency increase. However, one should never take this extra power into account when designing an optical link, since cladding modes eventually disappear when the POF gets longer. Moreover they exit the POF at large angles, which makes it difficult to capture them by a detector at the end of the link.

Finally, the coupling efficiency can be influenced by the variation on the numerical aperture of the POFs. Since the numerical aperture can vary between 0.45 and 0.55, variations of $\pm 5\%$ on the coupling efficiency are possible.

Diameter mismatch It is obvious that in case the diameter of the RCLED is larger than that of the POF core, extra coupling losses are generated. For this thesis we used RCLEDs developed in the framework of the OIIC project and hence the diameters are smaller than, or more or less equal to, those of the POF cores. The mesa diameters are 52 and 70 μm corresponding to respectively a 32 and a 50 μm mirror diameter [7]. The mirror area is the real emitting area of the RCLED and hence further on in this thesis, we will use the mirror diameter to indicate the device diameter. The RCLEDs used for our experiments were bottom-emitting, this means that the light has to travel through the substrate before it reaches the end facet of the device. As can be seen in figure 5.22, 3 InGaAs quantum wells are placed in a cavity, made by a gold mirror on the top and a 5 pair GaAs/AlAs Distributed Bragg Reflector on the bottom. The light leaves the device via the DBR on the bottom side. The structure of the RCLED has been chosen in that way in view of their implementation in the OIIC System Demonstrator [8]. The bottom emitting structure, with the electric contacts on the top side, allows flip-chip mounting of RCLEDs arrays on CMOS chips, an important issue for simple and compact optical interconnection of those chips.

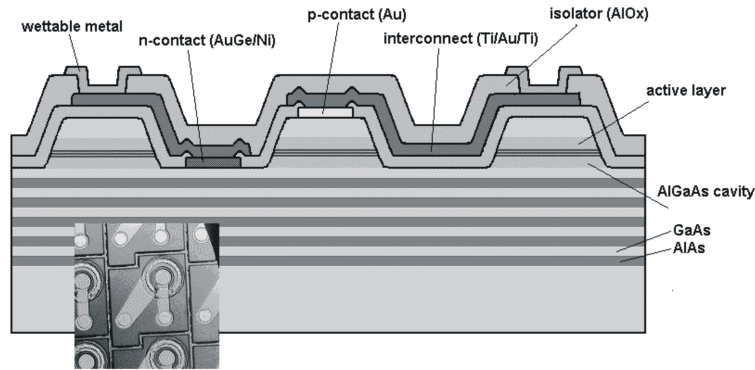


Figure 5.22: Structure of the 980 nm bottom-emitting RCLEDs

The GaAs substrate has a typical thickness of $150\ \mu\text{m}$ and has a refractive index of 3.5. It is clear that since the light has to travel through this substrate, the effective diameter of the emitted beam at the end facet is larger than the specified device diameter. Figure 5.23 explains this. The POF only accepts light emitted

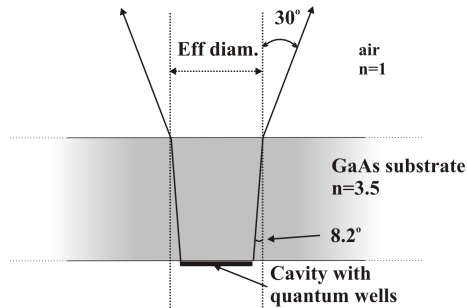


Figure 5.23: Bottom-emitting RCLED: the effective emitting diameter of the light beam is larger than that of the mirror

at angle smaller than 30° in air, corresponding to an angle $\arcsin(\sin(30^\circ)/3.5) = 8.2^\circ$ in the substrate. The effective radius at the end facet of the RCLED therefore will be: $\text{diam}_{RCLED} + 2 \tan(8.2^\circ) \cdot L_{substr}$, with L_{substr} the thickness of the substrate. For RCLEDs with diameter 32 and $50\ \mu\text{m}$ the effective diameters become 74 and $92\ \mu\text{m}$ respectively. It is clear that in case of butt coupling of the Toray $116\ \mu\text{m}$ core POF to these RCLEDs, there will be no coupling loss due to diameter mismatch. However, for the Asahi $61\ \mu\text{m}$ core the effective RCLED diameter is larger than the core diameter and power will be lost. We used the above described ray tracing model to calculate the optical coupling efficiency as a function of the RCLED diameter. As can be seen on figure 5.24, about 27 % of the emitted light is coupled into an Asahi $61\ \mu\text{m}$ core fibre up to a RCLED diameter of $20\ \mu\text{m}$. At diameters 32 and $50\ \mu\text{m}$ the efficiency decreases to 26 and 22 % respectively. Hence it seems that the combination RCLED-Asahi POF is not the preferred option to be implemented in an optical link, at least for the dimensions we consider. Further calculations on alignment tolerances will confirm

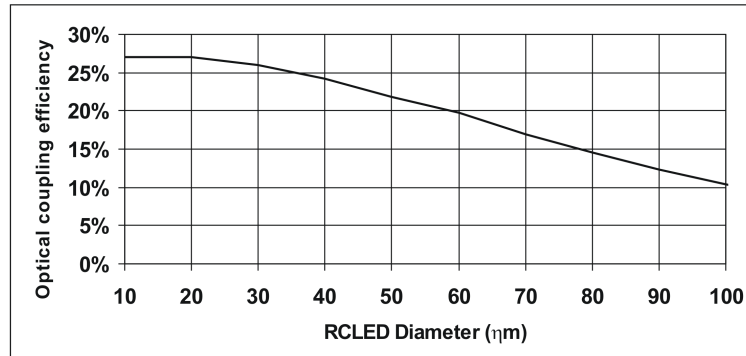


Figure 5.24: Optical coupling efficiency as a function of the RCLED emitting surface diameter for a substrate thickness of $150\ \mu\text{m}$ an Asahi $61\ \mu\text{m}$ core POF

this conclusion. Finally, we calculated the loss that is caused by the varying diameter of the POF. We obtained a maximum of 0.1 dB. Hence this loss is very limited.

Axial offset Due to the rotational symmetry of RCLEDs and optical fibres, misalignments can be decomposed in three components: two translations (axial and radial offset) and one rotation (figure 5.25). With axial offset, or separation, the misalignment following the Z-axis in figure 5.25 is meant. This is a critical

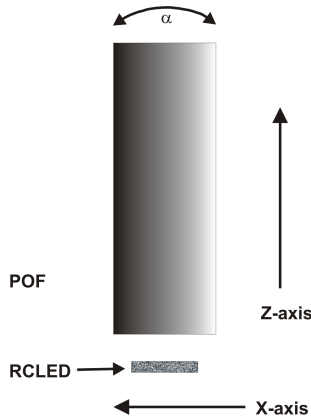


Figure 5.25: The alignment axes for a RCLED/POF interface

parameter in connector design since, as we discussed in Chapter 4, often a spacer is put around the RCLED in order to avoid physical contact between the device and the POF. A critical issue is then to design a spacer thick enough to prevent contact damage on the one hand, and thin enough not to loose too much power transmission.

Simulations The losses in function of axial offset have been simulated for several RCLED-POF combinations using the ray trace model. As can be seen in

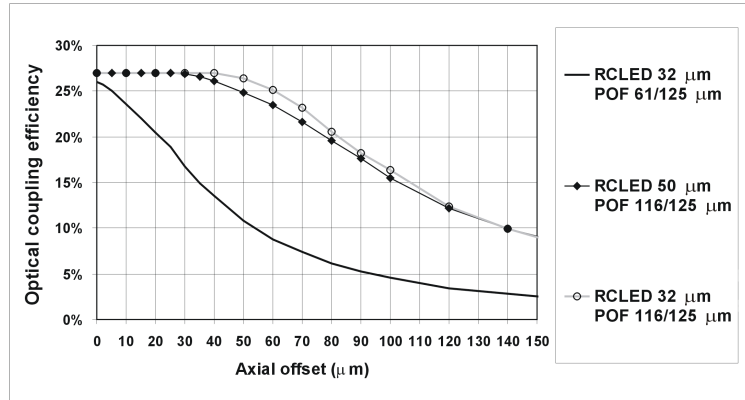


Figure 5.26: Optical coupling efficiency as a function of axial offset for different RCLED/POF combinations

figure 5.26 for the 30 μm RCLED in combination with the 61/125 μm Asahi POF, the efficiency decreases quickly when source and POF are separated. For instance a 10 μm separation decreases the efficiency to 23.5 %, in other words results in 0.4 dB extra loss. For the RCLED combination with the 116/125 μm Toray POF tolerances are larger. For the 32 μm RCLED a separation of 23 μm causes no extra losses, for the 50 μm RCLED there are no extra losses up to 40 μm separation. The low tolerance on the axial offset in case of the Asahi fibre can be increased by thinning the substrate of the RCLED. This has been done in our department: in parallel with the 980 nm RCLEDs, other bottom-emitting RCLEDs at 850 nm wavelength have been developed in the framework of the OIIC project. However, since the GaAs substrate absorbs strongly at 850 nm, the substrate has been almost completely removed, until only a few μm remained. For these RCLEDs, with a diameter of 32 μm , a maximal axial offset of 25 μm without extra losses is possible, in combination with the Asahi POF. A graph of the maximal axial offset as a function of the substrate is given in figure 5.27. The thinner the substrate,

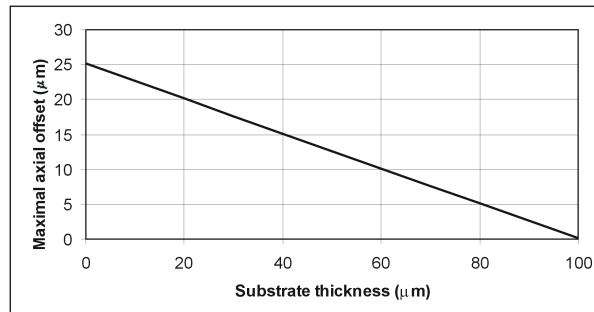


Figure 5.27: Maximal axial offset as a function of the substrate thickness for a 32 μm RCLED and a 61/125 μm Asahi POF

the larger the maximal offset. However, a thin substrate makes the RCLED array brittle and easy to damage. This has been noticed clearly for the developed 850 nm RCLEDs. Hence, for loose tolerances at the RCLED-POF interface, it is indicated to use the thinnest substrate possible that assures mechanical stability of the array. As a matter of fact, the 150 μm thick substrate used for the OIIC system demonstrator is very satisfactory from the mechanical point of view.

Experiments The ray tracing model has been verified experimentally using the setup described in section 5.2. Two POFs were coupled and after optimizing the coupling, a slowly increasing axial offset was introduced by the alignment system. Simultaneously the output power of the outgoing POF was measured. Following equations 5.4 and 5.6, the coupling efficiency is calculated, and compared to the theoretical value. Small divergences between theory and experiment can be seen in figures 5.28 and 5.29. At low separations the model underestimates the efficiency probably due to cladding modes (those are not included in the model). Since the measurements have been carried out with short pieces of POF (30cm) the cladding modes are likely to be present at the end facet of the outgoing POF. One can notice that for larger separations the model overestimates the efficiency. This can be explained by the fact that the rays emitted by the first fibre that are causing the cladding modes do not reach the second fibre anymore. Indeed, since they

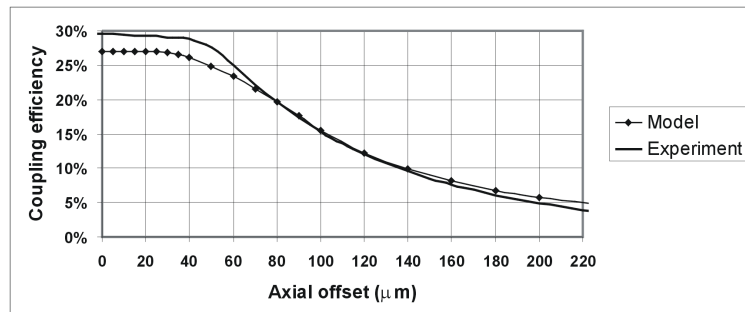


Figure 5.28: Optical coupling efficiency as a function of axial offset for 50 μm RCLED in combination with a 116/125 μm Toray POF

are emitted at a larger angle than the acceptance angle of POF they will "miss" the second fibre at smaller separations than light emitted within the numerical aperture of the POF. So at larger separations both the model and the experiment will only involve rays within the numerical aperture and a good agreement should be expected. However the model does not include losses due to the imperfect end facet of the fibres, resulting in a small overestimation. While designing an optical link though, one is more interested in reasonably small separation. While estimating the coupling loss using the model, with bringing the imperfect end facets into account, one is surely overestimating the coupling loss and as a consequence, playing it on the save side. The model is hence a useful tool for the make up of a link power budget.

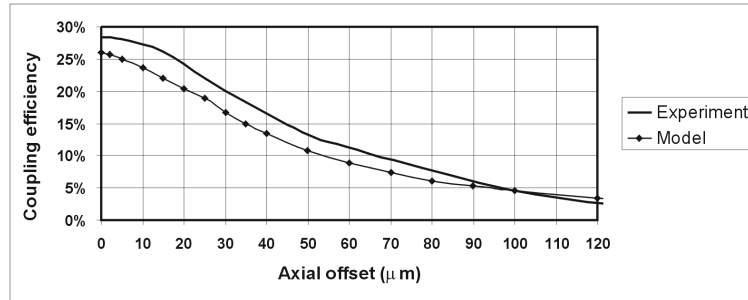


Figure 5.29: Optical coupling efficiency as a function of axial offset for 50 μm RCLED in combination with a 61/119 μm Asahi POF

Radial offset

Simulations With radial offset, the misalignment following the X-axis in figure 5.25 is meant. The result of the simulations with ASAP can be seen in figure 5.30. We can see that for the RCLED-POF combinations with the 116/125 μm

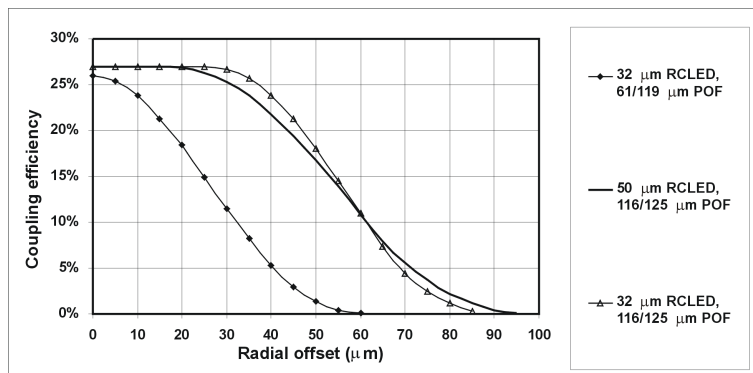


Figure 5.30: Optical coupling efficiency as a function of radial offset for different RCLED-POF combinations

POF there is no misalignment loss up to an offset of 20-30 μm . This is due to the fact that the effective emitting surface at the end facet of the RCLED is smaller than the POF core diameter. This is not true for the 32 μm RCLED in combination with the 62/119 μm POF. At 5 μm offset the transmission drops already to 25 %. Hence the alignment is clearly more critical in this case and a link with a Toray POF would be preferable to one with an Asahi POF from this point of view.

Experiments The results of comparisons between reality and experiment can be seen in figures 5.31 and 5.32. Here again the influence of the cladding modes is clearly visible. Not only is the measured power higher than expected, but also it remains higher over a larger offset range, probably due to cladding

modes coupled in via the cladding. This last effect is relatively larger in the case of the 61/119 μm POF, since the cladding is thicker for this kind of POF. Hence

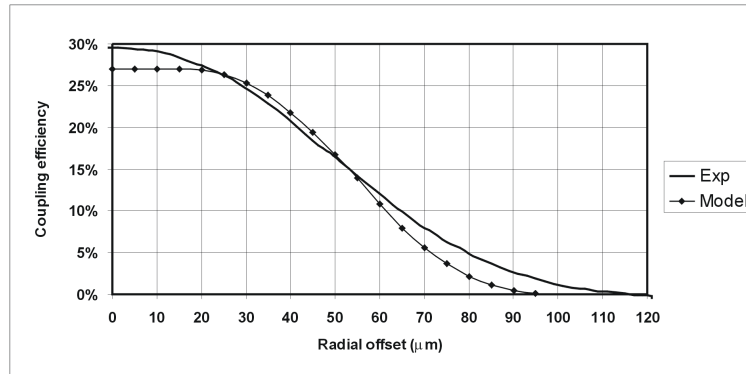


Figure 5.31: Optical coupling efficiency as a function of radial offset for a 50 μm RCLED in combination with a 116/125 μm Toray POF

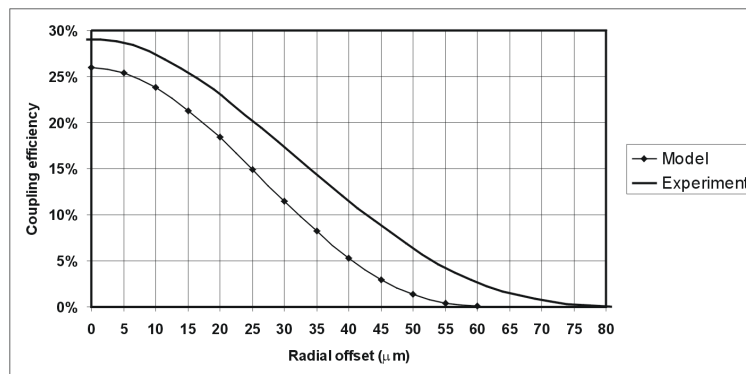


Figure 5.32: Optical coupling efficiency as a function of radial offset for a 32 μm RCLED in combination with a 61/119 μm Asahi POF

also for axial offset, assuming the modeled loss value and adding the possible end facet loss is a conservative way to estimate optical link losses. Finally, it is possible to loosen the tolerance on the axial offset by introducing a material, that has a higher refractive than that of air, between the emitter and the fibre. The higher refractive index makes the emitted bundle less divergent. Polymers are a suitable material for this purpose. It is common practice to use such a polymer in liquid form, called index matching gel, in fibre/fibre interfaces. It was though more complicated to use such a gel on our RCLEDs since it would spread all over the module. However, in [9] an UV-curable adhesive with refractive 1.5 was used to form an encapsulating glob top. The ferrule with the POFs is easily butt-coupled to the glob-top. A spacer becomes unnecessary and there is no air gap between

the POF and the emitter.

Angular offset In optical interfaces, angular offset is often caused by non-parallelism of the mating end facets. An example is given in figure 5.33 a. A badly produced spacer causes the end facet of the ferrule to be tilted with respect to the RCLED array. As can be seen on the figure, besides the angular offset an axial offset z , depending on the position of the fibre in the ferrule, is introduced as well as a smaller radial offset. This axial offset can be substantial. Let us take an example in which a 1×8 array, as shown in figure 5.33 a, is tilted over an angle of 5° . The z difference between the POF on the left hand side and that on the right hand side is about $150 \mu\text{m}$, for an array with pitch $250 \mu\text{m}$. So there is at least an axial offset of $150 \mu\text{m}$ for the left side POF. The radial offset is smaller: under the same circumstances the POF pitch projected on the plane of the RCLED array is about $249 \mu\text{m}$. With an optimized alignment this means a maximal offset of $4 \mu\text{m}$ per fibre. In certain cases neither a radial nor an axial offset is introduced, as

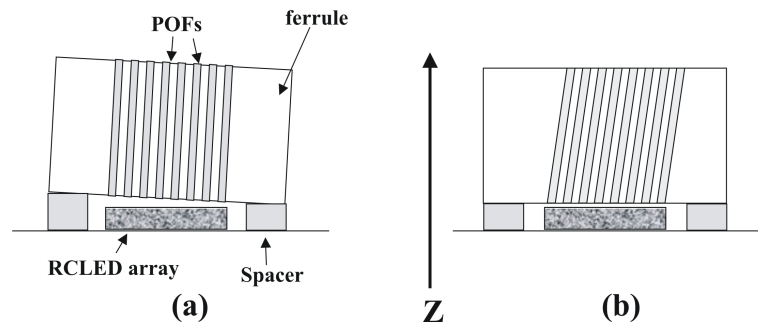


Figure 5.33: (a) A badly produced spacer causes the complete ferrule to tilt. (b) The POFs are obliquely mounted in the ferrule, but the end facets are parallel.

shown in figure 5.33 b. It is e.g. possible that the fibres are obliquely mounted inside the ferrule but that the end facets are well aligned with the RCLED array. In this case, one can visualize the coupled light as that part of the emission pattern of the RCLED that falls within the acceptance cone, similar as in paragraph 5.4.1.1. Only here, the POF is tilted with respect to the RCLED and hence the coupling loss is a function of the overlap between a tilted far field emission pattern of the RCLED and the acceptance cone of the POF (fig 5.34). The coupling loss has been simulated with ASAP, yielding figure 5.35. The coupling efficiency does not decay considerably until an offset of 10° , due to slowly varying intensity for emission angles up to 30° . Hence the broadness of the emission pattern of a RCLED makes that only a part of the emitted power is launched into the aperture of the POF on the one hand, but on the other hand it renders the coupling efficiency quite independent from angular offset. Let us come back now to the more common case of figure 5.33 a. We want to set up a design criterion for the tilt tolerances that only involves the losses caused by the tilt itself, not by the associated radial and axial offset. The tolerances on these two last misalignment types, are set by their

Figure 5.34: An angular offset α of the POF makes that light emitted at lower angles contributes to the light captured in the numerical aperture of the fibre. A typical acceptance angle of 30° is shown.

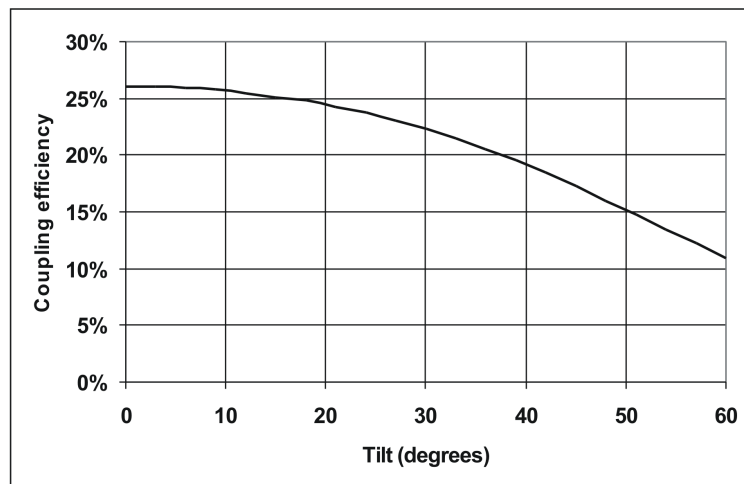
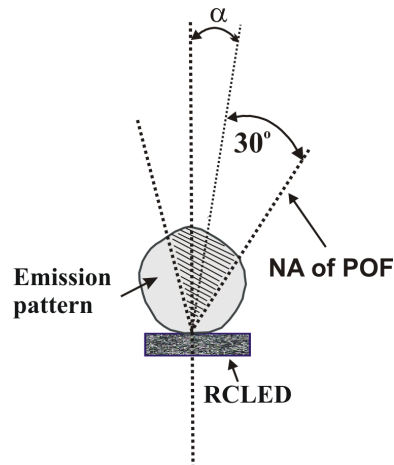


Figure 5.35: Power coupling efficiency as a function of angular offset, without separation between RCLED and POF

own specific criterion. Therefore we will disregard the possible radial and axial offsets and reduce the coupling to a configuration in which the remaining (partial) separation z' is caused by, and only by, the rotation of the fibre end facet with respect to the RCLED, as shown in figures 5.36 a and b. The POF is well aligned with respect to the X and Y axes, i.e. the optical axes of the VCSEL and the POF cross each other at the end facet of the POF. In comparison with the coupling in 5.33 b, here the losses are not only caused by the tilt of the emission pattern, but also due to the gap between RCLED and POF, through which part of the emitted light “escapes” (figure 5.36b). Simulations of the coupling loss with a ray tracing model yielded for the Toray and the Asahi POF the curves given in figure 5.37. We can see that for the Toray POF in combination with the two sizes of RCLEDs

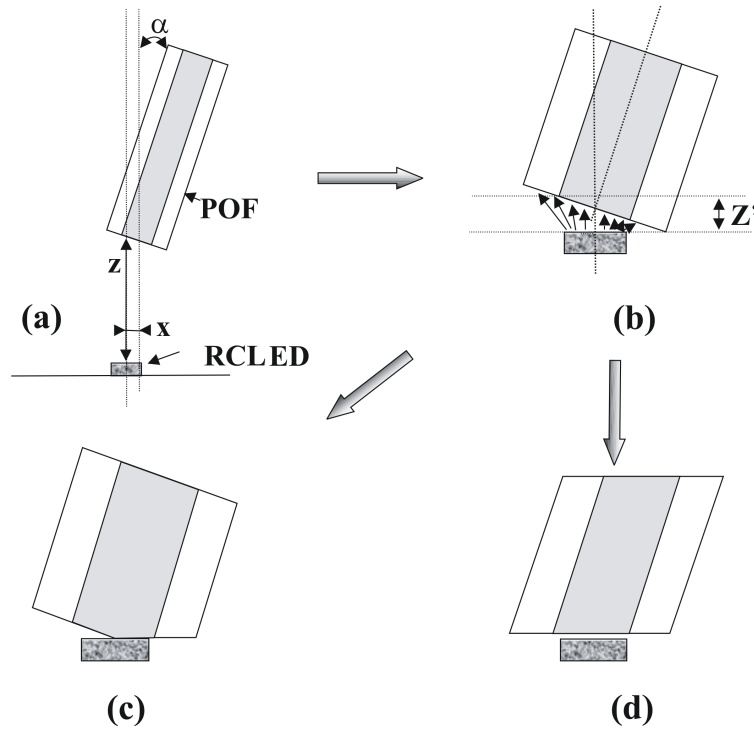


Figure 5.36: Tilt in a RCLED/POF interface is often coupled to separation (a). For tolerance calculations the configuration is reduced to one with a minimal separation (b). In a system with butt-coupling one can reduce this separation by applying force on the connectors ((c) and (d)).

there is no loss up to an angle of 3° , then the coupling efficiency drops very slowly to 25.7% for an offset of 10° . We can state that for the Toray POF the losses due to tilt are negligible. For the Asahi POF in combination with a $32\ \mu\text{m}$ RCLED the transmission is more sensitive to tilt. It drops to $\pm 23.3\%$ at 5° and to 21.5% at 10° , corresponding to an extra loss of 0.4 dB and 0.7 dB respectively. Since the tilt of the emission pattern with respect to the acceptance angle of the POF is of no influence up to 10° , the loss is entirely due to light escaping from the gap between RCLED and POF. This effect occurs at smaller angles for an Asahi POF than for a Toray fibre because of its small core diameter in comparison to that of the Toray POF.

Until now, no deformation of the fibre end facet was considered. In reality it is possible that the POF is pushed against e.g. a glob-top and that only a partial air gap or no air gap at all remains at the interface as shown in figures 5.36 c and d. The last case is similar to the configuration in figure 5.33 b. However,

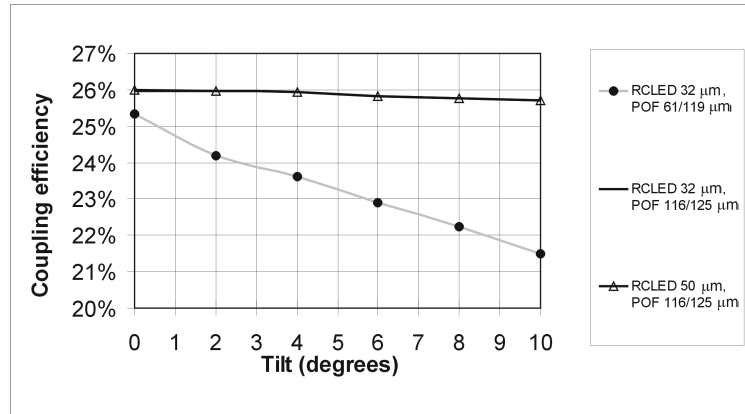


Figure 5.37: Power coupling of a RCLED to POF interface as a function of angular offset. (with gap)

the interface without deformation of the POF represents the “worst case” scenario and therefore this case is taken for the estimation of the angular coupling loss.

Experiments The strong linkage between angular and axial offset in connectors makes it difficult to verify experimentally the influence of tilt on the coupling efficiency: the ferrule in which the POF is mounted will increase the axial offset when tilted, due to its external edges (figure 5.38 (a), a problem that does not occur when measuring radial and axial offset. To circumvent this obstacle the external part of a ferrule was removed so that the POF lays at the edge of the ferrule (figure 5.38 b). However, even now a certain axial separation between POF and RCLED had to be respected in order not to damage the RCLED with the sharp edge of the adapted ferrule. The result of a coupling experiment between a 50 μm RCLED and a 116/125 μm Toray POF can be seen in figure 5.39. As can be seen, the measured coupling efficiency drops rapidly as a function of the tilt in comparison to the model. This can only be explained by axial offset. For more reliable experiments a more adequate setup should be designed. For instance a setup in which the distance RCLED-POF is monitored optically could offer a solution. This was not feasible within the time frame of this PhD. We will hence assume that, following the theoretical model, the losses purely due to tilt are negligible or very small for typical offset in the order of a few $^\circ$ (up to 10° for Toray POF).

Conclusion RCLED/POF interface alignment tolerances Comparing the tolerance estimations for the different possible offsets at a RCLED/POF interface we can state that radial offset is the most critical parameter. Although, for Toray POF a quite large alignment tolerance of 20-30 μm is valid for the radial offset. The estimations also showed that from an “alignment” point of view, Toray POF is clearly a better choice than Asahi POF. Finally the influence of tilt is very limited. It is zero for Toray POF, and small for Asahi POF,

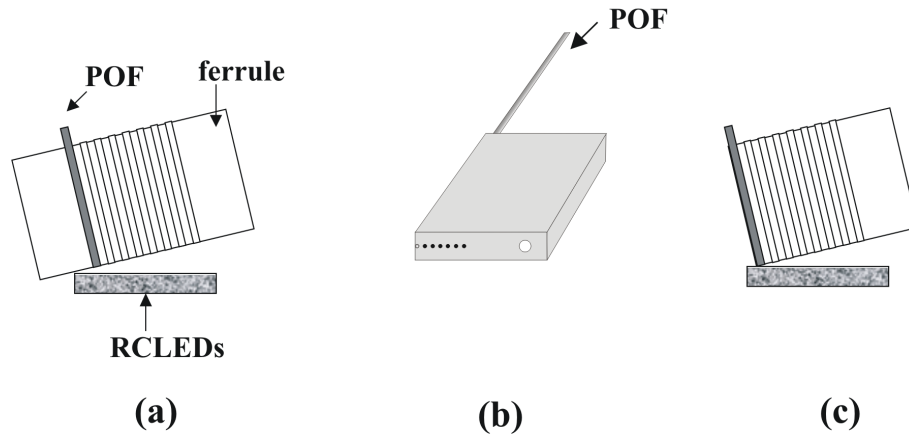


Figure 5.38: Adapted ferrule for RCLED-POF angular offset (a) The size of the ferrule introduces an extra axial separation (b) The outer part of the ferrule removed (c) The POF can be brought closer to the RCLED

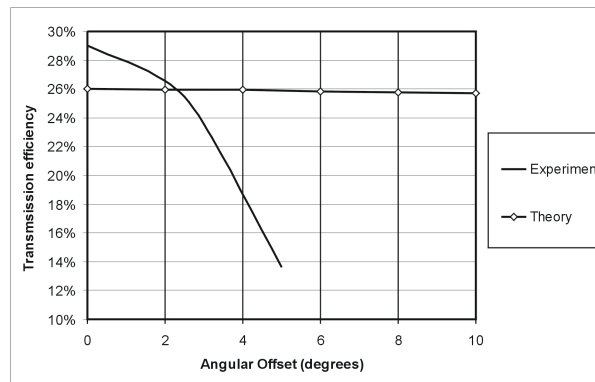


Figure 5.39: Comparison between model and experiment for angular offset. A $50 \mu\text{m}$ RCLED is coupled to a 116/125 Toray POF

5.4.1.2 VCSEL/POF interface

Thanks to their narrow emission pattern and the typical dimensions of VCSELS, the coupling alignment tolerances are clearly looser than in the case of RCLEDs. The radius of the emitting surface of a VCSEL typically measures $10 \mu\text{m}$ (large radial offset tolerance) and they emit the light in a beam with a typical divergence angle of 20° . Single mode VCSELS emit beams with a Gaussian irradiance profile. However, most of the VCSELS, including the ones used within the OIIC project, are multimode devices. However, given the VCSEL's small diameter and low beam divergence, we can use a Gaussian beam approximation for the VCSEL-POF coupling. This means that there are no intrinsic coupling losses and it leads to large axial and angular offset tolerance. No VCSELS were available for coupling

experiments during this thesis. However, some brief and simple calculations can show the loose tolerances on a VCSEL/POF alignment. Consider therefore the Gaussian approximation of the field emission pattern of a VCSEL: This means that the irradiance obeys:

$$S = S_0 \exp \left[-2 \left(\frac{x}{w_x} \right)^2 - 2 \left(\frac{y}{w_y} \right)^2 \right], \quad (5.13)$$

with x and y perpendicular to the propagation direction of the light. The irradiance drops with a factor e^{-2} with respect to the on-axis value S_0 when x and y equal w_x and w_y respectively. For circular symmetric beams $w_x = w_y = w$, a condition generally fulfilled for a single mode VCSEL. The spot size w is function of the distance z from the VCSEL:

$$w = w_0 \sqrt{1 + \left(\frac{\lambda z}{\pi w_0} \right)^2} \approx \frac{\lambda z}{\pi w_0}, \quad (5.14)$$

with w_0 the beam waist: the spot size where the beam is the narrowest, at $z = 0$. The right hand side approximation is valid only for $z \gg z_R$, with $z_R = \frac{\pi w_0^2}{\lambda}$ the Raleigh range parameter. At this z range the spot size increases linearly as a function of the travel distance, in other words the beam spreads with a constant diffraction angle:

$$\theta_0 = \arctan\left(\frac{\lambda}{\pi w_0}\right) \approx \frac{\lambda}{\pi w_0}. \quad (5.15)$$

In general this angle is small. For instance the 980 nm VCSELs used in the OIIC system demonstrator have a diffraction angle equal to 10.2°

The total power transmitted through an aperture with radius a for a beam with spot size w is then obtained by the integration of 5.13 over the surface of the aperture a ;

$$P_a = \int \int_A S dA = S_0 \int_0^{2\pi} \int_0^a \exp \left(-2 \left(\frac{r}{w} \right)^2 \right) dr = \frac{\pi S_0 w^2}{2} \left[1 - \exp \left(-2 \left(\frac{a}{w} \right)^2 \right) \right] \quad (5.16)$$

Hence the fractional power emitted in the centered circular cross-section of the beam is given by:

$$P_a/P_\infty = 1 - \exp \left(-2 \left(\frac{a}{w} \right)^2 \right), \quad (5.17)$$

with a the radius of the cross section. This equation tells us that 86 % of the beam power is emitted within the spot size w and 99.9 % of the power is confined in a circle with radius $2w$. Hence while designing optical pathways, taking $2w$ as the radius of the VCSEL beam is a very save rule of thumb.

Axial offset equation 5.16 can be used to give a rough estimation of the misalignment loss for axial offset by setting a equal to the radius of the POF core. As an example we take the VCSELs used for the OIIC system demonstrator, i.e. divergence angle 10.2° , emitting diameter $7 \mu\text{m}$ and wavelength 980 nm. The

curves in figure 5.40 show that the alignment tolerance is clearly greater than in the case of RCLED/POF couplings. For the Asahi POF a separation up to $70\ \mu\text{m}$ is possible without transmission loss (neglecting Fresnel losses). For the Toray POF this maximal working distance equals $150\ \mu\text{m}$. So not only is the alignment

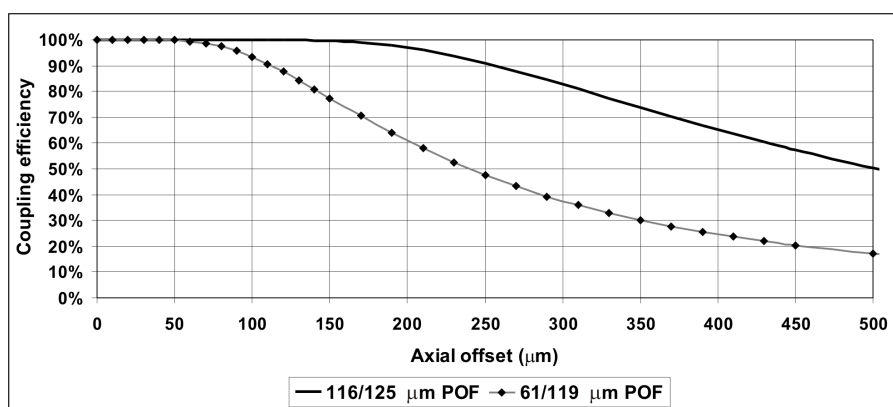


Figure 5.40: Transmission efficiency for a VCSEL-POF coupling as a function of axial offset

tolerance higher, but moreover all the emitted power of the VCSEL is coupled into the POF, in contrast with a RCLED, that only emits part of its total power into the numerical aperture of the POF.

Radial offset Since the irradiance of the Gaussian beam is well described by equation 5.13 it is quite simple to calculate the coupling efficiency as a function of radial offset. The algorithm is illustrated in figure 5.41: firstly the irradiance profile is calculated for a 2-dimensional cross section of a Gaussian beam. Then the power captured by the POF core is calculated using the integral:

$$P = \int_S I ds, \quad (5.18)$$

with S the surface defined by the overlap of the radially translated POF core and the cross section of the VCSEL beam. This integral is calculated numerically. The rate P/P_{total} , with P_{total} the total emitted power by the VCSEL, gives the coupling efficiency. This has been calculated for butt-coupled devices and the result can be seen in figure 5.42. It can be seen that no loss is introduced for an offset up to $20\ \mu\text{m}$ for the Asahi POF, and up to $45\ \mu\text{m}$ for the Toray POF. For larger offset the efficiency decays rapidly.

Angular offset Similar to the RCLED-POF coupling let us consider the configuration as shown in figure 5.36 b. The POF is tilted but its well aligned with respect to the X and Y axes, Z is minimal. For small tilt values the losses can easily be estimated. Let us therefore distinguish the two contributions that might

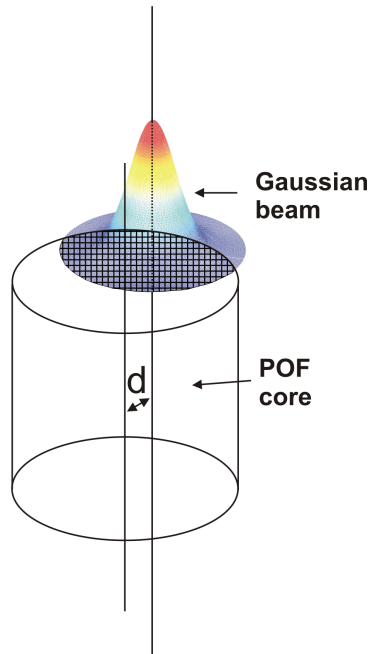


Figure 5.41: The estimation of the power coupled from a VCSEL into a POF is done by calculating the volume integral of the VCSEL beam profile limited by the hatched zone: the overlap between the beam cross section and the POF core, translated over a distance d

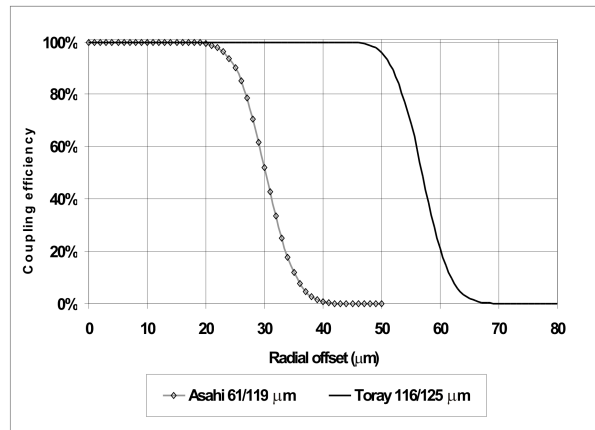


Figure 5.42: Coupling efficiency for a VCSEL to a POF as a function of radial offset

cause coupling loss: (1) due to the tilt some VCSEL light is not captured in the numerical aperture of the fibre, and (2) due to the gap between VCSEL and the POF some light does not reach the POF core. For small tilt values the latter is negligible. Consider therefore figure 5.43: which each tilt α corresponds an offset Z , following the relationship

$$Z = L \cdot \sin(\alpha), \quad (5.19)$$

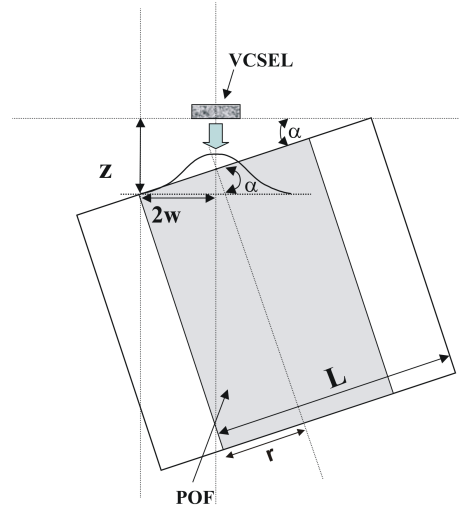


Figure 5.43: Angular offset for a VCSEL to POF coupling

with $L = r_{POF} + r_{core}$. For a certain maximal value Z_{max} , and hence α_{max} , the beam edge, taken as $2w$, will reach the POF core and losses are introduced. In other words:

$$2w(Z_{max}) = r_{core} \cdot \cos(\alpha_{max}) \quad (5.20)$$

Substituting equations 5.19 and 5.14 in equation 5.20 yields:

$$\tan(\alpha_{max}) = \frac{\pi}{2} \sqrt{\frac{r_{core}^2 - 4w_0^2}{\pi^2 w_0^2 + \lambda^2 L^2}} \quad (5.21)$$

For Toray POF this angle equals 37° , for Asahi POF 28° . Hence the losses caused by this contribution are completely negligible for small angular offset.

Let us now come back to the former possible contribution to tilt loss. In the far field a the VCSEL ray can be described by its radiant intensity:

$$I = I_0 \exp \left[-2 \left(\frac{\theta}{\theta_0} \right)^2 \right], \quad (5.22)$$

with θ_0 the diffraction angle given in equation 5.15. This means that all the power (99.99 %) of the VCSEL is emitted within angle $2\theta_0$ of the optical axis. So, for the given VCSELs $2\theta_0$ equals 20° . Since the spot size is clearly smaller than the POF core, the launching efficiency is not determined by the near-field distribution, but it is limited in the far field distribution [3, 10]. The considered POFs have a numerical aperture of 0.5, so an acceptance angle of 30° . This means that the VCSEL can be tilted over 10° , and still all the emitted light will fall within the acceptance angle of the fibre and will be guided.

Hence, as a an overall conclusion we can state a VCSEL-POF coupling does not suffer from transmission losses up to a tilt of 10° , an hence the tolerances for angular offset are very loose.

Conclusion VCSEL/POF interface alignment tolerances Due to its very low divergence angle the tolerance on axial offset is extremely loose (100 and 200 μm lossless for Asahi and Toray POF respectively). The alignment in radial direction is more critical but is still relatively easy (until 25 and 45 μm no loss for Asahi and Toray respectively). Tilt losses are negligible. Contrary to the considered RCLED/Asahi POF combinations, the VCSEL/Asahi POF combination seems totally acceptable, at least for alignment reasons.

5.4.2 POF/POF coupling

Fibre/fibre couplings are extensively described in literature [3–5, 11]. However, most of the models start from the assumption that Equilibrium Mode Distribution (EMD) is reached, and this is certainly not the case in interconnect links. It is thus worthwhile to compare the model with some experimental results in order to appreciate the influence of parameters like launching conditions, fibre length and bends on the coupling efficiency. We based our model on the discussion of the alignment tolerances given in [3]. The theoretical coupling model in this work starts from the assumption that the end facet of a fibre acts as a truncated Lambertian light source, i.e. it emits equal amounts of power per unit of projected area and per unit of solid angle from each part of its emitting surface. This optical power per unit of projected area and per unit of solid angle is called the radiance L ($\text{W m}^{-2} \text{sr}^{-1}$) and is constant over the emitting surface. Considering the POF as a truncated Lambertian emitter simplifies the calculations for power coupling efficiency and allows to approximate the coupling loss due to misalignments by analytical equations, at least for small offsets. We used this theoretical model for comparison with experimental results obtained with small-diameter POF.

5.4.2.1 Intrinsic losses

The influence of the geometrical and optical properties of the POFs on the coupling efficiency has already been discussed thoroughly in Chapter 3. It was shown that the variation on the numerical aperture causes an average coupling loss of 0.06 dB, with a maximum of 1.75 dB. The variation on the core diameter causes an average coupling loss of 0.04 dB for the Toray POF (maximal 0.3 dB) and 0.32 dB for the Asahi POF (maximal 2 dB). The impact of the variation of the outer diameter and the core-cladding non-concentricity is a more complex problem. The effect of those anomalies is a radial offset of the POF core, and the extent of that offset depends on the used alignment technology. It has been shown in Chapter 3 that with a standard fibre-hole-technology used in MT^{TM} ferrules the average induced loss is 0.19 dB for Toray POF. This has not been investigated for Asahi POF, but given the fact that the outer diameter of this POF varies more than that of the Toray POF, losses will be greater. In fact it can easily be calculated that a loss up to 2 dB is theoretically possible for this POF when aligned with MT^{TM} -technology.

Radial offset Following [3] the coupling efficiency is determined by the ratio of the overlapping area of two circles with radius r of the fibre core, and centers $2d$

apart, d being half the offset (figure 5.44). The coupling efficiency is given by

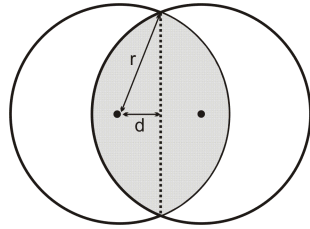


Figure 5.44: Two fibres with radial offset $2d$

$$\eta = \frac{2}{\pi} \left(\arccos\left(\frac{d}{r}\right) - \frac{d}{r} \sqrt{1 - \frac{d^2}{r^2}} \right) \quad (5.23)$$

It can be seen that the efficiency is independent of the numerical aperture. For small separations the equation simplifies to:

$$\eta = 1 - \frac{4d}{\pi r} \quad (5.24)$$

This means that for the Asahi POF a $5 \mu\text{m}$ offset generates a loss of 0.5 dB, for the Toray POF the same loss occurs at a $10 \mu\text{m}$ offset. The above expressions have been verified experimentally for Toray and Asahi POF. The comparison between experiment and model can be seen in figures 5.45 and 5.46. For the Asahi POF as

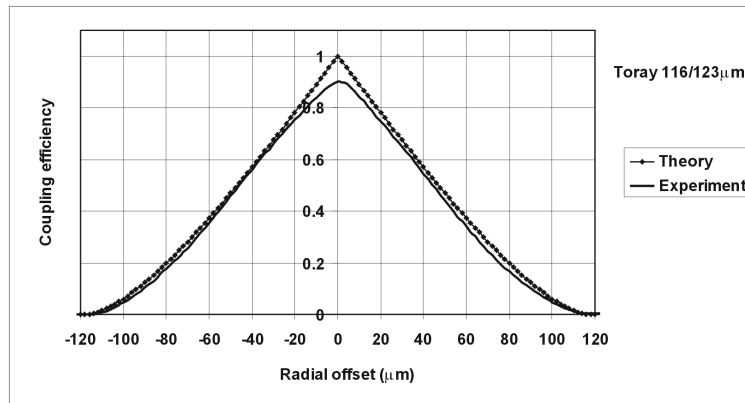


Figure 5.45: Coupling efficiency as a function of radial offset for Toray POFs, with butt-coupling

well as for the Toray POF there is a 10 % difference between theory and experiment at zero offset, due to the end facet roughness and intrinsic losses (difference in numerical aperture and core diameter). The POFs have been terminated with hot knife cutting. For the Toray POF the difference between model and experiment stays within a 10 % boundary up to an offset of about $80 \mu\text{m}$. For larger offset this

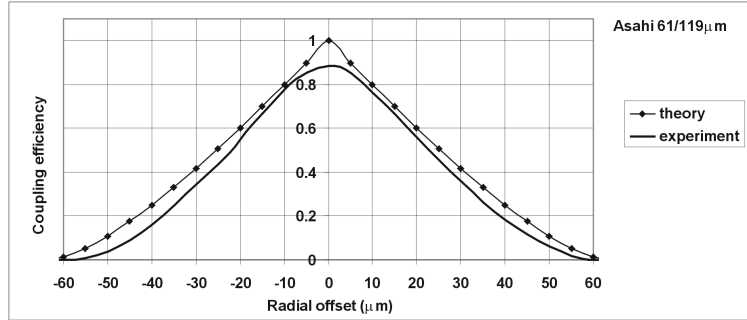


Figure 5.46: Coupling efficiency as a function of radial offset for Asahi POFs

difference becomes somewhat larger. However, for larger offset the measured power is very small and measurements less precise. For the Asahi POF the conclusions are similar, but the difference between model and experiment becomes larger than 10 % for separations larger than $25 \mu\text{m}$, which is a relatively smaller offset than in the case of the Toray POF. This could indicate that, at least for this sample, the roughness of the end facets is higher at the periphery of the core than at the centre. This phenomenon has been observed with most of the hot knife terminated Asahi POFs.

As a conclusion we can state that for radial offsets up to more or less the radius of the POF the model predicts the coupling losses well, taking into account the typical losses due to end facet roughness and intrinsic losses.

Axial offset The theoretical modeling is somewhat more complicated than in the case of radial offset. Here the emission pattern of the POF plays a role as the fibres are separated. In [3] the theoretical loss for small separations is given by:

$$\eta = 1 - \frac{z}{r} \frac{2}{\pi (NA)^2} \left[\arcsin(NA) - NA \sqrt{1 - (NA)^2} \right], \quad (5.25)$$

with r the radius of the POF and NA the numerical aperture. This equation does not take into account Fresnel losses at the end facets of the fibres, so another 8 % loss should be added. In reality the Fresnel loss is often compensated by applying index matching glue at the fibre coupling. The equation predicts a loss of 0.5 dB at an offset of $14 \mu\text{m}$ for the Asahi POF, the same loss is obtained for an offset of $27 \mu\text{m}$ for the Toray POF. Due to the strong dependence on the numerical aperture the POFs are relatively sensitive to axial offset, since they have a relatively large NA of 0.5. Moreover, since the emission pattern influences the coupling efficiency, experiments show a dependence on the mode distribution of the emitting fibre. This can be noticed in figures 5.48 and 5.49. During an experiment light is coupled from a HeNe Laser into a $62.5/125 \mu\text{m}$ step index glass fibre via a grin lens (figure 5.47). This glass fibre is coupled to a 30 cm long POF, that is in its turn coupled to another 30 cm of POF with the alignment system. The numerical aperture of the silica fibre has a typical value of 0.2. Hence the

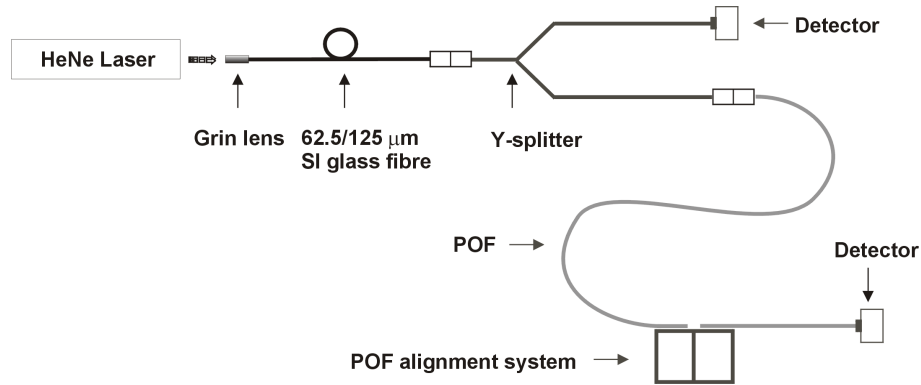


Figure 5.47: Experimental setup for the measurement of the effect of axial offset on the transmission efficiency at a POF to POF coupling

higher order modes in the first POF are not directly excited by the coupled light, resulting in a narrower emission pattern. This can clearly be seen in figure 5.48 for Toray POF. Not taking into account the 10 % end facet losses, the experiment shows less transmission loss than the model. This can be explained by the fact that the emission pattern of the emitting POF is narrower than for EMD. A second experiment confirmed this assumption. In order to broaden the emission pattern, we laid a few bends with radius 2mm in the first fibre and measured again the coupling efficiency as a function of the offset. As can be seen in figure 5.48 the coupling efficiency decreases faster for the fibre with bends, so that it agrees better with the model. A similar experiment with Asahi POF shows the same phenomenon (figure 5.49). However, the effect of the bending is smaller, which

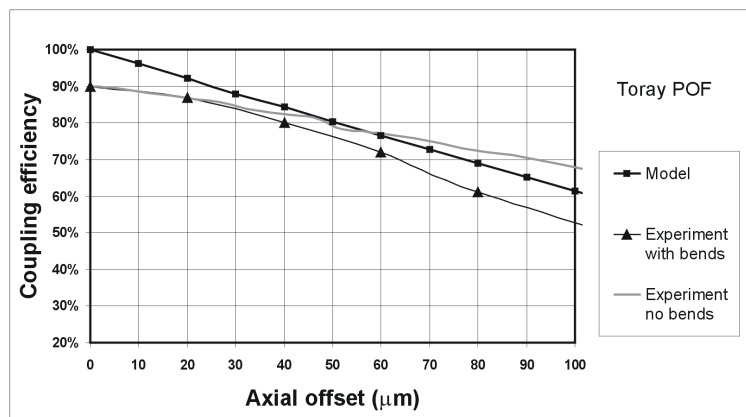


Figure 5.48: Coupling efficiency as a function of axial offset for Toray POFs

seems reasonable since the mode mixing is depending on the ratio :

$$\frac{\text{bending radius}}{\text{radius fibre core}}$$

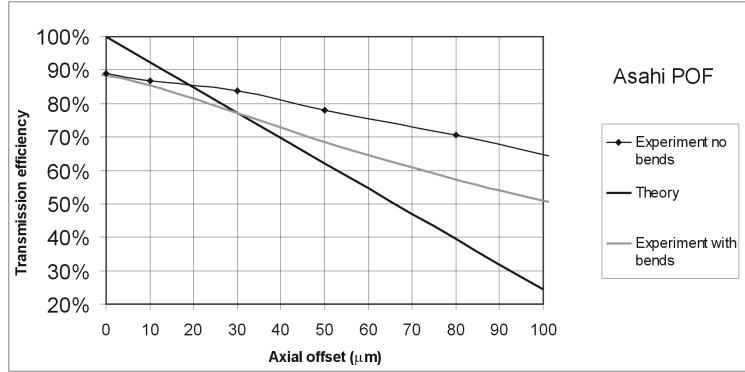


Figure 5.49: Coupling efficiency as a function of axial offset for Asahi POFs

The smaller the rate, the larger the mode mixing, hence the effect is larger for the Toray than for the Asahi POF. As a matter of fact, if we neglect the 10 % end facet losses, the experimental curve can be quite well matched with a theoretical curve for a numerical aperture of 0.2, the numerical aperture of the silica fibre. Analogously, the curve after the bending can be fitted with a model with $NA = 0.5$ for the Toray POF. For the Asahi POF the “new” numerical aperture only equals 0.3. These experiments show that axial offset in real interconnect links can be of less importance than predicted by the model, however while designing a link one can not take this into account, since bends and roughness influence this behaviour. Moreover if sources with a broad emission pattern, such as RCLEDs, are used, the model will give an accurate estimate, if one takes into account end facet roughness and Fresnel losses.

Theoretically it is possible that interference phenomena occur when the fibres are separated [3]. The parallel end facets of the fibres form, for small separations, a Fabry-Perot cavity. Hence the transmission efficiency does not follow a smooth curve as depicted in figure 5.48, but shows “fast” oscillations, for the first few micrometers of separation. In practice we never saw this phenomenon, probably because one needs very parallel and smooth end facets, a condition we did not easily achieve.

Angular offset For small angles, theory predicts a dependence of the transmission efficiency on angular offset as follows [3]:

$$\eta = \frac{2}{\pi} \left(\arccos\left(\frac{\gamma}{\sqrt{2\Delta}}\right) - \frac{\gamma}{\sqrt{2\Delta}} \sqrt{1 - \frac{\gamma^2}{2\Delta}} \right), \quad (5.26)$$

with $\gamma = \sin(\alpha)$, and α equaling half the tilt. The equation starts from the assumption that the mated fibres are in full physical contact as depicted in figure 5.50a. This is reasonable since in general a rather strong force is applied when ferrules are mated in order to assure physical contact (up to 20 N for standard connectors containing silica fibres). We only applied 1 N in order not to deform

the end facet of the POF, as mentioned in paragraph 5.3.3. Note that the radius

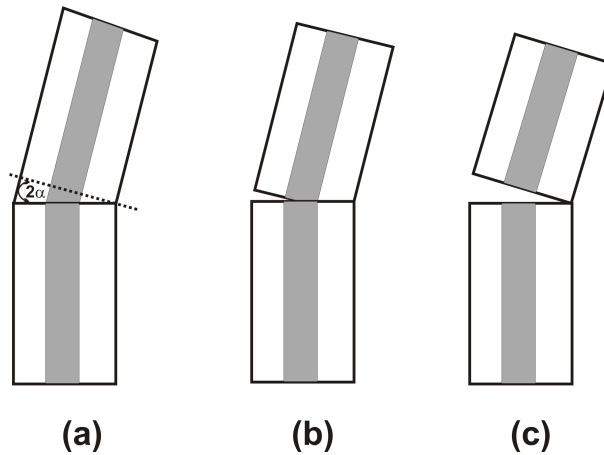


Figure 5.50: Possible configurations for POF/POF interfaces

of the fibre does not appear in the equation. For both the Asahi and the Toray POF the model estimates a loss of 0.5 dB for a 5° tilt. Similarly to axial offset the efficiency depends on the numerical aperture of the fibre, and hence on the mode distribution. This can be seen in figure 5.51 and 5.52. For the experiment

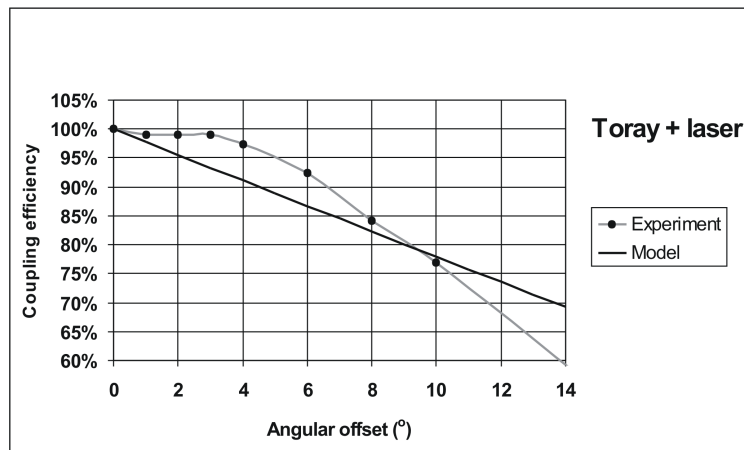


Figure 5.51: Coupling efficiency as a function of angular offset for Toray POFs with a HeNe Laser as light source

of figure 5.51 a similar setup as in figure 5.47 was used, i.e. a HeNe laser served as a light source, and two 30 cm pieces of POF were coupled. Also a MT^{TM} ferrule with a removed external part, as depicted in figure 5.38 b was used. We can see that, probably due to the absence of higher order modes in the emitting POF, the experiment shows no loss for small angular offsets, besides the end facet

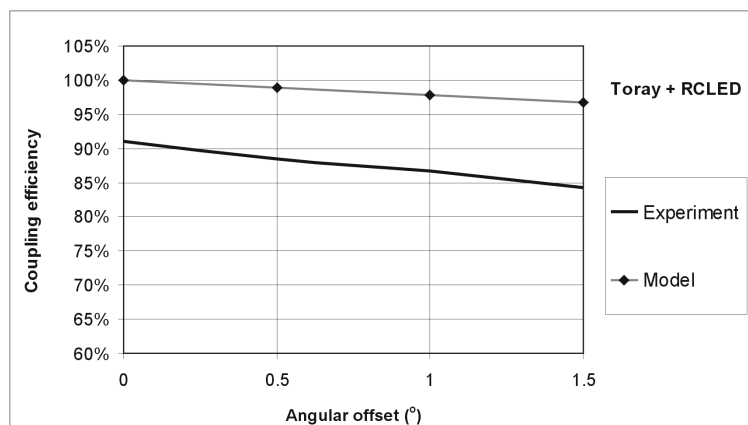


Figure 5.52: Coupling efficiency as a function of angular offset for Asahi POFs, with a RCLED as light source

roughness loss. Indeed, if the first POF does not guide higher order modes, it emits light at lower angles than in EMD. Hence even with some tilt, the emitted light will fall within the acceptance angle of the receiving fibre. For larger offsets the transmission efficiency drops faster than for the model, which is again compatible with a narrower emission pattern. Moreover, due to the fact that we only use a coupling force of 1 N, there might be only a partial physical contact between the fibre facets, especially for larger angles (figures 5.50 b and c), which could decrease the transmission efficiency even more. When a light source with a broad emission pattern is used, such as a RCLED, the higher order modes are excited and the experiments confirmed the model. As shown in figure 5.47, for which a 980 nm RCLED was used, the difference between theory and experiment is solely due to end facet loss.

Conclusion POF/POF interface alignment tolerances Clearly the most critical parameter to control is the radial alignment (5 and 10 μm for 0.5 dB, Asahi and Toray respectively). Axial offset is roughly spoken 3 times less stringent than radial offset (14 and 27 μm for 0.5 dB, Asahi and Toray respectively). The consequences of tilt are not negligible: for 5° a loss of 0.5 dB is estimated.

5.4.3 POF-to-detector coupling

Similarly to the emitter/fibre side of the link the chosen geometrical and optical parameters of the fibre and the detectors strongly influence the coupling efficiency. For instance, the smaller the numerical aperture of the POF, the looser the tolerance on separation [2]. Or in case the detector diameter is smaller than the POF core diameter, intrinsic losses will be introduced and alignment tolerances are tightened. Also the presence of a substrate between the POF and the active area of the detector causes losses. This is for instance the case for the detectors

used in the OIIC system demonstrator: the InGaAs/InP PIN photodiodes contain

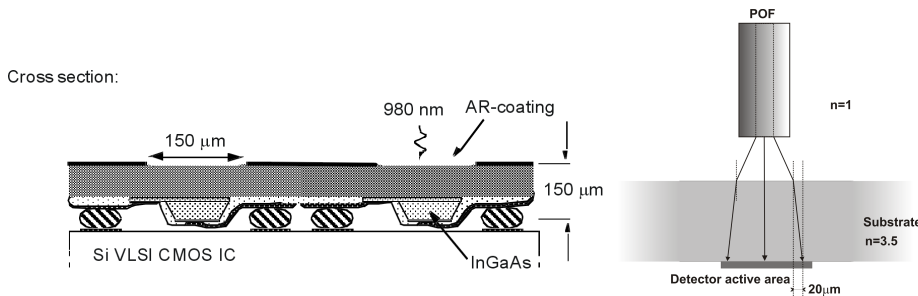


Figure 5.53: Structure of a flip-chipped InGaAs/InP detector

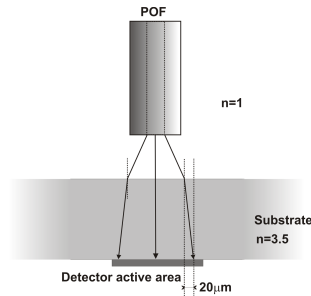


Figure 5.54: Optical pathway at the POF-detector interface

a 150 μm thick InP substrate (figure 5.53). Since they are flip-chip mounted the incoming light has to pass the substrate and hence there is a separation between the fibre end facet and the InGaAs/InP layers. Hence the light spot emitted by the fibre is broadened until it reaches the detector. Given that the refractive index of the substrate is about 3.5, one can calculate that the radius of the spot emitted by POF, increases by about 20 μm when it reaches the detector area (figure 5.54). As a consequence one was obliged to use a relatively large detector diameter (150 μm in combination with Toray POF) for the system demonstrator, in order to capture sufficient power for signal detection. This increased the capacity of the detector, and reduced its speed. Therefore the OIIC system demonstrator worked at the limited data-rate of 150 Mbit/s per channel [1]. An option to circumvent this problem is to remove the substrate, so that the POF end facet can be brought closer to the active area of the detector and smaller detector areas can be used. This solution was chosen for the OIIC Gigalink, which was designed to work at a data rate of 1 Gbit/s per channel [1] and optimized for a 850 nm wavelength. The InP substrate of a 90 μm InGaAs/InP detector was removed with wet-chemical etching, until only 1 μm remained. This allowed to obtain high coupling efficiencies from Asahi POF to the detectors. Unfortunately there have been problems with the yield of the 850 nm sources and as a consequence the 150 nm detector with substrate has been used in combination with the Asahi POF. We estimated the alignment tolerances for the POF/detector combinations proposed in the framework of the OIIC project. Therefore we calculated the coupling losses as a function of the offset using the ASAP ray tracing software, for the following combinations: Toray POF/detector 150 μm /150 μm substrate, Asahi POF/detector 150 μm /150 μm substrate, Asahi POF/detector 90 μm /1 μm substrate. The modeling results could not be validated experimentally since no detectors were available for separate alignment tolerance measurements.

Intrinsic losses We used the ray tracing program ASAP to calculate the coupling losses due to the varying diameter and numerical aperture of the POF. For all the configurations the losses are non-existent or negligible.

Axial offset The results for axial offset modeling can be seen in figure 5.55. The Asahi POF allows an offset of $30\ \mu\text{m}$ and $50\ \mu\text{m}$ without any coupling loss in combination with the $90\ \mu\text{m}$ and $150\ \mu\text{m}$ detector respectively. The curve of the Toray POF shows a different behavior: due to the larger diameter of the POF, coupling losses are introduced as soon as fibre and detector are separated. At $40\ \mu\text{m}$ a loss of 0.5 dB is seen. Note that the curve for the detector with thin substrate drops more steeply than for the detectors with $150\ \mu\text{m}$ substrate, for larger separations. This is evidently due to the smaller diameter of these detectors.

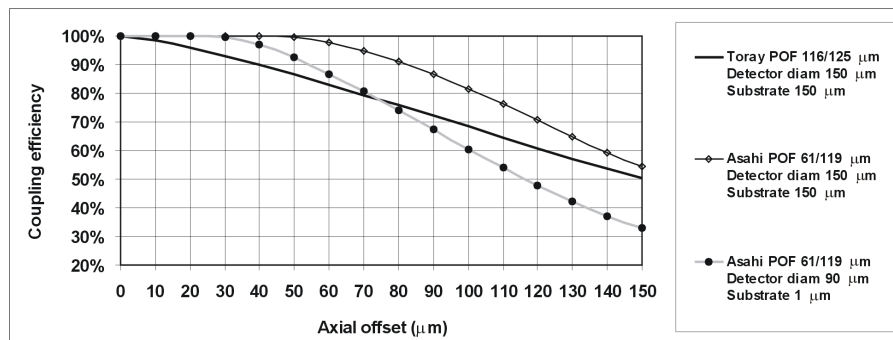


Figure 5.55: Coupling efficiency as a function of axial offset for a POF-to-detector coupling

Radial offset Following our calculations the combination Asahi POF/ $150\ \mu\text{m}$ detector allows an offset of $25\text{--}30\ \mu\text{m}$ without any loss (figure 5.56). For the Asahi/POF with the $90\ \mu\text{m}$ detector this value decreases to $15\ \mu\text{m}$, for greater offsets the efficiency decreases rapidly. For the Toray POF in combination with the $150\ \mu\text{m}$ detector losses are present as soon as an offset is introduced. For an offset of $25\ \mu\text{m}$ a loss of 0.5 dB is calculated.

Angular offset We will only consider the most general configuration for tilt as depicted in figure 5.57. The POF is tilted but not deformed. A small separation z is introduced but solely due to the rotation of the POF end facet. In case the POF is pushed against the detector or an intermediate medium, so that the remaining separation vanishes, the coupling efficiency can only be better than in the case we consider. The configuration we chose is hence part of a conservative approach. It can be seen in figure 5.58 that the Asahi POF in combination with both detector types can be tilted up to 12° without causing coupling loss. For the Toray POF a loss is introduced when the fibre is tilted. However it is limited: 0.18 dB for an angular offset of 10° . Hence we can state that for the POF-detector combination we consider, losses due to tilt are negligible.

Conclusion for the POF-detector interface The most critical parameter to control at the fibre-detector interface is radial offset. It yields losses roughly twice

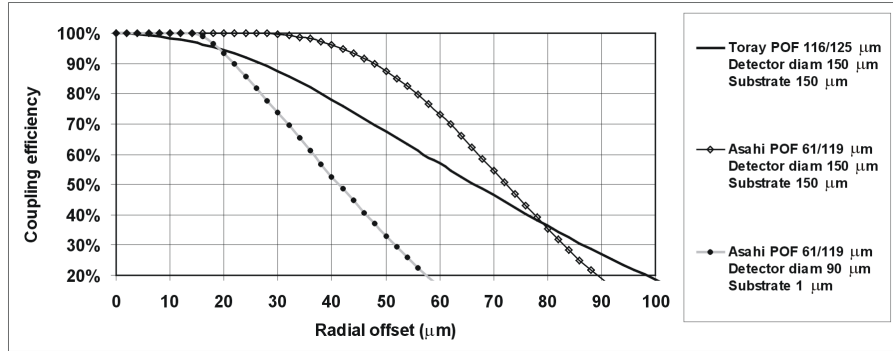


Figure 5.56: Coupling efficiency as a function of radial offset for a POF-to-detector coupling

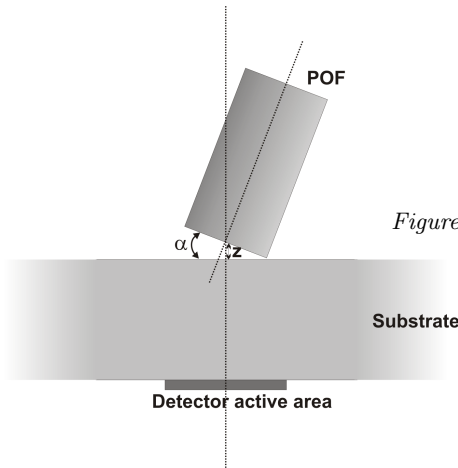


Figure 5.57: Configuration of the angular offset at the POF-detector interface

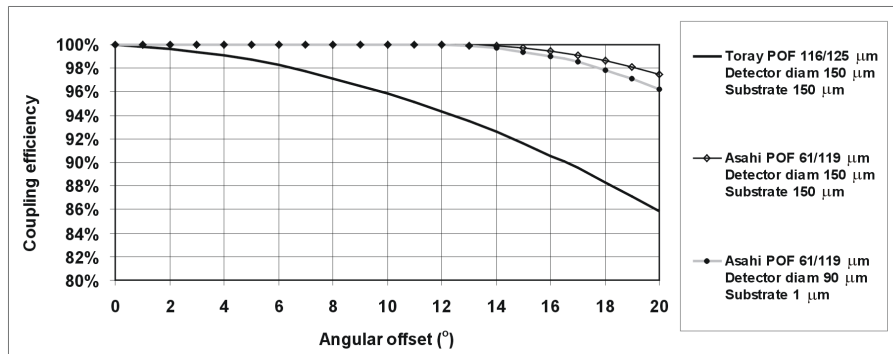


Figure 5.58: Coupling efficiency as a function of angular offset for a POF-to-detector coupling

as large as those caused by axial offset. Tilt losses are negligible.

5.5 Optical cross-talk

One speaks of optical cross-talk when light from one optical channel reaches another, adjacent, channel. The risk of cross-talk depends on the optical and geometrical properties of the optical devices on the one hand, and on the distance between the different elements on the other hand. In general cross-talk will occur when the end facets of the mating devices are considerably separated. The minimal separation z for which cross talk can occur can be calculated analytically.

POF/POF interface We consider POFs at a pitch of $250\ \mu\text{m}$, the standard distance in parallel optical links and in the framework of the OIIC program. From figure 5.61 it can easily be seen that crosstalk will occur when the light emitted at the maximal angle of 30° reaches the core of the neighbouring POF. Or

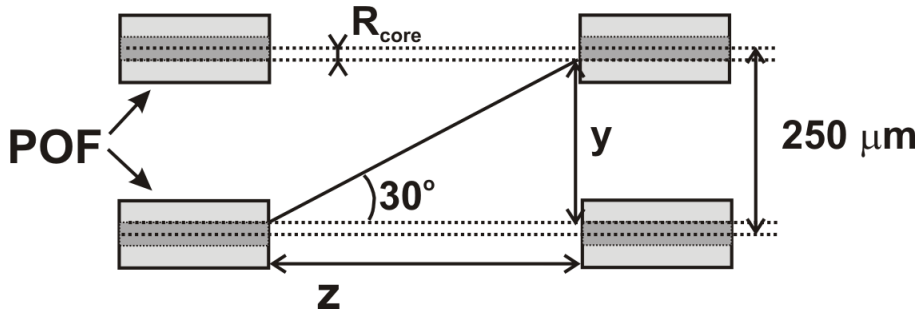


Figure 5.59: Optical cross-talk at the POF/POF interface

mathematically:

$$y + 2 R_{POF} = 250 \quad (5.27)$$

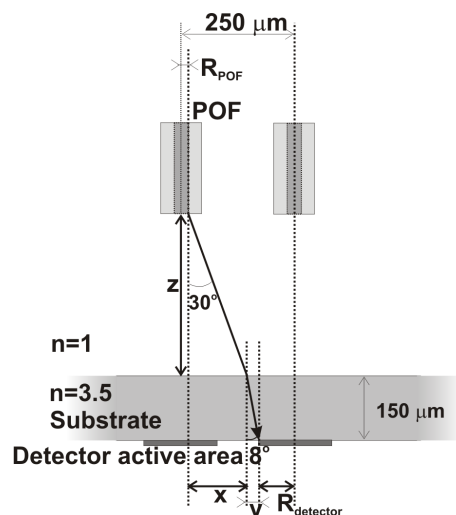
Given that $y = z \cdot \tan(30^\circ)$, z can easily be extracted. For Toray POF this gives a separation of $232\ \mu\text{m}$, for Asahi POF this becomes $327\ \mu\text{m}$. These are values that are far above real separations that occur in systems, and hence optical cross-talk will not occur at POF/POF interfaces.

POF/detector interface The situation is quite similar to the POF/POF interface: if light emitted from the POF at the maximal angle of 30° reaches an adjacent detector, cross-talk occurs (figure 5.60). Only here a small part through the detector substrate has to be added to the optical path. This leads to the following condition for cross-talk:

$$R_{POF} + x + y + R_{detector} = R_{POF} + z \cdot \tan(30^\circ) + 150 \cdot \tan(8^\circ) + R_{detector} = 250 \quad (5.28)$$

From which z easily extracted. The 8° angle in the substrate is of course derived from Snell's law at the air/substrate interface. For Toray POF in combination with

Figure 5.60: Cross-talk at the POF/detector interface, with detector substrate thickness $150\ \mu\text{m}$



the $150\ \mu\text{m}$ detector a separation of $116\ \mu\text{m}$ is calculated, for the same detector with the Asahi POF, $214\ \mu\text{m}$ is found. For the detector without substrate the path through the substrate is negligible and z equals $300\ \mu\text{m}$, in combination with an Asahi POF. It is clear that those numbers are very large and that hence optical cross-talk is not an issue at the POF/detector interface.

Emitter/POF interface At the emitter/POF interface one has to distinguish two possibilities. Either the source emits at angles larger than the acceptance angle of the fibre, or it does not. In the former case z is defined by the acceptance angle of the POF. This can be seen in figure 5.61a, where a RCLED/POF interface is shown. The condition for cross-talk is similar to equation 5.28, just $R_{detector}$ needs to be replaced by R_{RCLED} . In the latter case, which is the case of the VCSEL, z is defined, not by the acceptance angle of the fibre, but by the maximal emission angle of the emitter (figure 5.61b). Given the fact that the VCSEL beam has a low divergence, cross talk only occurs with a large separation. Taking twice the divergence angle as maximal emission angle for the POF, we calculated a $500\ \mu\text{m}$ minimal separation for cross-talk. For RCLED-POF interfaces we found separations between 250 and $300\ \mu\text{m}$. It is hence clear that, with the optical devices we consider in this thesis, and at a pitch of $250\ \mu\text{m}$, optical cross-talk does not form a problem at any of the interfaces.

5.6 Power budget: calculations on examples

The choice of the elements to be implemented in an optical interconnect link is basically driven by the following question: how do we optically transfer a digital signal from transmitter to receiver with the lowest power consumption and the highest data rate? The solution to this question not only depends on the underlying electronics of the link, but also on the characteristics of the optoelectronic

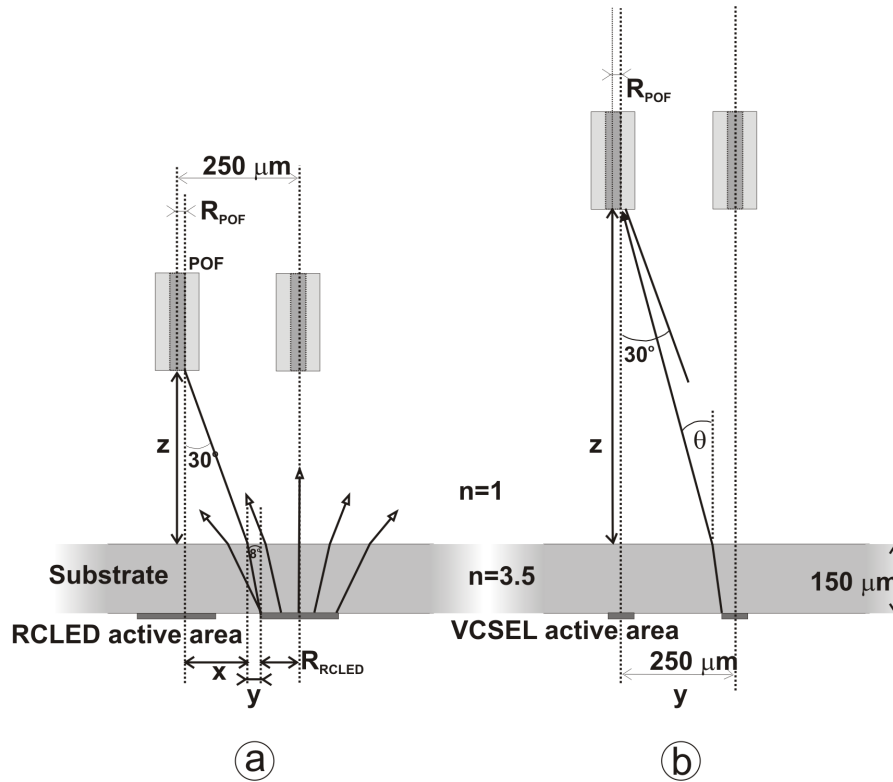


Figure 5.61: Optical cross-talk at the POF/POF interface (a) RCLED light source (b) VCSEL light source

and optical devices. In general a balance has to be found between speed, coupled optical power, power consumption, and of course, technical feasibility. This issue has been thoroughly studied in the framework of the OIIC and the consortium has come up with a couple of link configurations, implemented in the System Demonstrator(s) and the Gigalink [1]. After the setting of the parameters for the devices in the link, it is then the task of the optical engineer to investigate what the power transmission efficiency of the optical pathway needs to be. Better said, how much losses can be permitted and still couple enough power in order to transmit data from detector to receiver. In other words, after taking into account intrinsic and end facet losses, what alignment offsets can we tolerate at the optical interfaces? We will try to solve this question for some typical link configurations, for which we get our inspiration in the proposed OIIC links.

Link configuration and power budget In this chapter we discussed the coupling of following elements: Toray POF 116/125 μm , Asahi POF 61/124 μm , RCLED 31 μm , RCLED 50 μm , VCSEL, Detector 150 μm , Detector 90 μm . We will limit the devices in the examples to devices that were made for 980 nm wavelength,

since they were eventually found to be the most reliable during the OIIC program. This choice sets the boundary conditions at the POF/detector side of the link. The 150 μm detector for 980 nm needs a minimal power of 34 microwatt (-14.7 dBm) for signal detection. At this stage we can already make a selection for the light source. Let us therefore firstly consider the POF, and more precisely the length of it. Typical lengths we are aiming for is e.g. 20 cm and 50 cm. However, at 980 nm, absorption losses in the POF are about 10 dB/m, and hence half a meter corresponds to 5 dB, a reduction by a factor three. The shorter POF of 20 cm will show a loss of 2.2 dB (40 % loss). For Asahi POF this is even slightly higher: 5.7 dB for 50 cm, and 2.6 dB for 20 cm. On the detector side of the link on the other hand, drive current for the emitters is limited. For instance in the OIIC system demonstrator this about 3 mA [12]. In case of the RCLEDs this current yields between 300 and 350 microwatt output (-5.2 to -4.6 dBm) power for a 50 μm RCLED, and about 150 microwatt (-8.2 dBm) output power for a 30 μm LED [7]. At the same current a VCSEL easily reaches 1 mW output power. Taking into account the RCLED/VCSEL to POF coupling efficiencies we can calculate the maximal power that will be emitted by the POF end facet and that is incident on the detector.

Table 5.2: Power emitted at POF end for different light sources and different POF lengths, at 3 mA drive current

	Toray 20 cm	Toray 50 cm	Asahi 20 cm	Asahi 50 cm
RCLED 30 μm	24 μW -16.1 dBm	13 μW -18.8 dBm	22 μW -16.5 dBm	11 μW -19.6 dBm
RCLED 50 μm	52 μW -12.8 dBm	28 μW -15.5 dBm	39 μW -14.1 dBm	19 μW -17.2 dBm
VCSEL	600 μW -2.2 dBm	316 μW -5dBm	549 μW -2.6dBm	266 μW -5.7dBm

This table does not take into account end facet losses and assumes perfect alignment with butt-coupling. In this case the power emitted by the POF equals the power received by the fibre. A 100 % coupling efficiency of VCSEL to POF is considered as well as typical 27 % RCLED to POF efficiency (5.7 dB loss). Given the fact the detectors need a minimal power of 34 microwatt, one can notice that a RCLED can only be used in combination with a 20 cm Toray POF, and it should have a diameter of 50 μm . The combination 50 μm RCLED with 20 cm Asahi

POF is just above the limit, but the margin is too small for an adequate link. On the other hand, it is clear that the VCSEL/POF combination delivers more than sufficient power, for both lengths of POF

Hence we will limit our calculations to the following three combinations

- VCSEL/50 cm Toray POF
- VCSEL/50 cm Asahi POF
- RCLED 50 μm /20 cm Toray POF

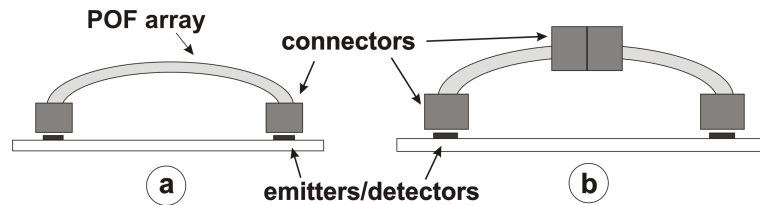


Figure 5.62: Possible configurations of the optical pathway: (a) only connectors at the end of the fibres (b) with an intermediate connector

In addition to the choice of the link elements also the number of connectors will influence the losses in the link. Within the framework of the OIIC program the configuration of figure 5.62a was chosen: one connector at the detector side and one at the emitter side. Yet it is possible that one wants to increase the routing flexibility of the POF links and in that case adding an intermediate POF/POF connector would be an option (figure 5.62b). Of course, introducing an extra interface means introducing extra losses. As has been mentioned, the table above only takes into account maximal RCLED/VCSEL-POF coupling efficiency and fibre transmission losses in order to calculate the minimal loss over the link. However some other factors have to be taken into account: end facet roughness and Fresnel losses as well as varying diameter and numerical aperture of the POF add to the minimal loss of the link. The 27 % coupling efficiency at the RCLED/POF interface is based on experimental results and hence the intrinsic losses are already included. For the VCSEL/POF the influence of the varying POF is negligible, only some end facet roughness and Fresnel losses have to be taken into account, estimated at 0.2 dB average. At the POF/POF interface we measured an average loss of 9 % or 0.40 dB. At the POF/detector interface also only Fresnel and end facet roughness have to be taken into account: 0.2 dB. Nowhere we considered the influence of the varying outer diameter. Since, the impact of this variation on the coupling efficiency is closely related to the implemented alignment technology it is hard to estimate a common value for loss. Since the effect of varying outer diameter is a radial offset of the core anyway it simpler to consider it as being part of the radial alignment accuracy. Finally we assume that there are two 90° bends with bending radius 2 mm in the optical path, corresponding to a loss of

0.4 dB. We can now calculate the power budget of the considered link configurations, under circumstances of perfect alignment. The results for a link with two connectors can be seen in table 5.3. With “budget” we mean the loss that can still

Table 5.3: Power budget estimated for a link with two connectors

	Power at source	Link loss	Power at detector	Budget
RCLED 50 μm 20 cm Toray	-4.9 dBm	8.5 dB	-13.4 dBm	1.3 dB
VCSEL 50 cm Asahi	0 dBm	6.5 dB	-6.5 dBm	8.2 dB
VCSEL 50 cm Toray	0 dBm	5.8 dB	-5.8 dBm	8.9 dB

be afforded while having a functional link. We can see that for the VCSELs there is still enough room for some “power waste”. For the RCLED-based link though, the specifications are very tight. For links with three connectors the budget decreases with another 0.4 dB. A RCLED-based link with three connectors has then a budget of 0.9 dB, which does not leave much room for misalignments. In the VCSEL-based links on the other hand, a third connector can easily be introduced.

Alignment tolerances for a link without intermediate POF/POF connector.

RCLED-based link: Since the connector technology at detector and source side are the same the accuracy on the alignment will be the same. Hence the sum of the coupling losses on both interfaces can be calculated as a function of a single offset parameter per axis. We calculated the total coupling loss in function of axial and radial offset, tilt can be neglected. As can be seen from figure 5.63 the loss as a function of radial offset reaches 0.15 dB at 15 μm , and then increases rapidly for greater offsets. Hence 15 μm is a good guide number for radial offset. It is then possible to increase the axial offset up to 50 μm , yielding an extra loss of 1 dB. However, a 15 μm radial offset yields slightly higher losses at 50 μm separation than at butt-coupling. This can be noticed when we calculate the loss generated by radial offset at 50 μm separation. In this calculation we do not take into account the loss caused by the separation, but solely the additional loss caused by the radial offset at that particular separation. The result can be seen in figure 5.64, where the coupling loss as a function of radial offset is given, at an axial offset of 50 μm and with butt-coupling. A radial offset of 15 μm creates an extra loss of 0.3 dB. This means that in the worst case one will obtain a loss of 1.3 dB,

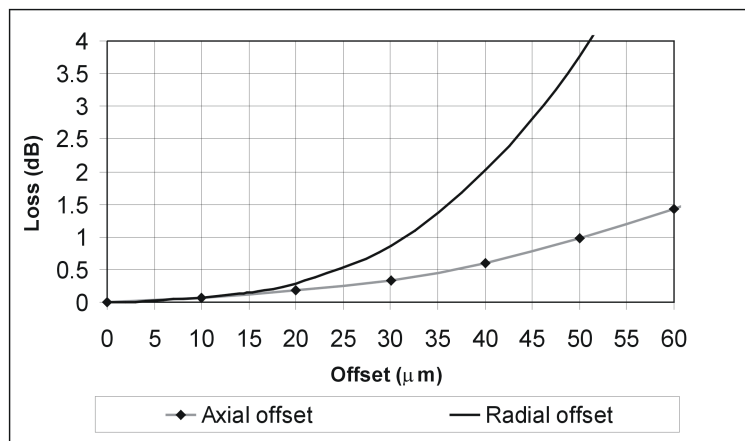


Figure 5.63: Total coupling loss for a $50\ \mu\text{m}$ RCLED/ 20 cm Toray POF link

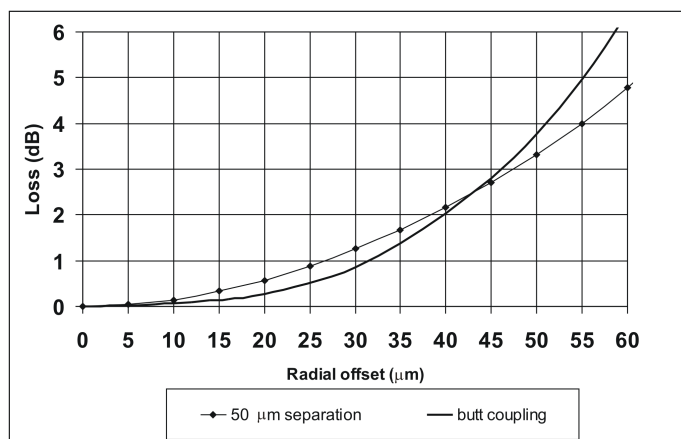


Figure 5.64: Total coupling loss for a $50\ \mu\text{m}$ RCLED/ 20 cm Toray POF link as a function of radial offset at a separation of $50\ \mu\text{m}$

exactly the power budget we have estimated. It also means that the alignment tolerances really have to be obeyed, otherwise the link will not work well. By keeping a separation between detector/RCLED and POF damages at the optoelectronic elements can be avoided. In order to stay under $50\ \mu\text{m}$ separation, it is e.g. an option to aim for a $30\ \mu\text{m}$ separation, and try to achieve a $20\ \mu\text{m}$ accuracy on the z-positioning.

VCSEL-based link: Similar to the RCLED-based link, losses due to tilt are negligible. However, the high output power of the VCSELs allows to use a larger separation between optoelectronics and POF. It has been suggested in the framework of the OIIC project to aim for a $50\ \mu\text{m}$ working distance. From the calculations in

section 5.4.1.2 one notices that there are no coupling losses at this axial offset for a VCSEL/POF interface, neither for the Asahi-, nor for the Toray POF. Hence the limitation on axial offset will rather come from the POF/detector than from the VCSEL/POF interface. The total coupling loss as a function of axial offset for a two-connector link has been calculated for the two kinds of POF and can be seen in figure 5.65. For a separation of $50\ \mu\text{m}$, the total loss is about 0.6 dB for the Toray POF and is negligible for Asahi POF link. It is hence an option to e.g.

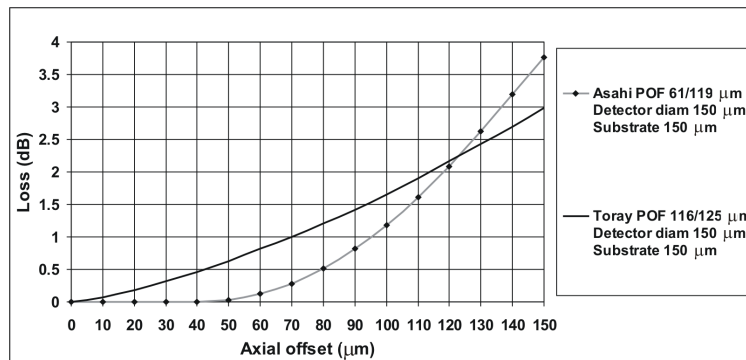


Figure 5.65: Total coupling loss as a function of axial offset VCSEL/50 cm POF link with two connectors

aim for a separation of $50\ \mu\text{m}$, with an accuracy of $40\ \mu\text{m}$ on the z-positioning. We would obtain a maximal coupling loss of 1.4 dB for the Toray POF and 0.8 dB for the Asahi POF (at $90\ \mu\text{m}$ separation).

For the radial offset the differences between Asahi and Toray POF are larger as shown in figure 5.66, where the coupling efficiency in function of radial offset is given for butt-coupling. For the Asahi POF the losses increase considerably for offsets greater than $20\ \mu\text{m}$. This is almost entirely due to coupling loss at the VCSEL-POF side. At this offset the laser beam touches the edge of the POF core and losses increase rapidly (figure 5.42), while for the same misalignment at the POF to detector side the efficiency remains around 100% (figure 5.56). For the Toray POF the situation is reversed: the losses are caused by the POF to detector interface: for an offset of $25\ \mu\text{m}$ the coupling efficiency at the VCSEL/POF interface is 100% (figure 5.42), while at the POF to detector side the loss reaches already 15% (figure 5.56).

As pointed out previously, it is an option to aim for a separation of $50\ \mu\text{m}$ with a tolerance of $\pm 40\ \mu\text{m}$. However, radial offset induces a different loss at different separations. This can be seen in figure 5.67: the loss due to radial offset in a VCSEL/Asahi is given for different separations. Here again we do not take into account the loss caused by the separations but only the additional loss due to radial offset at that particular separation. For offsets under $30\ \mu\text{m}$ the loss is the highest at $90\ \mu\text{m}$. For higher offsets the loss is larger for lower separations. If we set a radial offset tolerance of $25\ \mu\text{m}$, the radial loss is limited to 2.5 dB at $90\ \mu\text{m}$. This means that if we set $25\ \mu\text{m}$ for radial and $40\ \mu\text{m}$ axial tolerance, the maximal

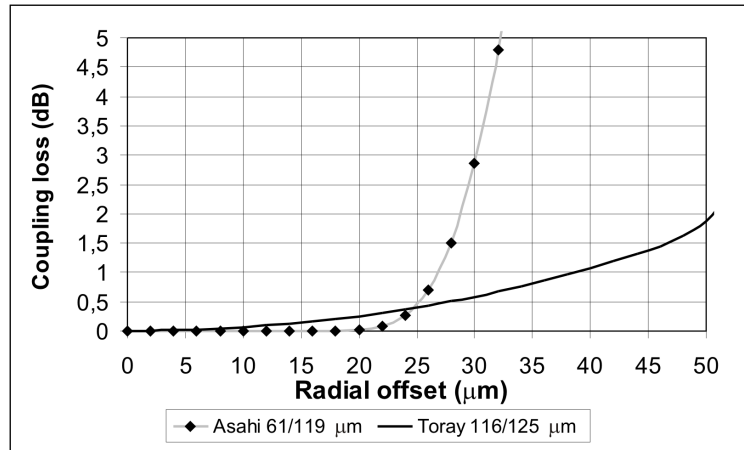


Figure 5.66: Total coupling loss as a function of radial offset for a VCSEL/50 cm POF link with two connectors and butt-coupling

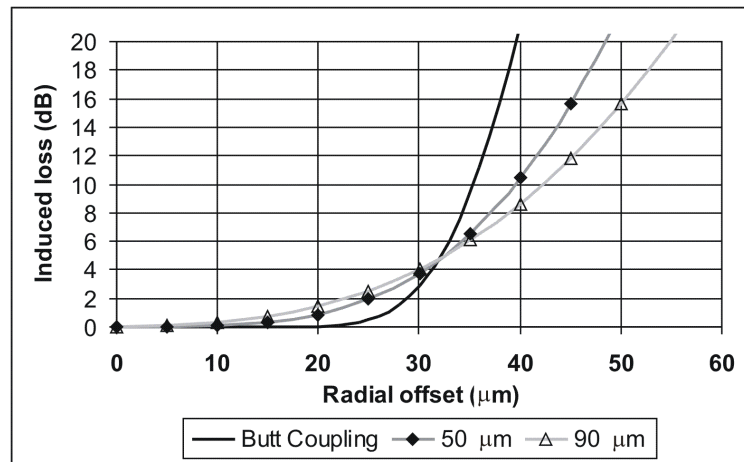


Figure 5.67: Loss induced by radial offset for different axial offsets in a VCSEL/50 cm Asahi POF link

alignment loss is limited to $2.5 \text{ dB}(\text{radial}) + 0.8 \text{ dB}(\text{axial}) = 3.3 \text{ dB}$. This can be afforded since we calculated a 8.2 dB power budget (table 5.3).

For the Toray POF a larger radial misalignment can be tolerated. This can be seen in figure 5.68 where we plotted the total coupling loss as a function of radial offset at different separations. Up to $40 \mu\text{m}$ the losses are very similar at the different separations. For higher offsets the loss increases steeply, especially for the butt-coupled case. By taking the radial offset limit $40 \mu\text{m}$, we limit the radial offset loss to 1.15 dB . A maximal loss of 1.15 dB , will be found in that case. Adding the loss at $90 \mu\text{m}$ separation (1.4 dB) and the loss at $40 \mu\text{m}$ radial offset (1.15 dB) yields a

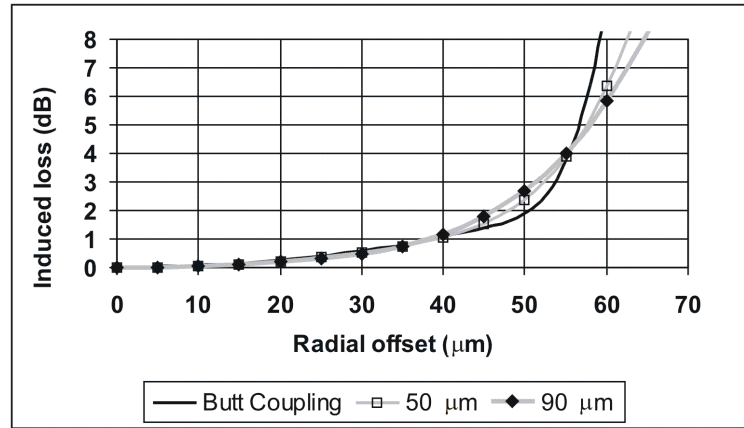


Figure 5.68: Loss induced by radial offset for different axial offsets in a VCSEL/50cm Toray POF link

Table 5.4: Power budget estimated for an optical link with two connectors

	Axial accuracy	Radial accuracy	Coupling loss	Total loss	Budget
50 μm RCLED Toray 20 cm POF	20 μm	15 μm	1.3 dB	9.8 dB	0 dB
VCSEL Asahi 50 cmPOF	40 μm	25 μm	3.3 dB	9.8 dB	4.9 dB
VCSEL Toray 50 cm POF	40 μm	40 μm	2.55 dB	8.35 dB	6.35 dB

total coupling loss of 2.55 dB. Since we calculated a power budget of 8.9 dB, this loss should cause no problem (table 5.3).

Taking into account the coupling losses for the different link configurations we obtain a new power budget in table 5.4.

Alignment tolerances for a link with intermediate POF/POF connector.

Table 5.4 shows that introducing an intermediate POF/POF connector in the RCLED-based link is impossible. For the VCSEL-based links it is feasible though. POF/POF couplings are done with butt-coupling since there are no great risks for damage, and a coupling force can be applied on the ferrules. We will hence neglect the axial misalignment. However, in POF/POF interfaces tilt loss also

plays a (modest) role. Since angular loss is only function of the tilt angle and of the numerical aperture the losses are equal for both Asahi and Toray POF. The coupling loss as a function of tilt is given in figure 5.69. A tilt of up to 5° can be

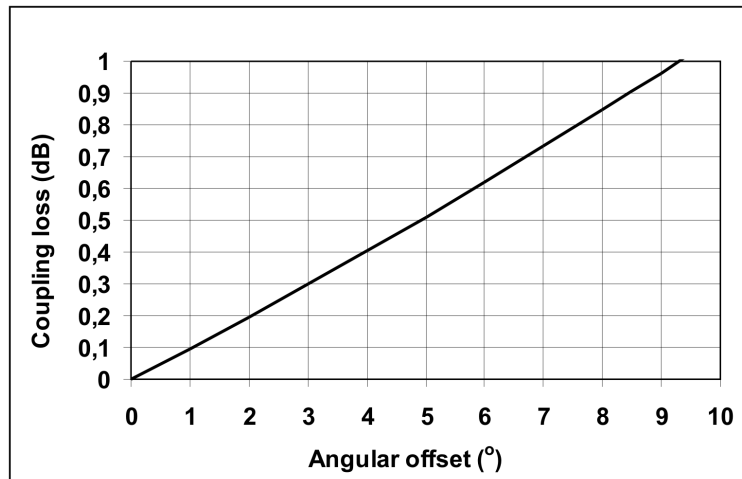


Figure 5.69: Coupling loss as a function of angular offset for Asahi and Toray POF

tolerated if loss of 0.5 dB is accepted.

For radial offset the behaviour is different for Toray and Asahi POF. As shown in

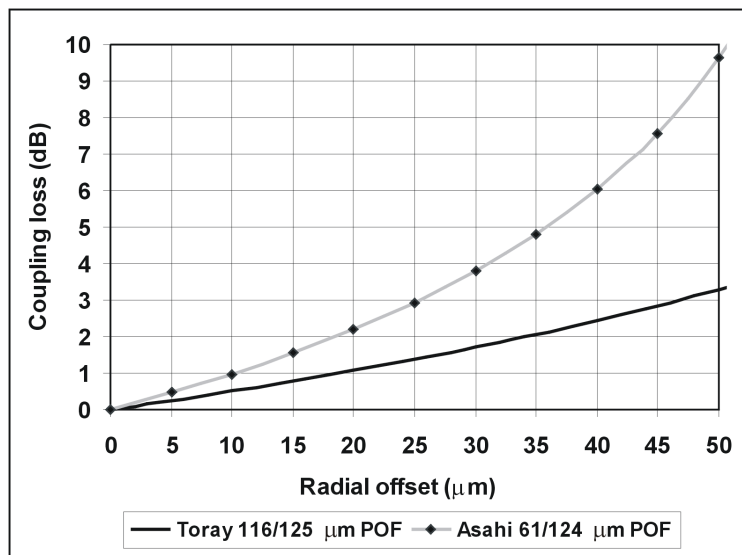


Figure 5.70: Coupling loss for a POF/POF interface as a function of radial loss with butt-coupling

figure 5.70 for a radial offset of $20\ \mu\text{m}$ at an Asahi POF/POF interface, a 2.2 dB offset is found. Adding tilt and radial offset we obtain a total maximal coupling loss of 2.7 dB at the Asahi POF/POF interface, resulting in 2.2 dB remaining budget. In other words for a 5° tilt- and $20\ \mu\text{m}$ radial tolerance at the POF/POF interface we would still end up with 40 % too much power. For the Toray POF the tolerances are looser. An offset of $40\ \mu\text{m}$ means a loss of 2.5 dB. If we add the 0.5 dB tilt loss we obtain a power budget of 3.35 dB. So we dispose of more than twice the power we need at the detector. An overview of the power budget calculation for VCSEL-based links with intermediate POF/POF connector can be found in table 5.5.

Table 5.5: Power budget estimated for a VCSEL-based link with three connectors

	Angular accuracy at POF/POF	Radial accuracy at POF/POF	Total loss	Budget
VCSEL Asahi 50 cmPOF	5°	$20\ \mu\text{m}$	12.5 dB	2.2 dB
VCSEL Toray 50 cm POF	5°	$40\ \mu\text{m}$	11.35 dB	3.35 dB

5.7 Conclusions

We can summarize this chapter as follows: we have modeled and measured coupling efficiencies as a function of offsets that occur at the interfaces in optical links. We found that model and experiment are in good agreement. After characterizing coupling losses we used the results to set alignment tolerances at the optical interfaces. It turned out that those tolerances are a lot tighter in a RCLED-based link than in a VCSEL-based link. Therefore we concluded that a RCLED-based link with an intermediate POF/POF connector is not feasible. In VCSEL-based links on the other hand, an intermediate POF/POF connector can be included. We obtained guide numbers for the allowed tolerance in these links that can be summarized in table 5.6.

Table 5.6: Guide numbers for alignment tolerances in RCLED and VCSEL links (*NA* = non applicable). VCSEL-based links can have an intermediate POF/POF connector, RCLED-based links cannot.

Link	Radial source/detect - POF	Axial source/detect - POF	Radial POF-POF	Tilt POF/POF
50 μm RCLED Toray 20 cm POF	15 μm	20 μm	NA	NA
VCSEL Asahi 50 cmPOF	25 μm	40 μm	20 μm	5°
VCSEL Toray 50 cm POF	40 μm	40 μm	40 μm	5°

Bibliography

- [1] <http://oiic.intec.ugent.be/>.
- [2] V. Baukens, *Scalable Micro-Optical Modules for Short Distance Photonic-VLSI Interconnections*. PhD thesis, Vrije Universiteit Brussel, 2001.
- [3] W. van Etten and J. van der Plaats, *Fundamentals of Optical Fiber Communications*. Hertfordshire, UK: Prentice Hall, 1991.
- [4] D. Gloge, "Offset and tilt loss in optical fibre splices," *Bell System Technical Journal*, vol. 55, pp. 905–916, September 1976.
- [5] K. Taylor and B. L. Anderson, "Misalignment losses in fiber optic joints due to angular misalignment for arbitrary energy distribution," *Optical Engineering*, vol. 34, pp. 3471–3479, December 1995.
- [6] A. Van Hove, *Termination and Interconnection Technology for Parallel Optoelectronic Systems*. PhD thesis, Ghent University, Faculty Applied Sciences, Dept of Information Technology, Sint Pietersnieuwstraat 41, 9000 Gent, Belgium, 2001.
- [7] R. Bockstaele, *Resonant Cavity Light Emitting Diode Based Parallel Interconnections*. PhD thesis, Ghent University, Faculty Applied Sciences, Dept Information Technology, St-Pietersnieuwstraat 41, 9000 Ghent, Belgium, 2000.
- [8] R. Bockstaele, T. Coosemans, C. Sys, L. Vanwassenhove, A. Van Hove, B. Dhoedt, I. Moerman, P. Van Daele, R. Baets, R. Annen, H. Melchior, J. Hall, P. Heremans, M. Brunfaut, and J. Van Campenhout, "Realisation and characterisation of 8x8 resonant cavity LED arrays mounted onto CMOS drivers for POF-based interchip interconnections.," *IEEE Journ. Sel. Topics Quant. Electr.*, vol. 5, pp. 224–235, March 1999.
- [9] R. Bockstaele and P. De Pauw, "Fabrication of a low-cost module for gigabit ethernet transceivers," *Proceedings of SPIE 4942, VCSELs and Optical Interconnects*, vol. 55, pp. 905–916, September 2000.
- [10] H. Sunak and M. Zampronio, "Launching light from semiconductor lasers into plane-ended multimode optical fibres," *Applied optics*, vol. 22, pp. 2337–2243, August 1983.
- [11] P. Di Vita and U. Rossi, "Theory of power coupling between multimode optical fibres," *Optical and Quantum Electronics*, vol. 10, pp. 107–117, September 1978.
- [12] M. Brunfaut, W. Meeus, J. Van Campenhout, R. Annen, P. Zenklusen, H. Melchior, R. Bockstaele, L. Vanwassenhove, J. Hall, B. Wittman, A. Neyer, P. Heremans, J. Van Koetssem, R. King, H. Thienpont, and R. Baets, "Demonstrating optoelectronic interconnect in a FPGA-based prototype system using flip-chip mounted 2d-arrays of optical components and 2d POF ribbon arrays as optical pathways," in *Proceedings of the SPIE' 46th annual meeting*, (San Diego, California), July 2001.

6

Fabrication of one-dimensional POF arrays

OUR design for parallel POF connectors is based on the stacking of one-dimensional arrays, a principle that was elaborately discussed in Chapter 4. The following pages will focus on the fabrication of such one-dimensional arrays. Two manufacturing technologies will be discussed: the “fibre-in-groove” method and the “embedded fibres” method. A comparative study of the experimental results of both techniques is carried out.

6.1 Introduction

As has been thoroughly discussed in detail in Chapter 4, the first step in the manufacturing of a POF array connector consists in making a one-dimensional $1 \times N$ POF array. This array should assure an alignment of the POF in a row with pitch $250 \mu\text{m}$, and with an acceptable accuracy. Further on, it should be possible to stack these arrays at a pitch of $250 \mu\text{m}$. In other words, the thickness of those arrays should be below $250 \mu\text{m}$. The most simple approach is to fabricate thin plates with U-grooves in which the POF can be laid and fixed. These plates have been made within our laboratory by means of laser ablation. However, it turned out that, despite the fact that the grooves were made with high accuracy, the alignment of the POFs was of moderate quality, due to the varying diameter of the fibres. In particular for the Asahi POFs the misalignment was unacceptable. Therefore an alternative method was developed, which we baptized “embedded fibres”. It consists of pre-aligning the POFs using V-grooves and embedding them in UV-curable glue. After hardening the glue, one obtains a $1 \times N$ array with enhanced alignment.

In the next paragraphs we will describe both methods in detail and discuss their results. We start off with the most obvious option: fibre in groove.

6.2 The “fibre in groove” method

One of the main problems during the development of this method is the search for an adequate fabrication technology for the plates with grooves. This method had to combine production flexibility with a relatively low cost for prototype series of typically few tens of pieces. Several manufacturing methods, including embossing, micro-machining and deep proton lithography, were considered. Most of the methods that would meet the technical requirements turned out to be expensive or lack flexibility. For instance, embossing needs a mold: a very precise, and hence expensive, tool. The necessity of a mold makes embossing only affordable at a larger production scale, which makes this method only suitable for mass production. Moreover it lacks flexibility: for each new design a new mold needs to be manufactured. Other methods like deep proton lithography are more flexible, but the production cost per hour makes it a very expensive method for the fabrication of prototype serials. Finally, we took the option to use laser ablation, a technology available in-house. It combines a relatively low production cost with a high degree of flexibility. A detailed explanation of this technology can be found in [1]. A clear overview of the main micro-fabrication techniques is given in [2] and can be seen in figures 6.20 and 6.21 at the end of this chapter .

6.2.1 Laser ablation

Laser ablation can be defined as controlled local removal of material through laser pulse - substrate interaction. A substrate is irradiated with a high-power laser beam (energy density $0.07 - 4 \text{ J/cm}^2$). The light interacts with the material and particles are ejected (figure 6.1). In this way a micro-hole is created. This tech-

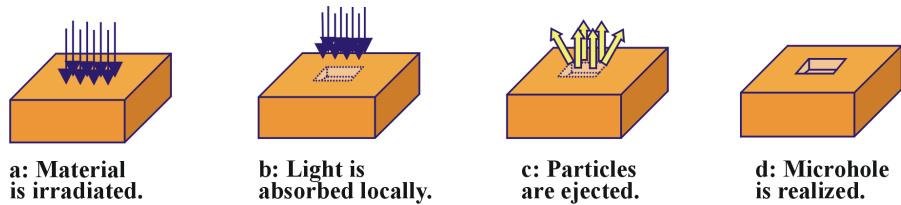


Figure 6.1: Principle of laser ablation

nique has several advantages: it is a non-resist technique, it does not require severe conditions, neither on the ablation environment, nor on the substrate. However, the material should be highly UV-absorbing. Finally, it is a very versatile and fast prototyping technique. A scheme as well as a picture of the laser ablation setup can be seen in figures 6.2 and 6.3 respectively. The setup contains a Lumonics Pulse Master 848 excimer laser, suitable for both KrF and ArF gas mixtures and emitting at 193 nm (ArF) or 248 nm (KrF). Two UV-absorbing materials, namely polycarbonate and polymethylmetacrylate were irradiated with these two wavelengths. In addition two production methods were used: the ‘aperture method’ and the ‘hybrid mask method’. The former method involves the use of a square

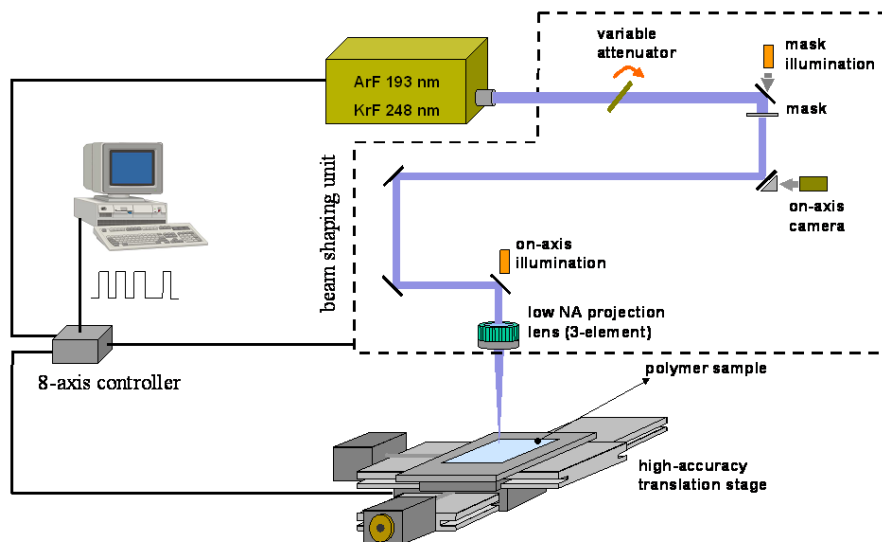


Figure 6.2: Scheme of the ablation setup

aperture which shapes the excimer beam so that its size in the substrate plane

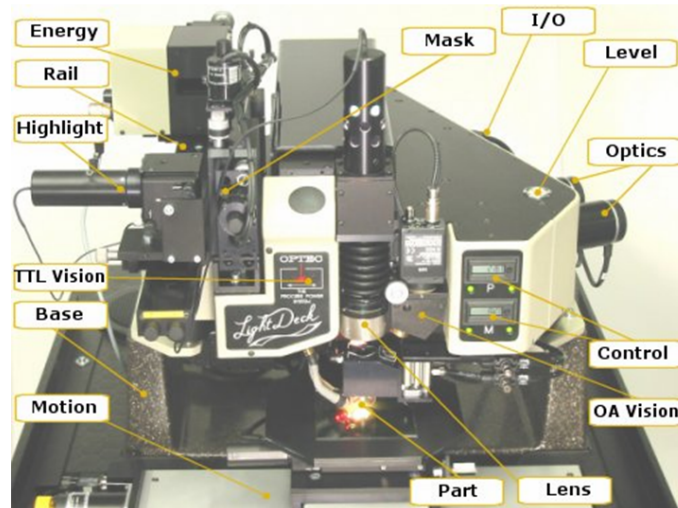


Figure 6.3: Picture of the ablation setup

is exactly the desired width of the groove. Translation of the substrate during illumination ('scanning') allows the creation of one groove. Since the size of the aperture is limited to the width of the groove, this method is very time consuming and the fabrication of an array of grooves can take several hours. The latter method refers to the use of a more complex mask pattern for shaping of the laser beam. Depending on the pattern size, scanning might not be necessary anymore. Although it may be beneficial to the resulting ablation quality of the grooves: by partially overlapping pulses (slow translation of the substrate), one averages depth variations of the ablated surface due to spatial inhomogeneity of the laser beam. The ablation procedure is finalized by a cleaning step in which the substrate surface is cleaned by water and pressurized air in order to remove particles - "debris" - which remain in (the neighbourhood of) the groove structure.

Polycarbonate and PMMA plates containing 8 grooves of 9 mm length at a pitch of $250\ \mu\text{m}$ were made, with both wavelengths¹. PMMA plates irradiated with 193 nm generated the best results [1, 3]. A picture of such an ablated groove in PMMA can be seen in figure 6.4. Very steep sidewalls (78°) were obtained. The depth of the groove is $127\ \mu\text{m}$ ($\pm 1\ \mu\text{m}$) and the width has been optimized to carry an optical fiber taking the finite steepness of the groove into account. It also provides a few micrometer space to allow easy insertion of the fibres as well

¹All ablation work carried out by Kris Naessens, Dept. of Information Technology, Ghent University. More details can be found in [1]

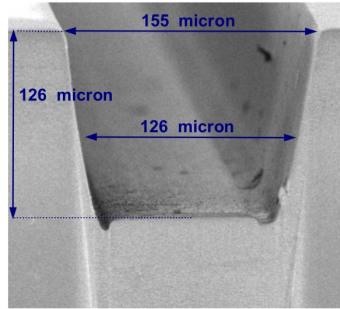


Figure 6.4: Cross section of an ablated groove in a PMMA plate

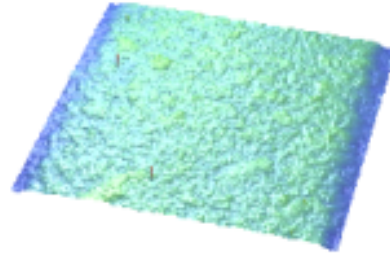


Figure 6.5: Roughness at the bottom of the groove (Wyko interferometer)

as penetration of the UV-curing epoxy for the fixation of the inserted fibres. A low RMS roughness ($0.33 \mu\text{m}$) at the bottom of the grooves was measured with a Wyko interferometer as illustrated in figure 6.5². The grooves are ablated with the mask method; the laser light passes a mask containing a pattern of 4 grooves of length 2.5 mm ($500 \mu\text{m}$ on substrate level, taking an imaging from mask to sample with demagnification 5 into account) and is limited in size by the aperture of the projection lens. It consists of a quartz substrate (transparent for both excimer wavelengths) on which a metal pattern has been deposited. The maximum allowed energy density is about $100 \text{ mJ}/\text{cm}^2$. While the laser is irradiating the material with consecutive pulses (frequency 10 Herz), the sample is translated. Since a large area is irradiated and since 4 grooves are ablated simultaneously the whole procedure takes only about 15 minutes for a plate with 8 grooves of 9 mm long (instead of 11 hours for the “aperture” method!). A picture of a complete plate can be seen in figure 6.6.

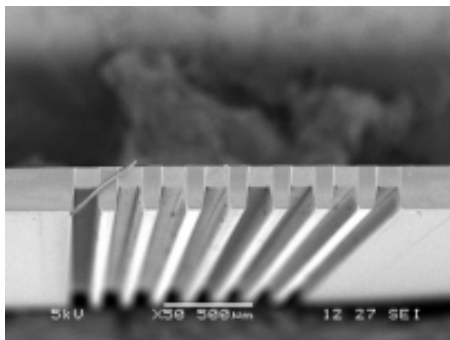


Figure 6.6: A PMMA plate with 8 grooves ablated at 193 nm wavelength, pitch is $250 \mu\text{m}$

²This measurement was carried out at the Photonics Department of the Free University Brussels.

6.2.2 Fixing the POF in the grooves

After the production of the grooves, fibres need to be introduced in the grooves. Special attention has to be paid to a homogenous insertion of the fibres: every fibre needs to be at the same position relative to its groove. Moreover this positioning needs to be maintained over the full length of the inserted part of the fibre. Introducing the POFs in the grooves starts with pre-aligning a 1×8 array by means of two standard MTTM-ferrules (figure 6.7). As can be seen in this figure the 1×8 POF array is stretched between two MTTM ferrules. Then the PMMA

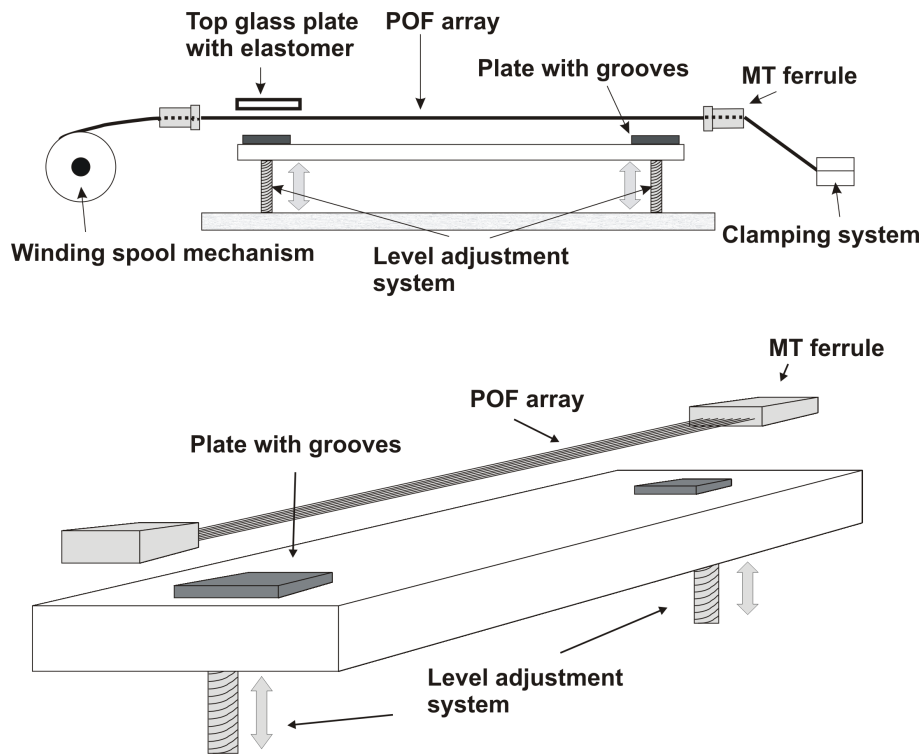


Figure 6.7: Set-up for introducing POFs in the grooves

plates, which are lying on a translation table under the array, are slowly moved upwards until they reach the POF array. Then the positions of the PMMA plates are re-adjusted by hand so that the POFs can easily slide into the grooves. Finally the table is still moved upwards so that the POFs are introduced in the grooves. The tension in the POFs is strong enough to turn the grooves completely parallel with the fibres. The final step is to pour some small quantity of glue on the fibres after which it is UV-cured. We used NOA 72 glue from Epotecny. During the curing process a glass plate covered with a layer of flexible elastomer is pushed on top of the array in order to maintain the alignment of the fibres. The glue does not stick to the elastomer and hence the plate can easily be removed. The applied glue should be of low viscosity so that it can easily penetrate and fill the left-over

space in the U-groove after insertion of the POF. Moreover it should be adhesive to PMMA, basic material for the plate and the POF. Finally, it should have more or less the same hardness as the POF and the plate. This is important for the termination of the array, since the end facet is obtained by a hot knife cutting procedure. The cleanest end facets are obtained with a uniform hardness. During the cutting the plate is held firmly between a bottom glass plate with an elastomer layer and a top glass plate, then the knife slides along the edge of the glass plate as depicted in figure 6.8. A picture of a plate with terminated Asahi POFs, as

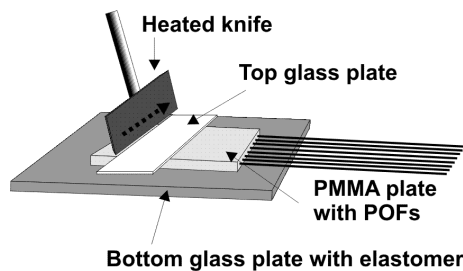


Figure 6.8: Facet termination of the “fibre in groove” POF array using a hot knife

well as a cross section of it, can be seen in figures 6.9 and 6.10. From figure 6.10

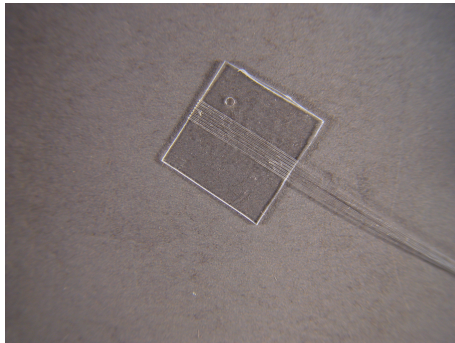


Figure 6.9: A grooved PMMA plate with inserted POFs

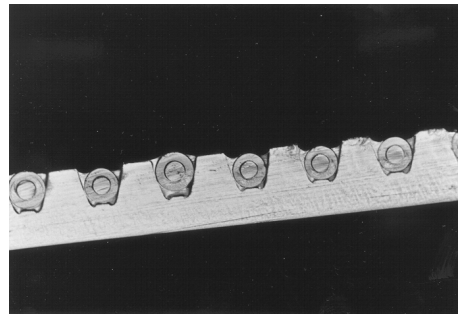


Figure 6.10: Asahi POFs in a PMMA plate with grooves

one can immediately notice the main problem with this technology: due to the varying outer diameter the alignment is severely disturbed. Some fibres have too large a diameter and do not enter the groove on the one hand, and some fibres have too small a diameter and are not well aligned by the groove on the other hand. This can also be seen in the positioning accuracy measurements carried out on those plates. The position of the POFs in the PMMA plate was measured by scanning the end facet of the POF array with a light source and measuring the evolution of the power at the other end of the fibres as a function of the scan position (figure 6.11). The maxima of the power output were corresponding with the position of the centres of the POFs in the array. The results of this experiment can be seen in table 6.1. The terms “pitch average” and “pitch standard deviation” are self explanatory. “Maximum deviation pitch” gives the difference

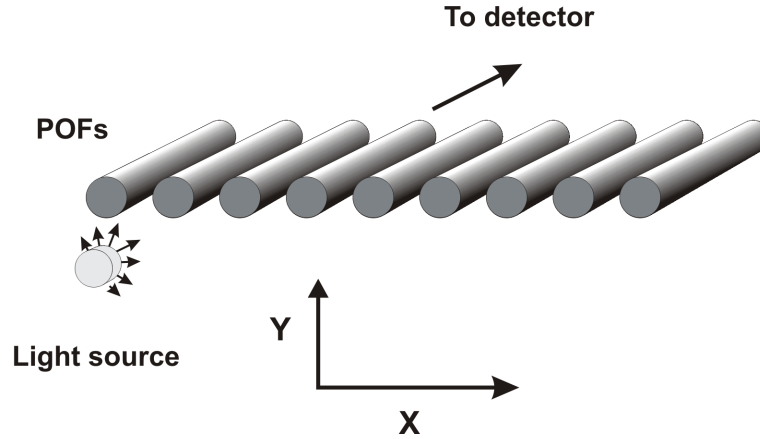


Figure 6.11: The fibres are scanned with a light source in the X-Y plane. By monitoring the power output of the POFs as a function of the scan position, the exact position of the POFs can be found. A multimode 62.5/125 μm glass fibre with HeNe laser light was used as a light source.

Table 6.1: Accuracy on positioning of the POFs for the “fibre in groove” technology

	pitch (μm) average	pitch (μm) standard deviation	pitch (μm) maximum deviation	Y (μm) standard deviation	Y (μm) maximum deviation
Toray	250	4	10	4	9
Asahi	250	9	20	10	18

between the average and the measured pitch that differs the most from the average. The term “standard deviation” gives the standard deviation of the measured Y-values (figure 6.12), in other words it gives the spread of the Y values around the median, $Y_{average}$, “Y maximum deviation” gives the measured Y value that differs the most from this median. It can be seen that for both Toray and Asahi POF the average pitch is 250 μm , but especially for the Asahi POF the spread around the average is large. Also in the Y direction there is a large spread. How does this affect the radial offset when such arrays are coupled to other arrays or to a detector/emitter? Therefore we simulated optimal couplings and calculated the maximal radial offset. In other words, we calculated the position of a coupled array with the least coupling losses, and then looked for the maximal radial offset of an individual POF in that configuration. We performed this simulation for

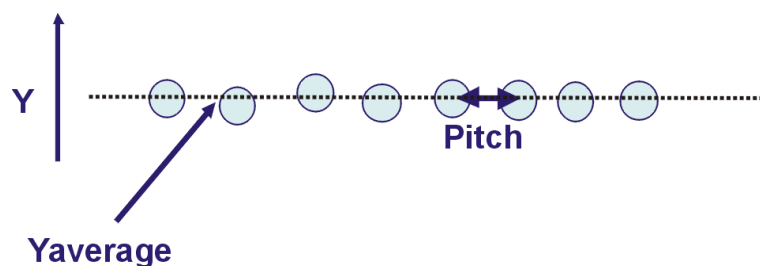


Figure 6.12: Axes on a one-dimensional array

different combinations POF/POF and POF/detector-emitter. We neglected the offset caused by the detector/emitter arrays since they are negligible compared to the misalignments in the POF array. The results of these simulations can be seen in table 6.2. By comparing these values with those in table 5.6 (Chapter 5), we

Table 6.2: Maximal radial offset in 1×8 coupled arrays based on “fibre-in-groove” technology

	emitter/detector to POF	POF to POF
Toray	$9 \mu\text{m}$	$14 \mu\text{m}$
Asahi	$27 \mu\text{m}$	$40 \mu\text{m}$

can see that for the Toray POF the radial offset is acceptable for a VCSEL-based link. For a RCLED-based link with no intermediate connector, the difference between the total tolerance and the offset caused by the “fibre-in-groove” technology is only $6 \mu\text{m}$. This is rather small, thus an improvement is recommended. For the Asahi POFs the values are unacceptable and definitely another technique had to be developed.

6.3 The “embedded fibres” method

From the discussion in the previous paragraph it is clear that a u-shaped groove, that fits exactly the diameter of the fibres, can only align POFs adequately if the outer diameter of the POF is well controlled. Hence we had to come up with an alignment technique that is less dependent on the outer diameter of the POF. Therefore we decided to align the fibres with v-shaped grooves instead of u-shaped

ones. The pitch of the aligned fibres then becomes totally independent of the outer diameter of the fibre. Also the alignment in the Y-direction becomes somewhat less dependent on the POF diameter. These V-grooves can be made very precisely with an etching process on silicon substrates. In addition we decided not to use the very precise, and hence expensive from a mass production perspective, V-grooved plates for the final connector. Instead we decided to use these plates only during the production process of the connector, and encapsulate the aligned fibres in a cheap polymer material. In this way, the core of a cheap and easy to produce connector for two-dimensional POF arrays is created.

6.3.1 Principle and set-up

The principle of the “embedded fibres” technology is depicted in figure 6.14. In a first step a 1×8 array of fibres is pre-aligned by two silicon plates containing V-grooves at a pitch of $250 \mu\text{m}$ (see also figures 6.15 and 6.16). The grooves

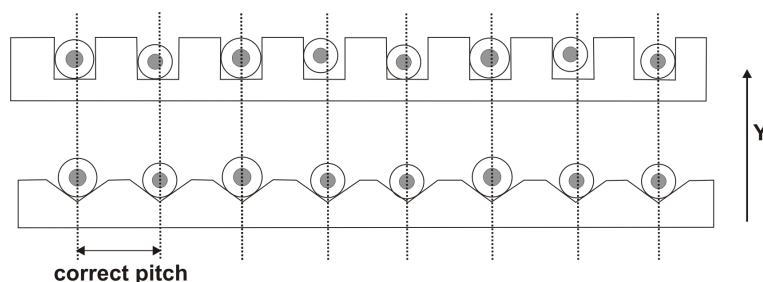


Figure 6.13: The “embedded fibre” setup

are etched and contain only part of the fibre. Note that this makes it easy to push the fibres well into place in the groove. As a result, the pitch is completely independent of the diameter of the POF. Moreover, the spread in the Y-direction is also reduced: in case of U-grooves, the groove could not always assure an alignment in the Y-direction, here the V-groove always aligns the fibres (figure 6.13). The spread in the Y-direction is reduced to the net variation of the outer diameter of the POF (+ non-concentricity core-cladding). A bottom plate is placed under the POFs. Subsequently UV-curable glue is poured over the POFs, and a top plate is placed on the fibres (figure 6.17). In this way the glue forms a flat film of about the thickness of the fibres. Then the glue is cured and the top plate removed. A 1×8 array is obtained by peeling off the cured glue together with fibres from the bottom plate. The end facet is made by cutting the array with a heated knife in the same way as for the grooved PMMA plates. A lot of research was done on the definition of the best glue, bottom plate and top plate. The glue needs to adhere to the PMMA of the POF but not to the top and bottom plates. Moreover, it needs to be of the same hardness as the fibres and last but not least it should show a minimal shrink during the curing, otherwise the alignment loses precision. After testing a range of different glues we obtained the best results with NOA 72 from Epotecn. For the bottom plate the best material was polycarbonate and for

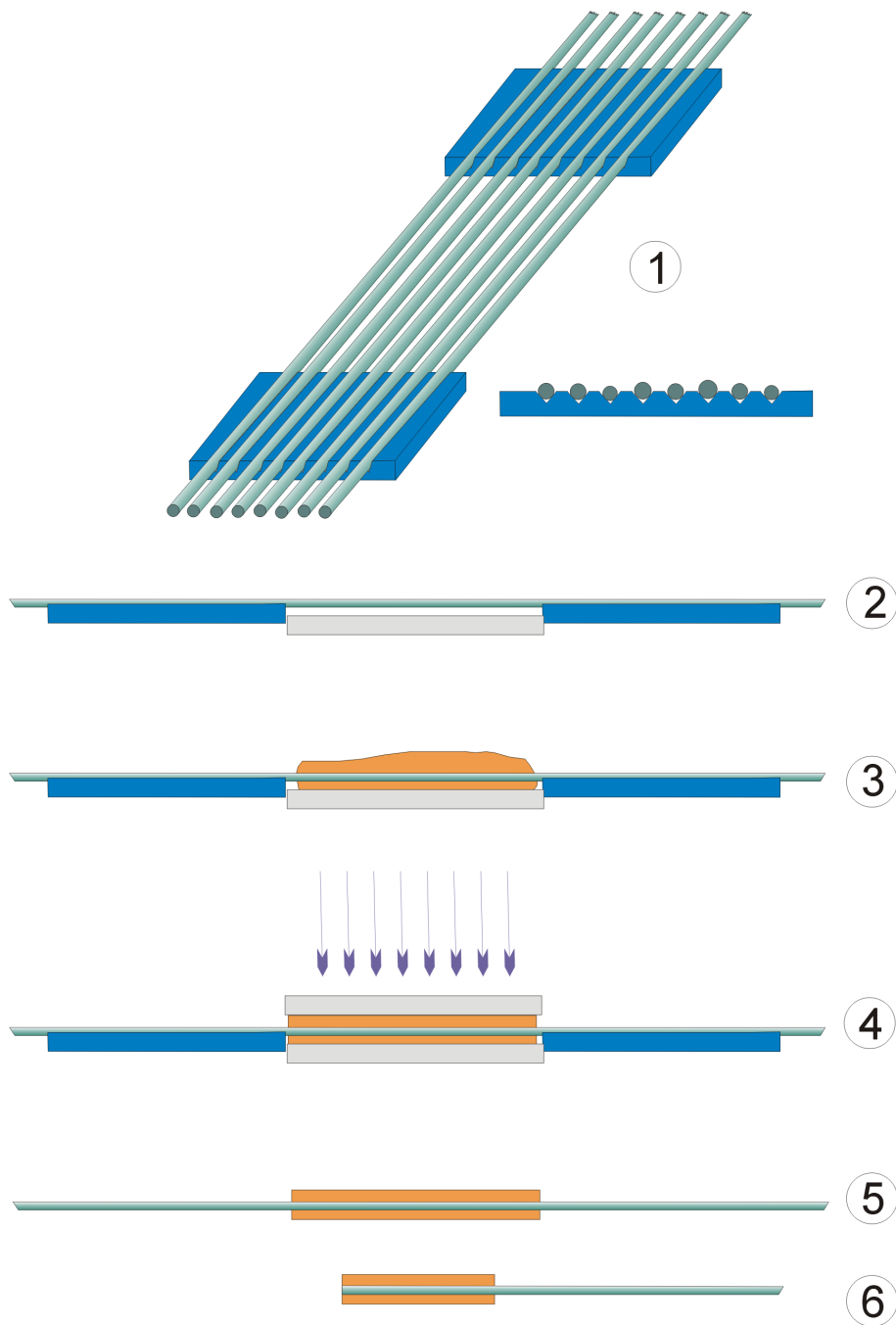


Figure 6.14: Principle of embedded fibres

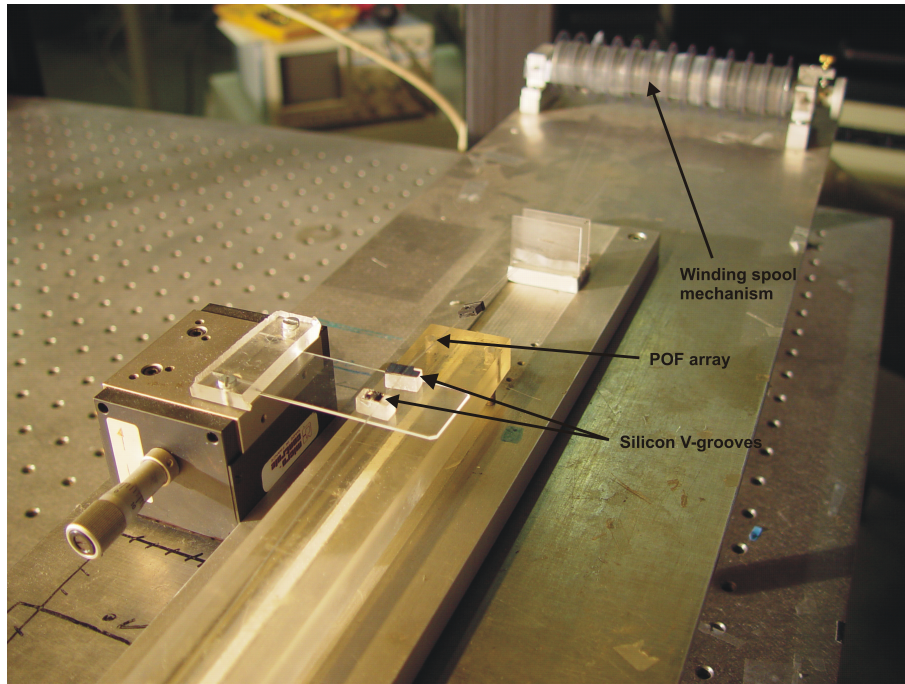


Figure 6.15: The “embedding fibre” setup

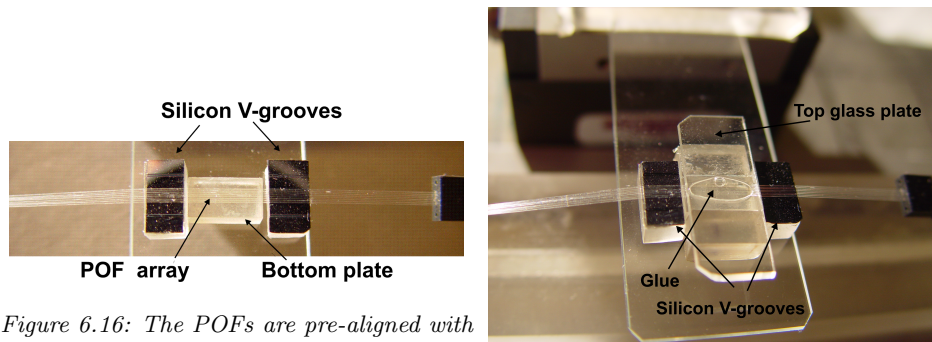


Figure 6.16: The POFs are pre-aligned with silicon V-grooves

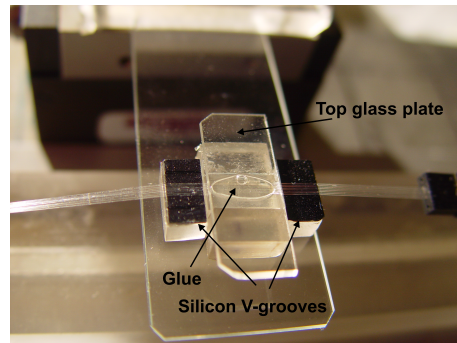


Figure 6.17: Glue is poured over the array, and a top glass plate is placed

the top plate it was glass. Ideally the top plate was also made of polycarbonate, but this material appeared to absorb too much the UV curing light. In order to diminish the adhesion between the glue and the top and bottom plate, a spray with teflon micro-fibres was applied on the plates prior to the gluing. During the curing the top glass plate was let loose so that only its weight was shaping the cured glue film. This resulted in a varying thickness of the cured glue film, depending on

the amount of glue that was applied. However, we did not want to increase the pressure on the top glass plate because this was disturbing the alignment of the fibres. A picture of a one-dimensional arrays can be seen in figures 6.18 and 6.19

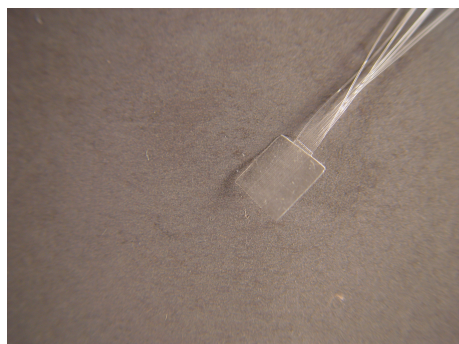


Figure 6.18: A 1×8 “embedded POF” array



Figure 6.19: A cross section of a 1×8 “embedded POF” array

6.3.2 Experimental results

We used the scanning experiment described above to measure the positional accuracy of the POFs. An overview of the results can be seen in table 6.3. If we compare these values to those in table 6.1 we see a small improvement for the Toray POF, and certainly a strong improvement for the Asahi POF ($18 \mu\text{m}$ difference!). For the alignment in the Y direction the accuracy improves with a factor

Table 6.3: Accuracy on positioning of the POFs for the “embedded fibre” technology

	pitch (μm) average	pitch (μm) standard deviation	pitch (μm) maximum deviation	Y (μm) standard deviation	Y (μm) maximum deviation
Toray	250	3	6	2.5	4
Asahi	250	3	7	5	8

2, while for the pitch the improvement equals a factor 3. What the improvement means in terms of radial offset when embedded fibre arrays are coupled, can be seen in table 6.4. For the Toray POF the improvement is modest, but for the Asahi POF a reduction with $23 \mu\text{m}$ is achieved. When we compare these values to the

total radial tolerance shown in table 5.6 (Chapter 5), we can see that the radial offsets caused by the “embedded fibre” technology are within these tolerances, at least for the VCSEL-based links. For a RCLED-based link with Toray POF, the result is still close to the edge. Much will depend on the accuracy of the stacking procedure as well as on the connector completion with the U-blocks.

Table 6.4: Maximal radial offset in 1×8 coupled arrays based on “embedded fibre” technology

	emitter/detector to POF	POF to POF
Toray	8 μm	12 μm
Asahi	9 μm	17 μm

6.4 Conclusions

We developed two methods for the fabrication of one-dimensional POF arrays. The fibre-in-groove method did not completely fulfill the expectations, despite the fact that grooves at a high precision were made: it is satisfactory if the outer diameter of the POF is well controlled. This was the case for the Toray POF: we measured that the achieved accuracy of the fibre alignment was sufficient for connectors in VCSEL-based links. For RCLED-based links with Toray POF, the results were close to the maximal allowable tolerance and no firm conclusion could be made. For the Asahi POF, the fibre-in-groove method was clearly inadequate, due to the variable diameter of this fibre. Another method, based on pre-aligning the POFs with V-grooves, and subsequently embedding them in UV-curable glue yielded better results. Measurements showed that the “embedded fibre” method could be used in VCSEL-based links with Asahi POF. For the Toray POF the improvement was modest and whether this technology can be used for a RCLED-based link, will depend on the accuracy of the subsequent processes for the completion of the connector.

Machining Method	Material/Annihilation	Typical Min./Max. Size Feature	IC Compatible	Tolerance	Aspect Ratio (Depth/Width)	Important Reference on Technique	Initial Investment Cost/Access	Final Investment
Group: Traditional Techniques (Not Involving Photolithography-Defined Masks)								
Chemical milling (S), (B)	Almost all metals	From submillimeters to a few meters (x,y); max thickness (z) ± 1 cm	Yes	Lateral tolerance 0.25 to 0.5 mm	±1	Harris ¹⁵	Low/good	
Electrochemical machining (S/A), (B)	Hard and soft metals, turbine blades, pistons, fuel-injection nozzles	Minimum size devices larger than in chemical milling because of the contacting need	Fair	Lateral tolerance < 10 µm	(S) 100	(A) Romankiw, ¹⁷ (S) Phillips ¹⁶	±\$400,000/good	Good
Electrodischarge machining (EDM) (S), (Se)	Hard, brittle, conductive materials used for tools and dies	Minimum holes of 0.3 mm in 20-mm thick plate	No	Lateral tolerance, 5–20 µm	100	Kalpakjian ¹³	High/good: equipment with numerical control is common	with numerical control is good
Electrodischarge wire cutting (EDWC) (S), (Se)	Hard, brittle materials; many punch-and-die applications	Minimum rods 20 µm in diameter and 3 mm long	No	Lateral tolerance, 1 µm	>100	Saito ¹³	High/good: does not require special dielectrodes	quite good
Electron-beam machining (EBM) (S/A), (Se)	Hard-to-machine materials	(S) most suited for large numbers of simple holes (<0.1 mm)	Fair	(S) ~10% of feature size (5 µm on a 50-µm hole)	(S) 10 is typical but 100 is possible	Taniguchi ¹⁶	Very high/fair ±100,000 when using modified SEM	then fixed SEM
Continuous deposition (A), (C); doctor's blade technology	With all materials available in inks, e.g., glucose sensors	Most suited for inexpensive disposables, from 100 µm to a few millimeters	No	15 µm	—	Harper ¹⁴	Low/good	
Focused ion-beam on a lathe (S)	Very pure IC materials	From submicrons to millimeters	Yes	(S) 50–100 nm	—	Vasilje ¹⁸	High/poor	
Hybrid thick film (A), (B)	Wide variety of materials available in inks	Minimum feature size 90 µm	Fair	12 µm	—	Harper ¹⁴	±\$30,000/good	
Laser-beam machining (LBM) (S/A), (Se)	Complex profiles in hard materials	(S) Holes from 10 µm to 1.5 mm at all angles	Fair	1 µm	(S) 50	Helvajian ¹⁹	±\$50,000 but up to \$400,000 for a five-axis system/good	up to a five-good tier
Plasma-beam machining (PBM) (S/A), (C)	Very high temperature materials	(A) only used for thick films > 25 µm; (S) for very thick films > 2.5 mm	No	(A) 20 µm for a 25-µm thick film; (S) typical ±3 mm but 0.8 mm is possible	—	Pfender ²²	Low/good	
Stereo lithography (S/A), (Se)	Polymeric photosensitive materials	Max. 10 × 10 × 10 mm (x,y,z)	Yes	Minimum solidification unit 5.5–3 µm (x,y,z)	—	Ikkat ²⁰	\$400 k/good	
Ultra-precision mechanical machining (S), (Se)	Form-stable materials	From submillimeters (e.g., 0.2-mm hole) to meters	No	1 mm by the year 2000	—	Boothroyd ¹	\$20 k/good	
Ultrasonic machining (S), (Se)	Hard and brittle materials	Holes from 50 µm to 75 mm	No	Lateral tolerance 10 µm	2.5 µm for a 250-µm hole	Bellows ²		
Ultrasonic (S), (Se)		75 mm			hole			

Figure 6.20: Overview of “traditional” microfabrication methods [2]

Machining Method ^a	Material Application	Typical Min./Max. Size Feature	IC Comparable	Tolerances	Important Reference on Technique	Aspect Ratio (Depth/Width)	Shape and Height/Depth	Initial Investment Cost/Access
Group: Nontraditional (Involving Photolithography-Defined Masks)								
Photofabrication (S)	Plastic, glass (ceramic), e.g., fluidic elements	Max. xy = 40 × 40 cm and max z = 0.6 cm	Yes	Lateral tolerance 20 μm	Trotter ²⁴	-3 for photoplastics; -20 for photoglass	xy is free; z = up to 6 mm	Medium/poor to medium
Photochemical milling (S)	Printed circuit boards, lead frames, shadow masks	Max. 60 × 60 cm; max. thickness < 0.5 mm	Yes	13 μm (printed circuits)	Allert ²¹	±1	xy is free; z = up to 0.5 mm	Medium/good
Wet etching of anisotropic materials (S)	Crystal Si, GaAs, quartz, SiC, InP	Max. wafer size, min. feature a few microns	Fair	1 μm	Kern ²⁴	100	xyz shape locked in by crystallography; z height of the wafer	Low/good
Dry etching (S)	Most solids	Max. wafer size, min. feature submicron	Good	0.1 μm	Manoge ²⁶	10	xy shape free; z = up to 200 μm	High/good
Poly silicon surface micromachining (S/A)	Poly-Si, Al, Ti, etc.	Max. wafer size, min. feature submicron	Good	0.5 μm	Howe ²⁶	—	xy free; z = 0.1 to 10 μm, but preferably 1–2 μm	High/fair
SOI (S)	Crystalline Si	Max. wafer size, min. feature submicron	Good	0.1 μm	Diem et al. ²⁷	—	xy free; z height depending on the epoxy; c/cg = 100 μm	High/poor
LIGA (S/A)	Ni, PMMA, Au, ceramic, etc.	10 × 10 cm or more, 0.2 μm	Fair	0.3 μm	Ehrfeld ²⁸	>100	xy free; z up to several cm	High (CoMOS)/ poor
UV transparent resists (S/A)	Polymide, SU-8, AZ-4000	Max. wafer size	Good	0.5 μm	Ahn et al. ²¹	10	xy free, z up to 100 μm	Medium/fair
Molded polysilicon HEXSEL (Keller) (S/A)	Poly-Si, Ni, etc.		Good	0.5 μm	Keller ²⁹	10	xy free; z up to 100 μm	High/poor
Erect polysilicon (Plater) (S/A)	Poly-Si		Good	0.5 μm	Plater ²⁷	10	xy free; z up to mm	High/poor

Note: S = subtractive, A = additive, Bz = batch, Se = serial, C = continuous.
 * All batches.

Figure 6.21: Overview of “non-traditional” microfabrication methods [2]

Bibliography

- [1] K. Naessens, *Excimer Laser Ablation of Microstructures in Polymers for Photonic applications*. PhD thesis, Ghent University, Faculty of Engineering, Dept of Information Technology, Sint Pietersnieuwstraat 41, 9000 Gent , Belgium, 2004.
- [2] M. Madou, *Fundamentals of microfabrication*. New York, USA: CRC Press, 1997.
- [3] T. Coosemans, A. Van Hove, K. Naessens, L. Vanwassenhove, P. Van Daele, and R. Baets, "Fabrication of a 2d connector for coupling a 4x8 array of small diameter plastic optical fiber (117/125 μm) to RCLED or VCSEL arrays," in *Proceedings of the 50th. Electronic Components and Technology Conference*, (Las Vegas, Nevada, USA), pp. 1236–1241, May 2000.

7

Fabrication of two-dimensional POF arrays

AFTER one-dimensional POF arrays are produced they need to be stacked in order to obtain a two-dimensional one. Therefor a method we called “virtual alignment” has been developed. In this chapter we describe this method and discuss experimental results.

7.1 Introduction

The second step in the production process of a connector is the stacking of the one-dimensional fibre arrays. Therefore the plates need to be positioned at an exact pitch of $250\ \mu\text{m}$. At first, having the fibre-in-groove method in the back of our heads, we investigated the idea of relying on the thickness of the plates. We looked for a production method and/or a manufacturer of plates with a precise thickness of $250\ \mu\text{m}$. The solutions we were offered where (a) not satisfactory and (b) very expensive. Moreover, in a later stage of the research we switched to “embedded fibre” technology and hence the thickness of the 1D-arrays was not very well controlled anyway. As a consequence we had to look for a technology that could align the 1D-arrays with high precision, and independent of the plate thickness. Moreover it would be an asset if we could use this technology also to align the housing, containing the guiding pins, with respect to the array. Thus this technology should be able to align two objects at a distance ranging from a few tens of μm up to a centimeter, with an absolute accuracy in the micrometer range. There were no standard solutions available on the market. Certainly commercial pick-and-place machines could achieve the necessary accuracy but their positioning system is software driven [1]. They can for instance place objects based on a pattern-recognition algorithm, which implies complex and expensive software tools. Pattern recognition can be avoided if the objects have well known dimensions. This is not very handy for prototype objects with variable dimensions, and in addition here again extensive software tools are necessary. What we were looking for was a simple and direct optical alignment technology, that does not need much software and is a relatively low cost product, like for instance a simple manual mask aligner [2]. However mask aligners work with two separate objectives, implying that the minimal distance between objects that such an aligner can actually align, is far too large for our kind of applications. As a result we eventually decided to design our own system and baptized it “virtual alignment”.

7.2 “Virtual alignment”

7.2.1 Principle and set up

The main problem that occurred to us while designing the alignment system is the fact that objects needed to be placed at distances in the order of a centimeter with an accuracy at micrometer scale. It is impossible to combine such a large field of view with the necessary magnification within one microscope objective. Hence two independent magnifying viewing systems need to be implemented. Unfortunately the distance between the different objects that have to be aligned is too small to use two separate microscope objectives, a principle used e.g in a mask aligner. Hence we developed an optical system that allows to use two independent cameras, each with a different field of view. However these fields can be at short distance from each other, varying from completely adjacent up to a distance of few centimeter. The solution we proposed is schematically depicted in figures 7.1, 7.2 and 7.3. One has a complete overview of the system in figure 7.1: at the bottom of the system

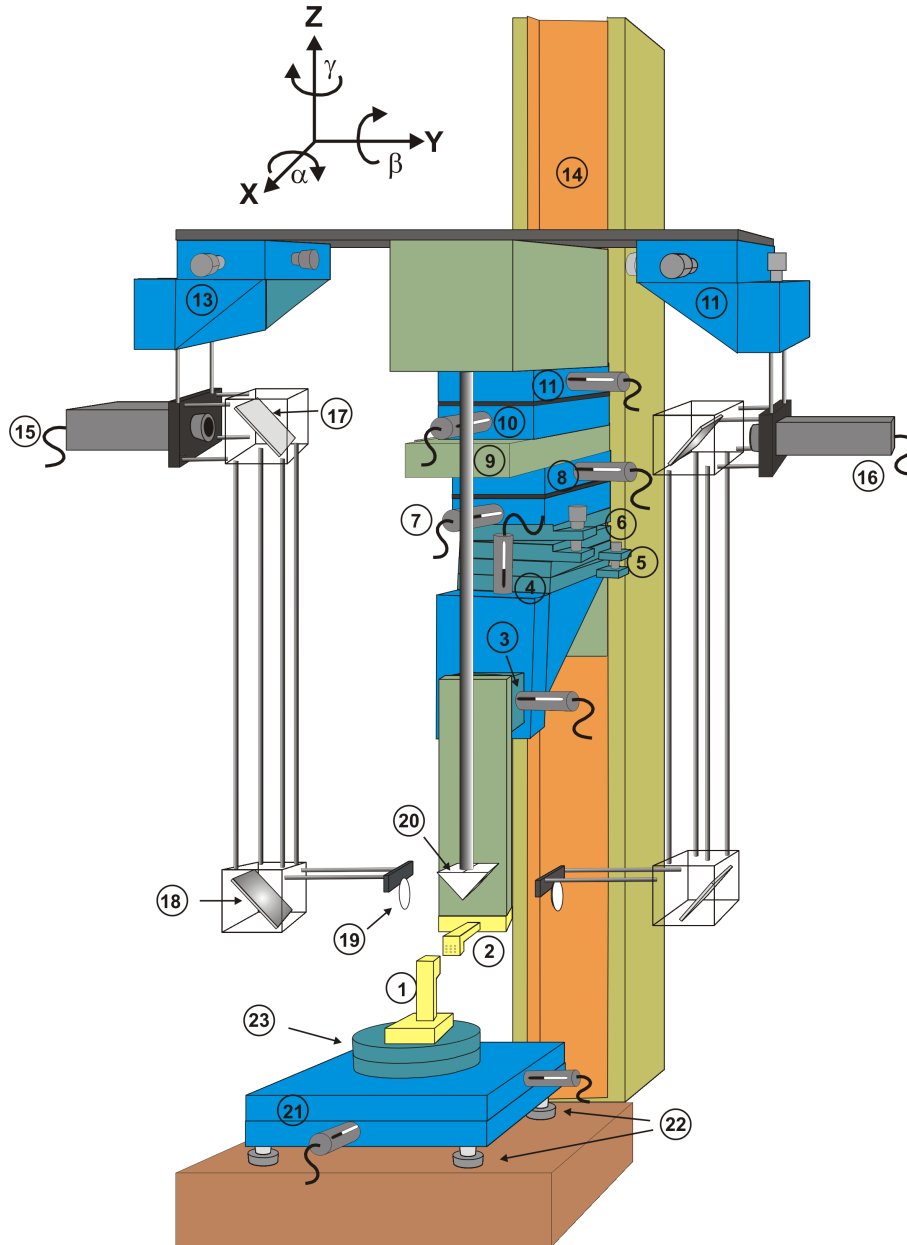


Figure 7.1: The virtual alignment setup

there are two independent holders (1, 2) that keep the two objects to be aligned. The holders use vacuum suction to grab the objects. One of the holders is placed on an automated X-Y-translation table with a resolution of $0.1\ \mu\text{m}$ and an absolute

accuracy of $\pm 0.2 \mu\text{m}$ (21). In addition the holder can be manually rotated around the γ -axis by means of a rotation stage (23). Four micrometer screws are used to position the translation table horizontally during the calibration procedure of the setup (22). The plane of this translation table is then used as reference

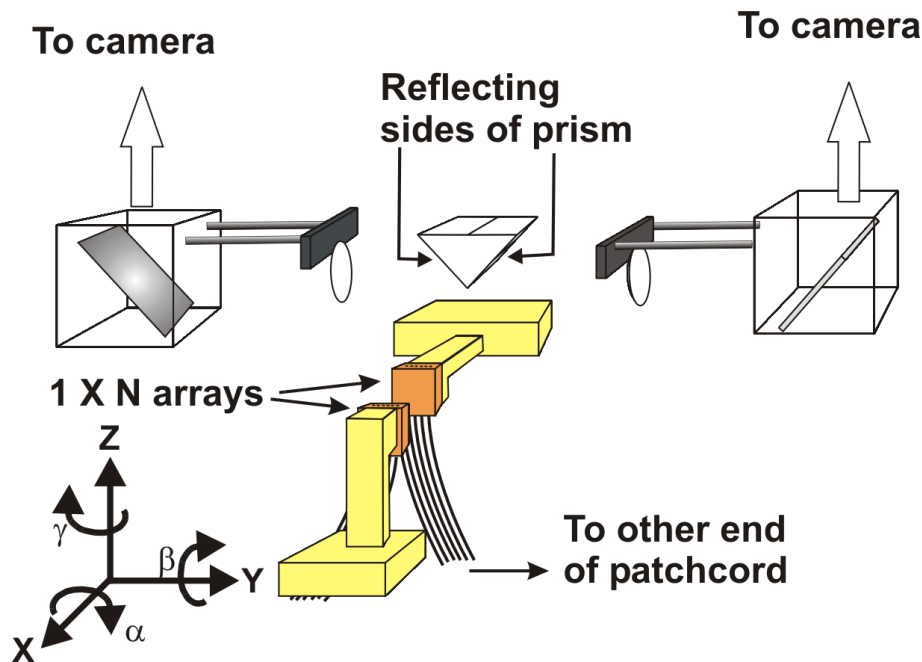


Figure 7.2: The virtual alignment setup: detailed look on the holders while two one-dimensional POF arrays are being aligned.

plane. The other holder is attached to motorized X, Y and Z-axes (7, 8, 4), as well as to a motorized α -axis (3) and to manual β - and γ -axes (5, 6). The two latter manual axes are used to bring the holder parallel with the reference plane, prior to the alignment procedure. The other axes are used during the alignment procedure. Given the fact that the second holder can be moved with six degrees of freedom one can bring the two objects in an arbitrary position with respect to each other. Besides the two holders, two cameras are implemented in the setup (11, 13). Both cameras can move independently following the X, Y and Z-axes with manual drives. In this way two viewpoints at an arbitrary distance can be monitored simultaneously. How the two fields of vision of the cameras are brought closely together is drawn in more detail in figure 7.2. Close to the objects a prism is mounted. The sides of the prism are silver coated and hence act as a mirror (20). In this way two optical pathways are created: one leading to the left camera, another one to the right camera. Since the cameras can move independently along the X, Y and Z axes, they each have an independent field of view. The maximal distance between these fields is defined by the size of the "prism-mirror" (20). The imaging is done by an achromatic doublet with f-number 0.2 (19) and two folding

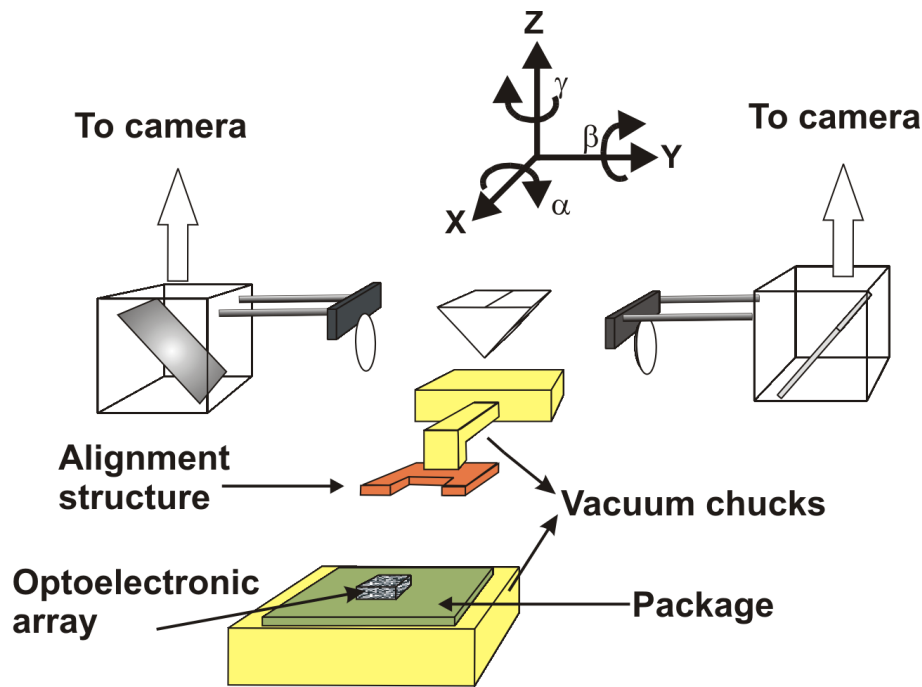


Figure 7.3: The virtual alignment setup: detailed look on the holders while a spacer is being aligned with respect to an optoelectronic die.

mirrors (17, 18). A focal distance of 2 centimeter was chosen in order to obtain a working distance large enough to allow easy movement of the holders during the alignment procedure. Also the optical path has to pass the "prism-mirror" before it reaches the achromatic lens, which requires a long enough working distance. The optical magnification equaled $20\times$, the electronic magnification from CCD camera to monitor equaled $32\times$. In total we obtained a magnification of $640\times$. This allowed us to visualize features in the order of a micrometer. Both cameras can be moved simultaneously in the X-Y plane by means of two motorized axes (10, 11). This possibility is used to bring the the field of view of both cameras roughly in the area of interest. The ensemble of cameras and holder 2 can move along the Z-axis by means of a carrier sledge that can move up and down a rail mounted on a granite base (14). This feature is used to bring holder 2 roughly at the same height as holder 1. The shape of the holders depends on the objects that have to be aligned. In figure 7.3, the holders for aligning an alignment spacer with respect to an optoelectronic die is shown. The complete system is placed on a pneumatic support in order to avoid vibrations.

The principle of virtual alignment is explained in figure 7.4. The stacking of two 1×8 arrays is taken as an example. The final goal is to fix the two plates at a $250\ \mu\text{m}$ distance. Therefore the first plate, that is fixed on holder 2 on the precise translation table, is positioned parallel with the cross hairs of the cameras. During

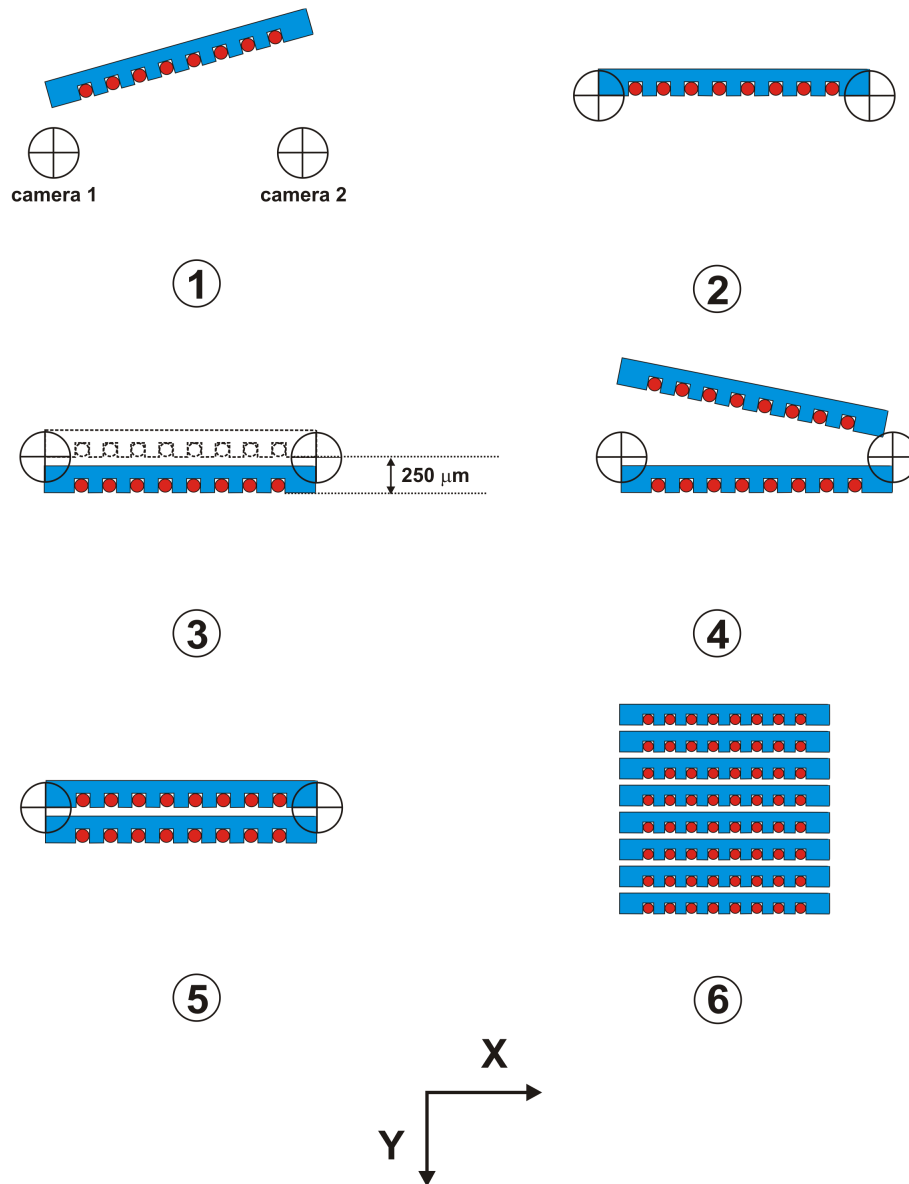


Figure 7.4: The principle of virtual alignment

the calibration of the set-up, the cross hairs are positioned in such a way that they are parallel with the X-Y-movements of the precise translation table. The cross hairs are then placed on two reference points of the plate array. In this example two corners of the plate are taken as reference points. In practice we mostly used the tops of the first and the last POF in the array. Then the plate is moved over a

distance of $250\ \mu\text{m}$ along the X-axis. The cross hairs are now placed again on the corners of the first array. Then the first array is moved back to its initial position. The cross hairs are now at $250\ \mu\text{m}$ from the reference points on the first array, and they indicate where the second array has to come. It forms a virtual master tool for the positioning of the objects, that’s why we baptized this method “virtual alignment”. Then the second array (on holder 1) is brought in the vicinity of the first one, it is put parallel with the cross hairs and the corners positioned on the cross hairs. At this moment the second plate is at its final position. Now some glue is deposited on the second panel and it is UV cured. In reality the last part went in two steps. First the second plate is roughly positioned correctly, and then it is pulled away from this position. Subsequently glue is applied and the array is put back in its position roughly aligned with the first plate. Finally the two arrays are precisely aligned and the glue is UV-cured. The fine alignment is only carried out after the application of the glue, since the capillary force of the glue sometimes changes the position of the plates.

7.2.2 Evaluation of the set-up

Prior to assembling the connectors, several experiments have been carried out in order to measure the accuracy of the setup. The precision of the positioning in the X-Y-plane is mainly determined by the X-Y-translation table of holder 2. On the other hand the alignment in the Z-direction is done by putting both arrays (or any other elements to be aligned) in focus. Hence the accuracy on the alignment in Z-direction is defined by the depth of focus of the magnifying optical system. Therefore we focused on the same image several consecutive times and we measured the range over which the micrometer was adjusted. We found that the adjustment stayed within an interval of $2\ \mu\text{m}$, hence the positioning based on focus adjustment had an accuracy of $\pm 1\ \mu\text{m}$. The quality of the imaging system has been quantified by means of patterns with increasing spatial frequency. A picture of such a pattern can be seen in figure 7.5. We could easily distinguish the dark lines of $1\ \mu\text{m}$, which proved that the viewing system was adequate enough to align objects with micrometer precision. However we noticed a vibration of the objects with respect to the viewing system: the hairlines were going back and forth over the image with an amplitude of half a micrometer. Hence the positioning accuracy was inherently limited to $1\ \mu\text{m}$ minimum. We also measured the positioning accuracy by fixing small pieces of indium phosphide on a Al_2O_3 substrate. We choose pieces of semiconductor because they have sharp edges and are rigid. In that way deformations of the objects during the glue curing process are avoided and deviations from the target position are entirely due to alignment procedure. We placed the elements at distances varying from $20\ \mu\text{m}$ up to 1 centimeter (figure 7.6). The accuracy of the placement has been measured with a Wyko interferometer¹. A relative accuracy of 2 % was found. In figure 7.7 a picture of two semiconductor pieces at $125\ \mu\text{m}$ distance is given. With the experiment described above we can evaluate the quality of the alignment procedure in X-Y-plane. In addition we investigated the alignment in the Z-plane. As mentioned before, this alignment is

¹Carried out at TONA, Vrije Universiteit Brussel

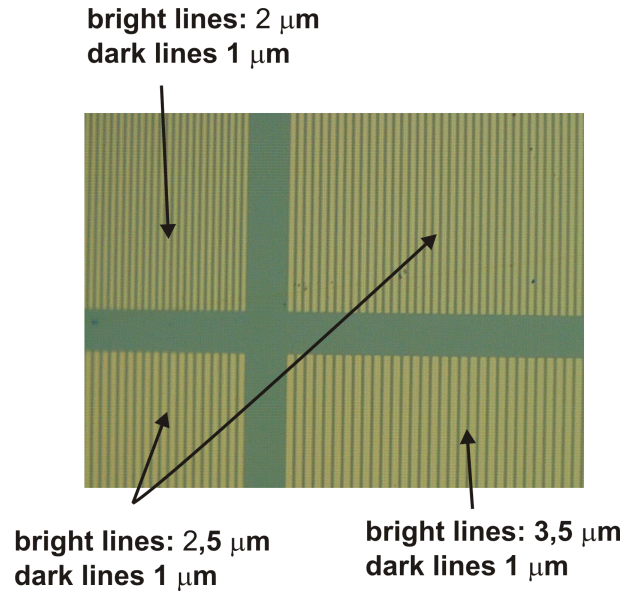


Figure 7.5: Pattern with varying spatial frequencies

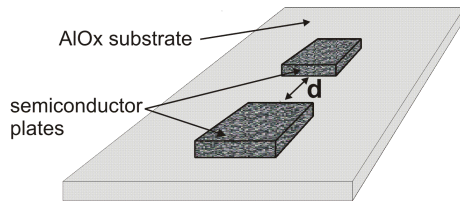


Figure 7.6: Semiconductor plates were placed at distance d varying from $20\ \mu\text{m}$ to 1 centimeter.

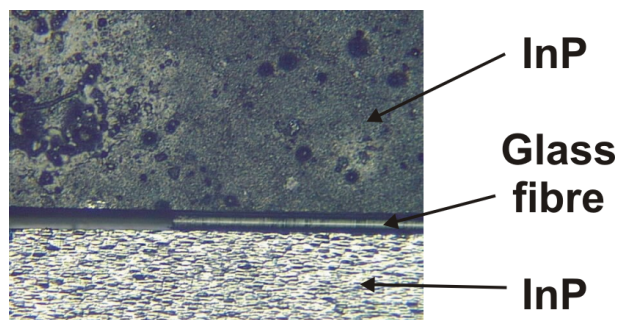


Figure 7.7: Positioning of two objects at $125\ \mu\text{m}$. In between the objects a silica fibre is placed to illustrate the distance between the objects.

based on the depth of focus of the imaging system. However, in order to evaluate the complete positioning procedure in the Z-direction, including the glue curing, we placed two plates vertically parallel at short distance, pretty much similar to a situation in which two $1 \times N$ arrays of POFs are aligned and stacked (figure

7.8). We found that the maximal “height” difference δz is $20\ \mu\text{m}$. This deviation

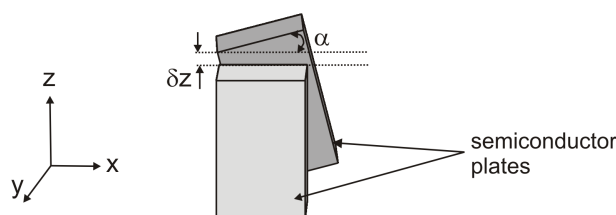


Figure 7.8: Vertical alignment test

was already noticeable after the curing with the viewing system of the virtual alignment setup. This indicates that sometimes the curing process was influencing the alignment of the devices. A similar effect was seen in the X-Y-plane: the plates were placed at $50\ \mu\text{m}$ distance on the X-axis originally, but after curing this distance varied between 50 and $45\ \mu\text{m}$. This might indicate some shrinkage or stress effects in the glue during the curing, although low shrink glue was chosen to do the assembly (Norland 121). However, in the case of stacked plates we decided to polish briefly the end facet of the stacked ferrule. In that way the end facet becomes flat and the accuracy in the Z-direction can be considered around $0\ \mu\text{m}$. As a conclusion we can state that the intrinsic alignment accuracy of the alignment is in the order of $2\ \mu\text{m}$ vertically and about 2% of the targeted distance in the horizontal X-Y plane. However, stress effects in the glue can decrease the quality of the alignment. Hence the choice of the kind of glue is critical for a precise assembly.

7.3 Stacking POF arrays: assembly of the ferrule

The “virtual setup” was used to stack the one-dimensional arrays to form a two dimensional array. We will present results for the stacking of embedded arrays as well as for stacked arrays based on “fibre in groove” technology. In this way the comparison of both technologies can be completed in depth. The accuracy of the stacking was measured with the same scanning technique as described in the previous chapter.

The positioning of the fibres in a two-dimensional array is defined by two contributions: the alignment within a one-dimensional array and the alignment of the one-dimensional arrays with respect to each other. The first contribution has been extensively discussed in the previous chapter. The contribution of the stacking in its turn can be split up into two components: accuracy in the Y-direction, and accuracy in the X-direction (figure 7.9). Both directions are differently influenced since e.g. the shrinkage of the glue will play a more important role in the Y-direction than in the X-direction. We limit ourselves to radial offset and neglected the offset in the Z-direction since the end facet is briefly polished. We

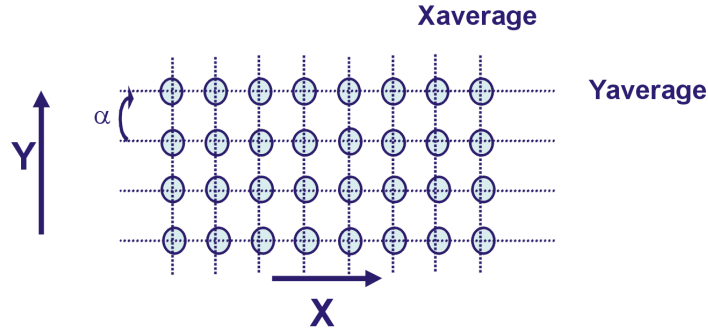


Figure 7.9: Offset axes at a 2D-array

neglected the angular offset as well since for the order of magnitude of offset we obtain, the losses are negligible (see Chapter 5). Let's go back to figure 7.9. We can calculate the average Y position for each row along the x-axis (Yaverage) and for each column along the Y-axis (Xaverage). The distribution of the fibres around Yaverage is mainly influenced by the accuracy of the alignment within one layer. The distance and the angle between the averages however, are mainly influenced by the stacking procedure. Hence we will use these parameters to characterize the stacking in the Y-direction. In the X-direction however, the distinction between the influence of the stacking and that of the single layer is more hazy. The parameter we use is the distribution of the fibres around the X-average columns. This is of course influenced by the variation on the pitch within one layer but also by the stacking.

Finally we evaluate the complete array by comparing the position of the fibres to that of a perfect array: we calculate the average offset between the real position of the fibres and the "ideal" position. For illustration purposes we also simulate the losses for an array-to-array coupling in case of best possible coupling alignment.

Stacked arrays based on "fibre-in-groove" technology We assembled 4×8 arrays of both Toray and Asahi POFs. The plates in which the grooves were made had a specified thickness of $250 \mu\text{m}$. However in reality they were slightly thicker, up to $260 \mu\text{m}$. So we decided to stack them at a pitch of $300 \mu\text{m}$.

For the Toray POF the average distance between adjacent rows was $300 \mu\text{m}$ (distance between medians of adjacent rows), but it varied between 285 and $315 \mu\text{m}$. Mostly the alignment of the one-dimensional arrays was based on the position of the centre of the outermost fibres. It is clear that the variation on the Y-position within the single plate influences the accuracy of the stacking alignment and explains part of this deviation. The angle between adjacent rows (angle between median of adjacent row) was 0.60° at maximum. The average distance between the columns is $250 \mu\text{m}$ (distance between median of adjacent columns), but the distribution of the POFs around the Xaverage value within a column had a standard deviation of $7 \mu\text{m}$. What this means in terms of radial offset can be seen in figure 7.10. We simulated the optimal position of a real array with respect to

an ideal array and calculated the radial offset between each POF and its ‘ideal’ equivalent. A typical example of such a radial offset distribution is given in figure 7.10. The maximal offset is around $17\ \mu\text{m}$, the average offset is $8\ \mu\text{m}$. This means that in case of best possible alignment the maximal radial offset at the emitter-detector/POF interface is $17\ \mu\text{m}$. We also simulated optimal couplings between ferrules and found a maximal $20\ \mu\text{m}$ radial offset between coupled POFs. If we look back at table 5.6 in Chapter 5, we can conclude that this technology is not usable for a link with Toray POF and RCLEDs. For Toray POFs in combination with VCSEL the technology is definitely acceptable. For the Asahi POFs the “fibre in

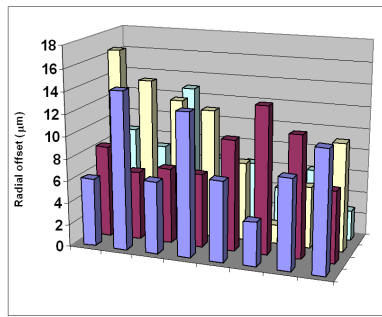


Figure 7.10: Radial offset distribution of a 4×8 Toray POF array with “fibre in groove” technology

groove” technology generates larger variations. A picture of (part of) a 4×8 array can be seen in figure 7.11. The average distance between adjacent rows is again

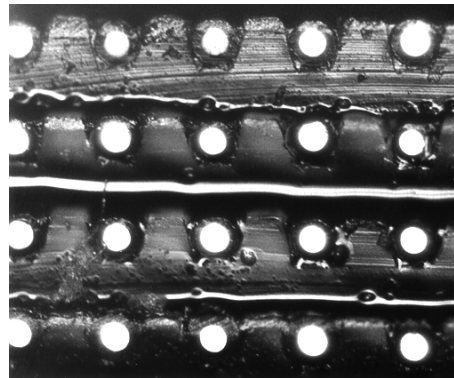


Figure 7.11: Picture of a Asahi POF array with the “fibre in groove” technology

$300\ \mu\text{m}$ but it varies between 260 and $340\ \mu\text{m}$. The angle between adjacent rows can go up to 1.5° . It is clear that the large variation on the positioning of the fibres within the grooves affects the stacking accuracy. The standard deviation of the fibre position distribution around the Xaverage value within a column is $10\ \mu\text{m}$. What all this gives in terms of radial offset compared to an ideal array can be seen from an example in figure 7.12. The average offset is $15\ \mu\text{m}$, the maximal offset is $40\ \mu\text{m}$. It is more than evident that the “fibre in groove” technology is completely inadequate for the Asahi POF.

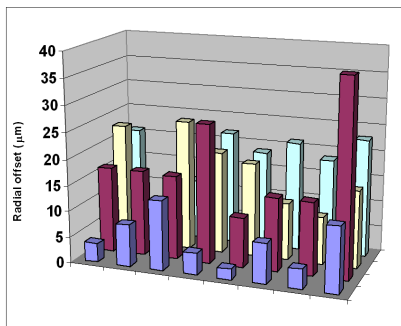


Figure 7.12: Radial offset distribution of a 4×8 Asahi POF array with “fibre in groove” technology

Stacked arrays based on “embedded fibre” technology The stacking of the single plate based on “embedded fibre” technology yielded some improvements. For the Toray POFs we obtained an average distance between adjacent rows of $250 \mu\text{m}$, with a variation $\pm 10 \mu\text{m}$. The maximal angle between adjacent rows is 0.3° . For the distribution of the POFs around Xaverage value we obtain a standard deviation of $5.5 \mu\text{m}$. In terms of radial offset with respect to an ideal array we obtain we obtain an average value of $7 \mu\text{m}$ with a maximum of $15 \mu\text{m}$. These numbers show a limited improvement compared to the “Toray in groove” case. The improvement is limited indeed, since we saw in the Chapter 6 that for Toray POF the change from “fibre in groove” to “embedded fibre” yielded a limited improvement. Referring to table 5.6 in Chapter 5, we can see that the “embedded fibre” technology, generates a maximal radial offset equaling the total radial tolerance for the RCLED/Toray link. This means that there is no room for additional offset caused by the coupling alignment. Hence we have to conclude that the embedded fibre technology in its current form is not adequate for the RCLED/Toray link. It is of course applicable for the VCSEL/Toray link. The situation is different for the Asahi POF. A picture of a 4×8 array assembled with “virtual alignment” can be seen in figure 7.13. The average distance between

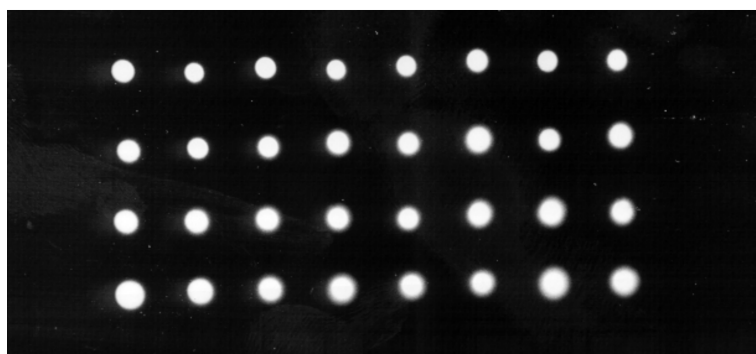


Figure 7.13: Picture of a 4×8 POF array with “embedded fibre” technology.

the Yaverage medians was $250 \mu\text{m}$ with a variation of $\pm 13 \mu\text{m}$, and the maximal

angle between them was 0.5° . The POF distribution around the Xaverage axis had a standard deviation of $7\ \mu\text{m}$. This shows a clear improvement with respect to the “fibre in groove” technology, but what does it mean in terms of radial offset? A typical example can be seen in figure 7.14. The average offset is around $11\ \mu\text{m}$,

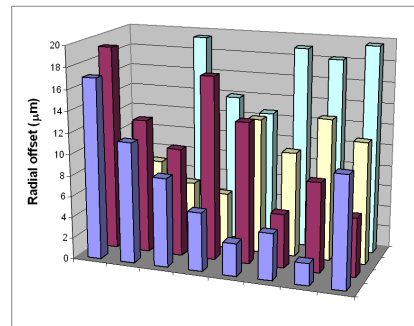


Figure 7.14: Radial offset distribution of an Asahi POF array with the “embedded fibre” technology

the maximum is $20\ \mu\text{m}$. Comparing this to the total offset tolerances in table 5.6 (Chapter 5), this radial offset is acceptable at the detector-emitter/POF interface. However we calculated the radial misalignment for optimized POF array/POF array couplings and we found a maximal offset of $23\ \mu\text{m}$, which is more than the allowed offset at the POF/POF interface. This means that the “embedded fibre” technology can be suitable for a VCSEL/Asahi link with two connectors, but not for a link with an intermediate POF/POF connector.

Gluing issues Although the “virtual alignment” method as such proved to be adequate some problems showed up, more precisely during the gluing step of the procedure. When the one-dimensional arrays are stacked they are in a vertical position. Although the glue is applied only towards the end of the alignment procedure, it still tends to go downwards and accumulate on the bottom of the arrays. This resulted in wedge-shaped ferrules (figure 7.15). The angles are in the order of a few degrees, which is too small to cause considerable optical losses, but given the fact that the length (L) of the ferrule is easily 5mm the difference in thickness (T) between the end facet and the back side was considerable. In addition we encountered another problem: it appeared that the thickness of the one-dimensional arrays was difficult to control during the “fibre-embedding” process. As a result the thickness of these arrays varied between $130\ \mu\text{m}$ and almost $250\ \mu\text{m}$. This made it very difficult to determine the amount of glue necessary during the stacking. Insufficient glue resulted in bad alignment, too much glue resulted in a glue layer on the end facet of the POFs. Of course this layer could be removed afterwards with a short polish procedure, but still it reduced the visibility of the fibre end facets during the alignment considerably. Moreover it increased the wedge-shaping of the ferrule. It is clear that those problems are not fundamental and can be resolved. A solution would consist of two steps. In the first place the one-dimensional array should be in a horizontal position when they are stacked. In this way wedge-forming is avoided. To achieve this, an adaptation of

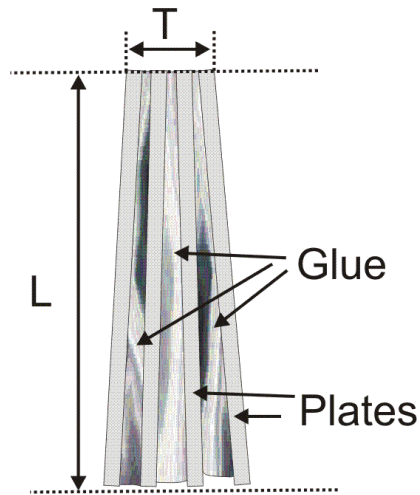


Figure 7.15: Influence of accumulated glue on the shape of the ferrule

the “virtual alignment” setup is necessary. Secondly the outer dimension of the one-dimensional arrays should be better controlled. During the development of the “embedded fibre” technology not much attention has been paid to this aspect, but curing of the glue when it is in a proper encasement should do the job. Well controlled sizes of the one-dimensional array should allow to use the same precise amount of glue for each stacking, and e.g. an automatic dispenser could be used. Unfortunately there was no more time available during this PhD to implement these enhancements.

7.4 Assembly of the complete connector

After the manufacturing of the POF ferrule it needs to be merged with a system that aligns it with a coupled device like an emitter/detector array or another POF ferrule. As pointed out in Chapter 4, for this purpose we made use of two so called U-blocks with sheaths for pins (figure 7.16). The assembly of the connector is done with virtual alignment as well. For the alignment procedure, the position of the POF array with respect to the alignment pins is used. More precisely, an alignment pin is cut in two and temporarily fixed in the grooves of one of the U-blocks. The cut has been carried out to obtain a flat end facet of the pin, so that optical system of the setup can easily focus on this end facet. (normally the ends of alignment pins are conical). After the alignment of the array with respect to the pins, it is fixed onto the U-block with UV-curing glue. Finally the pins are removed and the second U-block is placed on top of the first one and fixed with UV-curing glue. A picture of a U-block as well as a complete connector can be seen in figure 7.17. The depth of the central groove in which the ferrule fits had to be such that the cavity formed by these grooves is slightly larger than the ferrule. However, in the previous paragraph it was mentioned that the ferrules were wedge-shaped. In order to accommodate the broad (back)side of the ferrule, the central groove of the U-block had to be made relatively deep (d). As a consequence

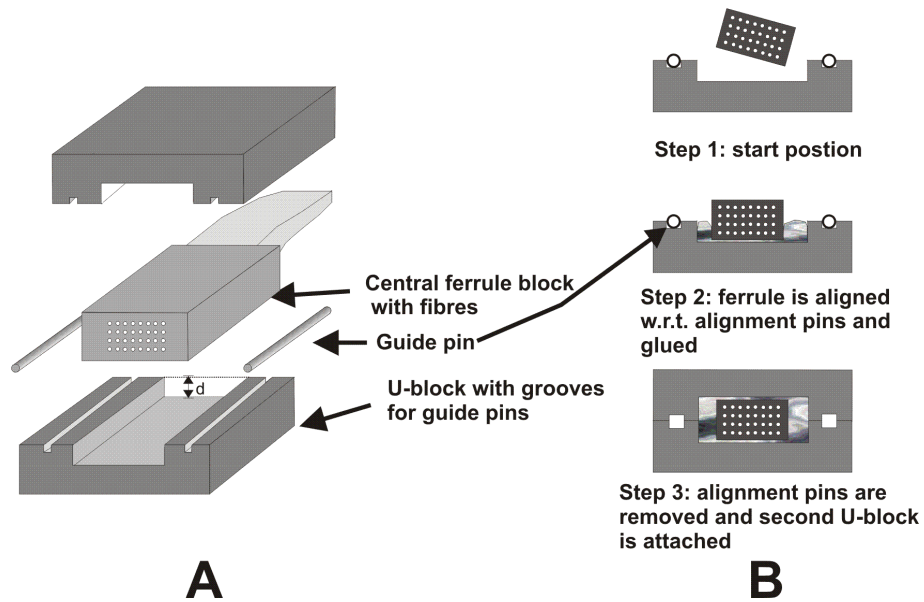


Figure 7.16: Assembly of a complete POF array connector: A) A central groove forms the cavity for the ferrule. Smaller grooves on the side from the sheaths for the guide pins B) The assembly can be split up in three steps

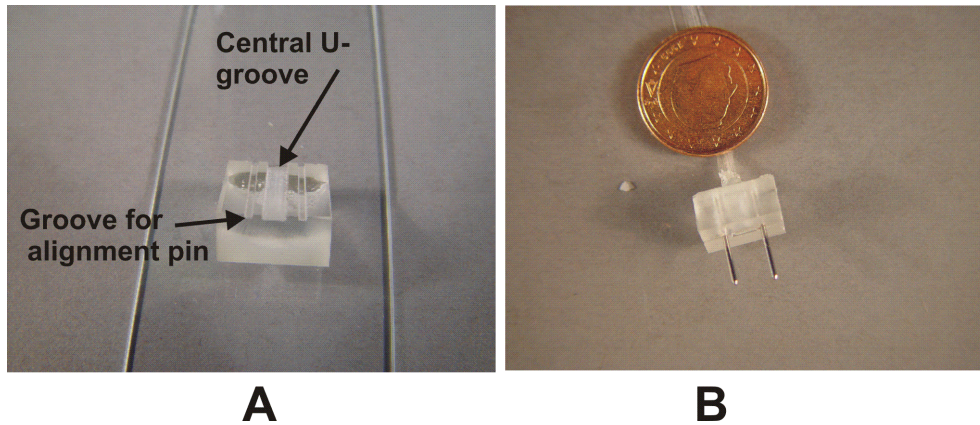


Figure 7.17: A) picture of a U-block B) Complete connector

too much glue needed to be applied, especially at the most critical place of the ferrule: at the end facet. Too much glue results in a severe loss of accuracy of the positioning during the UV-curing due to shrinkage effects. Hence the complete connectors we manufactured were of mediocre quality. This was clearly noticed during a coupling experiment in which we coupled POF arrays to each other. For instance the average transmission loss between coupled Toray POF arrays was 4

dB, for the Asahi POF arrays this equaled 5 dB. It is evident that the quality of these connectors did not come up to our demands. However, it is clear that by solving the gluing problems as described in the previous paragraph, the outer dimensions of the ferrule can be controlled more accurately and as a consequence it becomes possible to design a cavity that has dimension closer to that of the ferrule. In this way the applied amount of glue can be restricted to a minimum and the positioning of the ferrule with respect to the alignment pins can be carried out more accurately.

7.5 Assembly of a RCLED module

The connectors we developed until now allow to couple POF arrays to other POF arrays. However, the last hurdle that has to be taken for the completion of an (optical pathway of an) optical link is the realization of a POF to detector/emitter array coupling system. As described in Chapter 4, for this purpose we used a spacer plate containing precise holes for alignment pins. This spacer has to be placed next to the emitter/detector array in such a way that when the pins of the POF array connector are inserted in the holes, the POFs are well aligned with respect to the emitters/detectors. The placement of the spacer can be done in several ways. One can e.g. use a master tool that has features to align to the emitter/detector on the one side, and has features that aligns it to the spacer plate on the other side. Another way is to produce precise holes for the alignment pins directly in the substrate on which the emitter/detector array is mounted. These holes can be made by for instance micro drilling or laser ablation. In this case, the holes in the spacer on the other hand, do not need to be precise and hence the functionality of the spacer is reduced to one aspect: keeping a fixed distance between the end facet of the connector and the emitter/detector array. Both methods have been studied at Intec generating satisfactory results. An extensive report can be found in [3].

However, given the fact that the “virtual alignment” setup was built, we decided to investigate whether this method could be used for the placement of the spacer plate. In this way the versatility of the method is proved and, in addition it shows that the manufacturing of expensive master tools can be avoided.

For the assembly of emitter/detector modules did we had access neither to VCSEL arrays, nor to detector arrays. Hence we limited ourselves to the manufacturing of RCLED-based emitter modules. A basic “proof of principle” module we assembled consisted of 3 elements: a spacer with precise holes for alignment pins, a semiconductor (Si, InP, GaAs) chip carrier on which the RCLED array was flip-chip mounted [4], and an Aluminum Oxide (AlOx) or copper base plate on which the carrier and the spacer were mounted. A drawing and a picture of the complete module can be seen in figures 7.18 and 7.19. The base plate contains two drilled holes that are far wider (1-2 mm) than the 700 μm diameter of the alignment pins.

We have mounted the complete module on a testing Printed Circuit Board that allowed us to drive each RCLED in the array separately through SMA connectors (figure 7.20). In “real” operational systems the carrier and spacer are mostly di-

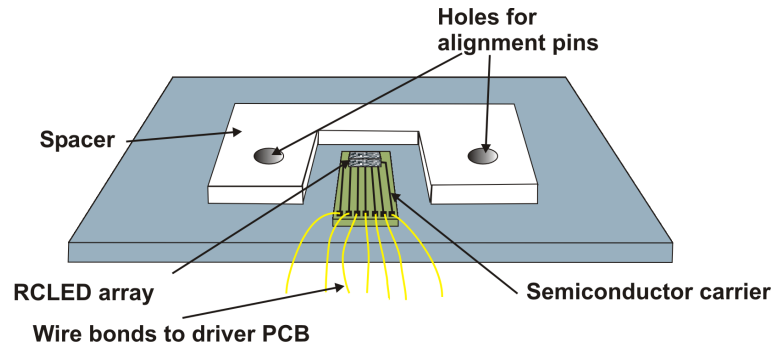
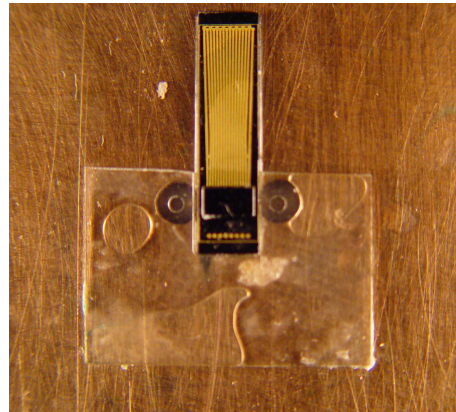


Figure 7.18: Schematic representation of a RCLED-based emitter module

Figure 7.19: A module containing a 2×8 RCLED array+ carrier, a spacer and a copper base plate



rectly mounted on an electronic package provided with for instance a pin- or ball grid array [3, 5]. The electrical connection to the PCB is ensured by wire bonds going from the semiconductor substrate to bond pads on the PCB. The RCLEDs are described in Chapter 3: they emit at a wavelength of 980 nm and have an active diameter of 50 or 32 μm . A semiconductor carrier was developed for driving 2×8 RCLED arrays. Its metallization layout can be seen in figure 7.21. The RCLED arrays are flip-chipped on the Au pads at the top end of the metal tracks. These long metal pads carry the signal away to the wire bonding pads. These pads are long enough ($\pm 8\text{mm}$) to allow a connector to be coupled to the arrays without damaging the wire bonds. A module with a coupled connector can be seen in figure 7.20. Above the RCLED array one can distinguish alignment crosses (figure 7.21). These were originally designed for use with a master tool [3]. However since they are at a fixed distance (1470 μm in the Y-direction, 0 μm in the X-direction) with respect to the RCLEDs they can serve as a reference point for the “virtual alignment” procedure. The thickness of the substrate was 300 μm . The thickness of the RCLED is 150 μm , so the total thickness of the carrier + RCLED array equals 450 μm , without taking into account the thickness of the flipchip- bonds, that can take an extra few μm s. The spacer on the other hand has a thickness

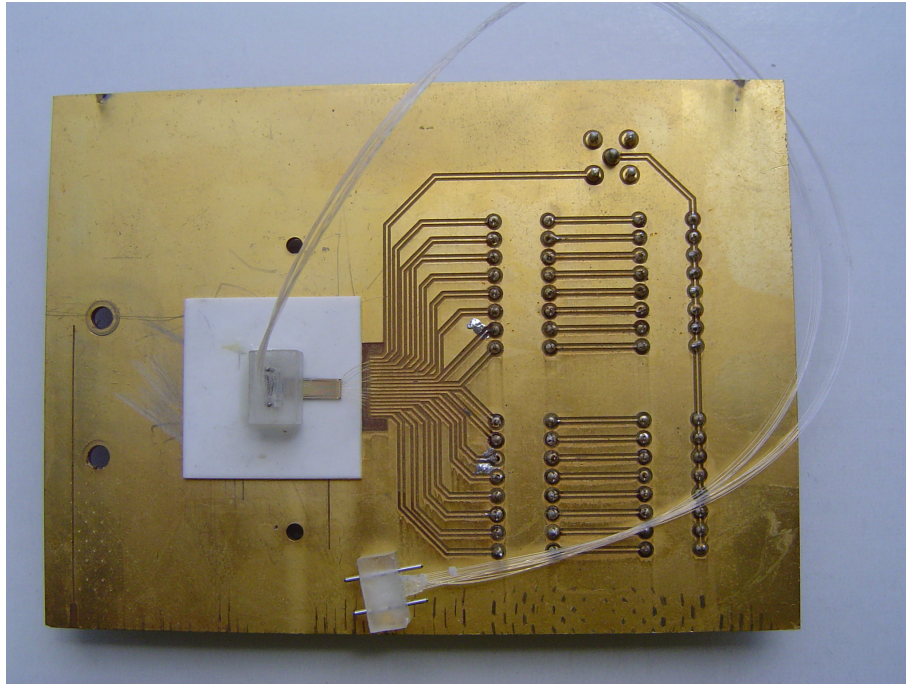


Figure 7.20: Module mounted on testing PCB

of $500 \mu\text{m}$, resulting in a “height” difference of $750 \mu\text{m}$ between the RCLED and the top of the spacer, \pm the variation on the thickness of the glue layer under the carrier and the spacer. The PMMA spacer has been produced at the Forschungszentrum Karlsruhe [6] and has a U-shape. It contains two micro-drilled holes with a diameter of $700 \mu\text{m}$ ($\pm 0.5 \mu\text{m}$) and at a distance of 4.6 mm ($\pm 2 \mu\text{m}$). They serve to guide the alignment pins of the coupled connector.

Experiments A module was scanned with a WYKOTM interferometer². It revealed that the placement of the “guide pin” holes is within $10 \mu\text{m}$ from the desired place. This means that the maximal radial offset due to misalignment from the spacer is

$$\text{maximal radial offset} = 875 \frac{10}{2300} \approx 4 \mu\text{m} \quad (7.1)$$

The origin of this equation can be seen in figure 7.22. This is a more than acceptable value for all the POF-based optical links we studied. However, the WYKOTM measurements also showed a height difference of 65 to $90 \mu\text{m}$ between the RCLED and the spacer, indicating that the gluing procedure was not uniform enough.

In order to further investigate the quality of the spacer placement, we used purchased MTTM connectors holding 1 by 8 $62.5/125 \mu\text{m}$ silica fibres. Those con-

²Carried out at TONA, VUB

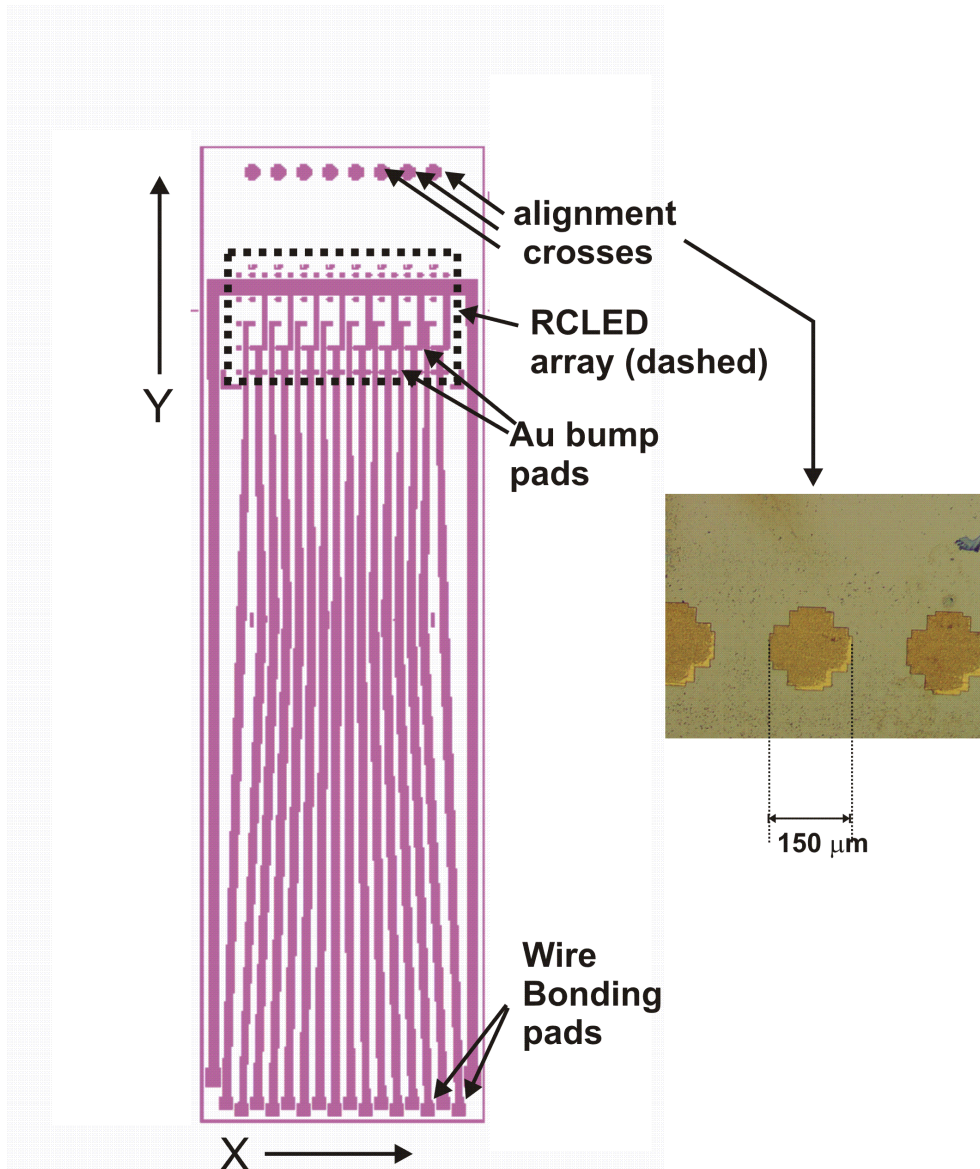
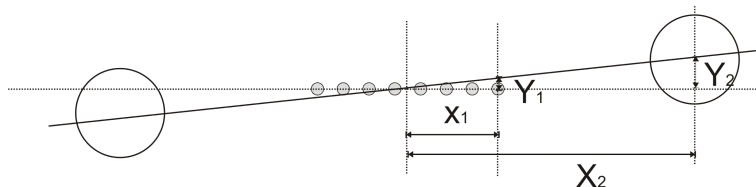


Figure 7.21: The layout of the semiconductor substrate

nectors assure a small radial offset of the coupled fibres, about $1 \mu\text{m}$ maximal [7]. Hence coupling such a connector to a $32 \mu\text{m}$ RCLED array gives us an idea about the accuracy of the spacer placement. We found coupling losses varying between 19 and 21 dB. These are perfectly normal numbers for the combination of $32 \mu\text{m}$ RCLEDs with $62.5/125 \mu\text{m}$ fibres with an NA of 0.20 at axial offsets between 65 to $90 \mu\text{m}$. The radial offset of the $4 \mu\text{m}$ at the pins does not have any influence on



$$\frac{X_1}{Y_1} = \frac{X_2}{Y_2}$$

Figure 7.22:

the coupling loss at this kind of axial offset.

7.6 Conclusions

We developed a method for alignment of opto-mechanical devices called “virtual alignment”. The intrinsic quality of the technology is satisfying. However, further investigations on the gluing mechanisms have to be carried out, since most of the inaccuracy is caused by bad gluing procedures. Using the “virtual alignment” technique in combination with the “fibre in groove” and the “embedded fibre” technology, we assembled ferrules that are usable in VCSEL-POF links and RCLED/POF links. An overview of which combination of technologies suitable is for what kind of link, can be seen in table 7.1. Also the assembly using “virtual alignment” at emitter-detector/POF interface showed a high potential.

Table 7.1: Applicability of the “virtual alignment” technique in combination with the “embedded fibre”- and the “fibre in groove” technology for the different types of optical links we have considered. (NA = not applicable)

Link	50 μ m RCLED + 20 cm Toray POF	VCSEL + 50 cm Asahi POF	VCSEL + 50 cm Toray POF
No intermediate POF/POF connector	NA	embedded fibre	embedded fibre + fibre in groove
With intermediate POF/POF connector	NA	NA	embedded fibre + fibre in groove

Bibliography

- [1] <http://www.ficontec.com>.
- [2] <http://www.suss.com/main.php>.
- [3] A. Van Hove, *Termination and Interconnection Technology for Parallel Optoelectronic Systems*. PhD thesis, Ghent University, Faculty Applied Sciences, Dept of Information Technology, Sint Pietersnieuwstraat 41, 9000 Gent, Belgium, 2001.
- [4] L. Van Wassenhove et al, "A room-temperature flip-chip mounting technique for laser diodes on silicon motherboards," in *IEEE Lasers and Electro-Optics Society 1995 Annual Meeting*, vol. 2, (San Francisco, CA, USA), pp. 127–128, Octobre 1995.
- [5] <http://oiic.intec.ugent.be/>.
- [6] <http://www.fzk.de>.
- [7] T. Statake, T. Arikawa, P. W. Blubaugh, C. Parsons, and T. Uchida, "MT multifibre connectors and new applications," *IEEE*, pp. 994–999, 1994.

8

Conclusions and perspectives

THIS concluding chapter will give a brief overview of the main thoughts, results and conclusions discussed in this thesis. It will also propose some ideas for further developments based on the work carried out for this PhD, and will modestly try to find a space for POF in tomorrow's world of short distance interconnect.

8.1 Highlights and conclusions

Roughly spoken we can summarize this PhD in terms of the 6 following contributions:

1. We studied and compared the different possible transmission media for highly parallel optical links at multi-chip-module-to-multi-chip-module and board-to-board level. We proposed small diameter POF for its high numerical aperture and small bending radius, two properties that allow very compact links. Moreover POF is very cheap and allows fast and simple end facet termination.
2. We studied in detail the mechanical and optical properties of two kinds of small-diameter POFs we acquired: a commercially available product and a prototype fibre. The former was a POF manufactured by Toray and had a core diameter of $116\ \mu\text{m}$ and an outer diameter of $125\ \mu\text{m}$, the latter was made by Asahi Chemical and had a core diameter of $61\ \mu\text{m}$ and an outer diameter of $124\ \mu\text{m}$. Both POFs were step index fibres and made of PMMA. It was noticed that the diameter of the Asahi POF was clearly varying more than that of the Toray POF. Also the Asahi POF appeared to suffer clearly more from mechanical shortcomings. Optical bending losses were found to be negligible down to a bending radius of 1 mm for both fibres. The transmission loss at various wavelengths was measured using a cut-back method.
3. We proposed a design for connectors for highly parallel POFs. We decided to realize the two-dimensional array of fibres by stacking one-dimensional arrays. The main source of inspiration for this approach was the unwillingness of the POFs to be introduced in classical connectors. Those connectors use the “fibre-in-hole” principle and due to the extreme flexibility of the POFs it is difficult, and hence time consuming and expensive, to introduce them in the narrow holes of the connectors. In order to obtain a complete connector, this two-dimensional array is placed in a housing containing two guiding pins. Those pins align the POFs to mating POFs or other optical devices. On the emitter-detector side of the coupling interfaces the alignment of the mating connector is done with a spacer containing holes for the guiding pins.
4. We studied the alignment tolerances at the optical interfaces in detail. We used models described in literature as well as our own ray-tracing model to estimate coupling losses as a function of offset. We compared the estimation to experimental results and obtained good agreement, taking into account end facet losses and light launching conditions.
5. We fabricated one-dimensional arrays of POFs with two different approaches: “fibre in groove” and “embedded fibres”. For the former technology, laser ablation was used to make grooves in thin PMMA plates. By fixing POFs in these grooves we obtained one-dimensional fibre arrays. This technique

yielded acceptable results for Toray POF. However, due to the varying diameter of the Asahi POFs, the accuracy of the alignment was not satisfactory for this fibre. The “embedded fibre” technology consisted in embedding a pre-aligned row of POFs in UV-curable glue. This technique yielded more satisfying results for usage in connectors with Asahi fibre. We obtained a precision of $9\ \mu\text{m}$ on the positioning of the fibres. Moreover these arrays can be terminated with a simple hot knife cutting.

6. We manufactured two-dimensional POF arrays by stacking the one-dimensional ones. For this stacking procedure a technique called “virtual alignment” was developed. This technique is based on the movement of two independent cameras and a very precise translation table. It allows to position two elements with respect to each other with an accuracy of 2 %, which is satisfactory for the assembly of devices in a POF-based optical link. However, problems occurred while fixing the aligned elements to each other, and an enhanced gluing system proved to be necessary. We manufactured 4×8 POF arrays that can be used in VCSEL-based optical links.

8.2 POF and interconnect: what is next?

As discussed in Chapter 1, how and when we will see optics implemented in intracabinet optical interconnects will depend on multiple factors, but it remains almost certain that some day in the future, parallel optics will be needed. Whether POFs will be used, remains an open question. Competition will most probably come from polymer waveguides. However, at this moment the implementation of highly parallel polymer waveguides in optical backplanes is still very complex and shows a lot of problems, in particular in relation to coupling light in and out of the waveguide plane. Much will depend on the maturity and cost of this technology at the moment parallel optics is needed. Still, small-diameter POF has some advantages that will be hard to beat:

- It is incredibly cheap, including the termination technology.
- Distances up to 1-2 meters can easily be covered.
- It allows making highly parallel links, that can follow a complex routing scheme.

In this perspective, small-diameter POF remains a candidate for short parallel data links. Moreover, the facts that low loss POF with small core diameter ($50\ \mu\text{m}$) is now commercially available and that a company like Nexans has developed a 1×8 POF ribbon (core diameter $62.5\ \mu\text{m}$), are quite encouraging [1, 2].

On the other hand, at this stage the behavior of small-diameter POF exposed to long term raised temperature/moisture is still inferior to that of silica fibre. This is of capital importance in a backpanel environment, and has to be further investigated and enhanced.

Finally there is the issue of the connectorization, the key question of this PhD.

An ideal connector is compact, cheap and can be made in an automated way. Prototypes of such a connector were developed by FCI in the framework of the IO project [3]. This project was the successor of the OIIC project and was carried out between September 2001 and November 2004, right after the research work for this PhD. The connectors were developed for 8×8 POF arrays, at a pitch of $250 \mu\text{m}$. The ferrules were made with ceramic moulding, resulting in very precise pieces. Adapted connector housings for the different interfaces within a data processing system were developed. The connectors that were coupled to the optoelectronic chips contained two protruding 8×8 ferrules. The goal of the protrusion was to bring the end facet of the POF array very close to the optoelectronic die without touching it. For the fibre-to-fibre backpanel connectors, ferrules with a flat interface were used. Given the fact that the POFs were bundled in 1×8 ribbons, one assumed that sliding the fibres into precise alignment holes would be considerably easier than in the case of single fibres. Hence a fibre-in-hole approach was adopted. However, the ribbons had to be partially stripped and severe problems due to the lack of stiffness of the POFs occurred while inserting the fibres into the holes. In this view, the ideas that we bring forward in this PhD stay relevant. We proposed a three-step process for making a connector: first making a one-dimensional array, then stacking these arrays to obtain a two-dimensional one, and finally adding a housing with features to align this array to another optical device. The two latter steps proved to be more complicated than the first one. Moreover, implementing an optical alignment method makes automation not impossible, but complex. The first step on the other hand, was clearly more simple and yielded very satisfactory results. Therefore the idea came to us to expand the first step to step 2 and maybe even to step 3. Therefore the “embedded fibre” technology needs to be expanded to a 2D-array. The idea for a production set-up is shown in figure 8.2. The pre-alignment of the 2D-array is carried out by, for instance, a plate with holes. Of course therefore the outer diameter of the POF needs to be reasonably controlled. The 2D-array is then embedded in a polymer, which is then hardened by for instance UV-curing. Once the first ferrule is made, it can be moved over a small distance following the Z-axis. In the cavity formed by the ferrule and the alignment tool, the POFs are now well aligned, and new polymer is added. In this way complete patchcords with good alignment can be manufactured. Moreover, one could try to add an alignment pin in the cavity, so that inside the patchcord a hole is created to guide these pins when coupling the patchcord to another optical device. This production process could easily be automated which would make it a cheap manufacturing method, resulting in cheap devices. It is clear though that especially the research for an adequate polymer would ask a large effort: it has to be flexible, heat resistant and compatible with the material of the POF.

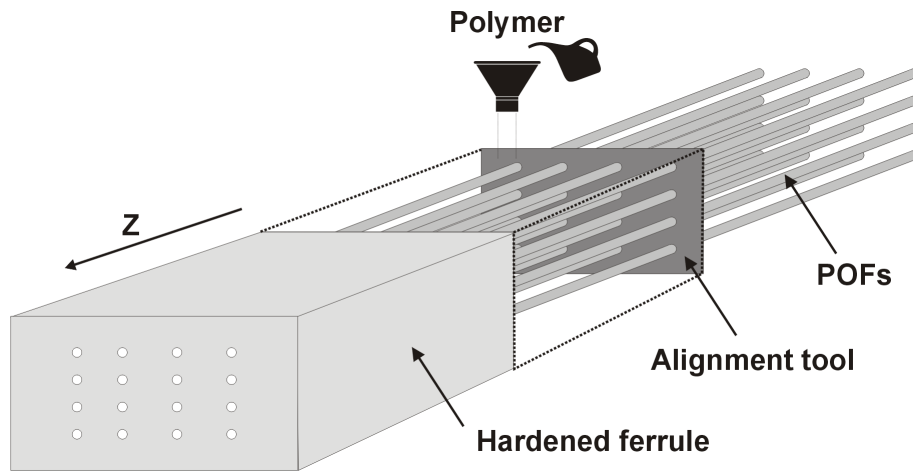


Figure 8.1: Set-up for the manufacturing of 2D arrays of POF, based on the “embedded fibre” technology

Bibliography

- [1] [HTTP://www.chromisfiber.com](http://www.chromisfiber.com).
- [2] T. Freeman, “POF eyes high-speed connections,” *FibreSystems Europe/Lightwave Europe*, pp. 11–12, June 2004.
- [3] <http://io.intec.ugent.be>.

